

INFORMATION TO USERS

The most advanced technology has been used to photograph and reproduce this manuscript from the microfilm master. UMI films the text directly from the original or copy submitted. Thus, some thesis and dissertation copies are in typewriter face, while others may be from any type of computer printer.

The quality of this reproduction is dependent upon the quality of the copy submitted. Broken or indistinct print, colored or poor quality illustrations and photographs, print bleedthrough, substandard margins, and improper alignment can adversely affect reproduction.

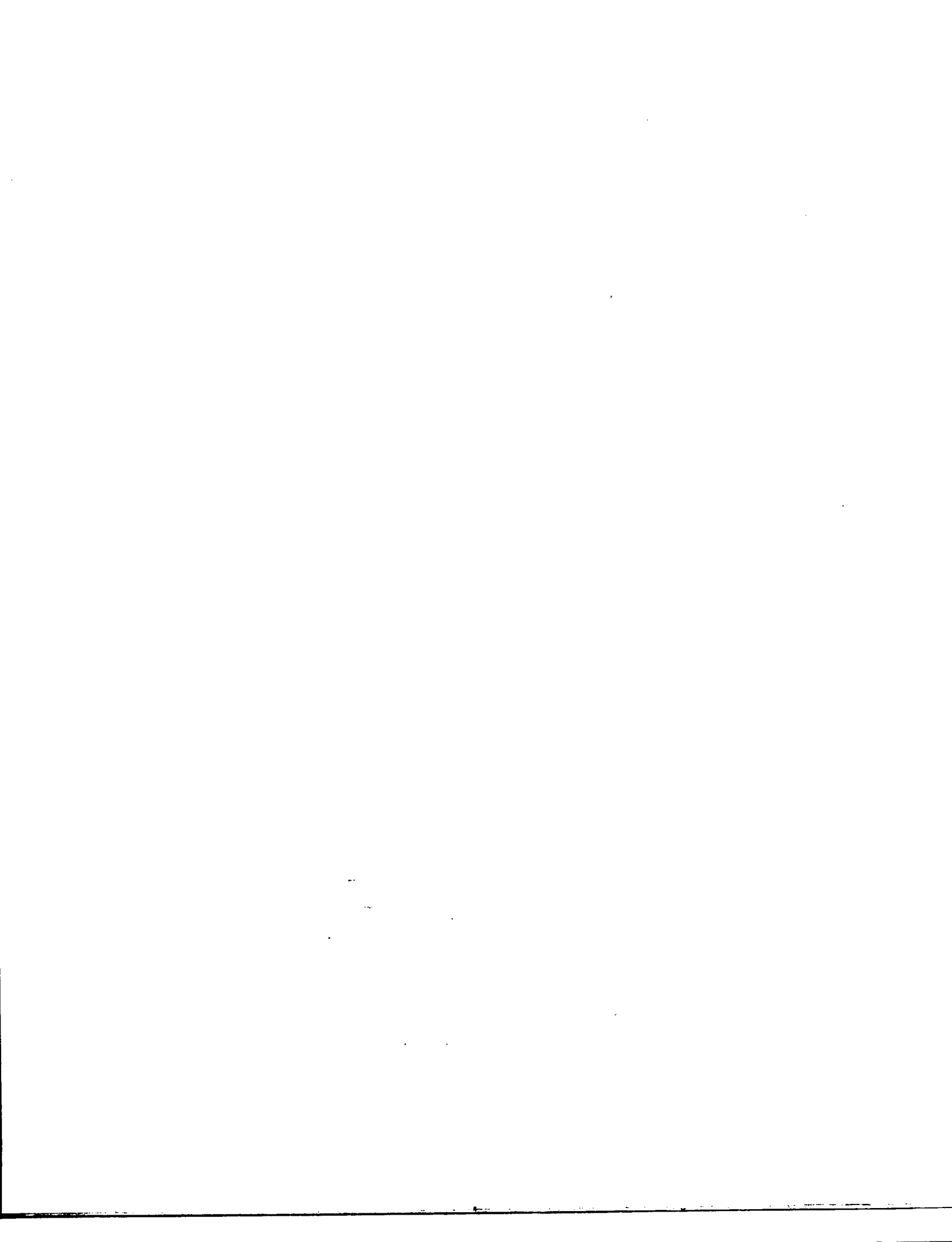
In the unlikely event that the author did not send UMI a complete manuscript and there are missing pages, these will be noted. Also, if unauthorized copyright material had to be removed, a note will indicate the deletion.

Oversize materials (e.g., maps, drawings, charts) are reproduced by sectioning the original, beginning at the upper left-hand corner and continuing from left to right in equal sections with small overlaps. Each original is also photographed in one exposure and is included in reduced form at the back of the book.

Photographs included in the original manuscript have been reproduced xerographically in this copy. Higher quality 6" x 9" black and white photographic prints are available for any photographs or illustrations appearing in this copy for an additional charge. Contact UMI directly to order.

U·M·I

University Microfilms International
A Bell & Howell Information Company
300 North Zeeb Road, Ann Arbor, MI 48106-1346 USA
313/761-4700 800/521-0600



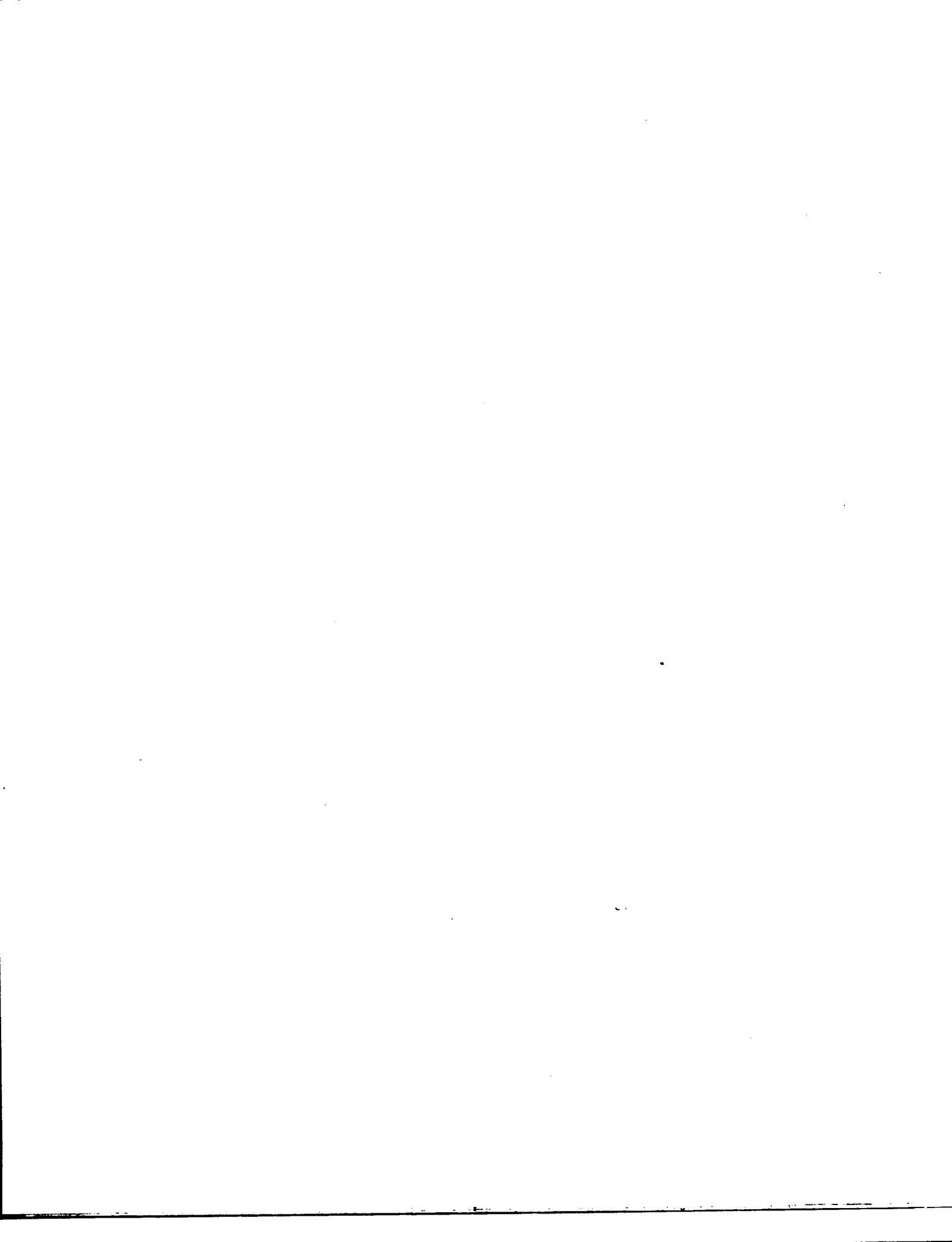
Order Number 9103462

Mechanics of headcut migration in rills

Stein, Otto Robert, Ph.D.

Colorado State University, 1990

U·M·I
300 N. Zeeb Rd.
Ann Arbor, MI 48106



DISSERTATION

MECHANICS OF HEADCUT MIGRATION IN RILLS

Submitted By:

OTTO R. STEIN

Department of Civil Engineering

In Partial Fulfillment of the Requirements

for the Degree of Doctor of Philosophy

Colorado State University

Summer 1990

COLORADO STATE UNIVERSITY

June 29, 1990

We hereby recommend that the dissertation prepared under our supervision by Otto R. Stein entitled "Mechanics of Headcut Migration in Rills" be accepted as fulfilling in part requirements for the degree of Doctor of Philosophy.

Committee on Graduate Work



Dr. Michael Harvey



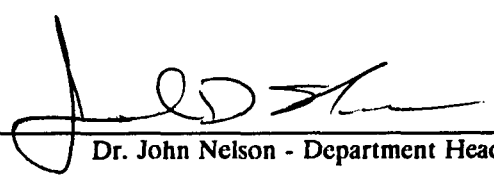
Dr. Dirk Van Zyl



Dr. Carlos Alonso - Co-Advisor



Dr. Pierre Juljen - Advisor



Dr. John Nelson - Department Head

Abstract of Dissertation

Mechanics of Headcut Migration in Rills

The proposed conceptual model relates two-dimensional headcut migration to sediment detachment just upstream and just downstream from a headcut. If upstream erosion dominates, the headcut tends to obliterate itself as it migrates upstream, eventually becoming indistinguishable from the eroding channel's bed slope. If downstream erosion dominates, the headcut face erodes from below and a definable headcut with a near vertical face migrates upstream with time.

A criterion to determine which migration mode occurs is formulated using both dimensional analysis and by equating hydraulic and sediment detachment equations. Dimensional analysis results in a time scale ratio of upstream to downstream erosion related to the upstream and downstream sediment detachment, bed slope, Reynolds number and the drop number, which represents the dimensionless headcut drop height. A physically based analysis of hydraulics and sediment detachment yields a relationship between the dimensionless terms. The resulting equation for headcut stability is favorably compared with a total of eleven laboratory measurements of headcut migration on cohesive soil.

The maximum scour depth and the total volume of eroded material produced by the impinging jet just downstream from a headcut are analyzed. A previously developed method for the prediction of the ultimate, or equilibrium, scour depth in non-cohesive bed material is modified to include scour from cohesive bed material. This method equates the sediment detachment potential of the bed material to the diffusion of a jet.

The same approach is used to determine the time rate of the maximum scour depth. Dimensional analysis relates the ratio, maximum scour depth at any time over the predicted ultimate scour depth, to the jet Reynolds number, Froude number and a dimensionless time scaled to jet properties. The change in scour depth is analytically shown to proceed as two distinct rates. For some period of time from the initiation of scour, scour rate is independent of time because the bed is within the jet potential core and diffusion has not reduced the maximum jet velocity. Beyond this time period jet diffusion decreases the rate of scour and this rate decreases with increasing time and scour depth. In the limit the predicted ultimate scour depth is approached. The dimensional and physically based analyses for scour depth compare favorably with experimental data. This data includes measurements of the ultimate scour depth and the change in scour depth with time for ten runs on cohesive soil, eight runs on sand $d_{50} = 1.5\text{mm}$ and six runs on sand $d_{50} = 0.15\text{mm}$.

Otto R. Stein
Civil Engineering Department
Colorado State University
Fort Collins, CO 80523
Summer, 1990

Acknowledgements

This has to be my favorite part of this dissertation if for no other reason than I get to express my thoughts in first person singular. I would first like to thank the people and organizations who have made this research possible, by providing support for both the project and myself. The majority of the funds have been provided by the wonderful people at the USDA-Agricultural Research Service, Hydro-Ecosystems Group in Fort Collins, and a special thanks goes to Donn DeCoursey who managed to bring me to CSU in the first place. Additional funding, especially in these last months, has been provided by the Center for Excellence in the Geosciences, Colorado State University. The Center is funded by the U.S. Army Research Office, Grant No. ARO/DAAL 03-86-K-0175.

I want to express my deep appreciation to my advisors, Pierre Julien and Carlos Alonso, who in their unique ways have provided me with an appreciation for engineering, research and academia, and the insight to keep it all in perspective with life's other goals. Without the skills they have taught to me this dissertation would not be worth reading.

I would also like to thank some of the many others who have helped me along the way; my other committee members Mike Harvey and Dirk van Zyl; people I have met through USDA, especially Virginia Ferreria, Mike Murphey, Rich Miskimins,

Leslie Bach, and Fernando Pons; and my fellow "Fellows" on the Geosciences project, Fred Ogden and Tom Burke. All of these people have provided invaluable technical assistance and/or much needed comic relief.

The one person who of course deserves more thanks than I will probably ever be able to return is Mary, my wife (who still hasn't gotten used to that label). Without her my ability to complete the last stages of this dissertation which seems to require every waking second would have been impossible. If only everyone could be as lucky to have a companion such as her.

I also thank my Mom and Dad, my brother and his family all of whom gave me the freedom to "leave the nest" and grow in ways I'm sure they never expected. Finally I would like to thank all my friends, both two and four legged, who have made life enjoyable for Mary and me.

Table of Contents

Abstract of Dissertation	iii
Acknowledgements	v
List of Tables	x
List of Figures	xi
List of Symbols	xiv
Chapter 1 Introduction	1
Chapter 2 Literature Review	4
2.1 Headcut Migration Studies	4
2.1.1 Brush and Wolman (1960)	5
2.1.2 Holland and Pickup (1976)	6
2.1.3 Begin (1979)	7
2.2 General Hydraulic Concepts	8
2.2.1 Continuity	8
2.2.2 Momentum	9
2.2.3 Energy: Resistance to Flow	10
2.2.4 Reynolds Number	11
2.2.5 Froude Number	12
2.3 Sediment Transport and Detachment	12
2.4 The Free Overfall	16
2.5 Hydraulics of Jet Scour	20
2.5.1 Free Plane Turbulent Jet	21
2.5.2 Impinging Plane Turbulent Jet	23
2.5.3 Scour from Impinging Jets	25
2.5.3.1 Kobus, Leister & Westrich (1979)	27
2.5.3.2 Rajaratnam (1981, 1982)	28
2.5.3.3 Yuen (1984)	29
2.5.3.4 Bormann (1988)	30
2.5.3.5 Similarity of Previous Studies	32
2.5.4 Time Scale of Jet Scour	34

Chapter 3 Analytical Development	37
3.1 Conceptual Model	37
3.2 Dimensional Analysis of Relevant Parameters	41
3.2.1 Dimensional Analysis of Headcut Stability	41
3.2.2 Dimensional Analysis of Upstream Scour	43
3.2.3 Dimensional Analysis of Downstream Scour	43
3.4 Normal Flow Region	44
3.4.1 Normal Flow Continuity	45
3.4.2 Normal Flow Momentum	45
3.4.3 Governing Equations	46
3.5 Accelerated Flow Region	47
3.5.1 Accelerated Flow Momentum Equation	49
3.5.2 Shear Stress in the Accelerated Flow Region	52
3.5.3 Bed Degradation in the Accelerated Flow Region	58
3.6 The Impingement Region	59
3.6.1 Maximum Applied Shear Stress	61
3.6.2 Ultimate Scour Depth	64
3.6.3 Change in Maximum Scour Depth With Time	65
3.6.3.1 Scour Rate Within the Potential Core	65
3.6.3.2 Scour Rate for the Diffusing Jet	67
3.7 Headcut Stability Analysis	72
Chapter 4 Materials and Methods	78
4.1 The Flume	78
4.2 Bed Material	80
4.3 Experimental Method	81
4.3.1 Measurement of Hydraulic Parameters	81
4.3.2 Constant Slope Runs	84
4.3.3 Non-Retreating Headcut Runs	85
4.3.4 Retreating Headcut Runs	87
4.3.5 Measurements of Changes of Profile	88
Chapter 5 Results and Discussion	89
5.1 Calibration of the Sediment Detachment Equation	89
5.2 Non-Retreating Headcut Runs	93
5.2.1 Ultimate Depth of Scour	102
5.2.2 Change in Scour Depth and Volume With Time	105
5.2.3 Sediment Concentration	113
5.3 Retreating Headcut Runs	116
5.3 Computer Simulation of Scour Profiles	125
Chapter 6 Conclusions and Recommendations	131
6.1 Conclusion Summary	138
6.2 Recommendations for Future Research	139

References	141
Appendix A	153
Appendix B	167
Appendix C	180
Appendix D	197

List of Tables

Table 3.1: Data from Rajaratnam and Muralidhar (1968)	53
Table 5.1: Hydraulic Parameters of Constant Slope Runs	90
Table 5.2: Hydraulic Parameters of Non-Retreating Headcut Runs	95
Table 5.3: Experimentally Varied Parameters for Ultimate Scour Depth ...	103
Table 5.4: Normalizing Parameters for Maximum Scour Depth	106
Table 5.5: Measured Headcut Stability Values	117

List of Figures

Figure 2.1: Free Overfall Definition Sketch	17
Figure 2.2: Free Plane Turbulent Jet Definition Sketch From Albertson et al. (1950)	21
Figure 2.3: Impinging Plane Turbulent Jet Definition Sketch From Beltaos (1972)	24
Figure 2.4: Scour Hole Forms From Kobus et al., (1979)	28
Figure 2.5: Equilibrium Scour Length J_e From Bormann, (1988)	32
Figure 2.6: Ultimate Scour Depth D_u From Bormann, (1988)	32
Figure 3.1: Initial Headcut Hydraulics	38
Figure 3.2: Headcut Migration: Upstream Hydraulics Dominate	39
Figure 3.3: Headcut Migration: Downstream Hydraulics Dominate	40
Figure 3.4: Normal Flow Control Volume	44
Figure 3.5: Accelerated Flow Region Control Volume	48
Figure 3.6: Pressure Distributions; Brink and Hydrostatic	48
Figure 3.7: Flow Depth vs. Distance Upstream From the Brink From Rajaratnam & Muralidhar, (1968)	54
Figure 3.8: Pressure Coefficient vs Distance Upstream From the Brink From Rajaratnam and Muralidhar, (1968)	54

Figure 3.9: Calculated Shear Stress Distributions; $q=0.00150 \text{ m}^2/\text{s}$, $S_b=0.023$	56
.....	
Figure 3.10: Hydraulics of the Impingement Region	60
Figure 3.11: Change in Scour Depth With Time From Eqs. 3.38 and 3.41	68
Figure 3.12: Change in Scour Depth with Time; Log-Log Scale	70
Figure 3.13: Headcut Stability for Initial Hydraulics and Low Critical Shear	
Stress	77
Figure 3.14: Headcut Stability Log-Log Scale	77
Figure 4.1: The Experimental Flume	79
Figure 4.2: Bed Material Particle Size Distribution	81
Figure 5.1: Sediment Discharge vs. Shear Stress; Constant Slope Runs	93
Figure 5.2: Typical Scour Profiles From Cohesive Soil	96
Figure 5.3: Typical Scour Profiles From Cohesive Soil	97
Figure 5.4: Typical Scour Profiles From Sand $d_{50}= 0.15\text{mm}$	98
Figure 5.5: Typical Scour Profiles From Sand $d_{50}= 0.15\text{mm}$	99
Figure 5.6: Typical Scour Progression With Time; Cohesive Soil	100
Figure 5.7: Typical Scour Progression With Time; Sand $d_{50}= 0.15\text{mm}$	101
Figure 5.8: Predicted vs Measured Scour Depths	104
Figure 5.9: Normalized Scour Depth vs Normalized Time; Large Sand	108
Figure 5.10: Normalized Scour Depth vs Normalized Time; Small Sand	108
Figure 5.11: Normalized Depth vs Normalized Time; Cohesive Soil	109
Figure 5.12: Measured vs Predicted Scour Depth with Time; Small Sand	111
Figure 5.13: Scour Depth vs Time; Soil Runs	112

Figure 5.14: Predicted vs Measured Sediment Concentration; Large Sand . .	114
Figure 5.15: Predicted vs Measured Sediment Concentration; Small Sand . .	115
Figure 5.16: Measured vs Predicted Sediment Concentration; Cohesive Soil .	115
Figure 5.17: Measured Headcut Stability Values	116
Figure 5.18: Scour Profiles Upstream Dominating Run	118
Figure 5.19: Scour Profiles Downstream Dominating Run	119
Figure 5.20: Measured Retreating Headcut Profile; All Soil	121
Figure 5.21: Headcut Retreat Showing Cantilevered Block Failure	123
Figure 5.22: Headcut Retreat Showing Cantilevered Block Failure	124
Figure 5.23: Comparison Measured and Predicted Profiles Non-Retreating	
Headcut	128
Figure 5.24: Comparison Measured and Predicted Profiles Retreating	
Headcut	129

List of Symbols

A, A', B, B'	Points defining an arbitrary normal flow control volume
B_d	Soil bulk density
C, C', D, D'	Points defining the accelerated flow control volume
C	Sediment concentration
C_d	General diffusion constant of a jet
C_f	Coefficient of friction
C_{fn}	Coefficient of friction in the normal flow region
$C_1 C_2$	Experimental diffusion constants of a jet
d_o	Diameter of a circular jet
d_{50}	Mean sediment size
D	Maximum depth of jet scour at arbitrary time
D_h	Initial drop height of the headcut
D_p	Depth of scour corresponding to potential core tip
D_u	Ultimate depth of jet scour
D	Normalized maximum scour depth (D/D_u)
f	Darcy-Weisbach friction factor
f_1	Constant of headcut stability analysis
F_d	Drop Froude number
F_o	Densimetric Froude number from Rajaratnam (1981)

F_r	Froude number
g	Gravitational acceleration
g_x	Gravitational acceleration in the x direction
h	Flow depth at a general cross section
H	Flow depth over normal flow depth
$h_{AA'}$	Flow depth at arbitrary cross section AA'
$h_{BB'}$	Flow depth at arbitrary cross section BB'
h_c	Critical flow depth
h_e	Flow depth at the free overfall brink
H_e	Flow depth at the brink over normal flow depth
h_n	Normal flow depth
h_t	Depth of tailwater
i	Rainfall intensity
J_c	Distance along a jet centerline
J_e	Distance along a jet centerline to impingement at equilibrium
J_i	Distance along a jet centerline to impingement
J_o	Length of a jet potential core
K	Pressure correction factor
K_e	Pressure correction factor at the brink
k_o	Pressure parameter from Kobus et al., (1979)
K_1 K_2	Constants of sediment discharge equation
L	Length of the accelerated flow region
L_c	Length of arbitrary control volume

P	Pressure at a general cross section
$P_{AA'}$	Pressure at arbitrary cross section AA'
$P_{BB'}$	Pressure at arbitrary cross section BB'
P_s	Excess static pressure from Kobus et al., (1979)
q	Unit flow discharge
q_b	Unit sediment discharge per unit area
R_e	Reynolds number
R_p	Particle size Reynolds number
S_b	Bed slope gradient
S_f	Friction slope gradient
t	General time
t_0 t_1 t_2 t_3	Incremental times in Figures 3.2 and 3.3
T_D	Time scale for downstream scour
T_p	Time scouring bed is within jet potential core
T_U	Time scale for upstream scour
T_n	Normalized time ($t U_o / y_o$)
u	Flow velocity in the x direction at a point
U_{mf}	Maximum diffused velocity of a free jet
U_{mi}	Maximum diffused velocity of an impinging jet
U_o	Initial velocity of a jet
U_*	Shear velocity
\bar{u}	Average flow velocity in the x direction
u_c	Average flow velocity at the brink

u_n	Average normal flow velocity
v	Flow velocity in the y direction at a point
w	Flow velocity in the z direction at a point
x	Longitudinal length scale
X_n	Longitudinal distance from brink to tailwater impingement
X_u	Normalized distance upstream from headcut brink
y	Vertical length scale
y_b	Thickness of a jet near the boundary
y_o	Initial thickness of a jet
z	Width length scale

Greek Characters

α	Average angle of scour hole boundary
β	Momentum correction factor
ΔS	Shift in pressure stagnation point for non-normal impingement
$\delta, \eta, \gamma, \xi, \epsilon$	Experimental exponents in Equation 2.2
θ_s	Shields parameter
θ_{cr}	Critical Shields parameter
ν	Fluid kinematic viscosity
ρ	Fluid density
ρ_s	Particle density
τ	Shear stress at a general cross section
τ_c	Critical shear stress for erosion initiation
τ_e	Shear stress at the brink

τ_i	Shear stress in the impingement region
τ_n	Normal flow shear stress
τ_{yx} τ_{zx}	Shear stresses in general momentum equation
ϕ	Sediment submerged angle of repose
χ	Angle of jet at tailwater impingement
ω_s	Sediment particle fall velocity

Chapter 1

Introduction

A headcut, also known as knickpoint or scarp, is an abrupt break in an ephemeral channel bed slope. When water flows over headcuts, they tend to migrate upstream and as one passes a cross section the channel becomes wider and deeper. If a headcut is on the upstream end of a channel it may define a break point between overland flow and channel flow. Therefore headcuts play a major role in drainage network evolution and microscale morphology. If the headcut is on a gully, or large scale ephemeral channel, it may undermine structures such as bridges or piers at a great economic loss.

Headcuts also form in rills, or micro-scale ephemeral channels, on roadcuts or in agricultural fields. A great deal of soil erosion takes place as the headcut migrates upstream. The loss of topsoil from fields is of great concern. The U.S. Soil Conservation Service has estimated thousands of acres of prime farmland, at a cost of billions of dollars in lost production, has been or will be severely eroded by the year 2000. This concern has prompted the United States and other countries to invest a great deal of money and research in predicting and mitigating the damage caused by soil erosion. However, little work has been done in predicting soil loss from headcuts, even though this mechanism may dominate others such as raindrop impact or general rill erosion. Two reasons explain this. First, the concept of

separating total soil loss into individual sub-processes is relatively new, only since the advent of super-computers to calculate the complex algorithms has this been feasible. Secondly, headcuts, especially those incised in rills, are often temporal, the reasons for their formation and eventual removal are poorly understood at best. On the other hand, raindrop impact and erosion in a rill will always occur if a given storm has sufficient intensity and duration to cause runoff.

This research is designed as both a theoretical and experimental investigation of the erosion phenomena in the vicinity of a headcut. The existence of a headcut is presumed, the study does not deal with headcut formation from a channel of constant slope. For a degree of simplicity only longitudinal and depth dimensions will be considered, width will be held constant.

There are two major objectives of this study. The first objective is to develop a criterion for headcut stability, defined as the conditions necessary for a headcut of given geometry under a given steady flow to be maintained indefinitely with time. With this definition a stable headcut with a relatively vertical face will propagate upstream and an unstable headcut will "wash out" with time and become indistinguishable from the channel bed slope. The second objective is to estimate the soil loss occurring in the vicinity of the headcut, especially just downstream, which can be attributed to the hydraulic conditions the headcut induces.

The approach is to determine the changes a headcut has on two-dimensional open channel flow hydraulics as compared to normal flow. Flow upstream of the headcut is similar to that of a free overfall and flow downstream is similar to that of an impinging jet. Both flow conditions increase the shear stress or dominant erosive

force applied to the bed. These changes are related to changes in the bed elevation of the channel near the headcut through a sediment detachment equation. This equation is based on both soil and flow properties. Mathematical descriptions of these changes will be provided in Chapter 3 and compared to experimental measurements in Chapter 5. In general however, water flowing from above the headcut impinges on the bed creating a plunge pool just downstream of the headcut. The pool is eroded both wider and deeper and the widening of the plunge pool in the upstream direction erodes the headcut face. At the same time erosion is increased in a region a few flow depths upstream of the headcut which tends to increase the bed slope in that region. The relative erosion rates of these two interdependent processes determine the stability, scour potential and upstream migration rate of a headcut.

Chapter 2

Literature Review

This chapter is divided into five main sections. First is an overview of the geomorphology of headcut migration, followed by sections on basic hydraulic concepts, general soil erosion and deposition, hydraulics of the free overfall, and hydraulics and scour potential of free and impinging jets.

2.1 Headcut Migration Studies

Many studies have attempted to define the shape and/or upstream migration of a headcut. The vast majority (Blong, 1985; Egboka and Okpoko, 1984; Piest et al., 1975; Patton and Schumm, 1975; Blong, 1970; Daniels and Jordan, 1966) report on field collected data most of which is qualitative and subjective. Usually these studies measure the changes in longitudinal position of a headcut with time. These measurements are usually made after a storm event. The change in position is often related to gross parameters such as peak flow rate of the previous storm. All are site-specific making comparison difficult.

Leopold et al., (1964 pp. 442-453) attempt to classify headcut shapes and suggest parameters which will cause a given shape to develop. One proposed hypothesis is that, at least for the case of headcuts in large gullies, seepage forces

through the soil may greatly alter the shape after the cessation of flow. Therefore the generalized shape measured after a storm event does not represent the shape determined by the flow hydraulics. However, upstream advancement is induced by the flow, which may explain the wide variance of migration and morphology data collected in the field.

Three studies stand out in their ability to explain fundamentals of headcut migration and reviewed below. It is no accident that all were conducted in laboratory flumes where conditions could be controlled.

2.1.1 Brush and Wolman (1960)

Brush and Wolman (1960) appear to be the first to relate knickpoint shape and migration to simple hydraulics. Their "knickpoint" was an oversteepened reach, 0.1 ft in 1.0 ft, in a channel of homogenous non-cohesive sand with an average slope ranging from 0.0012 to 0.0088 ft/ft. This stretches the definition of a headcut given above (an example of the difficulties in comparing studies) but their excellent observations relating knickpoint shape to hydraulics are quite general. They correctly show that shape changes must be related to differences in sediment transport at cross-sections near the knickpoint and assume sediment transport is related to applied bed shear stress. They qualitatively show shear stress and sediment transport to be a maximum at the upstream end of the knickpoint. The upstream end of the knickpoint migrates upstream as the maximum sediment transport at this point increases the slope.

Flow in the region just downstream of the knickpoint has more sediment than can be transported causing deposition which increases the slope just downstream. The knickpoint, originally defined as an oversteepened reach, grows both upstream and downstream but its slope decreases, approaching the average bed slope of the channel. Eventually the knickpoint becomes indistinguishable from the rest of the channel.

According to their analysis, the rate at which this shape change occurs is directly proportional to flow unit discharge and inversely proportional to sediment size. The change in shape of this knickpoint, or headcut, can be considered typical for homogeneous non-cohesive material.

2.1.2 Holland and Pickup (1976)

Holland and Pickup (1976) expand Brush and Wolman's study to include stratified cohesive and non-cohesive bed material. They define two general headcut types; a rotating headcut which tends to lose its shape with time, and a stepped headcut which tends to maintain a vertical face as it moves upstream. Brush and Wolman's study is an example of a rotating headcut. A stepped headcut is characterized by a plunge pool downstream from a vertical face and an oversteepened reach upstream. Any given headcut may show both characteristics at different times as it migrates upstream. For example, a stepped headcut may rotate if the plunge pool is filled by either upstream sediment supply or a crumbling of the vertical face. Conversely, a rotating headcut may step if a cohesive layer is exposed upstream allowing a plunge pool to develop. If the plunge pool becomes large

enough it may undermine the cohesive layer which collapses to fill the plunge pool and cause the headcut to once again rotate.

Holland and Pickup's study is significant in that it provides a mechanism which explains the incredible variability in headcut shape and migration rate found in the literature. Further, it shows that even for a constant discharge in a channel of constant slope the same headcut may change its shape and migration rate very rapidly depending on the differential properties of the bed material. However it makes no attempt to quantify any of the observed behaviors.

2.1.3 Begin (1979)

Begin's (1979) dissertation is the first attempt to develop a theoretically derived prediction of headcut migration this reader has found in the literature. In his study, which is summarized in two additional papers (Begin et al. 1980a,1980b), a headcut is created by base level lowering. The analytical approach combined sediment continuity and excess shear sediment transport equations to develop an equation for sediment production. This equation has the form of the well known heat diffusion equation. Sediment production is then related to headcut retreat. Solution of the diffusion equation for his boundary conditions shows headcut retreat to be rapid at early times and decrease to an asymptotic value.

While the attempt to apply fundamentals of sediment transport to headcut migration is admirable, several serious flaws exist in his analysis. First, he assumes headcut migration can be measured by sediment discharge at the flume exit. This measurement technique averages erosion over the entire length of channel and not

at the headcut. As he admits, the large scatter of his data could be caused by this averaging. No attempt is made to relate headcut retreat to hydraulics in the headcut vicinity. Second, in some (but not all) of his experimental runs precipitation was applied to the bed. Since this causes the flow rate at the headcut to decrease as the headcut moves upstream, it is natural to expect a decrease in migration rate. Therefore the decrease in migration rate for these runs may not be due to the hydraulics at the headcut. Finally, a closed form solution of the diffusion equation requires the exponent of the sediment transport equation to be identically equal to 1.5. While this is an often assumed value there is considerable debate. If the exponent is not equal to 1.5 the diffusion equation has lower order terms which do not cancel and his solution is invalidated. In defense of Begin's work it should be noted that his dissertation was primarily concerned with sediment production and not headcut migration.

2.2 General Hydraulic Concepts

2.2.1 Continuity

The basic physical phenomena the continuity equation describes is that matter can neither be created nor destroyed excluding energy transformations. For a fluid such as water this means the net outflow (or inflow) of mass from an arbitrary control volume must be equal to the decrease (or increase) of mass within the volume during a given time. Using principles of calculus to shrink the control volume and time span to infinitesimally small values, the differential form of the general continuity equation, 2.1, can be developed.

$$\frac{\partial \rho}{\partial t} + \frac{\partial \rho u}{\partial x} + \frac{\partial \rho v}{\partial y} + \frac{\partial \rho w}{\partial z} = 0 \quad (2.1)$$

In Eq. 2.1 ρ is the density of the fluid, t is time, x , y and z , are the cartesian coordinates and u , v and w are the fluid velocity components in the x , y and z directions respectively. Since water is an incompressible fluid, density is a constant (assuming constant temperature) and ρ can be eliminated from Eq. 2.1. Also because an initial assumption of this study is two dimensional flow the last term can be eliminated. Therefore Eq. 2.1 reduces to Eq. 2.2.

$$\frac{\partial u}{\partial x} + \frac{\partial v}{\partial y} = 0 \quad (2.2)$$

2.2.2 Momentum

The momentum equation is a mathematical expression of Newton's second law, namely that the sum of forces on a given mass in a given direction is equal to the time rate of change of linear momentum in that direction. For fluids a "given mass" is considered the mass within an infinitesimally small control volume. The cartesian coordinate system allows any given direction to be defined as the vector sum of three orthogonal directions x , y and z . A momentum equation must be defined in each direction. To derive the general momentum equation in any direction all the forces acting in that direction must be identified and be equated with the change in linear momentum in that direction. This study requires only the momentum in the longitudinal, or x direction shown in a differential form as Eq. 2.3.

$$\rho \left(\frac{\partial u}{\partial t} + u \frac{\partial u}{\partial x} + v \frac{\partial u}{\partial y} + w \frac{\partial u}{\partial z} \right) = \rho g_x - \frac{\partial P}{\partial x} + \frac{\partial \tau_{yx}}{\partial y} + \frac{\partial \tau_{zx}}{\partial z} \quad (2.3)$$

In Eq. 2.3, g_x is the gravitational acceleration in the x direction, P is the pressure, τ_{yx} and τ_{zx} are shear stresses in the x direction and all other terms are as defined for the continuity equation (2.1). The first term is eliminated if the flow is steady and the last term on both sides of Eq. 2.3 can be eliminated for two dimensional flow. With these assumptions Eq. 2.3 is reduced to Eq. 2.4 which will be used in future analysis.

$$\rho \left(u \frac{\partial u}{\partial x} + v \frac{\partial u}{\partial y} \right) = \rho g_x - \frac{\partial P}{\partial x} + \frac{\partial \tau_{yx}}{\partial y} \quad (2.4)$$

Further application of Eqs. 2.2 or 2.4 requires that all variables be defined at the boundary and either numerical solution or the following:

- 1) Select a control volume defining boundaries of the region of interest.
- 2) Integrate the equation over the control volume.
- 3) Use the divergence theorem to convert volume to surface integral.

Because each flow case has different values at the boundaries they will be evaluated separately.

2.2.3 Energy: Resistance to Flow

The first law of thermodynamics for a system shows that in the absence of a change in heat, mechanical work done by a system is dependent only on the initial and final energy states. If these states are equal energy is said to be conserved. The well known Bernoulli equation is a formulation of the conservation of mechanical

energy principle applied to irrotational flow. It shows that the energy state along a given streamline at any flow cross section is equal.

If flow is viscous and rotational, friction will dissipate energy and cause a resistance to flow. This loss can be accounted for mathematically if it is added to the downstream cross section. Dividing the head loss by the distance between cross sections yields the friction slope S_f . The Darcy-Weisbach equation relates the friction slope to other head terms if the flow is steady and uniform. In open channel flow the Darcy-Weisbach equation formulates as Eq. 2.5 where f is the Darcy-Weisbach friction factor, g the gravitational constant, \bar{u} the average uniform velocity and h_n the normal flow depth.

$$S_f = \frac{f\bar{u}^2}{8gh_n} \quad (2.5)$$

The friction factor has been determined from experiment for a variety of flow conditions. Julien and Simons (1985) report that four common equations can be used to approximate the friction factor depending on the flow condition. If the flow is laminar, it can be approximated as $24/R_e$ and for turbulent flow over a hydrodynamically smooth boundary the Blasius assumption yields $f = 0.22/R_e^{0.25}$ where R_e is the Reynolds number defined in Eq. 2.6. Manning's equation and the Chezy equation indirectly relate f to their respective coefficients.

2.2.4 Reynolds Number

Reynolds number is the ratio of inertial forces to viscous forces. For wide, uniform open channel flow this ratio is expressed in dimensionless terms as Eq. 2.6

where R_e is Reynolds number, \bar{u} is the average flow velocity, h is the flow depth orthogonal to the average velocity and ν the kinematic viscosity of the fluid. Reynolds number is important in determining the Darcy-Weisbach friction factor f and in distinguishing between laminar and turbulent flow.

$$R_e = \frac{\bar{u}h}{\nu} \quad (2.6)$$

2.2.5 Froude Number

Froude number is the ratio of inertial to gravitational forces. For wide, uniform open channel flow this ratio can be described in dimensionless terms as Eq. 2.7 where F_r is the Froude number, \bar{u} is the average flow velocity, h is the orthogonal flow depth and g is the gravitational constant. Froude number is important in distinguishing between supercritical and subcritical flow.

$$F_r = \frac{\bar{u}}{\sqrt{gh}} \quad (2.7)$$

2.3 Sediment Transport and Detachment

Sediment discharge can be defined as the amount of sediment, usually measured as mass or weight, passing through a cross section of flow per time. It is dependent on two distinct but often confused concepts, sediment transport capacity and sediment detachment capacity. Sediment transport capacity is the ability of a given flow to transport individual soil particles and sediment detachment capacity is the ability of a given flow to detach particles from the bed. Classic studies on

sediment discharge in open channels (see Simons and Senturk, 1977) usually have an infinite supply of non-cohesive bed material therefore transport capacity limits discharge.

Alonso et al. (1981) show that virtually all equations for sediment transport of non-cohesive bed material include the dimensionless Shields (1936) parameter θ_s , which relates hydrodynamically applied forces to a given sediment particle's resisting gravitational forces. For given sediment and fluid properties there is a level of shear stress in which these forces are in balance. This value of θ_s is defined as θ_{cr} and is related to another dimensionless parameter, particle Reynolds number R_* . The relation between θ_{cr} and R_* is usually given in graphical form or as Eq. 2.8 in which U_* is a shear velocity defined as $(\tau / \rho)^{1/2}$, where τ is the applied bed shear stress, ρ_s and ρ the density of the sediment particle and fluid respectively, g the gravitational acceleration, d_{50} the particle mean sediment size and ν the kinematic viscosity of the fluid.

$$\theta_{cr} = \left(\frac{\rho U_*^2}{(\rho_s - \rho)g d_{50}} \right) \propto R_* = \left(\frac{U_* d_{50}}{\nu} \right) \quad (2.8)$$

Sediment discharge of cohesive bed material is dependent on the lesser of transport or detachment capacity. Unless there is a large upstream sediment supply detachment capacity is usually limiting sediment discharge in channels of cohesive bed material (Brown et al., 1988). Confusion can arise in that both sediment transport and detachment are related to similar hydraulic parameters.

Julien and Simons (1985) proposed a general sediment discharge equation for overland flow on cohesive material based on dimensional analysis. Their result in

dimensional form, is shown as Eq. 2.9. In Eq. 2.9 q_s is the unit sediment discharge, S_b the bed slope gradient, q the unit flow rate, i the rainfall intensity, τ_c the soil resisting strength, τ the hydraulically applied bed tractive force (shear stress) and δ , η , γ , ξ , ϵ , experimentally determined constants. It makes use of the kinematic wave approximation where the slope of the energy gradient S_f can be considered equal to the bed slope S_b . The authors call Eq. 2.9 a transport capacity based sediment discharge equation but the last term $(1.0 - \tau_c / \tau)$ reflects soil resistance to erosion, and is therefore a detachment capacity not transport capacity term.

$$q_s = \delta S_b^\eta q^\gamma i^\xi \left(1.0 - \frac{\tau_c}{\tau} \right)^\epsilon \quad (2.9)$$

Foster and Meyer (1975) proposed the first form of Eq. 2.10 for sediment detachment in rills. It is mathematically equivalent to the second form which can be derived from Eq. 2.9 by assuming rainfall is absent or insignificant. The parameters K_1 and K_2 must be experimentally determined.

$$q_s = K_1 (\tau - \tau_c)^{K_2} = K_1 \left[\tau \left(1.0 - \frac{\tau_c}{\tau} \right) \right]^{K_2} \quad (2.10)$$

The form of Eq. 5.10 proposed by Foster and Meyer (1975) has gained wide acceptance as the rill erosion detachment component in many models of upland erosion (Foster et al., 1977; Knisel, 1980; Nearing et al., 1988). This is despite a clear understanding of the fundamentals of cohesive soil detachment. Foster and Meyer (1975) admit limited validation but relate their development of Eq. 2.10 for

detachment capacity to previous work of Partheniades (1965, 1972) and Partheniades and Paaswell, (1970).

Since 1975 some validation can be construed from work on sediment detachment by single drop impact (Al-Durrah and Bradford, 1982a,1982b). Their work clearly shows that sediment detachment is a function of the shear stress above a threshold value induced by an impacting water drop, below the threshold value no detachment occurs. Assuming that sediment detachment is related to the magnitude of shear stress and not the mechanism of application their study validates an excess shear model for sediment detachment. Partheniades initial study (1965) does relate erosion of a specific soil (San Francisco bay mud) to average shear stress above a threshold value but he notes that even below this value some erosion occurs. It should also be noted that this study was conducted in a flume 60 ft. long by 1 ft wide and erosion was determined from sediment concentration samples taken at the flume exit. This technique averages any local erosion and depositional patterns over the entire area.

The above discussions reveal the difficulty in calibrating a fundamentally sound, theoretically based sediment discharge expression for cohesive soil erosion. Theoretically, sediment discharge is the lesser of transport capacity or detachment capacity. In practice, it is difficult to quantitatively separate them. Therefore most researchers have used a simplified expressions such as Eq. 2.10. Most more rigorously developed expressions such as Eq. 2.9 can be reduced to the form of Eq. 2.10, an excess shear equation. This equation is quite general but has three parameters K_1 , K_2 and τ_c which may vary significantly. Studies, including those of

Partheniades, have attempted to relate these parameters especially τ_c to properties of cohesive soil. None can be considered adequate and for greatest accuracy they should be experimentally evaluated for each specific soil and flow condition. The first part of the present study's experimental program uses Partheniades method to evaluate K_1 , K_2 and τ_c for one particular soil under normal flow conditions. Results will be presented in Chapter 5.

2.4 The Free Overfall

This review of the hydraulics of the free overfall will be used in Chapter 5 to determine a shear stress distribution along the channel bed just upstream from a headcut. Virtually no previous studies on the free overfall consider shear stress, in fact most assume that shear stress in this region is constant so that other variables such as exit depth can be determined.

The free overfall, or the abrupt end of a long channel, is a hydraulic phenomena which has received considerable attention of past researchers. This was initially because it is a control section, theoretically in which discharge can be calculated from only geometric variables. Since early (pre 1950) studies, which assumed the free overfall was a case of flow over a weir of zero height, attention has focused on either applying the momentum or energy equations in some particular form or measuring in detail the various parameters involved. To arrive at a meaningful conclusion, both theoretical and experimental methods must be employed because the problem is one of rapidly varied flow which has neither uniform velocity

nor hydrostatic pressure distributions. All theoretical equations contain at least one constant which must be assumed or determined by experiment.

A definition sketch for the free overfall is given in Fig. 2.1. Steady uniform flow h_n approaches a brink in a channel of constant slope S_b . Assuming the flow detaches from the bed, pressure on the lowest streamline is zero at the brink. The pressure reduction causes the flow to accelerate and water surface profiles to decrease through a distance defined as the reach L . The minimum depth h_e occurs just at the brink, and can be related to the upstream normal flow depth h_n (if the flow is supercritical) or critical flow depth h_c (if the flow is subcritical as shown). Changes in pressure and flow depth affect the shear stress distribution within the reach L .

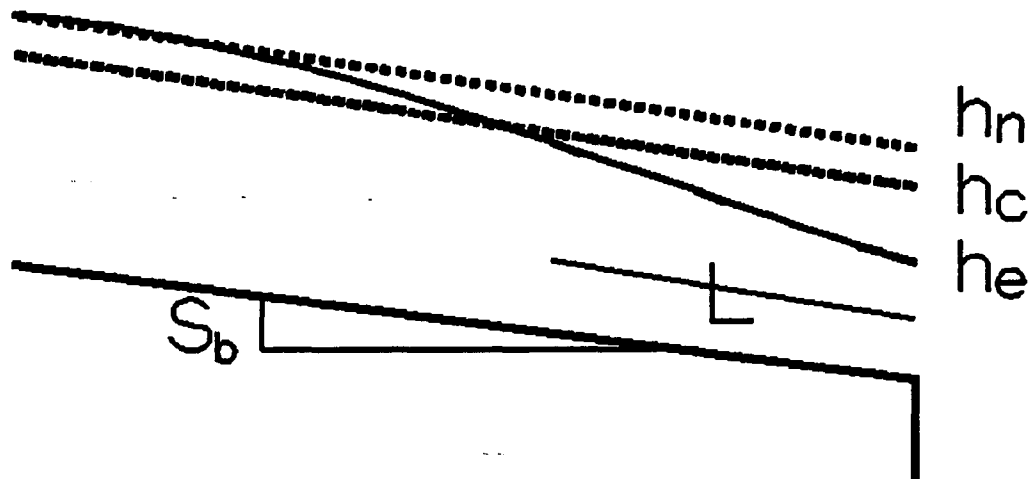


Figure 2.1: Free Overfall Definition Sketch

In one of the first publications on the topic Rouse (1936) uses the basic weir formula with weir height = 0 to determine for horizontal channels the exit depth, $h_e = 0.715 h_c$ where h_c is the critical depth of flow. He is the first to show that even

though brink pressures are zero at the upper and lower streamlines they are not zero through the entire brink profile, an assumption which is still often made. In a later publication Rouse (1937) gives measured pressure distributions for a horizontal bed for several cross-sections within the reach L .

Southwell and Vaisey (1946) use potential theory and a relaxation method to convert curvilinear streamlines to rectangular coordinates so that a finite difference method can be used to determine the flow profiles upstream and downstream from a free overfall. Markland (1965) refines Southwell and Vaisey's procedure, which is general, and uses it to calculate profiles for various upstream conditions. Since potential theory is used it is of no help in determining shear stress.

Fathy and Amin (1954) appear to be the first to apply the momentum equation to the free overfall. From a differential form of the momentum equation, a backwater profile curve which includes both momentum flux and pressure correction factors is proposed. Their experimentally measured values for pressures at the brink are negative and the emphasis of analysis is justifying these negative pressures. Discussion by Carstens and Carter (1955) shows that pressures cannot be negative and highlights other errors in analysis. Probably due to these errors the original paper has been largely dismissed, which is unfortunate because the initial approach is sound. Carstens (1955) later provides limited data on the relations between both h_c and L against S_b , the bed slope.

Delleur et al. (1956) provide a more detailed analysis of the relation between h_c and S_b . They develop the momentum equation for a control volume between the brink and an upstream control section, either where $h = h_c$ for a subcritical flow or

where $h = h_n$ for a supercritical flow. The length of the control section corresponds to the reach L . Both momentum flux and pressure correction factors are considered in the development but the first is later reasoned to be equal to unity. The weight and shear forces are assumed to cancel each other. The resulting relations give h_e in terms of a pressure correction factor at the brink K_e , and the bed slope S_b . Depths are experimentally measured for various slopes and a value for K_e can be graphically determined from fitted curves.

Rajaratnam and Muralidhar (1968) report on detailed experimental measurements of many parameters of the free overfall. Measurements of flow profiles; variation in K and β , the momentum flux correction factor; bed pressures; bed shear stress; and velocity profiles throughout the reach L are graphically represented for several combinations of discharge and bed slopes. Results show β increases slightly, K decreases significantly from 1.0 to 0.462-0.270 depending on bed slope and bed shear stress increases as the brink is approached.

Hager (1983,1984) uses an energy rather than momentum equation to determine changes in pressure and flow depth through the reach L . His determination for both exit depth and pressure are similar to previous studies using the momentum equation but he appears to be the first to provide an analytical equation for water surface profiles upstream from the free overfall. His relation for the exit depth h_e is given as Eq. 2.11 and the water surface profile is given by Eq. 2.12.

In these equations F_r is the Froude number, X_u is the distance upstream from the headcut divided by normal flow depth ($X_u = X / h_n$) and H the flow depth

$$\frac{h_e}{h_n} = \frac{F_r^2}{F_r^2 + 0.4} = H_e \quad (2.11)$$

$$X_u = -2 \sqrt{\frac{F_r^2}{3(F_r^2 - 1)}} \left(\operatorname{cotanh}^{-1} \sqrt{\frac{F_r^2 - H}{F_r^2 - 1}} - \operatorname{cotanh}^{-1} \sqrt{\frac{F_r^2 - H_e}{F_r^2 - 1}} \right) \quad (2.12)$$

divided by normal flow depth ($H = h / h_n$). Due to initial assumptions of Hager's analysis Eq. 2.12 is only applicable for supercritical flow ($F_r > 1.0$). Note that the originally published (1983) Eq. 2.12 erroneously used the hyperbolic arc tangent function. This is mathematically impossible as the argument is always greater than 1.0 and \tanh^{-1} is only defined for values less than 1.0. A reworking of Hager's analysis showed the error was in evaluating the domain of an integral required in the development of Eq. 2.12.

Several other papers are worth noting. Diskin (1961) and Rajaratnam and Muralidhar (1970) discuss the trapezoidal free overfall. Replogle's (1961) discussion of Diskin's paper provides more experimental results. Rajaratnam et al. (1976) include roughness effects on the free overfall. More recently, Christodoulou (1985) assumes a nonaerated free overfall where pressure is not atmospheric under the brink.

2.5 Hydraulics of Jet Scour

The hydraulics of jets has also received considerable attention of past researchers. Initial studies focused on a free jet in which the jet discharges into an identical fluid with infinite boundaries. More recently the effects of impervious

boundaries on jet hydraulics has been investigated. This configuration is often referred to as an impinging jet. Research concurrent to both has attempted to estimate the scour potential of impinging jets. The following sections review results from all three classes and will be used to determine the scour potential downstream from a headcut.

2.5.1 Free Plane Turbulent Jet

A definition sketch for a free jet taken from Albertson et al. (1950) is given in Fig. 2.2. The velocity field at several cross-sections is given. The jet has an initial width y_0 and average velocity U_0 . As the jet travels through the surrounding fluid it diffuses growing wider but decreasing in average velocity. For some distance J_0 from the nozzle along the jet centerline a potential core exists in which the velocity remains U_0 . Beyond this distance the entire velocity field is reduced by diffusion, but the maximum velocity U_{mf} remains at the jet centerline.

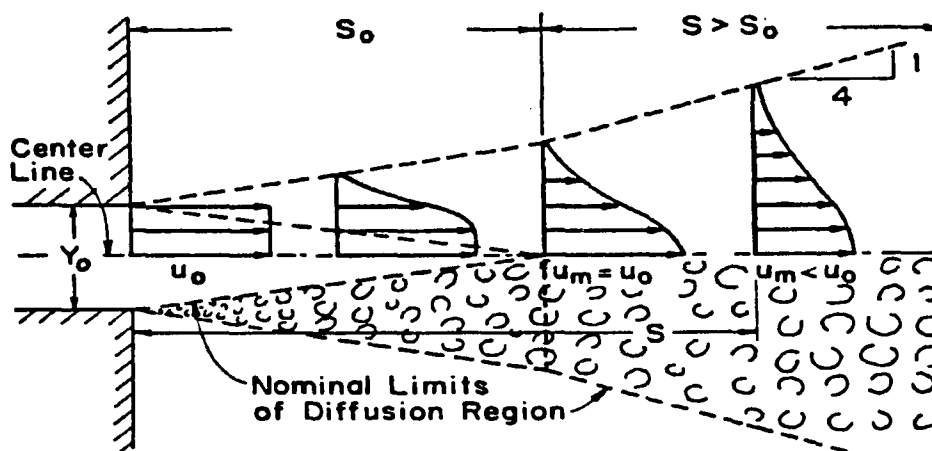


Figure 2.2: Free Plane Turbulent Jet Definition Sketch From Albertson et al. (1950)

Rajaratnam's (1976) text on jets is an excellent source for a wide variety of parameters. Of interest for this study is the relation between U_{mf} the maximum velocity, and J_c the distance from the nozzle along the jet centerline. He shows that U_{mf} / U_o is proportional to square root of $(1 / J_c)$ for J_c greater than J_o where J_c the distance along the jet centerline and J_o is the length of the potential core. In general, he proposes Eq. 2.13 where C_1 and C_2 are experimental constants ranging in various studies from 2.21 to 2.67 for C_1 and 0.0 to 1.20 for C_2 .

$$\frac{U_{mf}}{U_o} = C_1 \sqrt{\frac{y_o}{J_c + C_2 y_o}} \quad J_c > J_o \quad (2.13)$$

A solution attributed to Tollmien (1926) for perfect conditions, is $C_1 = 2.67$ and $C_2 = 0.0$. For this case Eq. 2.13 reduces to Eq. 2.14 in which the diffusion constant, $C_d = 2.67$. Equation 2.14 is the more generally accepted form and Rajaratnam suggests a mean value of C_d equal to 2.47.

$$\frac{U_{mf}}{U_o} = C_d \sqrt{\frac{y_o}{J_c}} \quad J_c > J_o \quad (2.14)$$

If J_c is less than J_o , $U_{mf} = U_o$. It is therefore necessary to know the length J_o to know U_{mf} at any cross section. Albertson et al., (1950) proposed Eq. 2.15 while Rajaratnam (1976) proposed Eq. 2.16.

$$J_o = 5.2 y_o \quad (2.15)$$

$$J_o = 5.96 y_o \quad (2.16)$$

In general, J_o is related to the same parameters which influence C_d especially the uniformity of U_o at the point of tailwater entry. Rajaratnam's value is again based on the Tollmien (1926) solution in which the velocity is completely uniform, such as that produced by a submerged perfect nozzle. Albertson et al.'s (1950) value is experimentally determined for a near perfect nozzle. Turbulence or non-uniform velocity at jet entry will influence both C_d and J_o . Solving Eq. 2.14 for $J_c=J_o$ when $U_{mf} = U_o$ yields Eq. 2.17.

$$J_o = C_d^2 y_o \quad (2.17)$$

2.5.2 Impinging Plane Turbulent Jet

The graduate work of Beltaos (1972,1974) provides an exhaustive theoretical and experimental study on plane and circular jets impinging on a flat impervious surface at normal or oblique angles. His results are summarized in several subsequent publications (Beltaos 1976a, 1976b; Beltaos and Rajaratnam 1973, 1974, and 1977). A definition sketch from Beltaos and Rajaratnam's (1973) study of plane normal impingement is given in Fig. 2.3 . For some distance along the jet centerline flow is analogous to a free jet. Beyond this distance the boundary forces the jet to deflect causing the velocity streamlines to curve and an excess static pressure to develop. Beyond some distance along the wall the excess pressure is dissipated and velocity streamlines resemble those of a wall jet.

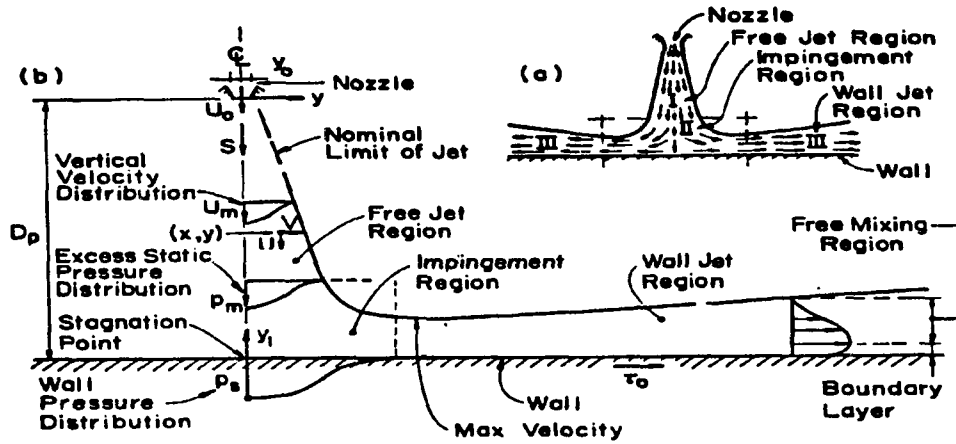


Figure 2.3: Impinging Plane Turbulent Jet Definition Sketch From Beltaos (1972)

The impingement region can be defined as the region in which either excess static pressure exists or streamlines resemble neither a free or wall jet. From either criterion the impingement region extends from approximately $0.30 J_i$ up from the wall to $0.35 J_i$ from the stagnation point along the wall where J_i is the distance along the jet centerline from the nozzle to impingement. Expressions for the maximum velocity in the free jet region U_{mf} and impingement region U_{mi} can be converted to the form of Eq. 2.14. Only the value of the coefficient C_d varies. They are shown as Eqs. 2.18 and 2.19.

$$\frac{U_{mf}}{U_o} = 2.50 \sqrt{\frac{y_o}{J_c}} \quad (2.18)$$

$$\frac{U_{mi}}{U_o} = 2.72 \sqrt{\frac{y_o}{J_i}} \quad (2.19)$$

The location of U_{mi} is approximately $0.30 J_i$ along the wall from the stagnation point. The location of the maximum shear stress on the bed τ_i coincides with U_{mi} and is approximated by Eq. 2.20.

$$\tau_i = 0.029 \rho U_o^2 \frac{y_o}{J_i} \quad (2.20)$$

Beltaos (1976b) shows the angle of impingement does not significantly effect the magnitude of the above expressions, but it does influence the location. This is because the stagnation streamline tends to intersect the wall at right angles. Therefore the stagnation point is shifted a distance ΔS from the intersection of the jet centerline and the bed. Schauer and Eustis (1963) approximate this shift with Eq. 2.21 where χ is the acute impingement angle measured from the horizontal.

$$\Delta S = 0.154 J_i \cot \chi \quad (2.21)$$

Robinson (1988,1989) has measured shear stress distributions along a flat impervious boundary produced by a plunging jet beneath a free overfall. No attempt is made to relate the measured shear stresses to flow hydraulics. His data shows that time averaged shear stress can be as much as one order of magnitude less than the maximum instantaneous value suggesting turbulence cannot be neglected.

2.5.3 Scour from Impinging Jets

Most early studies on the scour from impinging jets have taken a rather empirical approach. Only the best of these such as conducted by Van der Poel and Schwab (1985, 1988) use dimensional analysis. The usual dependent parameter is the

ultimate depth of scour D_u . Often these studies measure scour below dams (Spurr, 1985) or a scale model of one (Cola, 1965; Hartung and Häusler, 1973; Martins, 1973). Mason and Arumugam (1985) have reviewed a majority of these and determined that none of the developed equations accurately predict ultimate scour depth over the combined data sets. They propose as an improvement Eq. 2.22 in which q is the unit flow rate, D_h is the drop height, h_t is the depth of tailwater, g the gravitational acceleration, and d_{50} the mean sediment size. All of these studies make no attempt to relate the measured scour depths to the hydraulic conditions present.

$$D_u = 3.27 \frac{q^{0.60} D_h^{0.05} h_t^{0.15}}{g^{0.30} d_{50}^{0.10}} \quad (2.22)$$

Unlike the empirical studies above the following attempt to relate the ultimate scour depth, D_u , to parameters of an impinging jet. As in those studies, only non-cohesive materials considered. Before continuing the discussion, a few cautions on applying results obtained from studies such as Beltaos (1972, 1974) and Robinson (1989) are warranted. First, there are interactions between the shape of the boundary and parameters of the impinging jet. Equations 2.13 through 2.21 are derived for impingement on a flat bed. The shape of a scour hole changes dramatically with time. Streamlines in a concave scour hole must be deflected much more. This may effect the values of C_d and J_o and may increase τ_i . Certainly the location of U_{mi} and τ_i and the value of ΔS will be affected.

Secondly, an erodible bed is not impervious and an appreciable amount of the excess static pressure induced by jet impingement may be transmitted through the bed material. This effect is a function of the excess pressure magnitude and porosity

of the bed material. Kobus et al., (1979) examine this effect. Intuitively the transmission of pressure through the bed material tends to reduce the erosion while the concave shape tends to increase it, as compared to a flat impervious bed.

2.5.3.1 Kobus, Leister & Westrich (1979)

This excellent study examines impinging circular jets on smooth and rough impervious boundaries as well as scour from impinging circular jets. With regard to impervious boundaries they develop an empirical expressions for the shear stress distribution along the boundary. Roughness greatly increases the maximum measured shear stress as compared to smooth boundaries but they find that the location of maximum shear stress is only slightly effected by roughness and occurs at $0.15 J_i$ from the stagnation point. The same location was also measured by Beltaos (1974) for circular jets impinging on smooth boundaries. Solving the shear stress distribution on a smooth bed from Kobus et al. (1979) for the maximum yields Eq. 2.23 where d_o is the diameter of the jet at the nozzle. This result is of the same form as Eq. 2.20 from Beltaos (1973) except the constant is seen to be a weak function of Reynolds number.

$$\tau_i = 0.70 \left(\frac{U_o d_o}{\nu} \right)^{-0.17} \rho U_o^2 \left(\frac{d_o}{J_i} \right)^2 \quad (2.23)$$

No expression or relation for an ultimate scour depth due to jets impinging on an erodible bed is given, however they relate scour parameters to the sediment size and the excess static pressure induced in the impingement region. As noted earlier, this pressure is reduced by the porosity of the bed material. They describe two

distinct scour hole shapes dependent on a factor k_o defined in equation 2.24 where P_s is the excess static pressure on a horizontal bed, ρ_s the particle density, ω_s the particle fall velocity and U_{mi} the maximum velocity in the impingement region.

$$k_o = \frac{P_s}{\left(\frac{\rho_s \omega_s^2}{2}\right)} \propto \left(\frac{U_{mi}}{\omega_s}\right)^2 \quad (2.24)$$

Figure 2.4 shows the two forms for one particular sediment size. If k_o is between 1.2 and 3.0 form I develops because the deflected jet remains attached to the wall. If k_o is greater than 6.5 form II develops in which the deflected jet detaches from the wall. These two shapes are also noted by Akashi and Saitou (1986).

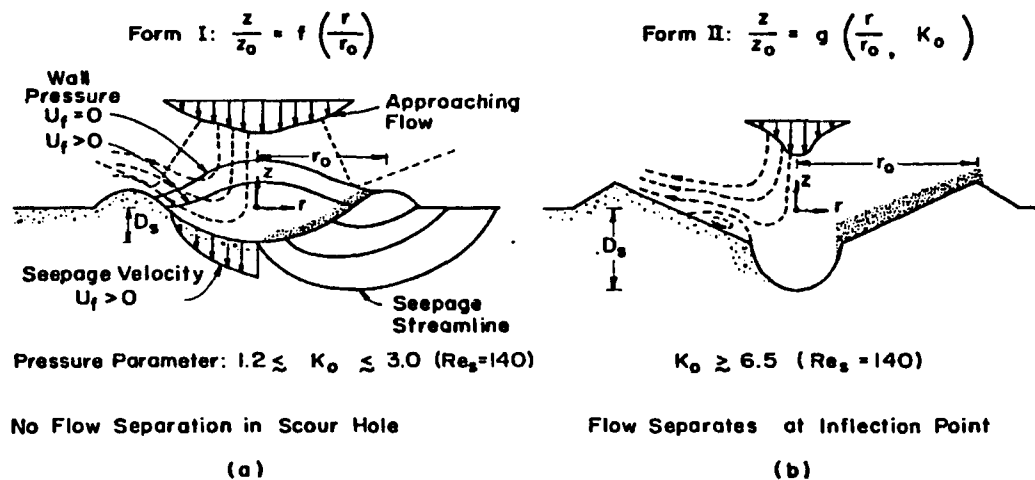


Figure 2.4: Scour Hole Forms From Kobus et al., (1979)

2.5.3.2 Rajaratnam (1981, 1982)

These studies expand Rajaratnam's and Beltaos' previous studies on impervious impingement to erodible beds. The earlier study, (1981) measures

parameters for deeply submerged wall and impinging jets. The second is for unsubmerged free-falling jets but is rather qualitative. No explicit equation for ultimate scour is given, however Rajaratnam proposes Eq. 2.25 from a simplified dimensional analysis where F_o is defined in Eq. 2.26, D_u is the scour depth measured from the unscoured bed and J_i is measured to the original unscoured bed elevation.

$$\frac{D_u}{J_i} \propto F_o \sqrt{\frac{y_o}{J_i}} \quad (2.25)$$

$$F_o = \frac{U_o}{\sqrt{\frac{\rho_s - \rho}{\rho} g d_{50}}} \quad (2.26)$$

The functional form of equation 2.25 is not evaluated. It is graphically shown to be different for air-sand and water-sand combinations. This could be expected as the fall velocities would be different and shows the need for an additional term such as $(\rho_s - \rho) / \rho$ if scour from different fluids are evaluated. Note the similarity between F_o and the Shields parameter, θ_s of Eq. 2.1 . Assuming U_o is related to U_o , Rajaratnam's F_o is the square root of Shields parameter. Mih and Kabir (1983) expand Rajaratnam's analysis to water jets on natural streambeds to study the effect of armoring.

2.5.3.3 Yuen (1984)

This thesis expands previous empirical work by Chee (Chee and Padiyar, 1969; Chee and Kung, 1971) and is summarized in Chee and Yuen (1985). It deals explicitly with the ultimate scour depth, D_u , and is based heavily on the work of

Beltaos (1972) for impervious impingement. Using dimensional analysis Yuen develops Eq. 2.27 for ultimate depth of scour where J_e is the value of J_i at an equilibrium scour depth. Note that it lacks a term for the depth of scour.

$$\frac{U_{mi}^2}{\frac{\rho_s - \rho}{\rho} g d_{50}} \propto \frac{d_{50} \sqrt{0.166 \left(\frac{U_o}{J_e}\right)^2 \frac{4.0 y_o^2}{\pi}}}{v} \quad (2.27)$$

Bormann (1988) exposes several discrepancies in Yuen's analysis including the above. Therefore Yuen's final predictive equation, which replaces d_{50} with J_i on the left hand side of Eq. 2.27 must be seriously questioned. Yuen does provide a rather large data set for scour of gravel sized particles from unsubmerged jets impinging at various angles from 45° to 90° . From these data Yuen concludes the jet follows a straight line to the bed at the same angle the jet makes with the horizontal upon tailwater entry. Therefore Eq. 2.28 can be used to determine the ultimate depth of scour for jets impinging at angles other than 90° where h_t is the depth of tailwater and χ is the angle the jet makes with the horizontal at tailwater entry.

$$D_u = J_e \sin \chi - h_t \quad (2.28)$$

2.5.3.4 Bormann (1988)

This study, summarized in Bormann (1989), uses original and previous data sets to determine the ultimate scour depth below grade control structures of varying slope face in which flow can be likened to an impinging jet. It provides a unifying methodology for prediction of scour produced by a large variety of jet configurations

from deeply submerged wall jets to impinging unsubmerged jets. It also has a two order of magnitude range of predicted scour depths. The latter point is quite remarkable in that virtually all other studies including the present have a range of less than one order of magnitude.

In general, Bormann relates the hydrodynamic forces of the jet to particle stability on the sloping scour hole boundary to determine the ultimate scour depth. This is the explicit approach taken by Yuen (1984) and implicitly taken by Rajaratnam (1981, 1982) as will be shown in Section 2.5.3.5. Bormann adds an approach similar to Stevens and Simons (1971) to account for particle stability on the sloping bed of the equilibrium scour hole. This may only be necessary if the scour hole has a form I profile as defined by Kobus et al., (1979). Bormann uses Eq. 2.28 to determine D_u and Eq. 2.29 to determine J_e where y_b is the thickness of the jet near the boundary, α is the average angle of the scour hole and ϕ is the angle of repose for the sediment.

$$J_e = \frac{\rho C_d^2 U_o^2 y_o \sqrt{\frac{y_b}{d_{50}}} \tan \alpha}{2.3 g (\rho_s - \rho) d_{50} \cos \alpha (\tan \alpha + \tan \phi)} \quad (2.29)$$

Figure 2.5 shows relatively good agreement between measured and predicted equilibrium scour length J_e . Figure 2.6 shows considerably more scatter for predicted versus measured ultimate depth of scour. This increased scatter is due to the problems of accurately determining the jet angle of impingement for the wide variance of conditions Bormann analyzed.

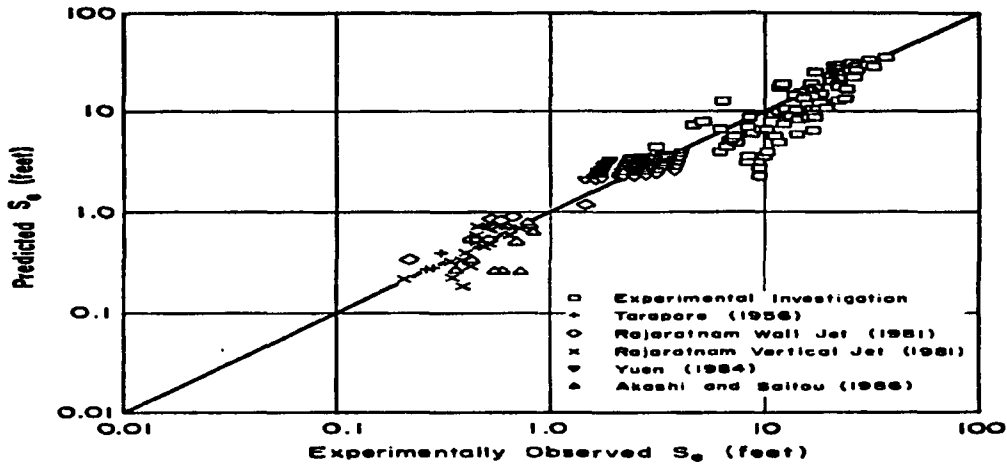


Figure 2.5: Equilibrium Scour Length J_e From Bormann, (1988)

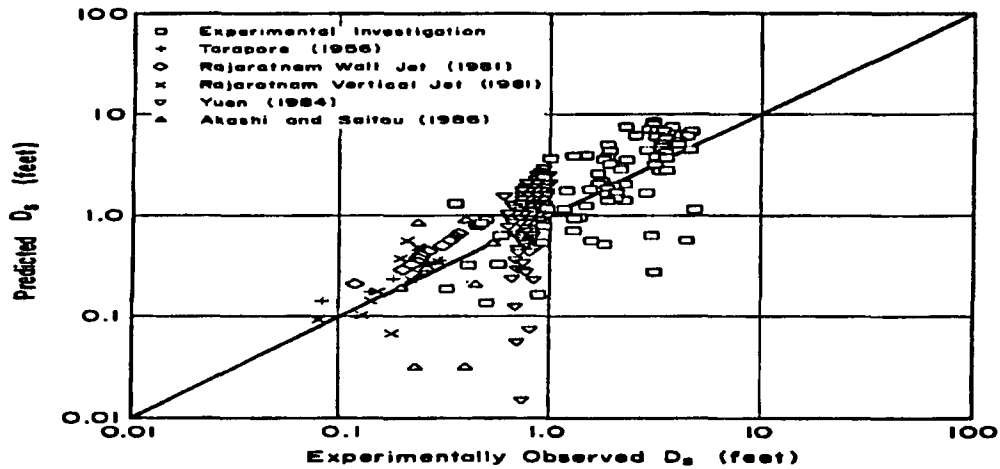


Figure 2.6: Ultimate Scour Depth D_u From Bormann, (1988)

2.5.3.5 Similarity of Previous Studies

The Rajaratnam, Yuen and Bormann equations for ultimate scour depth (Eqs. 2.25, 2.27 and 2.29) all relate jet diffusion to the Shields parameter in their analyses. The difference between them is the determination of the ultimate scour depth D_u in which the jet is sufficiently diffused so that $\theta_s = \theta_{cr}$.

Equation 2.25 from Rajaratnam (1981) is the most simplistic. He assumes that the shear velocity U_* is proportional to the jet nozzle velocity U_o therefore U_o can replace U_* in a modified Shields parameter defined as F_o . No attempt is made to incorporate the diffusion of a jet through the scour hole. He develops the term F_o from dimensional analysis apparently without ever considering principles of sediment transport. The fact that he identifies the correct relationship independently is a tribute to the excellent research he has conducted through the years.

Clearly the Shields parameter is the left-hand side of Eq. 2.27 developed by Yuen (1984) with U_* replaced by U_{mi} the maximum velocity in the impingement region. The right-hand side uses equations developed by Beltaos (1976a) for impervious jet impingement to transform of U_{mi} to τ_i and multiplies this by R , the particle Reynolds number to which θ_{cr} is related. Equation 2.20 is nothing more than a restatement of Eq. 2.8 developed by Shields in 1936. Equation 2.27 also assumes the shear stress required to move a particle in a scour hole exposed to a plane jet is identical to that produced by a circular jet impinging on a flat impervious boundary.

Bormann's Eq. 2.29 also can be reduced to a Shields parameter. The trigonometric terms account for the extra shear stress required to move a sediment particle up the sloping scour hole side wall and therefore considers non-flat geometry. It does not consider the effect of this geometry on jet diffusion. The terms C_d^2 , U_o^2 and y_o account for the diffusion of the jet velocity as it travels through the scour hole and $(y_b / d_{50})^{1/2} / 2.3$ is a relation proposed by Bogardi (1974) to convert a velocity near the bed, in this case U_{mi} , to a shear velocity U_* . Equation 2.29 correctly relates the forces which influence scour from jets, but difficulty arises in that C_d varies with

jet configuration and is not easily determined. Also Bogardi's analysis relating shear stress to a characteristic velocity has considerable scatter and is only applicable to flow over a hydrodynamically rough boundary. Still it is this writer's opinion that Bormann's methodology is the best available for determination of the ultimate depth of scour of non-cohesive bed material from impinging jets.

2.5.4 Time Scale of Jet Scour

All the above studies have attempted to predict the ultimate depth of scour from either dimensional analysis or relating jet diffusion to non-cohesive particle stability. However, headcut retreat is by nature a time dependent process therefore changes in scour parameters with time and not just ultimate dimensions are required. As will be discussed below there is considerable debate as to the validity of ultimate scour dimensions.

Limiting this discussion to the time dependency of the maximum depth of scour, which is by far the most often measured parameter, a first approximation attributable to Rouse (1940) is that scour depth increases with the log of time. This approximation invalidates the concept of an ultimate depth as scour will increase indefinitely with time. Laursen (1952) proposes convincing arguments for the concept of an ultimate depth and the method of equating jet diffusion to a Shields parameter demands it. At some time, however long, the scour hole will be sufficiently large to have diffused the jet enough for the maximum shear stress to be equal to the critical shear stress for the given bed material. This analysis of course ignores the effect of turbulent bursts on scour, which as Robinson (1988,1989) reports may have significant

magnitude. The debate may be more academic than practical in that the semi-log relationship of Rouse (1940) shows that scour increases very slowly at long times and it may take a time frame of years or even decades for the ultimate depth of scour to be reached. No studies have measured scour for that length of time.

The semi-logarithmic relationship has also been used by Breusers (1967), Rajaratnam (1981), Farhodi and Smith (1985) for scour induced by a hydraulic jump, Popova and Vedeneyev (1988) as well as Rouse (1940). These researchers normalize both depth and time to different parameters depending on the flow configuration therefore constants and exponents in the functional form vary. Also, no theoretical basis for a semi-log relationship has been proposed, it is merely a regression equation.

Analyzing the measured versus predicted plots of the above studies, the following generalities can be construed. Virtually all predictive equations underestimate the depth of scour at very short times. The length of this discrepancy appears to vary more with hydraulic parameters than sediment parameters, for larger scale models the increase in scour depth exceeds that predicted for a longer period of time. In the case of scour from impinging jets this may be due to the length of the potential core which increases with an increase in jet thickness. So long as the bed elevation is within the hypothetical extension of the potential core the maximum velocity and maximum shear stress is constant with time therefore the increase in scour depth should be linear with time.

The semi-log relationship is very good for the majority of the measured time span, however scatter with no apparent trend increases at the longest measured

times. During the mid-range time spans the jet is diffusing and the maximum velocity and maximum shear stress is decreasing as the scour hole grows with time. At the longest times the magnitude of shear stress is approaching the critical shear stress of the bed material and turbulent fluctuations become the dominant erosive force increasing scatter.

Blaisdell et al. (1981) regress semi-log, log-log and hyperbolic functions for maximum scour depth with time on the same data set. The semi-logarithmic equation gives the poorest fit even when early data points are removed. The hyperbolic function gives the best fit, however the nature of this equation requires determination of a focal point which must be determined by trial and error. Therefore the validity of the given equation for other data sets must be seriously questioned. A hyperbolic function does have an advantage over logarithmic relations in that it can be defined at $t = 0$ when scour depth is zero (and not negative infinity) and has a computable ultimate depth of scour. It is interesting to note that the predicted ultimate depth is reached 30,644 years after scour initiation for the Blaisdell et al. (1981) data set.

Chapter 3

Analytical Development

This chapter introduces a conceptual model which can be used to predict the mode of headcut migration. This model is mathematically formulated using a physically based analysis of sediment detachment and jet scour. Three flow regions, normal flow, an accelerated flow region, and an impingement region will be defined. The general hydraulic concepts developed in Chapter 2 will be applied to each region. Therefore this chapter is divided into several sections. The first introduces the conceptual model, the next develops general dimensionless equations for headcut migration and jet scour and others apply these concepts to each of the three flow regions.

3.1 Conceptual Model

The flow over an idealized two dimensional headcut formed in an infinitely wide slope is shown in Fig. 3.1. Steady, uniform flow of a given unit discharge, q , approaches at a normal depth, h_n , in a channel of constant slope S_b . A free overfall at the brink or headcut face causes the flow to accelerate through a distance L which is several flow depths long. Therefore the depth decreases to the exit depth h_e at the brink. This region is called the accelerated flow region. The flow then falls freely

until deflected by the bed which is lowered by a drop height D_h at the headcut face. This area is called the impingement region. At some distance downstream from the brink the flow has been completely deflected and returns to normal depth over a constant slope.

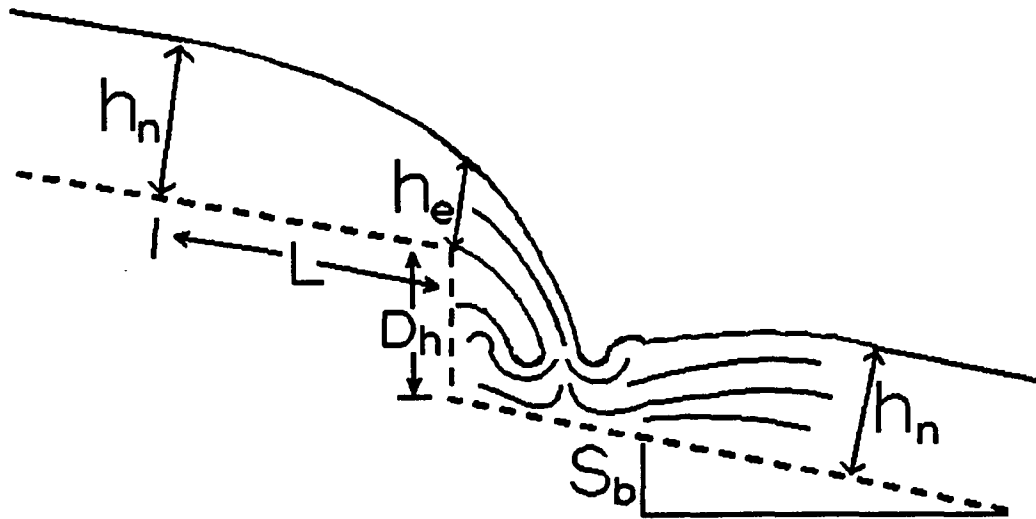


Figure 3.1: Initial Headcut Hydraulics

If the channel in Fig. 3.1 is of an erodible material this idealized shape will not be maintained with time. Accelerations developed in both the accelerated flow and impingement regions cause the applied bed tractive force or shear stress to increase as compared to normal flow. A detailed analysis of these increases will be provided in later sections. In summary, it can be shown that in the accelerated region shear stress increases in the longitudinal direction from a normal flow value to a maximum just at the brink. In the impingement region it can be shown that shear stress is at a maximum near the stagnation point which is where the nappe impinges on the boundary and diminishes in either longitudinal direction. Any increase in shear stress causes an increase in the erosion rate as compared to normal flow.

It is this increased erosion rate which causes the shape of the headcut to change with time. Two general classes of a headcut shape change exist depending on the relative increase in erosion rate in the upstream acceleration and downstream impingement regions. Fig. 3.2 diagrams the case where upstream erosion is of nearly the same or greater magnitude than downstream. This is similar to Holland and Pickup's (1976) rotating headcut. Figure 3.3 diagrams the case where downstream erosion dominates, similar to Holland and Pickup's stepped headcut.

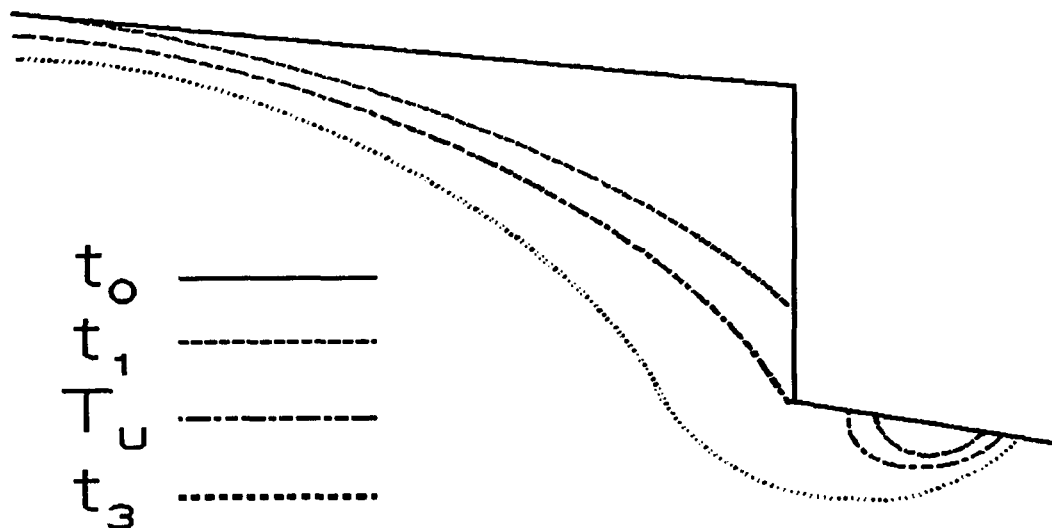


Figure 3.2: Headcut Migration: Upstream Hydraulics Dominate

At time t_0 in Fig. 3.2, the bed shape and hydraulics are the same as Fig. 3.1. At a future time t_1 , upstream sediment detachment has eroded some of the headcut face and a small plunge pool basin has eroded in the impingement region. The plunge pool has not yet affected the brink point and its deepest scour is near the stagnation point. At a later time T_U , upstream sediment detachment has completely eroded the headcut face before erosion in the impingement region has undercut the headcut face. At a still later time t_3 , a true headcut no longer existed but an

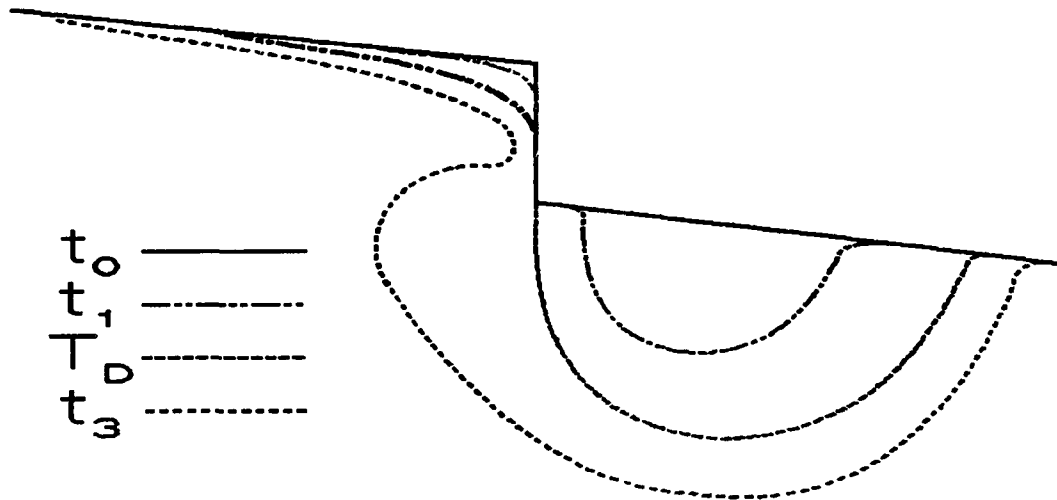


Figure 3.3: Headcut Migration: Downstream Hydraulics Dominate

oversteepened reach is migrating upstream. The slope of this oversteepened reach approaches the average bed slope at long times.

At time t_0 in Fig. 3.3 the bed shape and hydraulics are the same as Figs. 3.1 and 3.2 except that the drop height is larger. At time t_1 , the upstream erosion is similar to that in Fig. 3.2 but a considerably larger plunge pool has been eroded. At a future time defined as T_D , the downstream plunge pool has started to undermine the headcut face before upstream sediment detachment has completely eroded it. At a still later time t_3 , a definable near vertical headcut has retreated some distance upstream but shape of the headcut is considerably different than in Fig. 3.2.

Both of the above cases assume steady state flow and uniform soil conditions exist. With these simplifying assumptions a criterion to determine which type of headcut migration mechanism dominates, dependent on solely on hydraulics at the headcut, can be defined. Using the analytical tools developed in this chapter and experimental results presented in Chapter 5, a method for the determination of mode

of headcut retreat is presented. In addition, the rate of increase in the maximum scour depth in the impingement region independent of upstream scour is presented.

3.2 Dimensional Analysis of Relevant Parameters

The conceptual model developed in the previous section can be mathematically formulated through dimensional analysis providing a framework to meet the stated objectives in Chapter 1. The developed dimensionless equations will be functionally evaluated using either theory when possible or experiment when necessary.

3.2.1 Dimensional Analysis of Headcut Stability

A headcut is stable, that is have a definable near vertical face, if the time scale of downstream scour T_D exceeds that of upstream scour T_U and unstable if the converse is true. A criteria for headcut stability can be defined as the ratio of these time scales defined in Figs. 3.2 and 3.3. The upstream time scale can be defined as the time required for upstream erosion to completely erode the headcut face. The downstream time scale can be defined as the time required for the scour hole to start undermining the headcut face. The dependent variable is this time scale ratio. The independent variables are the upstream and downstream maximum applied shear stresses τ_e and τ_i , the upstream and downstream critical shear stresses τ_{cU} and τ_{cD} , the drop height D_h , the longitudinal distance from the brink to jet tailwater impingement X_n , and the physical constants ρ , ν , and g . Picking g , ν and τ_e as

repeating variables the dimensionless π parameters of Eq. 3.1 are obtained. The term F_d in π_6 is defined as a drop number with a form similar to a Froude number.

$$\begin{aligned}
 \pi_1 &= \frac{T_U}{T_D} \\
 \pi_2 &= \left(1 - \frac{\tau_{cU}}{\tau_e}\right) \\
 \pi_3 &= \left(1 - \frac{\tau_{cD}}{\tau_i}\right) \\
 \pi_4 &= \frac{\tau_i}{\tau_e} \\
 \pi_5 &= \frac{D_h}{X_n} \\
 \pi_6 &= \frac{v^2}{gD_h^3} = F_d^2 \\
 \pi_7 &= \frac{v^2 \rho^3 g^2}{\tau_e^3}
 \end{aligned} \tag{3.1}$$

Physically, the first term represents the dependent time scale ratio, all other terms are independent. The second and third terms represent the upstream and downstream sediment detachment capacity and the fourth a ratio between upstream and downstream shear stresses. The fifth term represents an erosion length scale ratio, the sixth term is the potential energy created by the drop height, and the last term represents the upstream shear stress. The last terms can be reduced to functions of Reynolds number, bed slope and drop number therefore the π terms of Eq. 3.1 reduce to Eq. 3.2. Proof of this reduction will be given in later sections.

$$\frac{T_U}{T_D} \propto \left[S_b R_e F_d \left(1 - \frac{\tau_{cU}}{\tau_e}\right) \left(1 - \frac{\tau_{cD}}{\tau_i}\right) \right] \tag{3.2}$$

3.2.2 Dimensional Analysis of Upstream Scour

The dependent variable for upstream scour is the time required to completely erode the entire headcut face which is analogous to the upstream time scale T_U . The independent parameters are flow rate, bed slope, drop height, applied shear stress, upstream critical shear stress, and the constants ρ , ν and g . Picking ρ , ν , and D_h as the repeating variables Eq. 3.3 can be developed.

$$\frac{T_u \nu}{D_h^2} \propto \left[S_b R_e F_d \left(1 - \frac{\tau_{cU}}{\tau_e} \right) \right] \quad (3.3)$$

Physically, the dependent term is a time scale, S_b and R_e represent the applied hydraulic forces, F_d is an erosion length scale and the last a sediment detachment term. Eq. 3.3 assumes the applied shear stress can be defined from bed slope and Reynolds number.

3.2.3 Dimensional Analysis of Downstream Scour

The dependent variable for downstream scour is the maximum depth of scour, the independent variables are the ultimate depth of scour the applied and critical shear stresses, time, the velocity and thickness of the jet at tailwater impingement and the physical constants ρ , ν , and g . Picking y_o , ρ and ν as repeating variables Eq. 3.4 can be developed.

$$\frac{D}{D_u} \propto \left[R_e \frac{q^2}{g y_o^3} \frac{t U_o}{y_o} \left(1 - \frac{\tau_{cD}}{\tau_i} \right) \right] \quad (3.4)$$

Physically the first term is the percentage of total erosion which has occurred at a given time, the second the Reynolds number, the third a Froude number, the fourth a time scale and the last a sediment detachment term.

3.4 Normal Flow Region

A control volume of unit width for normal flow is shown in Fig. 3.4. It is bounded by the points A, A', and B B'. The flow has constant normal depth h_n on a bed of constant slope S_b which exerts an average shear stress, τ_n to the flow. Hydrostatic pressure is exerted on both unit planes AA' (shown) and BB'. There is a mass flux, ρu , into the control volume at AA' and out of the control volume at BB' (shown). This can be averaged over the flow depth to yield an average mass flux $\rho \bar{u}$. Fig. 3.4 will be used to develop the continuity and momentum equations for normal flow.

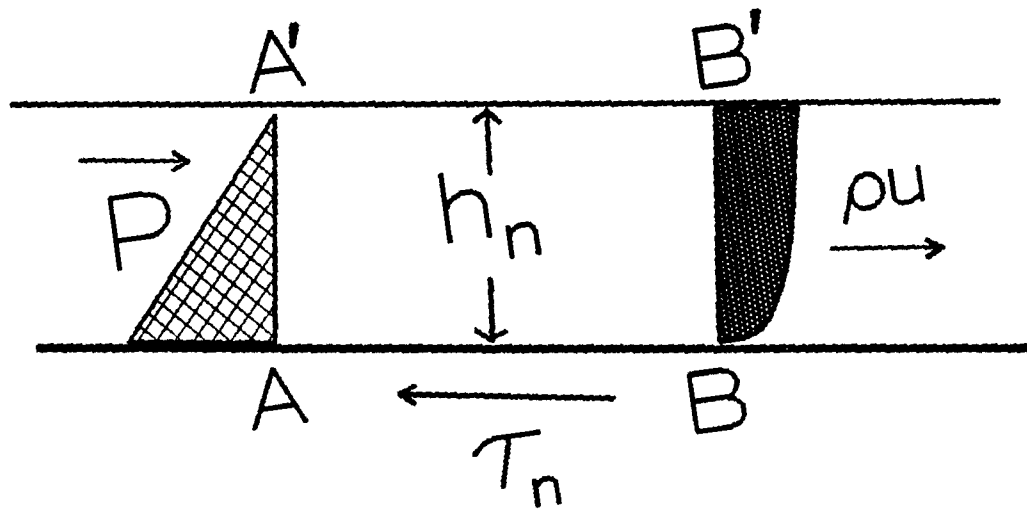


Figure 3.4: Normal Flow Control Volume

3.4.1 Normal Flow Continuity

The general continuity equation (2.2) can be reduced to Eq. 3.5 by realizing v , the velocity in y direction is zero everywhere.

$$\frac{du}{dx} = 0 \quad (3.5)$$

Integrating Eq. 3.5 over the control volume and applying the divergence theorem yields Eq. 3.6 .

$$- \bar{u}_{AA'} h_{AA'} + \bar{u}_{BB'} h_{BB'} = 0 \quad (3.6)$$

But since $h_{AA'} = h_{BB'} = h_n$ and $\bar{u}_{AA'} = \bar{u}_{BB'} = u_n$ the continuity equation for normal flow at any cross section is Eq. 3.7 .

$$q = u_n h_n \quad (3.7)$$

This mathematical exercise is trivial as Eq. 3.7 could be assumed by definitions of unit discharge and normal flow but the same procedure will be used to develop subsequent equations.

3.4.2 Normal Flow Momentum

The general momentum equation (2.4) can be simplified to Eq. 3.8 by again realizing $v = 0$, $\partial u / \partial x = 0$ from Eq. 3.5, and $\tau_{yx} = \tau_n$.

$$0 = \rho g_x - \frac{\partial P}{\partial x} + \frac{\partial \tau_n}{\partial y} \quad (3.8)$$

Integrating over the volume and applying the divergence theorem yields Eq. 3.9 where g_x is replaced by $(g S_b)$, and L_c is the length of the control volume.

$$0 = \rho g S_b h_n L_c - (P_{BB'} h_{BB'} - P_{AA'} h_{AA'}) + \tau_n L_c \quad (3.9)$$

Simplifying Eq. 3.9 by realizing $P_{BB'} = P_{AA'}$ and $h_{AA'} = h_{BB'}$ yields Eq. 3.10 the momentum equation for normal flow.

$$\tau_n = -\rho g h_n S_b \quad (3.10)$$

Equation 3.10 shows shear stress on the flow acts upstream and equals the product of fluid density, gravitational acceleration, normal flow and bed slope.

3.4.3 Governing Equations

As shown by Julien and Simons (1985) the normal flow region parameters average flow velocity, flow depth and bed shear stress can be stated as power functions of bed slope and Reynolds number by combining Eqs. 2.5, 2.6, 3.7 and 3.10. The functional form of these equations is dependent on the value of the Darcy-Weisbach friction factor. This value can be determined from one of four commonly used equations the Blasius, Chezy, Manning equations for turbulent flow and the laminar flow equation, depending on flow conditions. The Blasius equation is applicable for turbulent flow over a hydrodynamically smooth boundary, the Manning equation for turbulent flow over a hydrodynamically rough boundary and the Chezy equation is applicable for turbulent flow which is very deep. The Blasius equation assumes the friction factor $f = 0.22 / R_e^{0.25}$. Using this assumption Eqs. 2.5, 2.6, 3.7,

and 3.10 yield the following equations for flow depth and shear stress in the normal flow region.

$$h_n = \left(\frac{0.22}{8} \right)^{0.333} g^{-0.333} v^{0.667} S_b^{0.333} R_e^{0.583} \quad (3.11)$$

$$\tau_n = \left(\frac{0.22}{8} \right)^{0.333} \rho g^{0.667} v^{0.667} S_b^{0.667} R_e^{0.583} \quad (3.12)$$

Usage of either the Chezy, Manning or laminar flow equations change only the exponents in Eqs. 3.11 and 3.12 and not the form.

3.5 Accelerated Flow Region

A control volume is shown in Fig. 3.5. Flow at the cross section CC' approaches the free overfall, or brink, at a normal depth h_n . If the flow is subcritical ($F_r < 1.0$), the depth decreases as the brink is approached through the critical depth, h_c at a distance L above the brink to the exit depth, h_e . If the flow is supercritical ($F_r > 1.0$), as shown, h_n is less than h_c everywhere, but h decreases gradually through a distance L from h_n to h_c at the brink cross section DD'. In either case, the distance L is approximately 2 to 4 times h_n .

Upstream from the reach L flow is uniform but within this reach streamlines are curved. The pressure on the upper and lower streamlines must be zero at the brink because both are subjected to atmospheric conditions. Therefore, pressure at the bed varies from hydrostatic at cross section CC' to zero at cross section DD'. Fig. 3.6 shows typical pressure distributions with depth at hydrostatic (CC') and brink

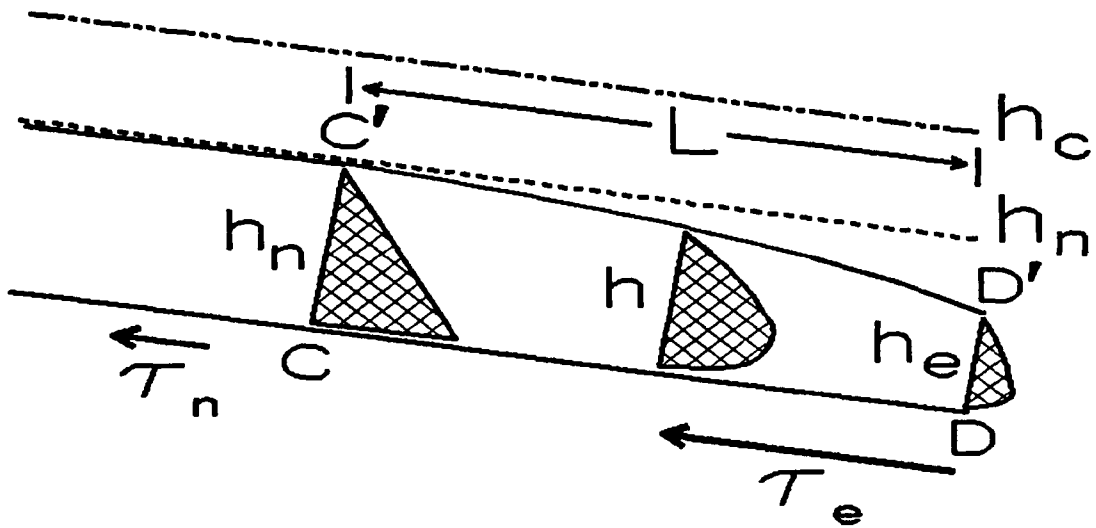


Figure 3.5: Accelerated Flow Region Control Volume

(DD') conditions. A pressure parameter K_e can be defined as the ratio of shaded areas in Fig. 3.6.

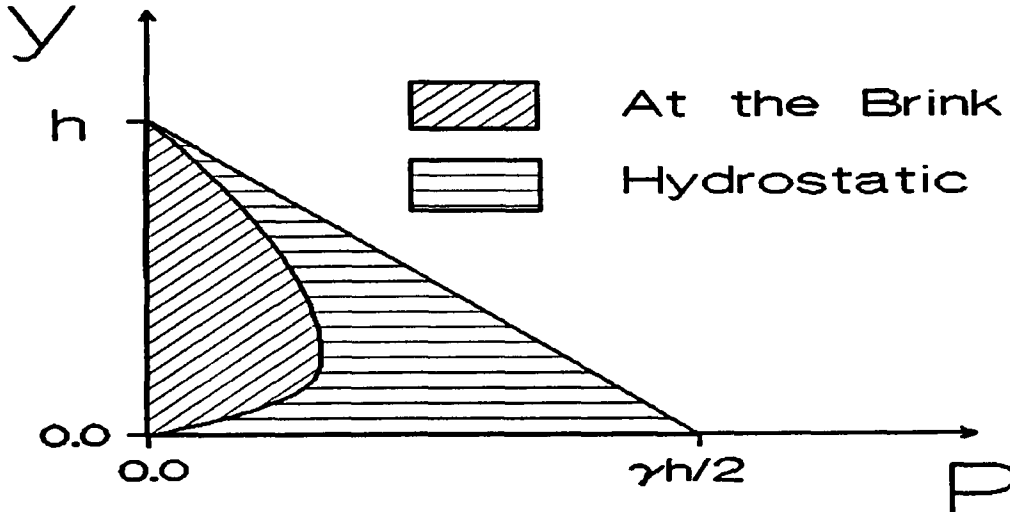


Figure 3.6: Pressure Distributions; Brink and Hydrostatic

Development of the continuity equation for the accelerated flow region proceeds identically to that of normal flow. However $\bar{u}_{DD'} = u_e$, velocity at the brink, and $h_{DD'} = h_e$, depth at the brink, therefore the continuity equation in this region is

given by Eq. 3.13 where q is the unit discharge u_n and h_n normal average velocity and depth respectively.

$$q = u_n h_n = u_e h_e \quad (3.13)$$

3.5.1 Accelerated Flow Momentum Equation

Only one simplification to the general momentum equation (2.4) can be made for this accelerated flow region, namely elimination of the term $v(\partial u/\partial y)$. At cross section CC' $v = 0$, and elimination is completely justified. As the brink section DD' is approached, v and $\partial u/\partial x$ attain finite but very small values due to streamline curvature. Therefore, while $v(\partial u/\partial x)$ is not identically zero at all points it is very small. On the whole the magnitude of this term is much smaller than other terms and its elimination is justifiable.

Using the above assumption and dividing through by ρ Eq. 2.4 reduces to Eq. 3.14 in the accelerated flow region.

$$u \frac{\partial u}{\partial x} = g_x - \frac{1}{\rho} \frac{\partial P}{\partial x} + \frac{1}{\rho} \frac{\partial \tau_{yx}}{\partial y} \quad (3.14)$$

Because shear stress at a cross section is desired Eq. 3.14 will be integrated over the flow depth and not the entire control volume. This is analogous to shrinking the control volume to a reach of infinitesimally small length. The following substitutions for the terms in Eq. 3.14 are used.

$$\int_0^h u \frac{\partial u}{\partial x} dy = \frac{\partial h \beta \bar{u}^2}{\partial x} \quad (3.15)$$

where: h is the flow depth
 \bar{u} is the mean velocity (hereafter $\bar{u} = u$)
 β is the momentum correction factor

$$\int_0^h g_x dy = ghS_b \quad (3.16)$$

where: g is the gravitational acceleration
 S_b is the bed slope

$$\int_0^h P dy = K \frac{\rho g h^2}{2} \quad (3.17)$$

where: ρ is the fluid density
 K is a coefficient to account for non-hydrostatic pressure.
 $K = 1.0$ if the pressure is hydrostatic and $K = 0$ if pressure is zero.

$$\int_0^h \frac{\partial \tau_{yx}}{\partial y} dy = -\rho g h S_f \quad (3.18)$$

where: S_f is the friction slope

Substituting Eqs. 3.15 to 3.18 into Eq. 3.14 yields Eq. 3.19.

$$\frac{\partial h \beta u^2}{\partial x} = ghS_b - \frac{g}{2} \frac{\partial K h^2}{\partial x} - ghS_f \quad (3.19)$$

Carrying out the differentiation, using the continuity relation $q = uh$, a local Froude number and solving for $\partial h / \partial x$ yields Eq. 3.20.

Equation 3.20 is a general backwater curve equation applicable when velocity distributions cannot be considered uniform and pressure distributions are

$$\frac{\partial h}{\partial x} = \frac{S_b - S_f - h \left(\frac{1}{2} \frac{\partial K}{\partial x} + F_r^2 \frac{\partial \beta}{\partial x} \right)}{K - \beta F_r^2} \quad (3.20)$$

non-hydrostatic. The familiar gradually varied backwater profile equation (Eq. 3.21) can be obtained by using the conventional assumptions that $K = \beta = 1.0$ at all points. A gradually varied profile assumes the pressure and acceleration terms of Eq. 3.14 can be approximated using normal flow values.

$$\frac{dh}{dy} = \frac{S_b - S_f}{1 - F_r^2} \quad (3.21)$$

To solve for the bed shear stress distribution along x , Eq. 3.20 is solved for S_f and multiplied by the quantity $(-\rho gh)$ shown in Eq. 3.22.

$$\tau = \rho gh \left[S_b - h \left(\frac{1}{2} \frac{\partial K}{\partial x} - F_r^2 \frac{\partial \beta}{\partial x} \right) - \frac{\partial h}{\partial x} (K - \beta F_r^2) \right] \quad (3.22)$$

If gradually varied flow is assumed, $K = \beta = 1.0$ and Eqs. 3.22, 3.21 and 3.10 reduce to Eq. 3.23, which is the ratio of actual shear stress to normal shear stress.

$$\frac{\tau}{\tau_n} = \frac{h}{h_n} \frac{S_f}{S_b} \quad (3.23)$$

To determine shear stress from Eq. 3.23 the value of S_f / S_b must be determined from the Chezy, Manning, Blasius or laminar flow equations. As stated previously, the only difference between these equations is the determination of Darcy-Weisbach friction factor. However the Chezy, Blasius and laminar flow equations all yield $S_f / S_b = (h_n / h)^3$. Manning's equation yields $S_f / S_b = (h_n / h)^{10/3}$. Therefore

Eq. 3.24 applies if the Chezy, Blasius and laminar flow equations are used. The exponent in Eq. 3.24 is replaced by 10/3 if Manning's equation applies.

$$\frac{\tau}{\tau_n} = \left(\frac{h_n}{h} \right)^2 \quad (3.24)$$

3.5.2 Shear Stress in the Accelerated Flow Region

There are three sets of assumptions which can be used to determine the shear stress distribution along the channel bottom above a free overfall. This distribution can be solved for shear stress at the brink τ_e as required by Eqs. 3.1, 3.2 and 3.3. The first, and most complex, is to use both momentum flux and pressure correction factors which are known to be relevant in the reach L. Under these conditions Eq. 3.22 must be used. Application of Eq. 3.22 requires all terms on the right hand side be known or calculated a priori. In the absence of equations to calculate the values of β and K, only experimental values can be used. An excellent source of this data is given by Rajaratnam and Muralidhar (1968).

A simplified solution can be obtained by assuming both K and $\beta = 1.0$, therefore the flow can be considered gradually varied. Only the flow depth h at the point x and the normal flow depth h_n calculated from the relevant equation (ie. Blasius or laminar flow) need be known to calculate the shear stress at the point x. The governing equation is Eq. 3.24. The most simple, and trivial, solution is to assume $h = h_n$ for all cross sections above the free overfall and Eq. 3.10 applies.

The applicability of these three levels of sophistication as expressed in Eqs. 3.10, 3.22 and 3.24 to headcut stability analysis are compared. Only one publication

(Rajaratnam and Muralidhar, 1968) appears to measure all of the parameters necessary to determine shear stress from Eq. 3.22, the most complex. Detailed measurements of all the relevant parameters for a variety of slopes from adverse to steep and various discharges are given. Two typical data sets are given in Table 3.1. These data are representative of both super-critical (steep) and sub-critical (mild) normal flow regimes. In addition to these data they provide graphs for the flow depth h and the pressure coefficient K with distance upstream from the headcut X_u within the reach L . These figures are reproduced as Figs. 3.7 and 3.8. No data for the change in momentum correction factor β with x are given, however they assume β is close to unity at the upstream control, therefore a linear change from 1.0 to the endpoint in Table 3.1 is assumed for the present analysis. This data set is used to define the values of terms on the right hand side of Eq. 3.22.

Table 3.1: Data from Rajaratnam and Muralidhar (1968)

Run	S_b	q (ft ² /s)	h_c (ft)	h_e (ft)	L (ft)	K_e	β_e
Mild	0.0005	1.582	0.427	0.307	2.417	0.340	1.085
Steep	0.0288	1.564	0.424	0.215	0.417	0.270	1.138

Since no functional form of the lines in Figs. 3.7 and 3.8 are given, non-linear regression using a natural growth model is used to determine K and h . Using this model which has a form h/h_n (or K) = $1.0 - a e^{-bx_u}$, depth and pressure asymptotically approach 1.0 as distance upstream from the brink is increased, as indicated from Figs. 3.7 and 3.8. The differential terms $\partial K/\partial x$ and $\partial h/\partial x$ are determined by

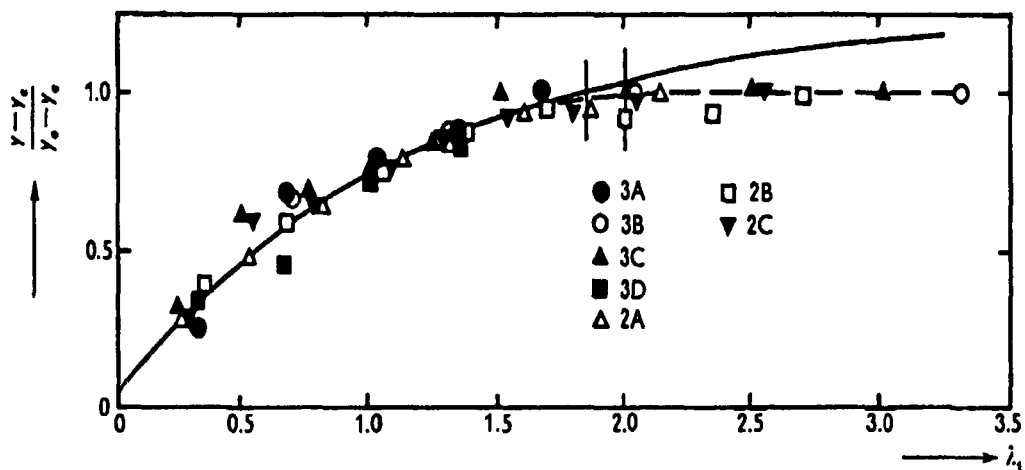


Figure 3.7: Flow Depth vs. Distance Upstream From the Brink From Rajaratnam & Muralidhar, (1968)

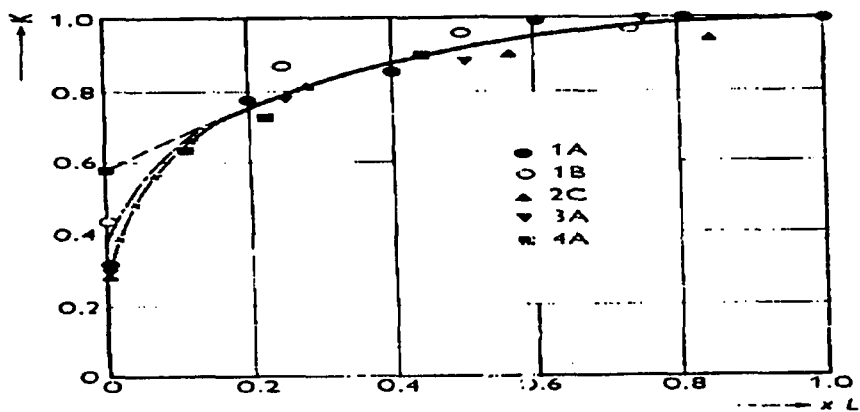


Figure 3.8: Pressure Coefficient vs. Distance Upstream From the Brink From Rajaratnam and Muralidhar, (1968)

differentiating the fitted curves. Note Eqs. 2.12 and 2.13 from Hager (1983) can be used to determine h and $\partial h / \partial x$ if the flow is supercritical.

The relative magnitudes of each term in Eq. 3.22 were analyzed to determine if any terms could be dropped. The term containing $\partial \beta / \partial x$ is two orders of magnitude less than the next smaller term for supercritical flow and one order less

for sub-critical flow and the term containing $\partial K/\partial x$ has the highest order of magnitude for both cases. The term containing $\partial\beta/\partial x$ can be dropped with no more than 1% error for sub-critical flow and no more than 10% error for super-critical flow. Dropping the terms with $\partial\beta/\partial x$ and making the approximation that $\beta= 1.0$, Eq. 3.22 reduces to Eq. 3.25.

$$\tau = \rho gh \left[S_b - \frac{h}{2} \frac{\partial K}{\partial x} - \frac{\partial h}{\partial x} (K - F_r^2) \right] \quad (3.25)$$

Since ρ , g , S_b and h are always positive, $\partial K/\partial x$ and $\partial h/\partial x$ are always negative, $0.0 \leq K \leq 1.0$ by definition, while $F_r > 1.0$ for all $h < h_c$, Eq. 3.25 shows the term containing $\partial K/\partial x$ increases shear stress while the term containing $\partial h/\partial x$ decreases shear stress as compared to a base value using only the bed slope. This condition will hold for all upstream cross sections if the normal flow is super-critical and for some distance upstream from the brink for sub-critical flow. Therefore, Rajaratnam and Muralidhar's data suggest that a gradually varied profile, which does not include the pressure terms K and $\partial K/\partial x$, will underestimate the applied bed shear stress at the brink.

If flow in the accelerated flow region can be approximated by a gradually varied flow profile, that is the pressure terms can be ignored, Eqs. 2.12, 3.10 and 3.24 can be combined to determine the upstream shear stress distribution. However, Eq. 2.12 applies only if the normal flow is super-critical. A simplistic solution would be to assume the flow is normal for all upstream cross sections and shear stress can be calculated from only Eq. 3.10. Typical shear stress distributions calculated from both non-trivial methods are compared in Fig. 3.9. In this figure shear stress is normalized

to normal shear stress and distance upstream from the brink is normalized to the normal flow depth. These shear stress distributions were calculated from a flow rate of $0.00150 \text{ m}^2/\text{s}$ and bed slope of 0.023.

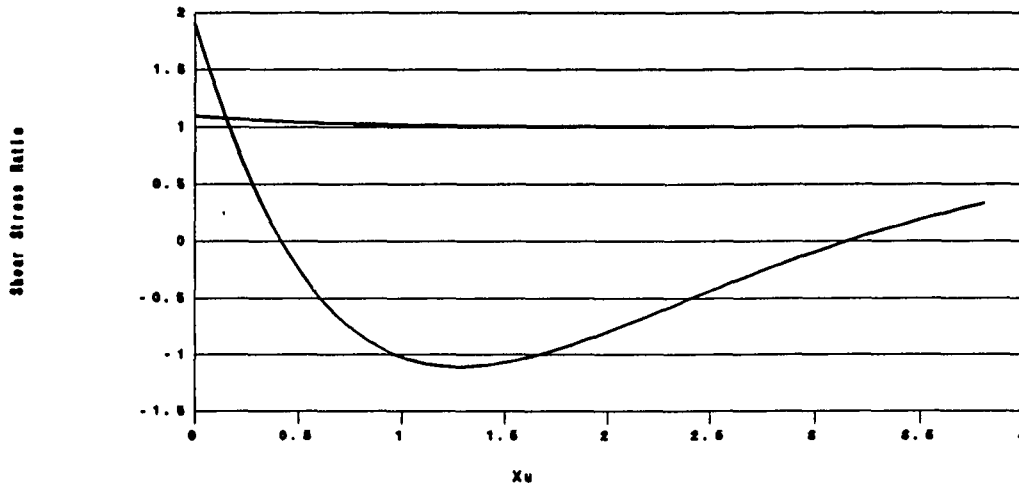


Figure 3.9: Calculated Shear Stress Distributions; $q=0.00150 \text{ m}^2/\text{s}$, $S_b=0.023$

Figure 3.9 shows that shear stress distributions calculated from a rapidly varied flow profile using Eq. 3.25 are unstable. Moving upstream from the brink (increasing x_u), shear stress rapidly decreases from a maximum of 190% of a normal flow value to a minimum value which is less than zero approximately 1.3 flow depths upstream from the brink, and gradually increases approaching normal shear stress far upstream. In no part of the channel should shear stress be less than the normal shear stress value calculated from Eq. 3.10 and negative shear stress in this case is a physical impossibility. While this example is an extreme case, many distributions calculated from Eq. 3.25 with different values for flow rate and bed slope show similar instabilities. The error stems from the aforementioned relative magnitudes of the terms in Eq. 3.25. The term in Eq. 3.25 adding shear stress $\partial K/\partial x$ and the term

subtracting shear stress $\partial h/\partial x$ are as much as two orders of magnitude higher than the base value computed from bed slope alone. The value of these terms is computed from the derivative of regression equations. These equations have no physical interpretation and although the fit of these equations is quite good small errors will be greatly increased when the derivative is taken. It is possible that the data can be equally represented by a regression model other than a natural growth curve resulting in small differences in the derivative values. Several regression forms were tried but with no appreciable improvement. Unfortunately, unless a numerical solution of Eq. 3.14 can be employed, or better data becomes available, Eq. 3.25 is too sensitive to values which can only be estimated to be of practical use.

The shear stress distribution calculated from a gradually varied flow profile using the combination of Eqs. 2.12 from Hager (1983), 3.10 and 3.24 shows no instability, it gradually increases from a normal flow value computed from Eq. 3.10 at about 2.5 flow depths upstream from the brink to a maximum of 110% of normal at the brink. This maximum is negatively correlated to upstream Froude number through Eq. 2.11. This method ignores the effect of the positive pressure gradient on shear stress included in Eq. 3.25 but includes the decreasing flow depth ignored in Eq. 3.10. Therefore this method represents the physics more accurately than Eq. 3.10 and at the same time does not display the instability of Eq. 3.25. For these reasons it will be used to determine the shear stress distribution and the maximum shear stress τ_e in the accelerated flow region.

3.5.3 Bed Degradation in the Accelerated Flow Region

Combining Eqs. 2.11, 3.11, 3.12, 3.13 and 3.24 yields Eq. 3.26 for shear stress at the brink τ_e calculated from a gradually varied flow profile from Hager (1983) and the Blasius assumption for the Darcy-Weisbach friction factor. Other assumptions for the friction factor (such as Manning's) change only the values of the constant and exponents of bed slope and Reynolds number.

$$\tau_e = \tau_n \left(1.0 + 0.022 S_b^{-1.0} R_e^{-0.25} + 0.000121 S_b^{-2.0} R_e^{-0.5} \right) \quad (3.26)$$

Equation 3.26 shows shear stress at the brink is equal shear stress in the normal flow region plus an increase due to the flow acceleration. This increase is negatively correlated to bed slope and Reynolds number. The last term in Eq. 3.26 is several orders of magnitude less than any other and can be ignored with no appreciable error. Subsequent equation development will ignore similar higher order terms.

Equations 3.12 and 3.26 show that the maximum shear stress is a function of only bed slope and Reynolds number confirming an assumption made in the development of the dimensional analysis relation in Eq. 3.3.

Sediment detachment at a channel cross section is directly proportional to the bulk density of the soil times the change in bed elevation with time. Therefore q_s ($M/L^2/T$) is proportional to $B_d (\partial Y/\partial t)$ where Y is the bed elevation and B_d the soil bulk density. The upstream erosion time scale was defined as the time required for the headcut drop height to be completely obliterated. Integrating the above expression from $t=0$ to $t= T_U$ yields $q_s \propto B_d D_n/T_U$. Substituting this relation into Eq. 2.10 and solving for T_U yields Eq. 3.27.

$$T_U \propto \frac{B_d D_h}{K_{1U} \tau_e^{K_{2U}} \left(1 - \frac{\tau_{cU}}{\tau_e}\right)^{K_{2U}}} \quad (3.27)$$

Equations 3.3, 3.12, 3.26 and 3.27 can be combined with the definition of F_d to determine an upstream scour potential given as Eq. 3.28.

$$\frac{T_U \nu}{D_h^2} \propto \frac{F_d^{-0.667}}{\left[S_b^{0.667} R_e^{0.583} (1 + 0.022 S_b^{-1} R_e^{-0.25}) \left(1 - \frac{\tau_{cU}}{\tau_e}\right) \right]^{K_{2U}}} \quad (3.28)$$

This equation is strictly applicable only for the initial time frame because shear stress at the brink is a function of bed slope at the brink which is a function of time if the shear stress distribution is not constant with channel length. This distribution is constant only if slope or Reynolds number are very large so that Eq. 3.26 reduces to $\tau_e = \tau_n$.

3.6 The Impingement Region

Flow in this region can be likened to that of an impinging jet. Therefore rather than develop a continuity and momentum expression for the entire region, as done in previous sections, properties of a jet will be used to determine shear stress and bed degradation. A general flow diagram for a jet produced by a free falling nappe entering a plunge pool is shown in Fig. 3.10. At impact with the water surface, the jet has an initial width y_0 and average velocity U_0 and impact angle χ . Diffusion of jet is similar to that of impinging jets described in Chapter 2.

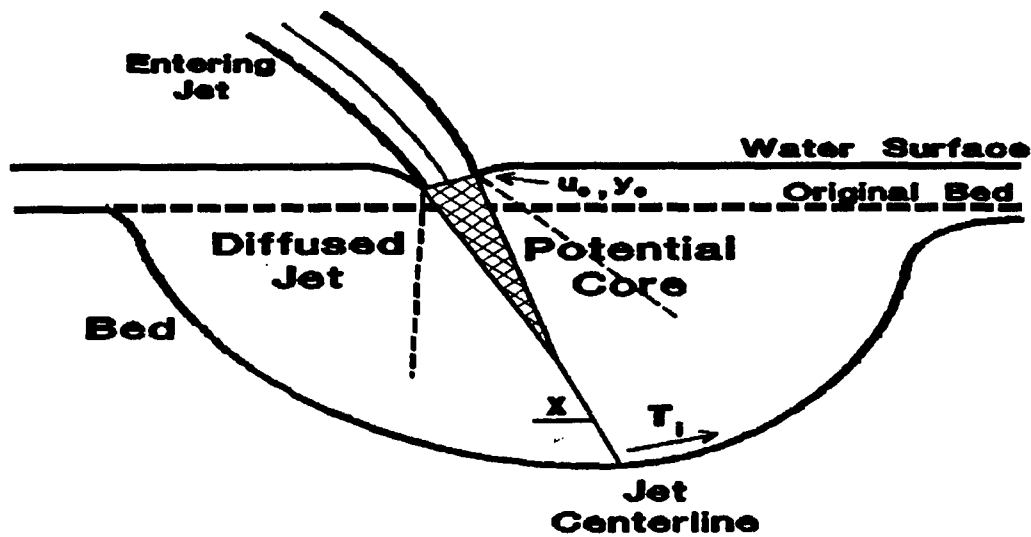


Figure 3.10: Hydraulics of the Impingement Region

Much of the ensuing analysis takes an approach similar to that of Rajaratnam (1981), Yuen (1984) and Bormann (1988) with three major differences. First the change in maximum scour depth with time and not just the ultimate scour depth is desired. Secondly, not just the maximum depth but the entire scour profile must be determined to determine headcut retreat. Fortunately many previous investigations of jet scour, (Poreh and Hefez, 1967; Chee and Kung, 1971; Rajaratnam and Beltaos, 1977; Kobus et al., 1979; Rajaratnam 1981; Akashi and Saitou, 1986; Blaisdell and Anderson, 1988a, 1988b) show a similarity of profile shape in which the maximum scour depth is a characteristic length. Finally, this study includes cohesive bed material in which particle stability cannot be considered the same function of sediment size as used in the Shields parameter.

3.6.1 Maximum Applied Shear Stress

The concept of shear velocity U_* introduced with the Shields parameter can be used to translate shear stress to velocity. Introducing a coefficient of friction C_f defined in Eq. 3.29, U_* can be replaced by a yet to be determined characteristic velocity.

$$C_f = \frac{\tau}{\rho U^2} \quad (3.29)$$

Bogardi's (1974) work on which Eq. 2.29 is based, shows C_f is related to the ratio of sediment size to a characteristic depth of flow on a hydrodynamically rough boundary. To determine maximum shear stress in the impingement region τ_i it follows that the characteristic velocity is the maximum velocity in the impingement region U_{mi} and Eq. 3.30 applies.

$$\tau_i = C_f \rho U_{mi}^2 \quad (3.30)$$

Combining Eqs. 2.14 through 2.19 with 3.30 yields Eqs. 3.31 and 3.32 for the maximum applied shear stress in the impingement region τ_i where J_i is the distance along the jet centerline from tailwater impingement to the eroding bed, J_o is the length of the jet potential core and U_o and y_o are the jet velocity and jet thickness at tailwater impingement.

$$\tau_i = C_f \rho U_o^2 \quad \frac{J_i}{J_o} \leq 1.0 \quad (3.31)$$

$$\tau_i = C_f C_d^2 \rho U_o^2 \frac{y_o}{J_i} \quad \frac{J_i}{J_o} > 1.0 \quad (3.32)$$

Equations 3.31 and 3.32 show τ_i and J_i are inversely proportional. Initially ($J_i < J_o$) the applied shear stress is a maximum and the scour hole grows rapidly. As the scour hole deepens and J_i increases to values greater than J_o the applied shear stress τ_i decreases, eventually approaching the critical shear stress for the bed material τ_c .

These equations incorporate the physics of jet diffusion and convert velocity of the jet near the bed to shear stress near the bed. They are general and can be combined with the Shields parameter to determine the ultimate scour depth from jets impinging on non-cohesive bed material as shown by Bormann (1988). In addition they can be used to determine the ultimate scour depth of cohesive bed material if the critical shear stress for that material is known. They can also be used to determine the sediment detachment at any time during the scouring process from scour initiation to ultimate depth by combining with Eq. 2.10.

Equations 3.31 and 3.32 can be applied to the scour hole below a headcut provided the impinging jet velocity U_o can be accurately determined. For a constant drop height a simple equation for a free falling nappe given as Eq. 3.33 can be used to calculate this velocity.

$$U_o = \sqrt{u_e^2 + 2gD_h} \quad (3.33)$$

The term u_e is the velocity at the brink and is given in Eq. 3.34 by combining Eqs. 2.7, 2.11 and 3.13. This derivation uses the upstream flow profile given by Hager (1983).

$$u_e = \frac{0.4 g h_n^3 + q^2}{q h_n} \quad (3.34)$$

The maximum shear stress applied on the bed in the impingement region occurs while the bed is within the jet potential core and is given by Eq. 3.31. By combining Eq. 3.31 with Eqs. 3.11, 3.12, 3.33 and 3.34 with the definition of F_d the maximum shear stress can be expressed as a function of bed slope Reynolds number and drop number shown as Eq. 3.35.

$$\tau_i = \tau_n \frac{C_f}{C_{fn}} \left(1 + 0.022 S_b^{-1.0} R_e^{-0.25} + 0.182 S_b^{-0.667} R_e^{-0.833} F_d^{-0.667} \right) \quad (3.35)$$

The term C_f is a coefficient of friction defined in Eq. 3.29 and C_{fn} is the value of C_f when u_n is the characteristic velocity. If the Blasius assumption for the friction factor is used C_{fn} is defined in Eq. 3.36.

$$C_{fn} = \left(\frac{.22}{8} \right) R_e^{-0.25} \quad (3.36)$$

Equation 3.35 shows the maximum shear stress in the impingement region equals the sum of normal flow shear stress and the increase due to the flow acceleration at the brink as given by Eq. 3.26 plus an additional increase related to the drop height through the drop number. This equation is only applicable if both the bed elevation is within the potential core of the diffusing jet so that the maximum

shear stress is given by Eq. 3.31 and if the drop height is constant with time so that Eq. 3.33 applies. Equations 3.35 and 3.36 will be used for headcut stability analysis.

3.6.2 Ultimate Scour Depth

If the bed material is non-cohesive, the method developed by Bormann (1988) using Eqs. 2.28 and 2.29 can be used to determine the ultimate scour depth. As previously discussed this method determines the depth of scour at which the ratio of shear stress applied by the diffused jet over the critical shear stress for the sediment particle equals one. The applied shear stress is calculated from a relation between shear stress and velocity over a hydrodynamically rough boundary and the critical shear stress from the Shields parameter adjusted for the sediment angle of repose and sloping side of the scour hole.

If the bed material is cohesive, a similar method can be used, however the boundary is more likely to be hydrodynamically smooth and the Shields parameter does not represent the critical shear stress. Equations 2.28 and 3.32 can be combined to yield Eq. 3.37 for the ultimate scour depth when $\tau_i = \tau_c$ and the depth of tailwater is insignificant.

$$D_u = \sin\chi \frac{C_d^2 C_f \rho U_o^2 y_o}{\tau_c} \quad (3.37)$$

Equation 3.37 is a general expression for the ultimate scour depth produced by an impinging jet for any jet configuration and bed material. Predictive equations developed by Rajaratnam (1981), Yuen (1984) and Bormann (1988) assume different flow conditions or bed material which change the values of parameters in Eq. 3.37.

All values in Eq. 3.37 are known constants or can be calculated with some degree of accuracy for a given flow configuration except the value of C_d which must be estimated. Rajaratnam (1976) suggests a value of 2.47 for a free jet. Beltaos' work (1972, 1974) with impinging jets suggests this value must be increased to 2.72 while Bormann (1988) used values as low as 1.8 for the case of developing jets on grade control structures. Comparison of Eq. 3.37 with an extensive data set for ultimate scour depth from an impinging jet produced by a free falling nappe will be discussed in Chapter 5.

3.6.3 Change in Maximum Scour Depth With Time

Dimensional analysis of the relation between maximum scour depth and time resulted in Eq. 3.4. This section will develop a relation between the same variables using the previously developed relations of sediment detachment and jet diffusion. The two methods will then be compared.

3.6.3.1 Scour Rate Within the Potential Core

Analogous with the reasoning used with upstream scour, sediment detachment at the point of maximum scour is directly proportional to the product of bulk density, a measure of porosity, and the change in scour depth with time. Therefore q_s ($M/L^2/T$) is proportional to $B_d (\partial D/\partial t)$ where D is the maximum scour depth at a given time. Substituting Eqs. 2.10 and 3.31, applicable while the bed is within the potential core into this relation yields Eq. 3.38.

$$\frac{dD}{dt} = \frac{K_{1D}}{B_d} (C_f \rho U_o^2 - \tau_{cD})^{K_{2D}} \quad (3.38)$$

Integrating Eq. 3.38 from $t=0$ to $t= T_p$ and solving for T_p yields Eq. 3.39 where T_p is the time at which the bed elevation is just at the tip of the potential core. The depth D_p corresponding to T_p (Eq. 3.40) is achieved by combining Eqs. 2.17 and 2.28, with the assumption tailwater depth is insignificant.

$$T_p = \frac{B_d C_d^2 y_o \sin \chi}{K_{1D} (C_f \rho U_o^2 - \tau_{cD})^{K_{2D}}} \quad (3.39)$$

$$D_p = C_d^2 y_o \sin \chi \quad (3.40)$$

Equation 3.38 shows that for some time from the initiation of scour given in Eq. 3.39 and corresponding to the time the bed is within the jet potential core, the maximum depth of scour increases linearly with time. This rate is directly proportional to the sediment detachment rate. Therefore at least while the bed is within the potential core scour depth cannot increase semi-logarithmically with time as reported by Rouse (1940) and others. This explains the underprediction of scour depth at early times when the semi-log relationship is used. The time T_p scour is controlled by the hydraulics of the potential core is inversely proportional to the sediment detachment rate as shown in Eq. 3.39, but the absolute depth D_p shown in Eq. 3.40 corresponding to this time is dependent only on hydraulics, especially jet thickness and not sediment detachment. Therefore, the significance of the potential core scour rate on the total scour process can vary considerably depending on the

relation between jet thickness and sediment detachment. This will be shown in the next section.

3.6.3.2 Scour Rate for the Diffusing Jet

If the bed elevation is beyond the length of the potential core Eq. 3.32 shows that the maximum shear stress decreases with increasing scour depth and therefore increasing time. This change is related to jet diffusion and the increasing depth of the scour hole. Using the same approach from which Eq. 3.38 was developed, Eqs. 2.10, 2.28, and 3.32, applicable when the bed is beyond the potential core, can be combined to yield Eq. 3.41, a non-linear ordinary differential equation.

$$\frac{dD}{dt} = \frac{K_{1D}}{B_d} \left[\frac{C_d^2 C_f \rho U_o^2 y_o \sin \chi}{D} - \tau_{cD} \right]^{K_{2D}} \quad (3.41)$$

Equation 3.41 is variable separable with the initial values given in Eqs. 3.39 and 3.40, however the resulting integral has an analytical solution only if the sediment detachment exponent K_{2D} is an integer. Assuming $K_{2D} = 1.0$, the solution to Eq. 3.41 is given as Eqs. 3.42 and 3.43.

$$-\frac{D}{\tau_{cD}} - \frac{C_d^2 C_f \rho U_o^2 y_o \sin \chi}{\tau_{cD}^2} \ln \left[1.0 - \frac{\tau_{cD} D}{C_d^2 C_f \rho U_o^2 y_o \sin \chi} \right] = \frac{K_{1D}}{B_d} t + C \quad (3.42)$$

$$C = -\frac{D_p}{\tau_{cD}} - \frac{C_d^2 C_f \rho U_o^2 y_o \sin \chi}{\tau_{cD}^2} \ln \left[1.0 - \frac{\tau_{cD} D_p}{C_d^2 C_f \rho U_o^2 y_o \sin \chi} \right] - \frac{K_{1D}}{B_d} T_p \quad (3.43)$$

Note the form of Eqs. 3.42 and 3.43, which includes both linear and logarithmic terms for depth, precludes an explicit expression for depth as a function of time, however time can be explicitly expressed as a function of scour depth. Selected solutions to Eqs. 3.38 and 3.41 the change in scour depth with time both within and beyond the potential core are shown on arithmetic scale in Fig. 3.11. The selected solutions represent from top to bottom measured values of Runs 9, 10, 6 and 13 described in detail in Chapter 5 and the sediment detachment exponent $K_{2D} = 1.0$.

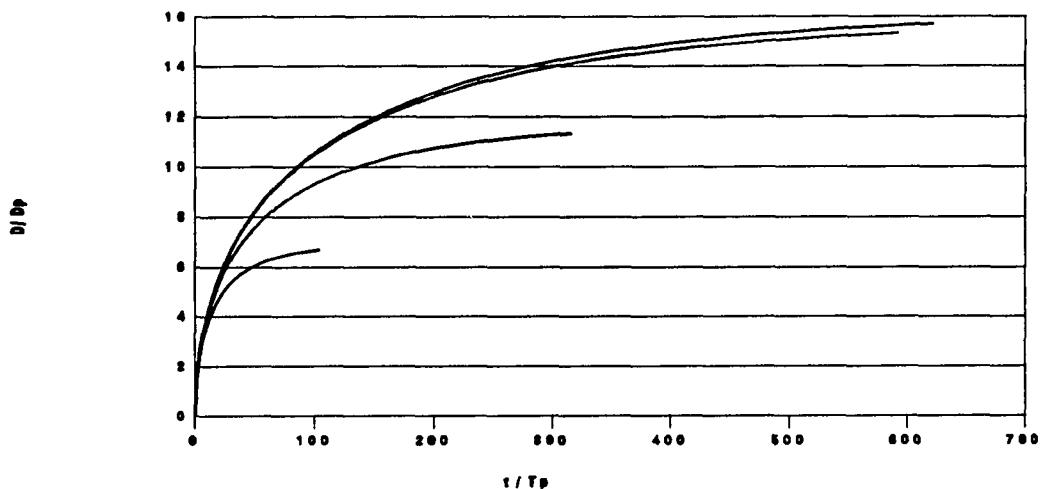


Figure 3.11: Change in Scour Depth With Time From Eqs. 3.38 and 3.41

In Fig. 3.11 maximum scour depth is normalized to the scour depth corresponding to the tip of the potential core D_p determined from Eq. 3.39 and time is normalized to the time T_p , determined from Eq. 3.40, corresponding to D_p . Therefore values of (t / T_p) and (D / D_p) less than one represent scour within the potential core and values greater than one represent scour from the diffusing jet beyond the potential core. The endpoint of each line corresponds to the ultimate scour depth determined from Eq. 3.37. As can be seen the total time of potential

core scour is an insignificant part of the total scour time but depth of potential core scour can be a considerable percentage of the ultimate scour depth determined from Eq. 3.37. This percentage varies considerably for different hydraulic conditions as discussed previously.

Figure 3.11 shows that scour depth as determined from Eq. 3.41 does not asymptotically approach the ultimate scour depth. Ultimate depth is reached within a finite time, though scour rate increases slowly as depth approaches the ultimate depth. The analysis from which Eq. 3.41 is developed is based on the time averaged shear stress and excludes turbulent fluctuations which may become significant (Robinson, 1989) as shear stress approaches the bed material critical shear stress. Turbulent fluctuations would therefore tend to scatter scour depth about the predicted lines in Fig. 3.11 with scatter increasing as the ultimate depth is approached. In addition, this scatter would not be random, it has a bias for increased scour depth at a given time because turbulent fluctuations above the mean would increase the scour depth while fluctuations below the mean would not affect the scour depth.

As was the case for scour within the potential core, the semi-logarithmic relation for the change in scour depth with time, used by Rouse (1940) and others, poorly approximates Eq. 3.41. A log-log transformation of the data in Fig. 3.11, shown in Fig. 3.12, graphically displays this fact.

Figure 3.12 shows the two unique scour rates depending on the position of the bed relative to the potential core. Scour rate controlled by the potential core, (D / D_p) and (t / T_p) less than 0 on log-log scale, is linear with a slope of one because Eq.

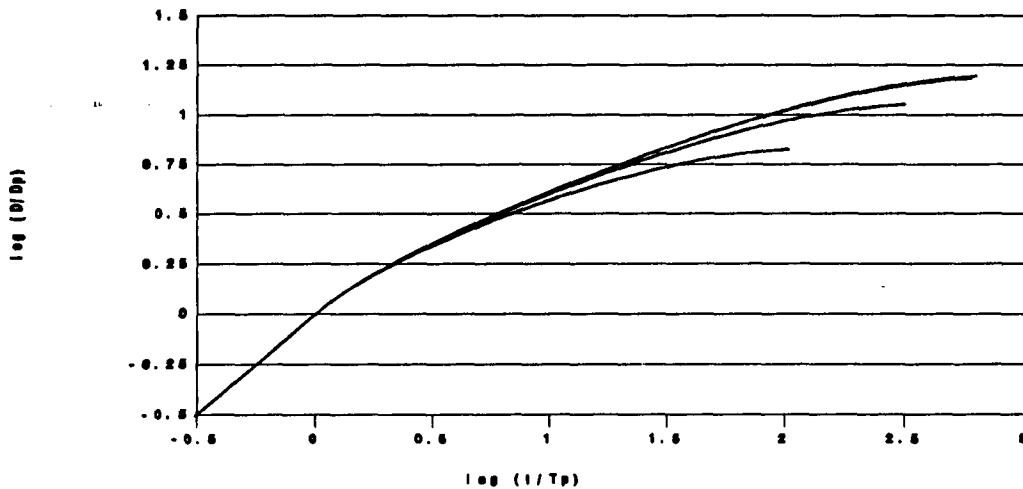


Figure 3.12: Change in Scour Depth with Time; Log-Log Scale

3.38 shows scour rate is linear with time. Additionally, scour depth with time for the diffusing jet plots on log-log scale as an approximately, but not identically, straight line for values of depth and time greater than D_p and T_p respectively. While the slope decreases slightly with increasing time it is in all cases less than one, indicating the scour rate for the diffusing jet is always less than within the potential core. Figure 3.12 indicates depth is accurately represented by a power function of time while the bed is within the potential core and can be approximated as a different power function of time for scour controlled by the diffusing jet. Considering that turbulent fluctuations increase the scour depth at a given time especially at long times, as discussed above, the power form may more accurately represent the change in scour depth with time than indicated in Fig. 3.12.

The log terms of Eqs. 3.42 and 3.43 can be approximated using a power series expansion. Considerable simplification of these equations results if the power series expansion is used in that the first term of the series expansion cancels with the first

term of both equations. The first three terms of the series expanded Eqs. 3.42 and 3.43 are given in Eq. 3.44. Each additional term increases by one the value of exponents of τ_{cD} , D , D_p and the bracketed denominator term.

$$t = T_p + \frac{B_d[D^2 - D_p^2]}{K_{1D}[C_d^2 C_f \rho U_o^2 y_o \sin \chi]} + \frac{B_d \tau_{cD}[D^3 - D_p^3]}{K_{1D}[C_d^2 C_f \rho U_o^2 y_o \sin \chi]^2} + \dots \quad (3.44)$$

Equation 3.44 confirms that a power or log-log function of the relation between scour depth and time should approximate Eqs. 3.42 and 3.43 developed by combining a sediment detachment function to jet diffusion. If the value of the sediment detachment exponent K_{2D} is not unity, Eqs. 3.42 through 3.43 are not solutions to Eq. 3.32, but the solution for any exponent should always be approximated as a power function.

Equation 3.41 is an analytically derived expression equivalent to Eq. 3.4 derived solely from principles of dimensional analysis as shown below. Substituting an expression for scour depth from Eqs. 2.28 (again assuming depth of tailwater is insignificant) and 3.32 into the argument of the log term of Eqs. 3.42 and 3.43, dividing depth in the first term of Eq. 3.42 by D_u given in Eq. 3.37, multiplying the entire expression by the quantity (U_o / y_o) and solving for $t U_o / y_o$ yields Eq. 3.45.

$$\frac{t U_o}{y_o} = - \frac{B_d C_d^2 C_f \rho \sin \chi}{K_{1D} \tau_{cD}^2} U_o^3 \left[\frac{D}{D_u} + \ln \left(1.0 - \frac{\tau_c}{\tau} \right) \right] \quad (3.45)$$

The term U_o^3 in Eq. 3.45 is the product of Reynolds number, Froude number squared and the constant νg , therefore Eq. 3.45 is an expression equivalent to the relation of Eq. 3.4 developed from dimensional analysis. Note however some terms of Eq. 3.45 are additive, a fact usually ignored when applying the π theorem of dimensional analysis.

In summary, the change in maximum scour depth with time produced by an impinging jet proceeds at two different rates depending on the position of the bed relative to the jet origin in this case taken as the original bed elevation. The rate is constant and given by Eq. 3.38 while the bed is within the jet's potential core, and decreases with increasing time thereafter. This decreasing rate cannot be determined directly, but can be computed from Eq. 3.44 if the sediment detachment exponent is unity. The dimensionless relation of Eq. 3.4 is shown to be equivalent to the analytically derived solution. For any value of the exponent and any scour depth less than the ultimate depth, scour depth and time should be approximately linear on log-log scale.

3.7 Headcut Stability Analysis

A dimensionless equation which is more physically revealing than Eq. 3.1 can be developed without use of the π theorem. The upstream time scale T_U was defined in Eq. 3.27. A similar relationship for ratio of the downstream time scale to length scale can be developed. The term T_D was defined as the time required for downstream erosion to reach the headcut face. The corresponding length scale is the longitudinal distance between the headcut face and impingement of the jet with the

original unscoured bed, X_n . This length scale is the scour hole half-width. Assuming the scour hole width is a function of the maximum scour depth at a given time yields the expression $q_b \propto \partial D / \partial t \propto X_n / T_D$. Solving the sediment detachment relationships of upstream and downstream scour for T_U / T_D yields Eq. 3.46 in which f_1 is a proportionality constant.

$$\frac{T_U}{T_D} = f_1 \frac{D_h \tau_i^{K_{2D}} \left(1 - \frac{\tau_{cD}}{\tau_i}\right)^{K_{2D}}}{X_n \tau_e^{K_{2U}} \left(1 - \frac{\tau_{cU}}{\tau_e}\right)^{K_{2U}}} \quad (3.46)$$

As will be shown below, all terms on the right hand side of Eq. 3.46 can be reduced to functions of S_b , R_e and F_d therefore it is equivalent to the relationship of Eq. 3.2. The shear stress terms τ_e and τ_i have been previously reduced to functions of S_b , R_e and F_d in Eqs. 3.26 and 3.35 using the Blasius assumption for the Darcy-Weisbach friction factor. The ratio of these stresses, assuming the ratio C_f / C_{fn} in Eq. 3.35 equals unity, is given as Eq. 3.47.

$$\frac{\tau_i}{\tau_e} = 1 + \frac{0.182 S_b^{-0.667} R_e^{-0.833} F_d^{-0.667}}{\left(1 + 0.022 S_b^{-1.0} R_e^{-0.25}\right)} \quad (3.47)$$

The downstream length ratio shown in Eq. 3.48 can be calculated from rearrangement of the same free falling nappe equation used to develop Eq. 3.33.

$$X_n = u_c \sqrt{\frac{2D_h}{g}} \quad (3.48)$$

Combining Eqs. 2.6, 3.11, 3.34, 3.48 with the definition of F_d yields the erosion length scale ratio given in Eq. 3.49.

$$\frac{D_h}{X_n} = 0.213 S_b^{-0.333} R_e^{-0.417} F_d^{-0.333} (1 + 0.011 S_b^{-1.0} R_e^{-0.25}) \quad (3.49)$$

Equations 3.47 and 3.49 correspond to two π terms developed in the dimensionless relationship of Eq. 3.1 for headcut stability. The final π term of Eq. 3.1 can be reduced to Eq 3.50 by combining Eqs. 3.12 and 3.26.

$$\pi_7 = \frac{36.363 S_b^{-1.0} R_e^{-1.5}}{0.066 + S_b R_e^{0.25}} \quad (3.50)$$

Equations 3.47, 3.48 and 3.50 reduce three dimensionless parameters of the relationship shown in Eq. 3.1 to functions of three different dimensionless parameters, bed slope, Reynolds number and drop number, confirming that the previously assumed equivalent dimensionless relationships for headcut stability shown in Eqs. 3.1 and 3.2 are indeed equivalent. Substituting Eqs. 3.26, 3.35 and 3.49 into Eq. 3.46 proves that this equation, formulated by equating the physical processes controlling erosion in the vicinity of a headcut, is also equivalent to the relationship in Eq. 3.2, developed solely from dimensional analysis.

If upstream and downstream sediment detachment equations are identical, a reasonable assumption if critical shear stress is small compared to either τ_i or τ_e , and if $K_{2U} = K_{2D} = 1.0$, Eq. 3.46 can be reduced to Eq. 3.51 by substituting Eqs. 3.47 and 3.49 where f_1 is an experimentally determined constant.

$$\frac{T_U}{T_D} = f_1 \left[\frac{F_d^{-0.333}}{S_b^{0.333} R_e^{0.417}} + \frac{0.011 F_d^{-0.333}}{S_b^{1.333} R_e^{0.667}} + \frac{0.182 F_d^{-1}}{0.011 + S_b^{1.0} R_e^{0.25}} \right] \quad (3.51)$$

Equation 3.51 relates headcut stability to three dimensionless parameters, bed slope, Reynolds number and drop number but assumes that all terms on the right hand side are independent of time. As discussed below it is strictly applicable only for the initial time frame as the relative magnitude of terms on the right hand side of Eqs. 3.26 and 3.35 for upstream and downstream shear stress respectively are formulated from initial conditions.

Equation 3.28 was shown to overestimate the upstream time scale because slope at the brink increases with time. This is because Eq. 3.26 will underestimate shear stress at the brink for all times greater than zero if slope or Reynolds number are not large. Conversely, the downstream time scale is underestimated because Eq. 3.35 will overestimate the maximum downstream shear stress for times greater than T_p , the time the bed is within the potential core, because the effect of jet diffusion on the maximum shear stress can no longer be neglected. This overestimation occur only if T_U is greater than T_p , however Eq. 3.35 will overestimate shear stress for all times greater than zero because upstream erosion decreases the drop height (and increases F_d) with time. Therefore the shear stress ratio given by Eq. 3.47 and used to develop Eq. 3.51 is a maximum and applicable only at $t=0$. The effect this has on the time scale ratio is partially offset by a decrease in X_n which increases the length scale ratio with time. The length scale X_n decreases with time because the effective drop height of Eq. 3.48 is decreasing with time. Note the upstream length scale remains constant and equal to the original drop height.

Equation 3.51 can only be considered a first approximation of the true time scale ratio because it is formulated from initial conditions which will change with time, however deviations are not expected to be great especially for large slope and Reynolds numbers. It is in all cases a conservative estimate of headcut stability, downstream erosion is overestimated implying the headcut will continue to migrate upstream when in fact it may rotate and obliterate itself. It is also limited to cases in which upstream and downstream sediment detachment equations are identical with an exponent equal to unity, and to supercritical flow over a hydrodynamically smooth boundary. If any of these conditions are not met, the more general Eq. 3.46 must be used for headcut stability analysis.

A criterion for headcut stability can be determined by solving the ratio (T_U / T_D) in Eqs. 3.46 or 3.51 for one. Values of this ratio greater than one indicate the upstream time scale T_U is larger and downstream erosion will reach the base of the headcut first. Conversely, values of (T_U / T_D) less than one indicate the downstream time scale T_D is larger and therefore upstream erosion dominates. Equation 3.51 is solved for $T_U / T_D = 1.0$ for various values of slope, Reynolds and drop number with a value of 0.07 for the experimental constant f_1 . This value is an average several computer simulations of headcut stability verified by experimentation as discussed in Chapter 5. A graphical representation this solution is shown on arithmetic scale in Fig. 3.13 and on log-log scale in Fig. 5.14.

Any set of conditions which plot above the lines of Fig. 3.13 are values of $T_U / T_D < 1.0$ therefore upstream erosion dominates and the headcut tends to obliterate itself with time. Conversely values below the lines indicate downstream erosion

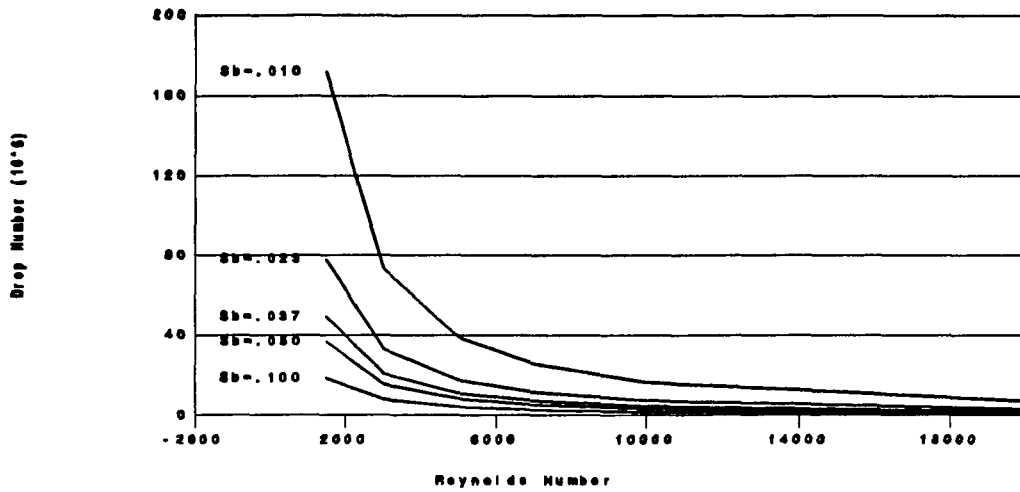


Figure 3.13: Headcut Stability for Initial Hydraulics and Low Critical Shear Stress

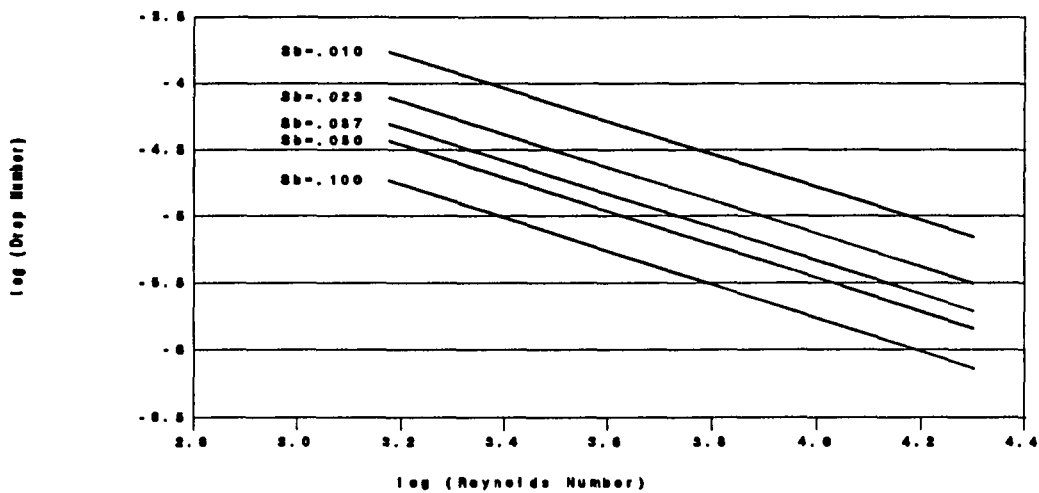


Figure 3.14: Headcut Stability Log-Log Scale

dominates and the headcut will migrate upstream. Considering Eq. 3.51 is conservative, that is it has a bias for downstream domination, it is remarkable that most combinations of slope, Reynolds and drop number indicate the headcut will obliterate itself if upstream and downstream sediment detachment rates are equal.

The validity of this headcut stability analysis will be discussed in Chapter 5.

Chapter 4

Materials and Methods

This Chapter discusses the materials and general procedures used in experimental part of this research. Details of the results are discussed in Chapter 5. All experimental runs were conducted in the Hydraulics Laboratory of the Engineering Research Center at the Foothills Campus of Colorado State University. The experimental program consisted of three main parts. The first runs, CS1 through CS6 were designed to calibrate the sediment detachment equation for one particular cohesive soil under normal flow conditions. The second part, consisting of Runs 1 through 4 and 6 through 27, had a plexiglass plate placed on the bed upstream from a simulated headcut. This allowed erosion in the impingement region to be measured without upstream erosion and was used to verify the ultimate and time scale analysis of jet scour. Three bed materials were eroded in these runs, the soil used in runs CS1 through CS6 and two sands of different sizes. Runs 5, and 28 through 40 allowed a given headcut to retreat and were used to valid headcut migration analysis.

4.1 The Flume

A flume for conducting experimental runs was constructed by modifying a narrow plexiglass tank previously used in a porous media study. Internal dimensions

of the tank are 10.4 cm wide by 200.0 cm long and 33.0 cm high. Modifications were as follows. The endwalls were lowered in height to allow water entry and exit. An exit plate which sits flush against the flume was constructed with its own sidewalls and floor, but which could be varied in height as compared to the entrance height. A headbox 20.4 cm long with the same width and height as the flume was fitted to the flume entrance. The entrance edge of the headbox and flume was rounded to minimize flow separation and other entrance effects. A support system was developed which allowed the flume and headbox to sit on a table or desk top with an adjustable slope range of 0 to 10 percent. A photograph of this flume is shown in Fig. 4.1.

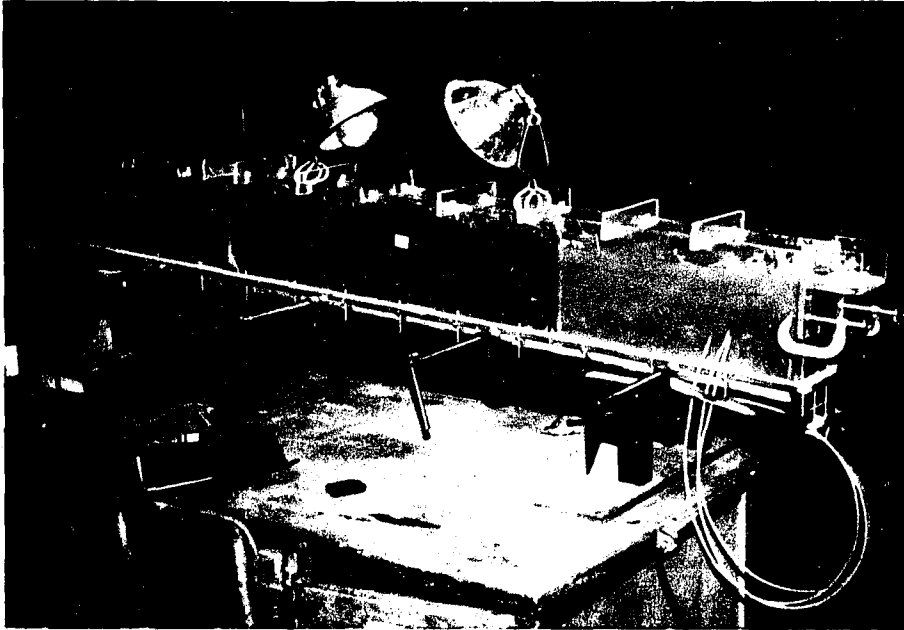


Figure 4.1: The Experimental Flume

Three identical plexiglass plates 10.2 by 66.0 cm were designed as a false floor capable of supplying a negative water potential to the soil matrix. A shallow depression (approx. 1 mm) was milled into the upper surface of these plates and a nipple fitted through the bottom. A porous plastic capable of holding up to 100 cm of water tension was glued to the upper surface of the plates. The milled depression served as a reservoir between the plate and porous plastic. Properties of this porous plastic can be found in Stieb's (1983) thesis. Hoses attached to the nipples can be fitted through watertight holes in the flume floor. These hoses act as a hanging water column to provide suction up to 100 cm of water. Though the physical setup allowed this small soil tension to be applied only a few preliminary runs were conducted under anything less than saturated conditions. these plates were set in the flume for all runs therefore the upper surface was approximately 5 cm above the flume floor. Vertical scaling for bed profile measurements used the top of the porous plastic as the origin. The flume entrance elevation was therefore 24.3 cm and exit elevation could be varied from 15.2 to 24.3 cm.

4.2 Bed Material

Three different bed materials were tested for erosivity in the flume. One, hereafter called large sand, has a mean diameter d_{50} of 1.5 mm another sand, hereafter called small sand, has a mean diameter of 0.15 mm. These sands were used to test scour in the impingement region independently from upstream scour. All other experimental runs used a typical agricultural soil which is susceptible to rill erosion and headcuts. It was collected from a wheat field in Logan County,

Colorado. The Soil Conservation Service (SCS) soil survey manual indicates the pit is located in Section 28 (T.6N.) R.51W. and the soil is a Norka, Fine silty, mixed mesic, Aridic Argiustoll 5-9% slope. A complete particle size break down of each material is given Fig. 4.2.

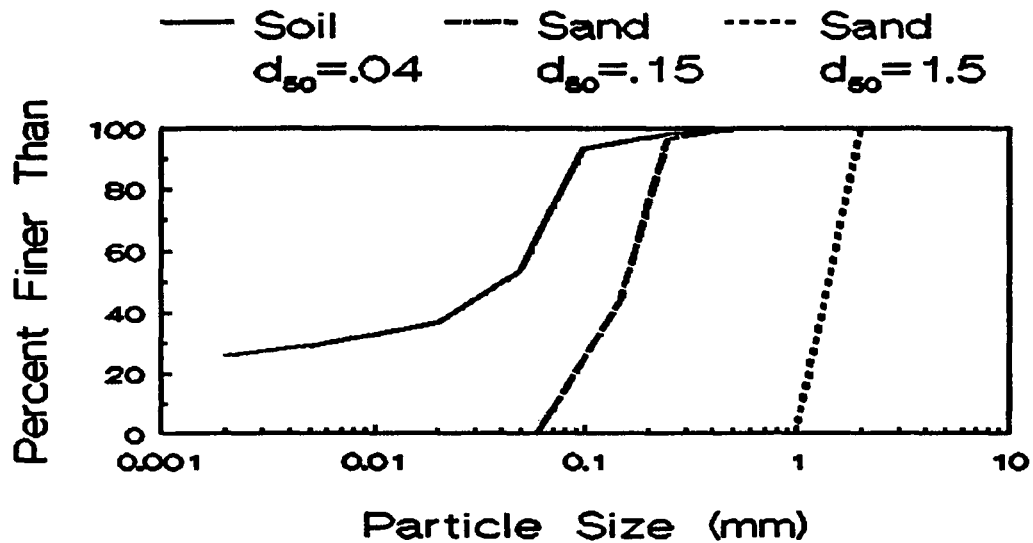


Figure 4.2: Bed Material Particle Size Distribution

To make cohesive soil conditions as uniform as possible, and to remove large pieces of organic matter, the air dried soil was passed through a 0.420 mm sieve. This destroyed all but the natural soil's micro-aggregate structure but allowed it to retain cohesive properties upon rewetting.

4.3 Experimental Method

4.3.1 Measurement of Hydraulic Parameters

Discharge was varied by use of a pressure regulator fitted to a Horsetooth Reservoir supply line of 3/4 inch pipe. The supply line carries water under great pressure (150 ft of head) but depending on the demands of other projects in the

Hydraulics Lab significant pressure variations were possible. The regulator delivers a steady discharge regardless of supply line variations and can be adjusted to deliver discharges ranging from 0 to 55 liters / min. For each run, a target discharge was achieved by measuring flow diverted through a bleed valve. Actual discharge to the headbox varied by as much as 10% from the target discharge depending on the relative resistance of each outlet but both discharges were recorded by one of the following procedures.

Initially, both target and actual discharges were measured by weighing a timed amount of flow, however several problems with this method were discovered during earlier experimental runs. First, at high discharges sample time was limited to as little as 10 sec. by the collection bucket size (15 liters). This was considered too short for the desired accuracy. Second, actual discharges were collected at the flume exit which in all cases consisted of sediment as well as water. These samples therefore had to be corrected for sediment concentration adding another source of error. Third, the time required to collect these samples prevented measurement of other parameters such as depth but especially sediment concentration which was measured by collecting a much smaller amount of soil and water discharge. This problem was especially acute in the critical first minutes of a run when sediment discharge was strongly time dependent. This method was abandoned after runs CS1 through CS6 and runs 28 and 29 which were conducted first.

Problems outlined above proved the need for a more automated method of discharge measurement. Therefore, a turbine flow meter was fitted into the supply line between the pressure regulator and the bleed valve. The turbine meter has a

magnetic sensor which counts the number of turbine blade passages. This count signal is electronically passed to a frequency meter giving a digital readout of counts per second. The count frequency was calibrated over the entire range of discharges by weighing the water discharged over a five minute time span in the calibration stand in the Hydraulics Lab. The calibration stand is completely automated to insure the greatest accuracy. The rating curve between counts and discharge proved to be linear over the flows tested with a replicability of 0.5%. This method was used to measure both target and actual discharge for all other runs.

Normal flow depth and bed profile measurements were made with a point gauge accurate to 0.001 ft (0.03 cm). Benchmark for these values is the flume top edge. Initial bed profile measurements were made on the flume centerline every 10 cm. Final bed profile measurements were made every 10 cm on 5 points along the cross-section (0.2, 2.7, 5.2, 7.8 and 10.2 cm). Flow was considered normal in cross sections 25 cm downstream from the entrance and 20 cm upstream from the headcut. Normal flow depth was determined by pointing the bed and water surface within this range. Average normal velocity can be calculated from depth and discharge measurements and the appropriate governing equation.

Sediment concentration samples were collected in 2.5 liter buckets at the flume exit. The time interval between collections varied depending on the time dependency of the sediment concentration. In the first minutes of the runs, samples were taken as often as every 10 seconds, but after 100 minutes, time periods as long as 10 minutes were not uncommon. Sediment concentration was calculated by weighing the combined water and sediment discharge to the nearest gram (0.05%

error), allowing the sediment to settle for 24 hours and decanting the water. The remaining water was allowed to evaporate at room temperature which required an additional 24-48 hours and re-weighed to the nearest 0.01 gram (0.3 to .01% error). Sediment discharge was determined by multiplying sediment concentration and flow rate.

Other data collected included water temperature which varied between runs from 6^o to 9^o C. Soil moisture samples were taken for runs which had soil. These samples were weighed, oven dried at 105^o C for at least 24 hours and reweighed to determine water content. Water content at saturation was $41 \pm 2\%$ for all runs at the observed bulk density.

4.3.2 Constant Slope Runs

The set-up procedure for these runs is as follows. The tension plates were soaked in water for at least 24 hours and seated in the bottom of the flume which was resting in the horizontal position. A filter of small sand 3 cm thick was placed over the plates to prevent possible clogging of the pores in the porous plastic by clay particles. Soil was then placed in layers usually 5 cm thick up to the equal entrance and exit elevation of 24.3 cm. For each layer a weighed mass of soil was placed in the flume to a thickness larger than desired. The flume sides were then vigorously tapped to settle the soil. Soil in excess of the desired thickness was removed by a specially designed leveling bar and weighed again. By this method an accurate weight per soil layer thickness could be evaluated to determine bulk density. Because the soil was sieved to a diameter of 0.420 mm or less this method achieved a very

uniform bulk density. Values for all layers in all runs were $1320 \pm 10 \text{ kg/m}^3$, better than anticipated. The soil was then slowly saturated by applying a small positive head to a reservoir below the saturated tension plates. The head was raised in 4 to 8 cm increments with each increment allowed to equilibrate from 3 to 12 hours. The final pressure head was set equal to the soil surface in the flume to insure full saturation but soil at the surface was wetted by capillary action, as indicated by a change of color, long before pressure head reached that level. At least 48 hours elapsed between the start of wetting and the beginning of all runs. Two moisture samples, one each near the flume exit and entrance, were taken to determine the saturated water content. At the completion of each run the maximum suction was applied to the tension plates for 24 hours. The soil was then removed, air dried and re-sieved for future use. The above procedure was repeated for each run.

Each run had a unique flow rate. The slope was successively increased from 1.0 to 2.3 to 3.7% for runs CS1 through CS5. Slopes for run CS6 were 1.0 and 5.2%. Relevant data were collected for each discharge/slope combination including final profile measurements made with the point gauge. In this way a total of 17 tests were conducted on saturated soil to determine the relation between sediment discharge and applied normal shear stress as given in Equation 2.10. Results will be given in Chapter 5.

4.3.3 Non-Retreating Headcut Runs

These runs were designed to determine the erosion rate in the impingement region below a free overfall. Bed material for runs 1 through 4 and 6 through 13 was

the same soil as used in the constant slope runs. Four discharge values were repeated at drop heights of 2.0 and 4.0 cm. The smallest and largest discharges were repeated a third time for a drop height of 1.0 cm for a total of ten runs on cohesive soil. Runs 14 through 21 repeated the discharge/drop height combinations for eight large sand ($d_{50} = 1.5$ mm) runs and runs 22 through 27 repeated all but the largest discharge combinations for six small sand ($d_{50} = 0.15$ mm) runs.

Set-up procedure was similar to the one used in the constant slope runs. Because bulk density was so consistent in those runs, initial filling for the soil runs was relaxed in that each layer was not individually weighed eliminating one tedious procedure. Also, because the amount of soil was finite and removing, drying, and re-sieving the soil through a 0.420 mm mesh was very labor intensive, it was decided to not empty and refill the entire flume for each run. Because erosion was limited to the impingement region, only soil in that region or where it had been disturbed was removed. It was, however, replaced by the same layering technique and wetted incrementally over a 48 hour period as before. The procedure for the runs with sand was the same as for soil except the incremental wetting time was reduced to 24 hours for the small sand and to 1 hour for larger sand. This was done because the large pore size of these materials allowed for more rapid water movement.

The desired headcut drop height was achieved by lowering the exit plate controlling downstream elevation the corresponding amount. The downstream bed material was leveled to this elevation. During set-up a piece of smooth styrofoam was wedged between the flume sidewalls at the headcut to create and preserve a vertical face. Upon wetting capillary attraction preserved the vertical face for soil

and small sand runs so that the styrofoam could be removed. However, it remained in place during the large sand runs.

To prevent the headcut from retreating a plexiglass plate 10.4 x 100.0 cm was placed on the saturated bed material upstream of the headcut. The upstream elevation of the bed material was leveled so that the top of the plate would sit flush with the flume entrance elevation (24.3 cm). This plate fit snugly between the flume walls so that it was tapped in place with a rubber mallet. The plate elevation was measured at various points. It was adjusted as necessary to insure no side or longitudinal slope as compared to the flume top. Finally a thin film of vaseline was applied at the interface between the plate and flume sidewalls to prevent any possible water leakage. All runs were conducted at 3.7% slope.

4.3.4 Retreating Headcut Runs

These runs were used to measure headcut migration and to calibrate the headcut stability analysis. Surface bed material for all runs was the cohesive soil. Two runs (28 & 29) allowed the headcut to retreat for some distance upstream and the later of these two had an underlying layer of large sand. This run demonstrates the effect of a much larger downstream sediment detachment potential and will be discussed in Chapter 5. All other runs (30 - 40) were used to measure headcut stability and were terminated when either upstream or downstream erosion clearly dominated. This allowed for several runs to be conducted in one flume packing. The setup procedure was nearly identical to the non-retreating cohesive soil headcut runs

except for the lack of the upstream plexiglas plate allowing for upstream as well as downstream erosion.

4.3.5 Measurements of Changes of Profile

Determining bed profile changes near a headcut both quickly and accurately was critical to this study, especially for the non-retreating runs measuring impingement erosion. The point gauge was used to determine initial and final bed profiles and periodic times between. However it is impossible to measure the entire profile at any instant during the run by this method. A photographic technique was developed to overcome this problem.

A 35 mm camera with a 50 mm lens was positioned so that an approximate 35 x 22 cm section of the flume side could be photographed. An intervalometer used in conjunction with an autowinder allowed the shutter to be automatically tripped at a variety of time intervals between 0.5 sec. to 24 hrs. Times of 5 sec to 10 min, depending on the rate of profile change, proved best. An opaque acetate paper on which millimeter grid lines were printed was adhered to the flume sidewall. Both bed and water surface profiles at the sidewall could be photographed through this paper which imprinted an accurate x - y grid. Slides taken by this method were projected onto paper and bed profiles traced. These traces were then digitized with the ERDAS geographical information system to store the x, y, t coordinates of the bed profiles. These data are used to determine bed profiles, volume of eroded material, and maximum depth of scour in the impingement region at instantaneous times.

Chapter 5

Results and Discussion

This Chapter details the results of experimental program of this study. Three sets of experiments were conducted in the flume described in Chapter 4. The first set of runs had a cohesive soil bed material with no headcut and was used to determine the critical shear stress and calibrate the sediment detachment equation for this bed material. The second set was used to determine the scour characteristics in the impingement region independent from any upstream scour. The main parameters measured are the changes in scour depth and volume with time, sediment concentration at the flume exit and the ultimate depth of scour. The third set of runs allowed the headcut to retreat and are used to validate the headcut stability analysis.

5.1 Calibration of the Sediment Deattachment Equation

Three terms of Equation 2.10 τ_c , K_1 and K_2 must be determined from experiment to determine sediment detachment of cohesive soil. Seventeen runs with different combinations of slope and discharge were conducted on one typical cohesive soil described in Chapter 4, but two of these (the CS6 set) were dropped from the analysis for reasons to be discussed below. Details of the experimental procedure for

these runs is given in Section 4.3.2. A summary of the measured hydraulic parameters is presented in Table 5.1.

Table 5.1: Hydraulic Parameters of Constant Slope Runs

Run	q (m^2/s)	S_b	h_{nM} (cm)	h_{nP} (cm)	R_e	F_r	τ_n (PA)
CS1A	0.00330	0.010	0.85	0.76	2357	1.58	0.75
CS1B	0.00330	0.023	0.61	0.58	2357	2.39	1.31
CS1C	0.00330	0.037	0.49	0.49	2357	3.03	1.79
CS2A	0.00470	0.010	0.98	0.94	3357	1.65	0.92
CS2B	0.00470	0.023	0.73	0.71	3357	2.50	1.61
CS2C	0.00470	0.037	0.64	0.61	3357	3.17	2.20
CS3A	0.00770	0.010	1.31	1.25	5500	1.75	1.23
CS3B	0.00770	0.023	1.25	0.95	5500	2.66	2.14
CS3C	0.00770	0.037	0.98	0.81	5500	3.37	2.94
CS4A	0.00050	0.010	0.21	0.28	357	1.09	0.27
CS4B	0.00050	0.023	0.14	0.21	357	1.65	0.47
CS4C	0.00050	0.037	0.14	0.18	357	2.10	0.65
CS5A	0.00127	0.010	0.34	0.38	907	1.74	0.37
CS5B	0.00127	0.023	0.31	0.29	907	2.64	0.65
CS5C	0.00127	0.037	0.21	0.24	907	3.34	0.89
CS6A	0.00480	0.010	0.91	0.95	3429	1.65	0.93
CS6B	0.00480	0.052	0.67	0.55	3429	3.77	2.80

Discharge varied from 0.00050 to 0.00770 m^2/s , slope from 1.0 to 3.7%, Reynolds number from 357 to 5500 and Froude number from 1.09 to 3.34. Flow therefore was always supercritical and was either laminar or turbulent for a given run. Predicted depths h_{nP} were calculated from either Eq. 3.11 from Blasius or Eqs. 3.7

and 2.5 with the laminar flow assumption for f , depending on Reynolds number. Shear stress was determined from the predicted depth and Eq. 3.10.

The experimental procedure produced a very smooth soil surface and the Blasius assumption seemed more appropriate than Manning's for turbulent flow (runs CS1-CS3,CS6). The maximum error between measured h_{nM} and predicted h_{nP} flow depths was 31.7% and the average absolute value error was 9.6%. This error is more likely due to measurement techniques than to the appropriateness of the Blasius assumption. The maximum and average error when the flow was clearly laminar (runs CS4-CS5) is greater, 34.9% and 18.8% respectively. However, the measured flow depths were so small that this error can be attributed to measurement error and the laminar flow assumption may still be considered valid.

The two runs of the set CS6 (corresponding to one flume packing) were eliminated from the sediment detachment analysis. During the set-up procedure the soil for these runs was saturated more quickly than other runs, causing the soil to swell about 1.5 cm vertically. The bed elevation was re-leveled but the swelling changed the soil properties, especially bulk density considerably. The measured sediment concentration and therefore sediment detachment was much larger than expected, however it was felt this increase was attributable to the soil swelling disturbance, did not represent the same conditions as other runs and was therefore dropped from the analysis.

Measured sediment concentration for all runs of the CS1-CS3 series displayed a time dependency. The maximum sediment concentration was always the first measurement taken within a run and consistently decreased with time. A

characteristic sediment concentration for each run was determined by curve fitting and determining the value of concentration at 60 seconds into the run. The CS4 and CS5 series, with the smallest shear stresses and sediment concentration did not display this time dependency. A simple average of all measured values was used to determine the sediment concentration for these runs.

Measured sediment concentrations were converted to sediment detachment rate measured as mass per unit area per time by dividing by the total flume area and multiplying by the total discharge and density of water. The sediment concentration and calculated sediment discharge data for each run is given in Appendix A. A plot of calculated sediment discharge versus predicted shear stress for each run is given as Fig. 5.1. Critical shear stress $\tau_c = 0.32$ Pa is taken as the x intercept. Sediment detachment appears to be linearly related to shear stress above the critical shear stress value for the range measured. This differs from many non-cohesive sediment transport equations but is an assumption currently popular for cohesive sediment detachment (Nearing et al. 1988,1989.).

Linear regression of the data in Fig. 5.1 was used to determine the constants of Eq. 2.10. The result with an $R^2 = 0.90$ is the solid line in Fig. 5.1 and given as Eq. 5.1.

$$q_s = 0.0258 \left[\tau \left(1 - \frac{0.32}{\tau} \right) \right]^{1.0} \quad (5.1)$$

This equation should only be considered an approximation of a differential form of a sediment detachment equation. No attempt was made to separate sediment detachment and sediment transport at any point along the flume channel,

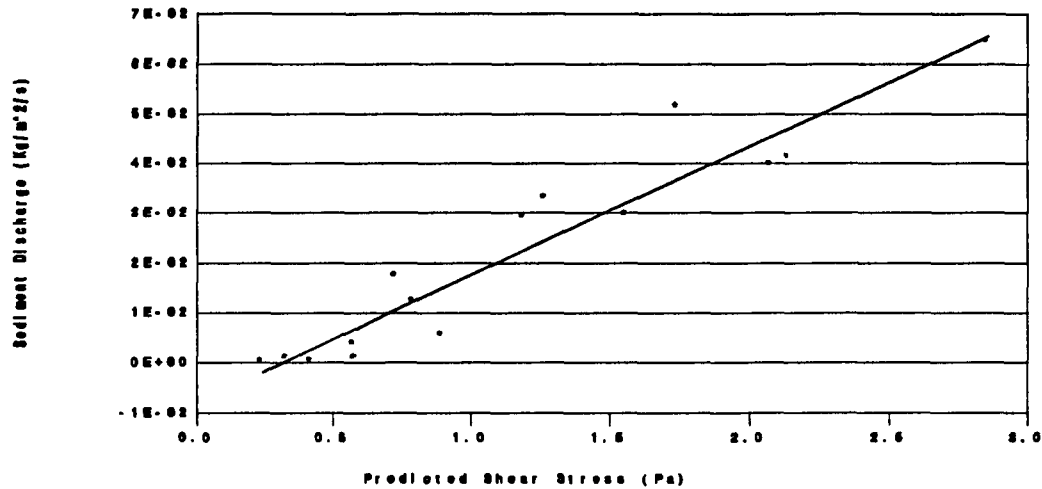


Figure 5.1: Sediment Discharge vs. Shear Stress; Constant Slope Runs

both were averaged over the entire erosional surface. The highest shear stress values in Fig. 5.1 represent the largest slopes. Because these data points are from the third in a set of three runs from one flume packing and therefore collected from a previously disturbed bed, a reduction in sediment detachment from what would otherwise have occurred is possible. This unavoidable bias is represented in Eq. 5.1. Despite these limitations this equation, being the best available, is used to determine the bed degradation in all regions which have cohesive soil.

5.2 Non-Retreating Headcut Runs

These runs had a plexiglas plate over the entire bed upstream from a simulated headcut, preventing any erosion. Flow from above the headcut produced a jet which impinged on three different saturated bed materials, a cohesive soil (Runs 1-4, 6-13; a total of ten different discharge and drop height combinations) and two sands, one with $d_{50} = 1.5\text{mm}$ hereafter called large sand (Runs 14-21; a total of eight

discharge and drop height combinations) and another with $d_{50} = 0.15\text{mm}$ hereafter called small sand (Runs 22-27; a total of six discharge and drop height combinations). Equations 3.33 and 3.34 were used to determine properties of the jet at impingement.

A summary of the measured hydraulic parameters is presented in Table 5.2. Discharge varied from 0.00154 to 0.00493 m^2/s , slope was held constant at 3.7%, Reynolds number varied from 1100 to 3521 and Froude number from 2.76 to 3.19. Flow therefore was always supercritical and was turbulent or near the border between laminar and turbulent for a given run. Predicted depths were calculated from Eq. 3.11 and shear stress from Eq. 3.12, based on the Blasius assumption for flow resistance. The laminar flow assumption was tried for Reynolds number below 2000, however it did not improve the measured versus predicted flow depths. All flow depth measurements were taken on the upstream plexiglas plate therefore the Blasius assumption for turbulent flow clearly applies. The maximum flow depth error is 39.4% and the absolute value average error is 9.6%, similar to the constant slope runs.

Longitudinal cross-sections of the scour progression with time were taken for all non-retreating headcut runs with the photographic technique described in Chapter 4. Photographs of profiles at three representative times for a typical non-retreating soil run (Run 10) are reproduced in Figs. 5.2 and 5.3. The times of these representative profiles are 0:00, 1:00, 1:00:00, 2:30:00. Similar profiles at 0:00, 1:05, 9:00 and 2:30:00 for a non-retreating sand run (Run 25) are shown in Figs. 5.4 and 5.5.

These and other photographs were digitized to provide x,y,t coordinates of the scour progression with time. Typically between 30 and 40 photographs were digitized

Table 5.2: Hydraulic Parameters of Non-Retreating Headcut Runs

Run	q (m^3/s)	S_b	h_{nM} (cm)	h_{nP} (cm)	R_c	F_r	τ_n (PA)
1	0.00224	0.037	0.55	0.39	1600	2.89	1.43
2	0.00236	0.037	0.46	0.41	1686	2.91	1.48
3	0.00226	0.037	0.34	0.40	1614	2.89	1.44
4	0.00225	0.037	0.34	0.40	1607	2.89	1.43
5	0.00264	0.037	0.46	0.43	1886	2.95	1.57
6	0.00450	0.037	0.64	0.59	3214	3.15	2.15
7T	0.00154	0.037	0.28	0.32	1100	2.76	1.15
8T	0.00172	0.037	0.32	0.34	1229	2.79	1.23
9	0.00458	0.037	0.67	0.60	3271	3.16	2.17
10	0.00354	0.037	0.55	0.51	2529	3.06	1.87
11	0.00346	0.037	0.56	0.51	2471	3.05	1.84
12	0.00489	0.037	0.70	0.62	3493	3.19	2.26
13T	0.00157	0.037	0.33	0.32	1121	2.76	1.16
14T	0.00168	0.037	0.31	0.33	1200	2.79	1.21
15	0.00235	0.037	0.40	0.41	1679	2.91	1.47
16	0.00353	0.037	0.55	0.51	2521	3.06	1.87
17	0.00480	0.037	0.70	0.61	3429	3.18	2.23
18	0.00493	0.037	0.70	0.62	3521	3.19	2.27
19	0.00347	0.037	0.55	0.51	2479	3.05	1.85
20	0.00257	0.037	0.43	0.43	1836	2.94	1.55
21T	0.00162	0.037	0.31	0.33	1157	2.77	1.18
22	0.00166	0.037	0.31	0.27	1186	3.82	0.97
23T	0.00166	0.037	0.31	0.33	1186	2.78	1.20
24	0.00349	0.037	0.56	0.51	2493	3.05	1.85
25	0.00337	0.037	0.54	0.50	2407	3.04	1.82
26	0.00242	0.037	0.41	0.41	1729	2.92	1.50
27T	0.00175	0.037	0.31	0.34	1250	2.80	1.24

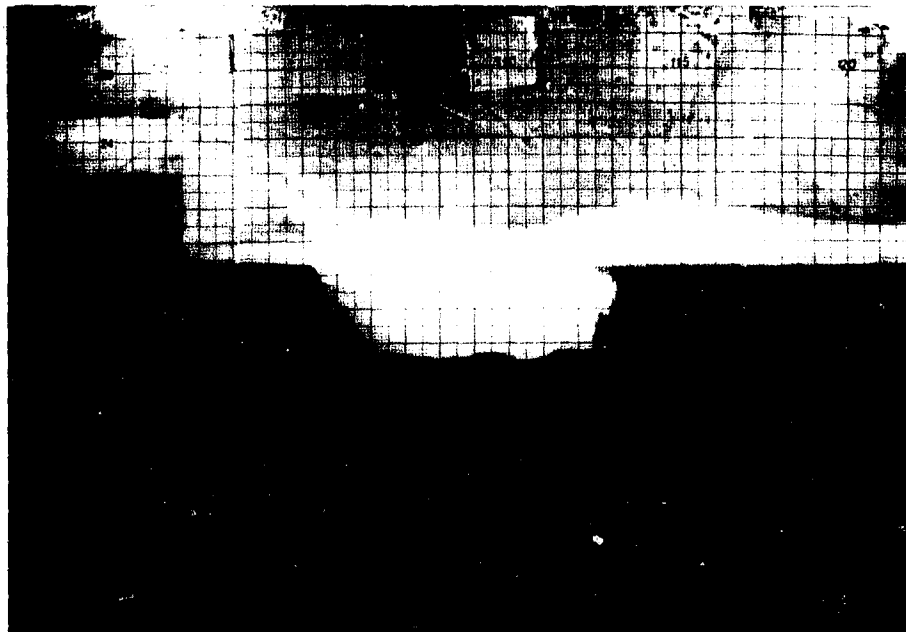
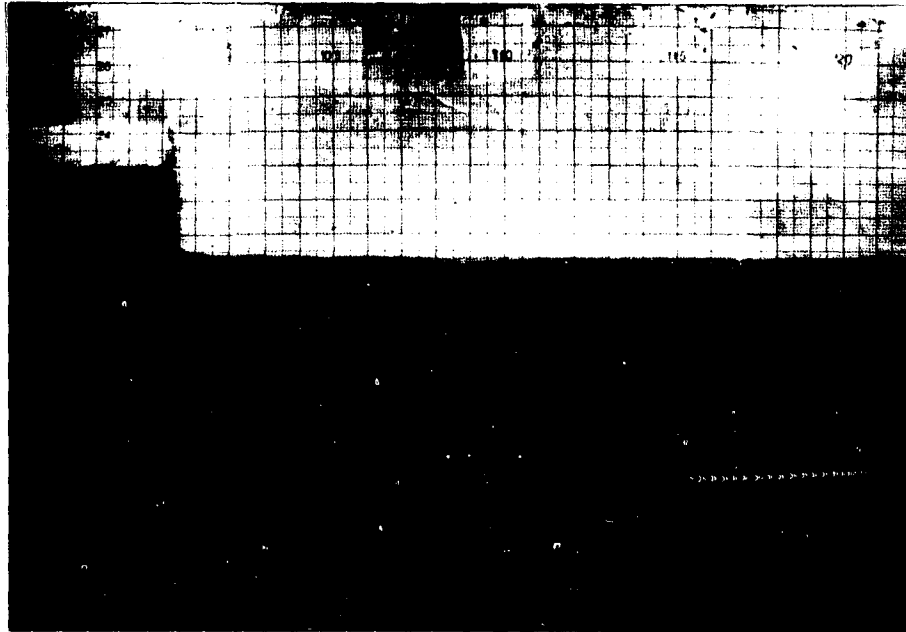


Figure 5.2: Typical Scour Profiles From Cohesive Soil

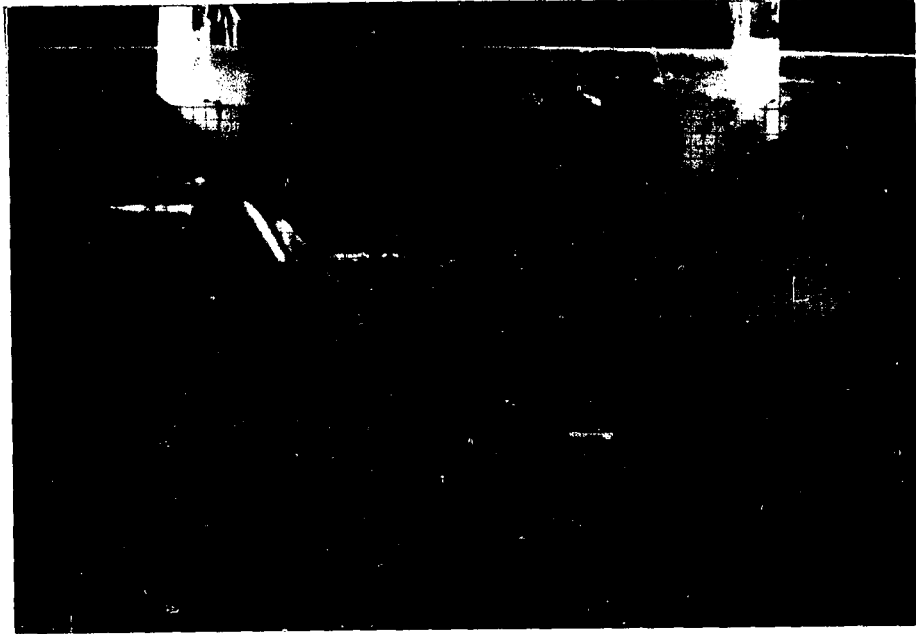


Figure 5.3: Typical Scour Profiles From Cohesive Soil

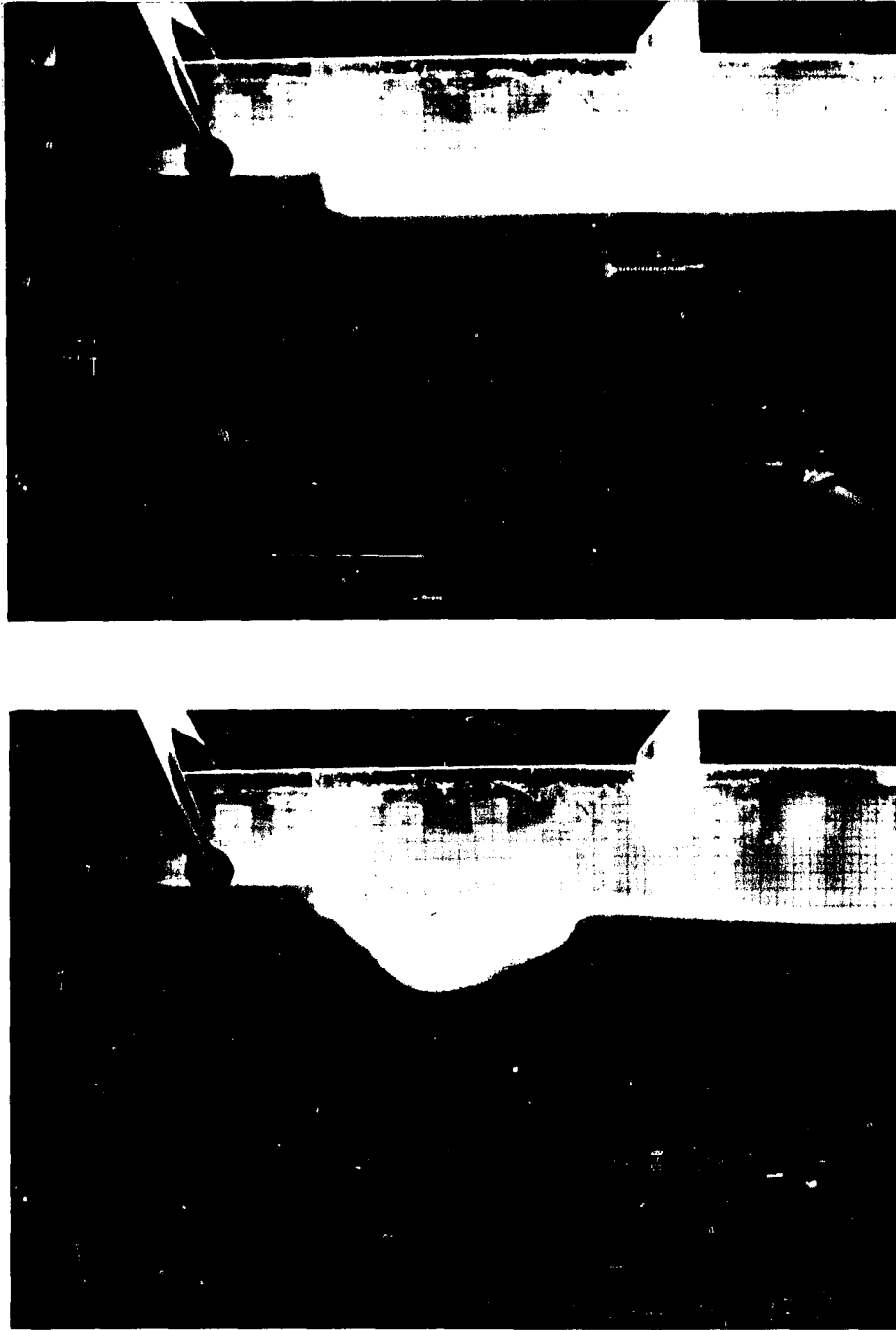


Figure 5.4: Typical Scour Profiles From Sand $d_{50} = 0.15\text{mm}$

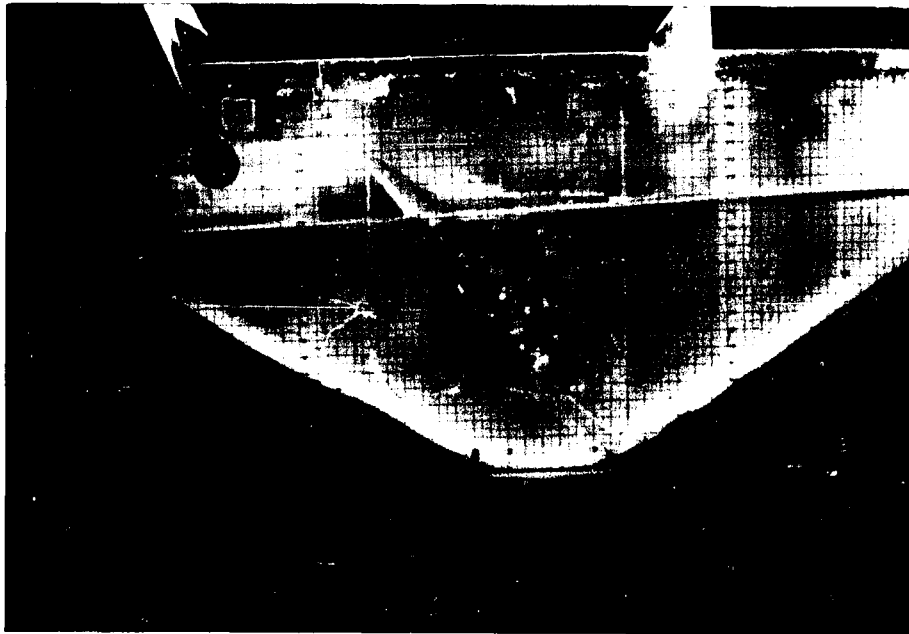
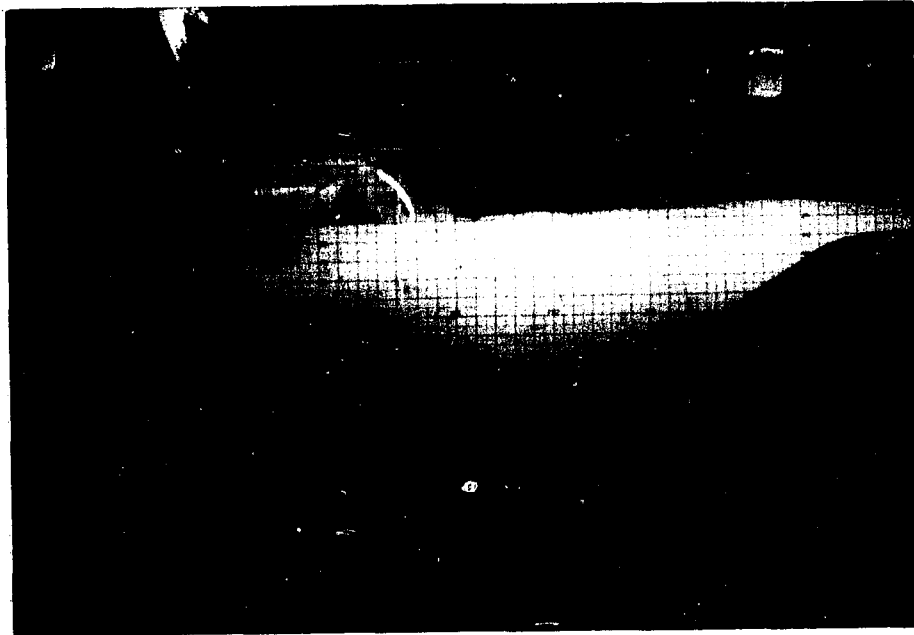


Figure 5.5: Typical Scour Profiles From Sand $d_{50} = 0.15\text{mm}$

for each run. Appendix B contains the resulting profile plots for all runs, and Appendix C contains the x,y,t coordinate of the maximum scour depth for each profile and run. The resulting plots for Runs 10 and 24 are also shown in Figs. 5.6 and 5.7. Total scour time for both runs is 2.5 hours. Time steps between lines in Figs. 5.6 and 5.7 are not equal and are dependant on the time interval between the digitized slide data. Time intervals are ten seconds for the uppermost lines and increase to ten minutes for the deepest scour lines. These figures show scour rate is most rapid at early times and decreases with increasing time. As expected, this was the case for all runs.

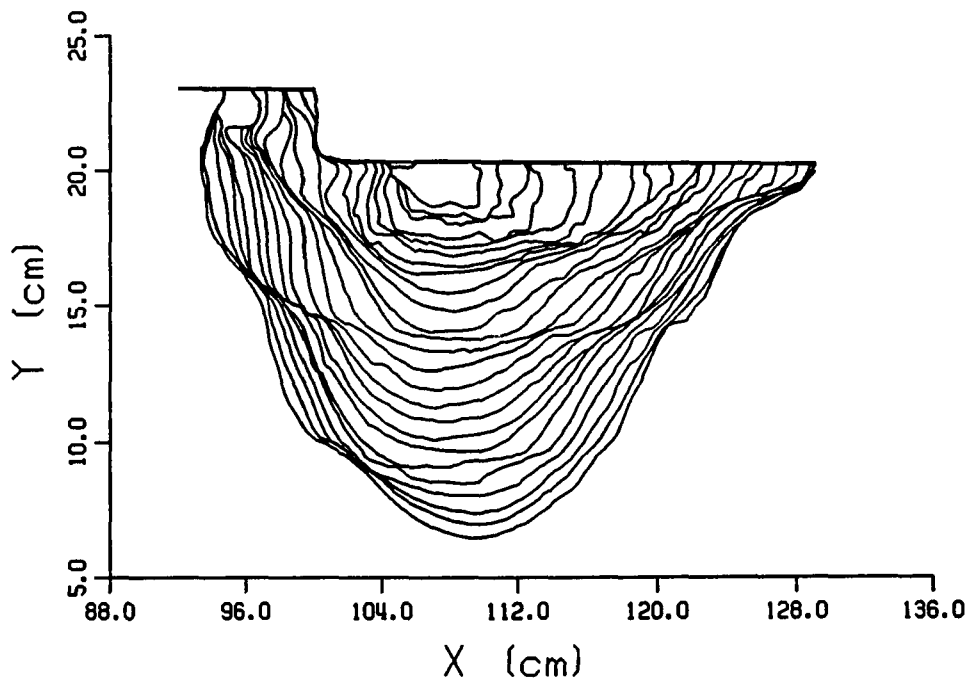


Figure 5.6: Typical Scour Progression With Time; Cohesive Soil

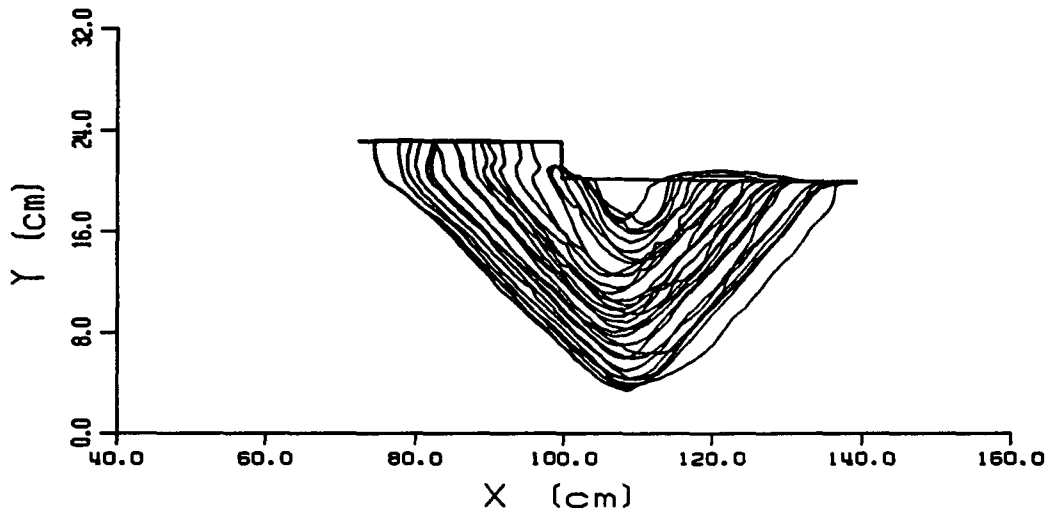


Figure 5.7: Typical Scour Progression With Time; Sand $d_{50} = 0.15\text{mm}$

Despite the efforts to minimize the heterogeneity of the cohesive soil, changes in the critical shear stress are apparent from the scour profiles of Fig 5.6. At repeating intervals of about 5 cm, corresponding to the layers of the set-up procedure, the scour hole erodes much wider for a given depth. After some time, the depth of scour once again increases relative to width. Apparently the resisting shear strength of the soil gradually increases with depth within a layer and decreases sharply as a new layer is breached. All runs with soil displayed this characteristic to some degree (Fig. 5.6 more pronounced), but as shown in Fig. 5.7 it was not observed in any runs with sand.

The total volume of eroded material at any time is strongly correlated to the maximum scour depth at that time, but the relationship is unique for each bed material. The slope of the scour hole profile approaches the submerged angle of repose for the sand runs but, due to the cohesive nature of the soil, slopes for these

runs tended to be more vertical. More scatter in the depth-volume relationship for these runs was observed as well, due to the layering effect described above.

The profile shape is approximately symmetrical about the maximum depth of scour with a slight skewness in the downstream direction for all runs. Maximum depth of scour is in the vicinity of the calculated centerline of the impinging jet, but unlike results of Yuen (1984) and as predicted by Schauer and Eustis (1963), this maximum is consistently shifted in the upstream direction. Equation 2.21 from Schauer and Eustis (1963), however, did not accurately predict the shift which for some runs was very small.

5.2.1 Ultimate Depth of Scour

Most previous research on non-cohesive scour from jets has focused on this parameter despite the questionable validity this concept. As discussed in Chapter 3, the most theoretically guided predictive equations can be simplified to Eq. 3.37. The validity of this equation was tested using the non-retreating headcut runs. Bormann's equation (Eq. 2.29) was used without modification for non-cohesive sands while Eq. 3.37 with $\tau_c = 0.32$ Pascal was used for the cohesive bed material. A value of 2.6 was taken for the diffusion constant C_d . This value is higher than used by Bormann (1.8-2.3) but is lower than that given by Beltaos (2.72) for diffusion in the impingement region. Bormann's experiments often had a poorly defined jet and Beltaos' were for a plane impervious boundary. The jet in these experiments was well defined but boundaries are neither plane (except for $t=0$) nor impervious.

Table 5.3: Experimentally Varied Parameters for Ultimate Scour Depth

Run	D_b (cm)	q (m^3/s)	U_o (m)	Y_o (m)	χ ($^\circ$)	D_{mP} (cm)	D_{mM} (cm)
13	1.0	0.00157	0.6818	0.0023	40.51	6.8	7.7
12	1.0	0.00489	0.9339	0.0052	28.31	15.9	11.2
7	2.0	0.00154	0.8105	0.0019	50.60	9.4	8.1
3&4	2.0	0.00225	0.8672	0.0026	46.24	12.5	8.4
11	2.0	0.00346	0.9500	0.0036	41.25	17.3	13.0
6	2.0	0.00450	1.0120	0.0044	38.24	21.1	12.2
8	4.0	0.00172	1.0363	0.0017	58.73	14.5	11.9
1&2	4.0	0.00230	1.0727	0.0021	55.66	18.0	10.8
10	4.0	0.00354	1.1420	0.0031	50.86	24.9	12.8
9	4.0	0.00458	1.1939	0.0038	47.89	30.2	14.2
21	2.0	0.00162	0.8173	0.0020	50.03	4.7	4.5
20	2.0	0.00257	0.8905	0.0029	44.70	6.3	5.8
19	2.0	0.00347	0.9506	0.0037	41.21	7.6	7.3
18	2.0	0.00493	1.0358	0.0048	37.21	9.6	8.2
14	4.0	0.00168	1.0337	0.0016	58.97	6.8	3.8
15	4.0	0.00235	1.0757	0.0022	55.43	8.3	5.7
16	4.0	0.00353	1.1415	0.0031	50.89	10.6	7.4
17	4.0	0.00480	1.2043	0.0040	47.35	12.9	9.7
22	2.0	0.00166	0.8206	0.0020	49.75	9.9	10.3
23	2.0	0.00232	0.8724	0.0027	45.89	12.2	13.2
24	2.0	0.00349	0.9518	0.0037	41.15	16.1	16.3
27	4.0	0.00175	1.0383	0.0017	58.55	14.0	13.4
26	4.0	0.00242	1.0799	0.0022	55.11	17.2	16.2
25	4.0	0.00337	1.1331	0.0030	51.42	21.2	17.5

The various parameters needed in Eqs. 2.29 and 3.37 are given in Table 5.3. The measured maximum depths are compared to predicted in Fig. 5.8. For depths less than 15 cm, agreement is generally good though measured values are consistently less than predicted, a conservative estimate. The error seems consistent for scour depths from about 5 to 15 cm and, at least for the large sand case, can be attributed to measurement error. The ratio of sediment size to scour depth is as high as 0.05 for the large sand, indicating as much as 5% error at the lowest predicted depths.

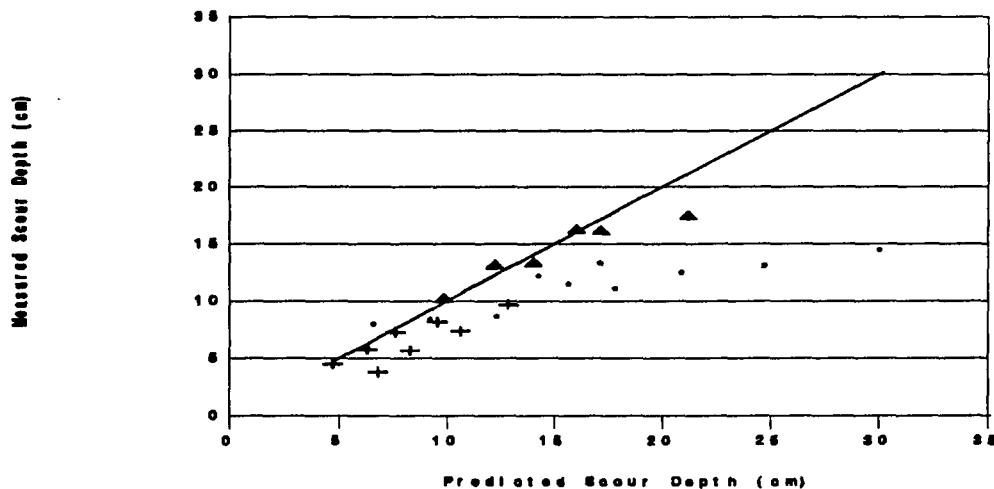


Figure 5.8: Predicted vs Measured Scour Depths

For predicted depths greater than about 15 cm, measured values become increasingly less than predicted. However the maximum measurable values in this experimental flume varied from 15 to 20 cm depending on drop height and bed material. Clearly several data points lie beyond this range. For the largest predicted value (Run 9), the maximum measurable depth was reached in only 67 minutes, while depth was clearly still increasing. Another possible reason for the conservative estimate is that the longest run time was 2.5 hours and most previous research

indicates this is too short for an ultimate depth to be reached. However the data for the sand runs presented in the next section shows measurable scour proceeds imperceptibly at the longest measured times.

5.2.2 Change in Scour Depth and Volume With Time

The non-retreating headcut runs are designed to determine the time rate of scour in the impingement region created by an impinging jet independent from upstream scour. Chapter 3 shows scour depth increases as two distinct functions of time depending on scour depth magnitude. For a short period of time from the initiation of scour, corresponding to the time the bed elevation is within the jet potential core, scour rate is constant with time. For times longer than this time T_p , the scour rate decreases with time and can be determined from either Eq. 3.4 developed from dimensional analysis or Eq. 3.44 developed from sediment detachment and jet diffusion. These equations were shown to be quite similar but the form of Eq. 3.44 suggests that D / D_p and t / T_p , rather than D / D_u and $t U_o / y_o$ as developed from Eq. 3.4, may be used to normalize data. The usage of these parameters would more clearly show the break between scour within the potential core and beyond. The normalizing parameters from either method and for all runs are given in Table 5.4.

Reynolds number is seen to vary from 1100 to 3521, Froude number defined at the point of impingement from 4.12 to 8.19, the quantity (U_o / y_o) from 178.4 to 636.0. These parameters are needed in Eq. 3.4. Rather than include sediment detachment as another variable in Eq. 3.4, each bed material is evaluated separately.

Table 5.4: Normalizing Parameters for Maximum Scour Depth

Run	R_e	F_r	U_o / y_o (1/s)	T_p (s)	D_p (m)	τ_c (PA)
13	1121	4.54	296.1	267.6	0.0101	0.32
12	3493	4.12	178.4	299.8	0.0168	0.32
7	1100	5.94	426.5	176.2	0.0099	0.32
3&4	1607	5.44	334.2	215.0	0.0127	0.32
11	2471	5.03	260.8	253.7	0.0162	0.32
6	3214	4.85	227.6	272.0	0.0186	0.32
8	1229	8.12	624.4	102.7	0.0096	0.32
1&2	1643	7.40	500.3	128.7	0.0120	0.32
10	2529	6.55	368.4	171.5	0.0163	0.32
9	3271	6.16	311.2	197.8	0.0192	0.32
21	1157	5.86	412.3	1.9	0.0103	1.14
20	1836	5.29	308.5	2.2	0.0137	1.14
19	2479	5.02	260.4	2.3	0.0163	1.14
18	3521	4.79	217.6	2.3	0.0195	1.14
14	1200	8.19	636.0	0.7	0.0094	1.14
15	1679	7.35	492.4	0.8	0.0122	1.14
16	2521	6.55	369.1	1.1	0.0162	1.14
17	3429	6.09	302.2	1.3	0.0198	1.14
22	1186	5.83	405.7	0.4	0.0104	0.11
23	1657	5.40	328.0	0.4	0.0129	0.11
24	2493	5.02	259.6	0.5	0.0163	0.11
27	1250	8.08	616.0	0.2	0.0097	0.11
26	1729	7.28	481.9	0.2	0.0124	0.11
25	2407	6.63	381.0	0.3	0.0157	0.11

The term T_p , defined in Eq. 3.39 is dependent on the sediment detachment rate which varies for different bed materials. However, the calibrated sediment detachment equation (Eq. 5.1) only applies to the cohesive soil. The Meyer-Peter sediment transport equation (see Simons and Senturk, 1977) can be converted to a sediment detachment equation by integrating over the initial jet thickness. This assumes the incoming jet is clear water and the entire transport capacity is filled at the point of maximum scour. For all experimental runs the first point is met, but the second can only be considered an approximation. Note also that the exponent K_2 has a value of 1.5 and the solutions to Eq. 3.41 previously presented are not valid. Using this modified Meyer-Peter detachment equation to determine T_p for the sand runs results in very small values. No profiles were measured within this time frame.

Using Eq. 3.4 developed from dimensional analysis as a model, arithmetic plots of maximum scour depth normalized to ultimate scour depth $D/D_u = D$ versus normalized time $t U_o / y_o = T$, are given for eight large sand runs in Fig. 5.9, six small sand runs in Fig. 5.10 and for ten soil runs in Fig. 5.11. These data are collected using the photographic technique described in Chapter 4 and allows more points in a relatively short time to be collected than in any previous study on the time progression of jet scour. The x,y,t coordinates of the maximum depth of scour for all runs is given in Appendix C.

As previously mentioned, errors in measurement of scour depth for the large sand can be significant due to the large sediment size to scour depth ratio explaining the small decreases in scour depth with time which occasionally occur. The bench-

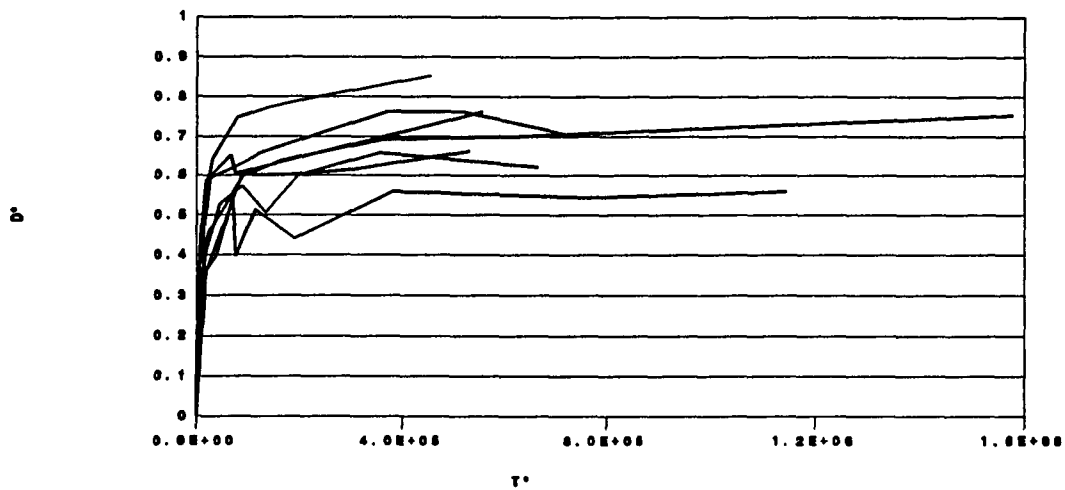


Figure 5.9: Normalized Scour Depth vs Normalized Time; Large Sand

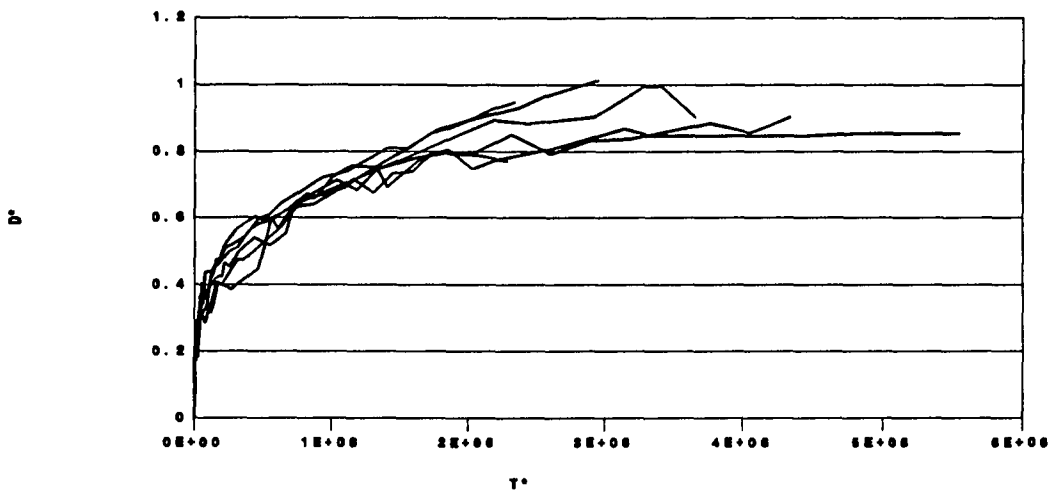


Figure 5.10: Normalized Scour Depth vs Normalized Time; Small Sand

like increase observed for some cohesive soil runs is probably due to the breaching of layers described previously.

All runs appear to asymptotically approach the ultimate scour depth but with considerably more scatter for large sand and cohesive soil, however, these plots do not include the effect of either Froude or Reynolds numbers, the additional parameters of Eq. 3.4 if sediment detachment is held constant. There is very little

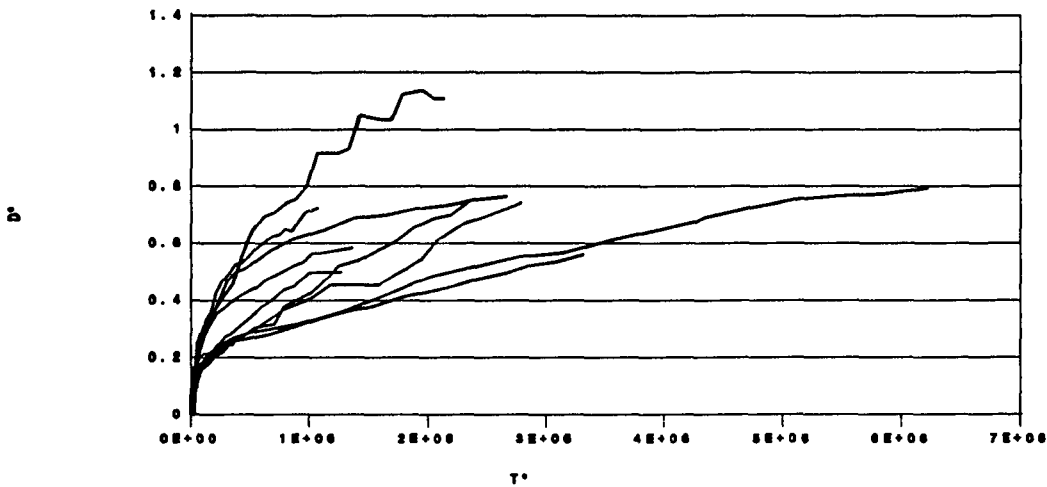


Figure 5.11: Normalized Depth vs Normalized Time; Cohesive Soil

scatter for small sand runs indicating the time scale is the only independent variable affecting depth of scour. Both the large sand and soil appear to have two major branching arms. Table 5.4 shows Reynolds number does not vary significantly but the impingement Froude number which is dependent on drop height has two distinct ranges and may explain the data separation as described below. Log-log regression of Eq. 3.4 with sediment detachment included in the experimental constant yields Eqs. 5.2 for large sand ($R^2 = .81$), 5.3 for small sand ($R^2 = .96$) and 5.4 for soil ($R^2 = .85$). All measured values for times less than T_p are eliminated from the regression analysis as Eq. 3.4 is not applicable for these times.

$$\frac{D}{D_u} = 1.111 F_r^{-0.931} T_p^{0.188} \quad \text{Large Sand (5.2)}$$

$$\frac{D}{D_u} = 0.01933 T_*^{0.258} \quad \text{Small Sand (5.3)}$$

$$\frac{D}{D_u} = 0.00666 F_r^{-0.840} T_*^{0.417} \quad \text{Cohesive Soil (5.4)}$$

The inclusion of Reynolds number in the above equations did not increase the accuracy of the predictions confirming that the effect of Reynolds number is insignificant within the range measured, as suspected from Figs. 5.9-11. This observation was also noted by Rajaratnam (1981). Also as expected from Fig. 5.10, the impingement Froude number did not increase the accuracy for the small sand prediction. Impingement Froude number affects the length of time the bed is within the potential core. Equation 3.39 shows that T_p is proportional to $1/F_r$. Therefore as Froude number decreases, scour rate is independent of time for a longer period of time. This can be seen as a vertical shifting of the curves in Figs. 5.9 and 5.11 for decreasing Froude number. However for the small sand, sediment detachment is so rapid and therefore T_p so small that its influence measured as a Froude number is insignificant.

Equations 5.2 through 5.4 show that the power form does approximate the relation between scour depth and time for the time periods measured. The semi-log relationship often used in previous research gives a very poor fit to the present data, as expected from Eq. 3.44. Deviations from the power form can be expected for long periods of time as the scour depth approaches the ultimate scour depth and shear stress approaches the critical shear stress. This can be seen in Fig. 5.12, a plot of the

small sand measured versus predicted (Eq. 5.3) scour depths. If either the predictive equation or the data trend is extrapolated to long times, depth will increase beyond the predicted ultimate scour depth, an impossibility. However, Eq. 3.44 is undefined when depth equals the ultimate depth and large deviations can be expected. The arithmetic plot of the same data in Fig. 5.12 shows the scour rate will be quite small when depth is near the ultimate depth.

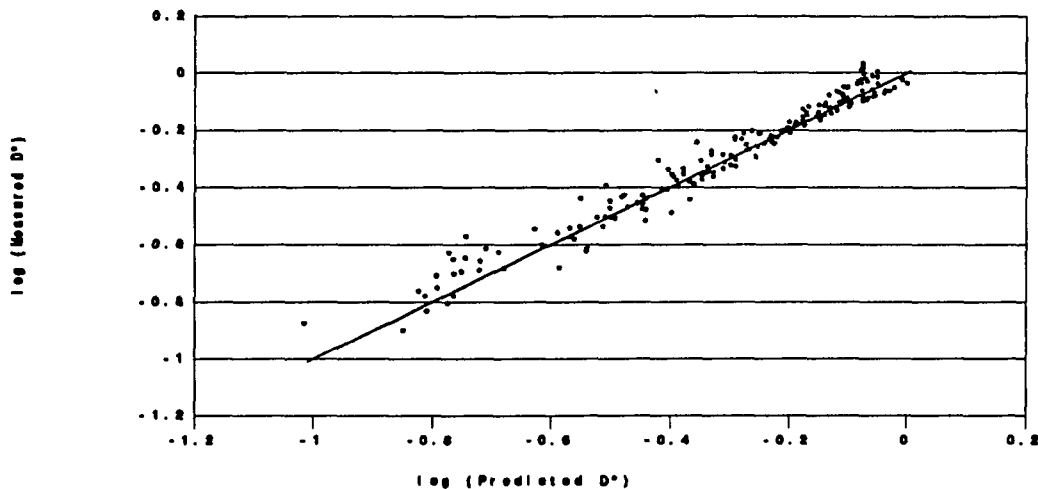


Figure 5.12: Measured vs Predicted Scour Depth with Time; Small Sand

The same data as plotted above can be normalized to the terms D_p and T_p to show the break between scour in the potential core and beyond. However as seen from Table 5.4, T_p is very small for the sand runs and no data was collected for times less than T_p . Figure 5.13 shows D/D_p vs t/T_p for the ten soil runs. From this plot it appears that the value for D_p from Eq. 3.40 fits the data quite well, however, Eq. 3.39 seems to underestimate T_p if Eq. 5.1 is used as the sediment detachment equation.

The digitized data can also be used to determine the volume of eroded

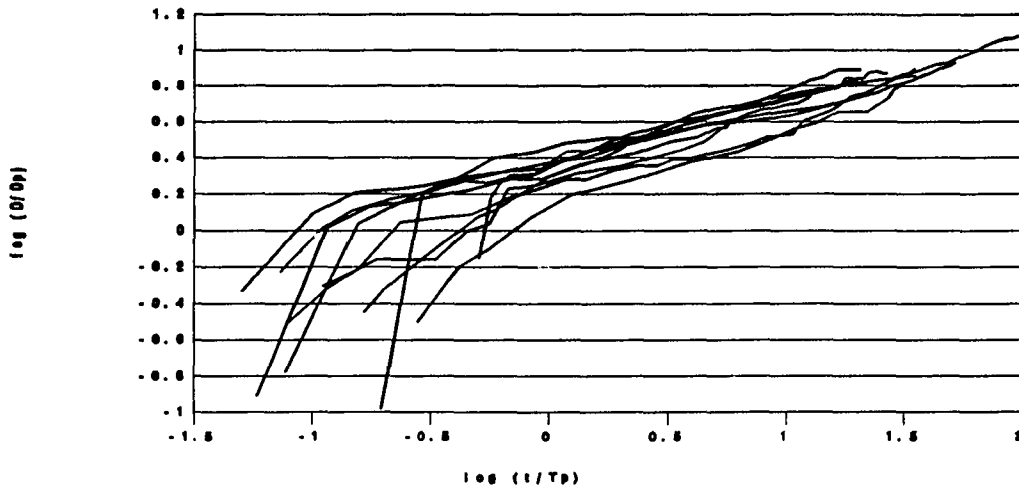


Figure 5.13: Scour Depth vs Time; Soil Runs

material. For all bed materials, the scour volume at any time is strongly correlated to the square the maximum scour depth at that time, however this function is not constant with time or between bed materials. The scour volume of non-cohesive sand is controlled by the sediment angle of repose which is in turn related to sediment size, therefore different bed materials should have different volume to depth ratios. Also as the scour depth increases the proportionate volume of eroded material necessary to increase the depth further increases therefore volume increases more rapidly than depth at long times. The relation between volume per unit width and scour depth for soil is given in Eq. 5.5.

$$\frac{vol}{D_u^2} = e^{0.453 + 1.651 \left(\frac{D}{D_u} \right)} \quad (5.5)$$

5.2.3 Sediment Concentration

For all runs sediment concentration C decreases with T_* . This would be expected as sediment concentration is inversely proportional to the change in scour volume with time. Measured concentration values with time are given in Appendix A. Values were as high as 4.9% (large sand runs) by weight during the initial seconds. The lowest measured values were less than 0.02% (cohesive soil).

Equations 5.6 through 5.8 show the relation between C , T_* and F_r for the large sand ($R^2 = .95$), small sand ($R^2 = .83$) and cohesive soil ($R^2 = .79$).

$$C = 24.378 F_r^{2.267} T_*^{-1.144} \quad \text{Large Sand (5.6)}$$

$$C = 0.199 F_r^{2.315} T_*^{-0.620} \quad \text{Small Sand (5.7)}$$

$$C = 0.0360 F_r^{1.438} T_*^{-0.417} \quad \text{Cohesive Soil (5.8)}$$

As was the case for depth of scour, all values for times less than T_p were eliminated from the analysis. However, because there was approximately one meter of channel between the scour hole and the flume exit where sediment concentration was measured, there exists a time lag between actual scour and concentration measurement. Also for the runs with sand especially the small sand, sediment detachment in the scour hole exceeded the downstream sediment transport capacity. Evidence of this can be seen at early times in Fig. 5.7 as small mound just downstream from the scour hole. This mound was later washed away as the scour rate in the hole decreased to below the downstream sediment transport capacity of the channel. Therefore, measured concentration values for T_* less than 10,000, which is greater than T_p , do not reflect actual scour and were eliminated for the analysis.

Figure 5.14 shows the measured versus predicted data for eight different drop height-flow rate combinations on the large sand. The ratio U_o / Y_o ranges from 222 to 637 s^{-1} . All measured points, including those that were eliminated, are shown.

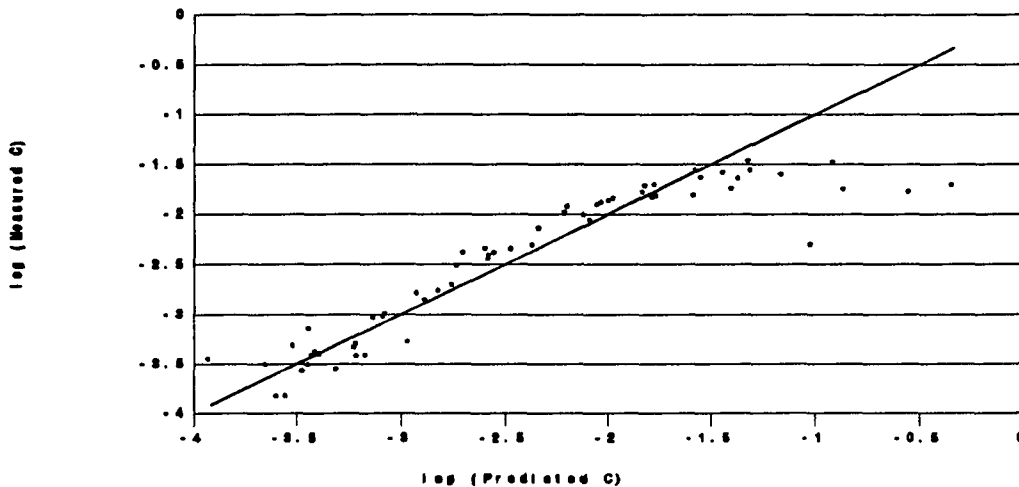


Figure 5.14: Predicted vs Measured Sediment Concentration; Large Sand

Figure 5.15 shows the measured versus predicted data for six different drop height-flow rate combinations on the small sand. The ratio U_o / Y_o ranges from 263 to 618 s^{-1} . While not as pronounced as for the case with the larger sand, measured concentrations are still less than predicted at T^* less than about 10,000 and were excluded from the analysis but are shown.

Figure 5.16 summarizes data for ten different drop height-flow rate combinations on the cohesive soil. The ratio U_o / Y_o ranges from 183 to 626 s^{-1} .

Comparison of the regression equations (Eqs. 5.6- 5.8) shows that the rate of decrease in concentration with time increases with sediment size, especially between sand sizes $d_{50} = 0.15$ and 1.5mm. The cohesive soil, with the smallest mean diameter, has the slowest decay but is similar to the smaller sand size. The maximum predicted

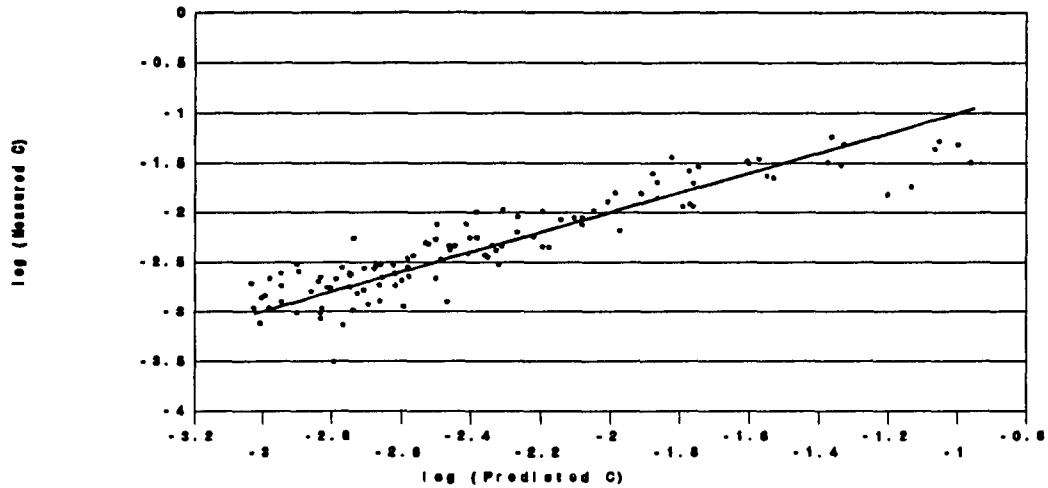


Figure 5.15: Predicted vs Measured Sediment Concentration; Small Sand

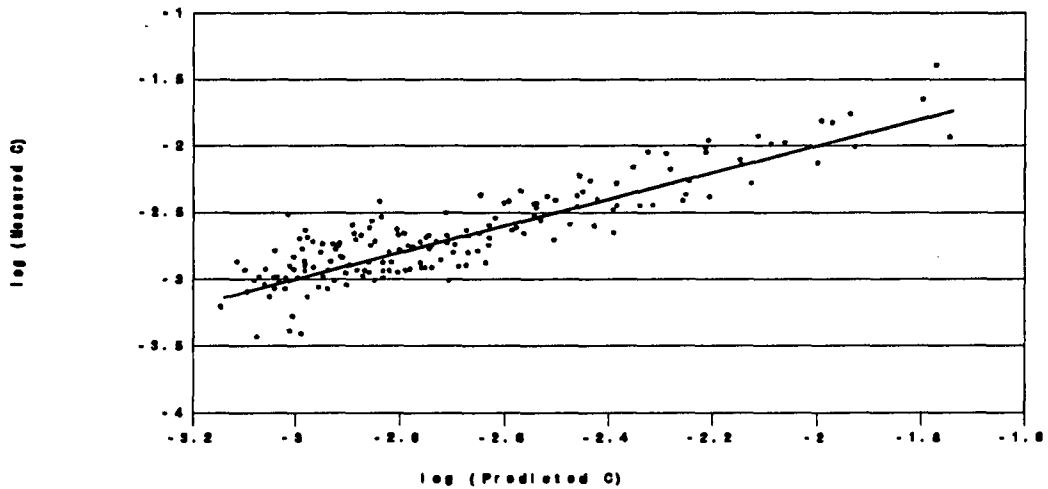


Figure 5.16: Measured vs Predicted Sediment Concentration; Cohesive Soil concentrations show a marked decrease with a decrease in sediment size, however as noted above, the equations for sand overestimate concentration at early dimensionless times ($T^* < 10,000$). Initial measured concentrations decrease slightly with a decrease in sediment size and varied from about 5 to 1%.

5.3 Retreating Headcut Runs

A total of thirteen runs with a preformed headcut which was allowed to erode were performed in the experimental flume. The upstream bed material was always cohesive soil and, for all but Run 29, was the downstream bed material as well. This run had the large sand as the downstream bed material and demonstrates the effect of different sediment detachment parameters on headcut stability. Run 28 was a full run in which the headcut retreated about 40 cm in approximately 15 minutes. Runs 30 through 40 are abbreviated runs which were terminated when either upstream or downstream erosion dominated. Table 5.5 provides the data required to determine the time scale ratio in Eq. 3.51 as well as the observed result from the abbreviated runs. The same data is graphically represented as a plot of T_U / T_D versus drop number in Fig. 5.17. The value of the constant f_1 was taken as 0.07 determined from an average of the computer simulations discussed in the next section.

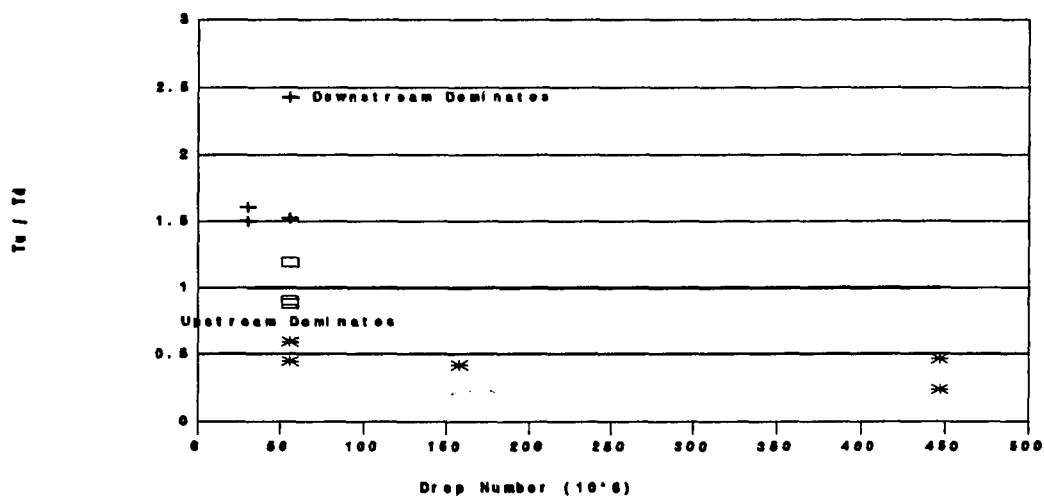


Figure 5.17: Measured Headcut Stability Values

Table 5.5: Measured Headcut Stability Values

Run	q (m ² /s)	D _b (cm)	S _b	R _c	F _d x10 ⁶	T _U / T _D	Result
28	0.00313	4.0	0.023	2236	55.88	0.88	Even
30	0.00127	1.0	0.059	907	447.05	0.24	Up
31	0.00142	1.0	0.018	1014	447.05	0.47	Up
32	0.00142	4.0	0.018	1014	55.88	2.43	Down
33	0.00266	4.0	0.014	1900	55.88	1.53	Down
34	0.00414	6.0	0.014	2957	30.42	1.61	Down
35	0.00267	6.0	0.027	1907	30.42	1.50	Down
36	0.00266	2.0	0.027	1900	158.06	0.42	Up
37	0.00417	4.0	0.027	2979	55.88	0.59	Up
38	0.00269	4.0	0.027	1921	55.88	0.90	Even
39	0.00415	4.0	0.040	2964	55.88	0.45	Up
40	0.00339	4.0	0.014	2421	55.88	1.19	Even

An example of the scour profiles for initial conditions and at the termination of a run are given Fig. 5.18 for an upstream dominating run and in Fig. 5.19 for a downstream dominating run.

Reynolds number varied from 907 to 2979, slope from 0.014 to 0.059 and Drop number from 30 to 447. The predicted time scale ratios varied from 0.24 to 2.43. It is virtually impossible to determine a quantitative time scale ratio from experiment. Clearly if upstream erosion dominates (ratio less than 1.0), downstream erosion will never reach the headcut face and the downstream time scale cannot be determined. If downstream erosion dominates (defined as downstream erosion reaching the headcut base before upstream erosion) but does not undercut the headcut face, the two processes appear to link. This could be described as upstream

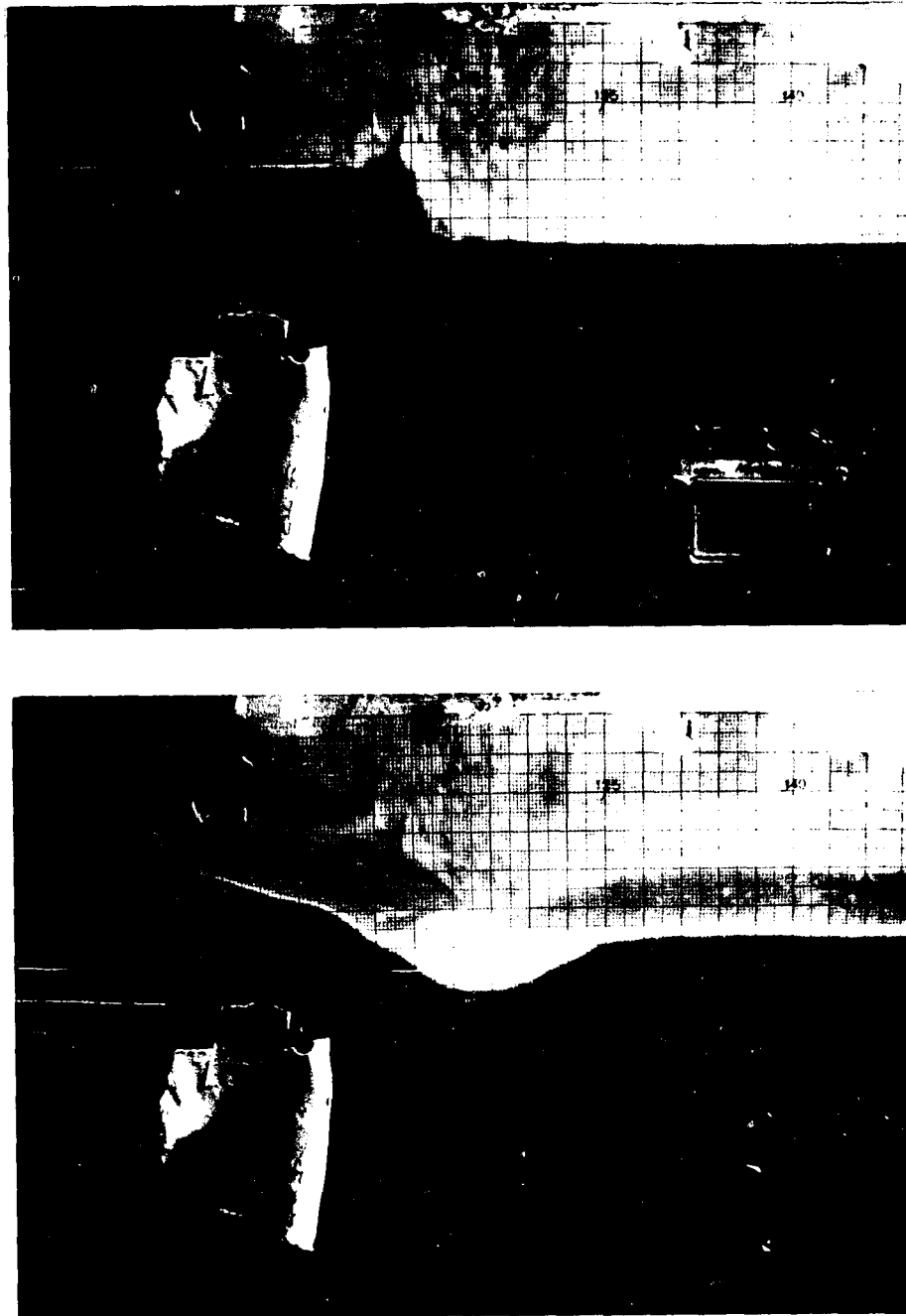


Figure 5.18: Scour Profiles Upstream Dominating Run

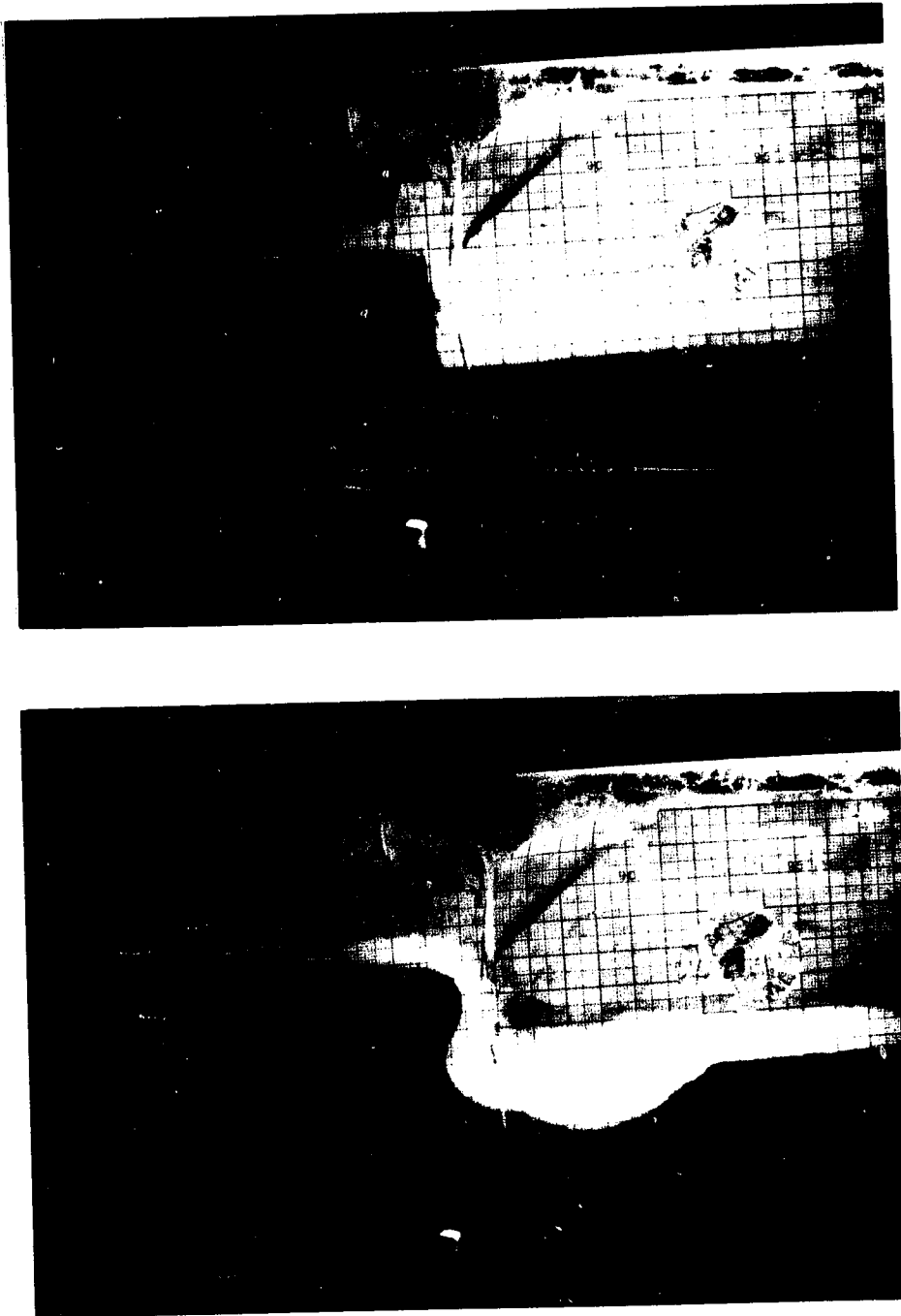


Figure 5.19: Scour Profiles Downstream Dominating Run

dominating because with time the headcut would tend to wash out. The first definition of headcut stability is used for the analysis because it is the one used to develop Eq. 3.51. The qualitative assessment in Table 5.5 is made with this definition.

These runs show the applicability of Eq. 3.51 with $f_1 = 0.07$ as a criteria for the mechanism of headcut migration in rills. All runs behaved as predicted including two runs with T_U / T_D close to unity. As predicted, both upstream and downstream erosion reached the headcut base at about the same time if $0.8 < T_U / T_D < 1.2$. This range can be considered a gray area in which neither upstream nor downstream erosion dominates. However as discussed above, the headcut will tend to wash out with time unless the downstream erosion undercuts the headcut face and this cannot happen unless the time scale ratio is considerably greater than one.

A few observations made from these runs are worth noting. The first was discussed above. Even if the downstream erosion reaches the headcut base before upstream erosion, upstream erosion may dominate in the long run if most of the headcut drop height has been eroded at that time. Second, it appears there is a minimum value for a combination of slope and Reynolds number for upstream erosion to dominate. There must be sufficient kinetic energy of flow at the brink to allow it to separate and impinge as a free falling nappe. Below this threshold value flow remains attached to the headcut face, such as when water is poured too slowly from a pitcher, and impinges directly at the base of the headcut. Under these conditions the headcut face is undermined almost immediately and Eq. 3.51

developed from a free falling nappe assumption cannot be expected to hold. Run 32 clearly displayed this characteristic.

Run 28, incised completely in cohesive soil, was allowed to retreat for some distance upstream. The value of T_U / T_D calculated from Eq. 3.51 for this run is 0.88. The computer simulation of this run discussed in the next section iterates Eq. 3.46 with time therefore reducing the downstream bias as compared to Eq. 3.51, as was discussed in Chapter 3. The simulated time scale ratio is 1.20, therefore Eq. 3.51 shows upstream erosion will dominate while the computer model shows downstream erosion dominates. Both values are within the gray zone discussed above suggesting that within the short run downstream erosion may dominate or at least be equal to upstream erosion but upstream erosion will eventually dominate. Figure 5.20 shows the measured profile changes of Run 28 with time.

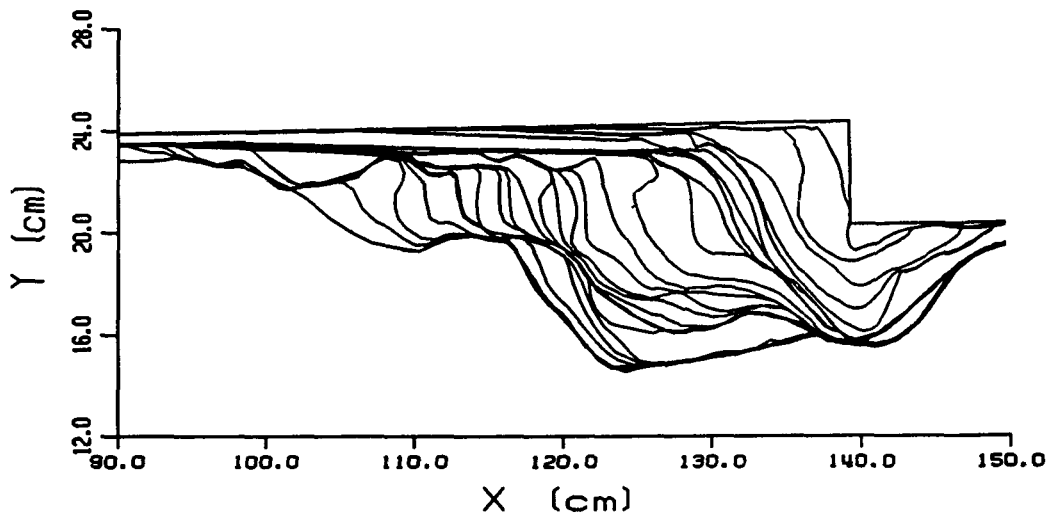


Figure 5.20: Measured Retreating Headcut Profile; All Soil

The headcut brink is eroded at about the same rate as the growth in scour hole width indicating the time scale ratio is indeed near unity. For early times of this run headcut migration is controlled by both upstream and downstream scour and neither one dominates the other. At longer times however, it is clear the vertical dimension of the headcut is decreasing while the horizontal dimension is increasing indicating upstream erosion is dominating and the headcut will wash out with time.

The headcut in Run 29 was created by overlaying a sand ($d_{50} = 1.5$ mm) with the cohesive soil. Photographs of the profile changes with time shown in Figs. 5.21 and 5.22 dramatically demonstrate the characteristic of undercutting and block failure of the headcut face when the sediment detachment rate in the impingement region dominates. The times of these profiles are 0:00, 0:10, 3:45, and 8:15.

While erosion is occurring completely on cohesive soil, scour is similar to that of Run 28. However, once the sand is exposed to erosion downstream erosion completely dominates. The sand is so quickly removed from beneath the cohesive layer a cantilever is formed which cracks and falls into the plunge pool. A new headcut is formed several centimeters upstream where the process repeats. Though there is erosion occurring in the upstream accelerated flow region it is insignificant compared to that in the impingement region.

Equation 3.51 with $f_1 = 0.07$, which assumes similar sediment detachment rates for upstream and downstream erosion cannot be used for this set of conditions. Equation 3.46, which can account for different sediment detachment rates, must therefore be used. However, no attempt has been made to calibrate this equation. It may be possible to use Eq. 3.51 if constant f_1 is increased to account for the

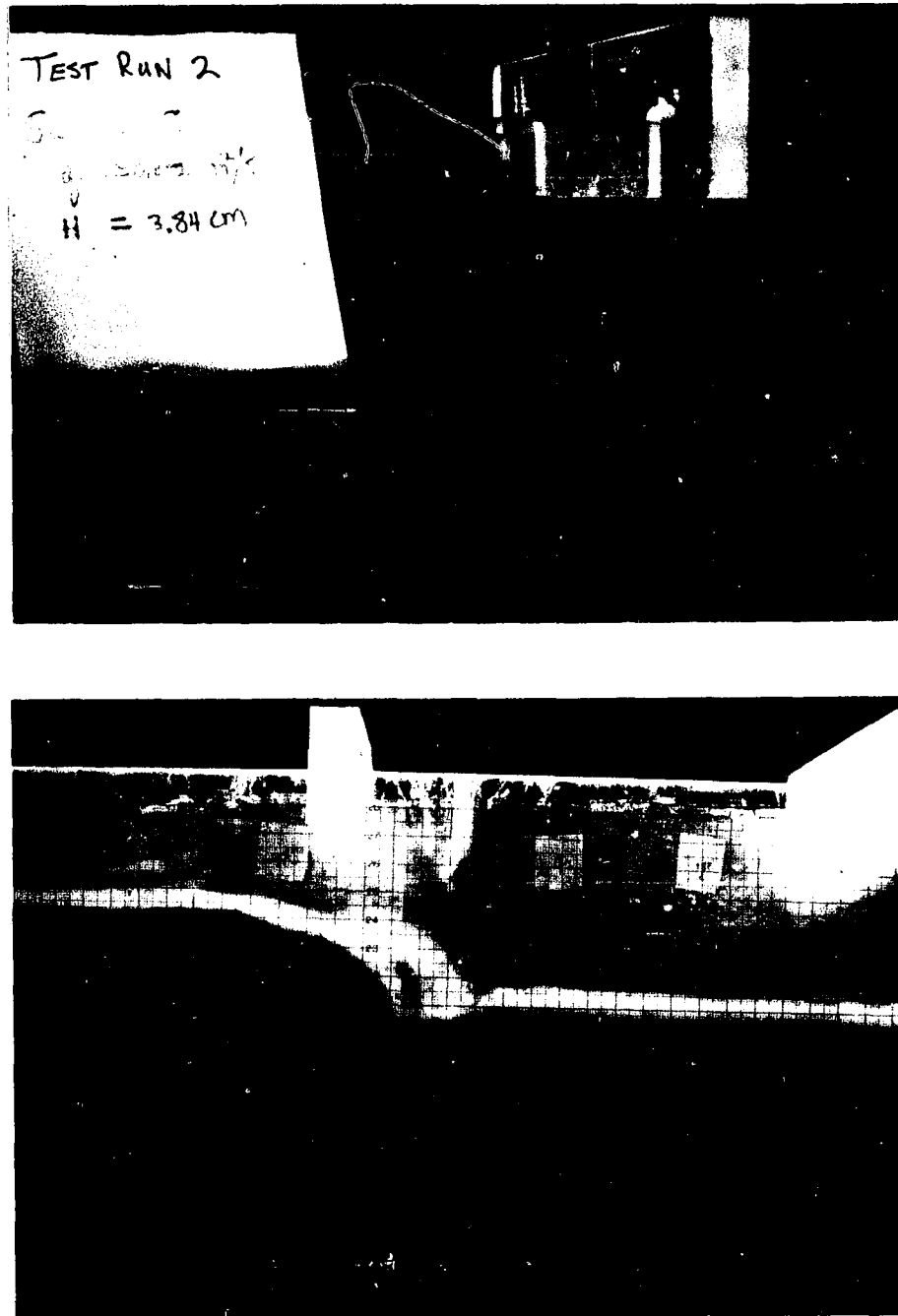


Figure 5.21: Headcut Retreat Showing Cantilevered Block Failure

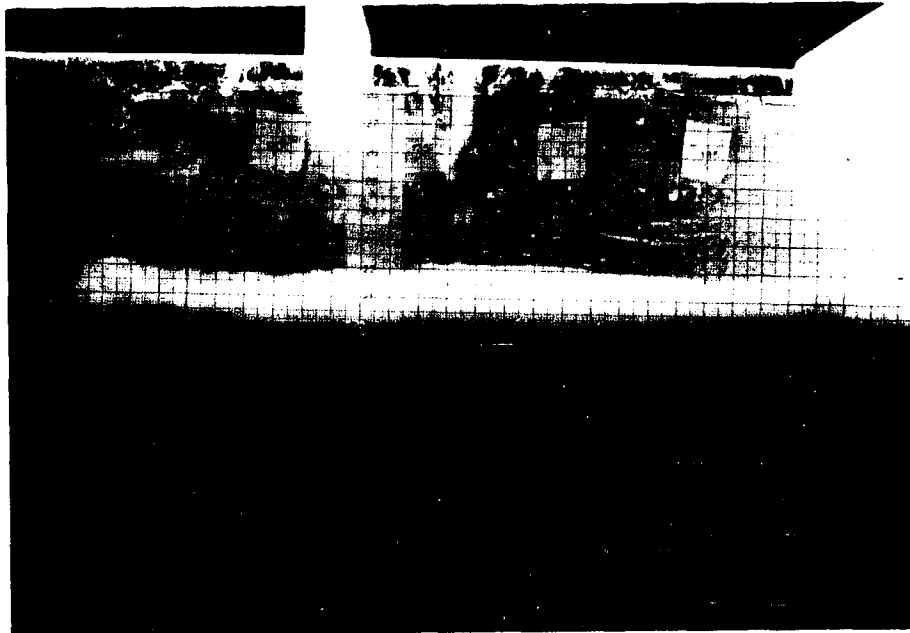


Figure 5.22: Headcut Retreat Showing Cantilevered Block Failure

different sediment detachment rates. This would shift the curves of Figs. 3.13 and 3.14 to the right and up, increasing the domain in which downstream erosion dominates.

5.3 Computer Simulation of Scour Profiles

A computer model which incorporates both upstream and downstream sediment detachment has been developed to determine the changes in bed profile in the vicinity of a headcut. Considerably more flexibility is possible with this model as compared to Eq. 3.51 in that virtually all parameters such as critical shear stress and the sediment detachment constants K_1 and K_2 can be varied and are not limited to integer values. The complete FORTRAN source code is presented in Appendix D. As presently developed the headcut is fixed in space for the entire erosion process but could be modified to simulate a retreating headcut.

Briefly described herein is the methodology used to calculate the bed profiles. Initial hydraulic values are determined by assuming a geometry as given in Fig. 3.1 and the change in bed profile over a small time step (1 to 5 sec.) is determined from these hydraulics values and a sediment detachment equation such Eq. 5.1. All subsequent hydraulic values are determined from the bed profile shape of the previous time step. The model can increase the time step if bed profile changes are very small. The channel is broken in to discrete longitudinal nodes which are either in the normal flow, accelerated flow or impingement region. The length of these regions is determined by the hydraulics and bed profile and vary with time.

Normal flow values are determined from either the laminar or Blasius assumptions for flow resistance depending on Reynolds number. Equation 2.12 from Hager (1983) is used to determine the water surface profiles at the nodes in the accelerated flow region. Shear stress at the nodes is then determined from the flow depth ratio using Eq. 3.24. For the initial time step, shear stress at the brink is given by Eq. 3.26. The change in bed elevation at each node is determined from the calculated shear stress and the sediment detachment equation. A one dimensional finite difference method is employed to determine the slope between nodes which increases as the brink is approached for all times greater than zero.

Equations 3.33 and 3.48 are used to determine the values of the free falling nappe at the original downstream bed elevation. The maximum depth of scour is determined from a combination of the sediment detachment equation and Eq. 3.31 or 3.32 depending on the bed elevation in relation to the length of the jet potential core. The x coordinate of the maximum depth of scour is determined from an adjustment of the jet centerline. The impingement region bed profile is calculated from the relation between scour depth and volume for the cohesive soil material, Eq. 5.5 assuming a parabolic shape. Bed elevation downstream from the impingement region is held constant.

Because all values are iterated with time the model may more accurately predict the headcut stability parameter T_U / T_D than Eq. 3.51 determined only from the initial hydraulics. The model was used to determine the ratio T_U / T_D for all retreating headcut runs and this value compared to that determined from Eq. 3.51. The value of the constant f_1 was shown to vary somewhat from about 0.04 to 0.11

with an average of 0.07. A small variation is expected because each run has unique sediment detachment ratio which was assumed equal to unity in Eq. 3.51. The model determined average for f_1 was used to calculate the plots of Fig. 3.13 and its applicability, at least for the ranges measured, was verified in Runs 30 - 40.

A comparison between measured and predicted bed profiles for a non-retreating cohesive soil run (Run 10) is presented in Fig. 5.23. The flow rate for this run is $0.00354 \text{ m}^2/\text{s}$, the bed slope 3.7% and the drop height 4.0 cm. Sediment detachment is determined from Eq. 5.26 and the value of the diffusion constant is 2.6, consistent with the previously developed analysis.

The time interval between the measured profiles varies from 10 seconds at the initial time steps and increases to ten minutes at the longest times. The final scour profile for both measured and predicted plots is at 9000 s. The time of each measured profile is given in Appendix C. Time intervals for the predicted profiles are similarly, but not identically, spaced because they were determined by the program. Figure 5.23 shows the predicted maximum depth of scour, the upstream and downstream ends of the scour hole, total volume of eroded material as well as the parabolic shape approximate the measured values. More scatter for the maximum depth of scour exists for some runs with about half overpredicting and half underpredicting the maximum scour depth at a given time. The error, which is relatively small for all runs but 1 and 13, is consistent within a run. However, the predicted scour hole endpoints, total scoured volume and general profile shape for a given predicted depth agree well with the equivalent measured depth, though the

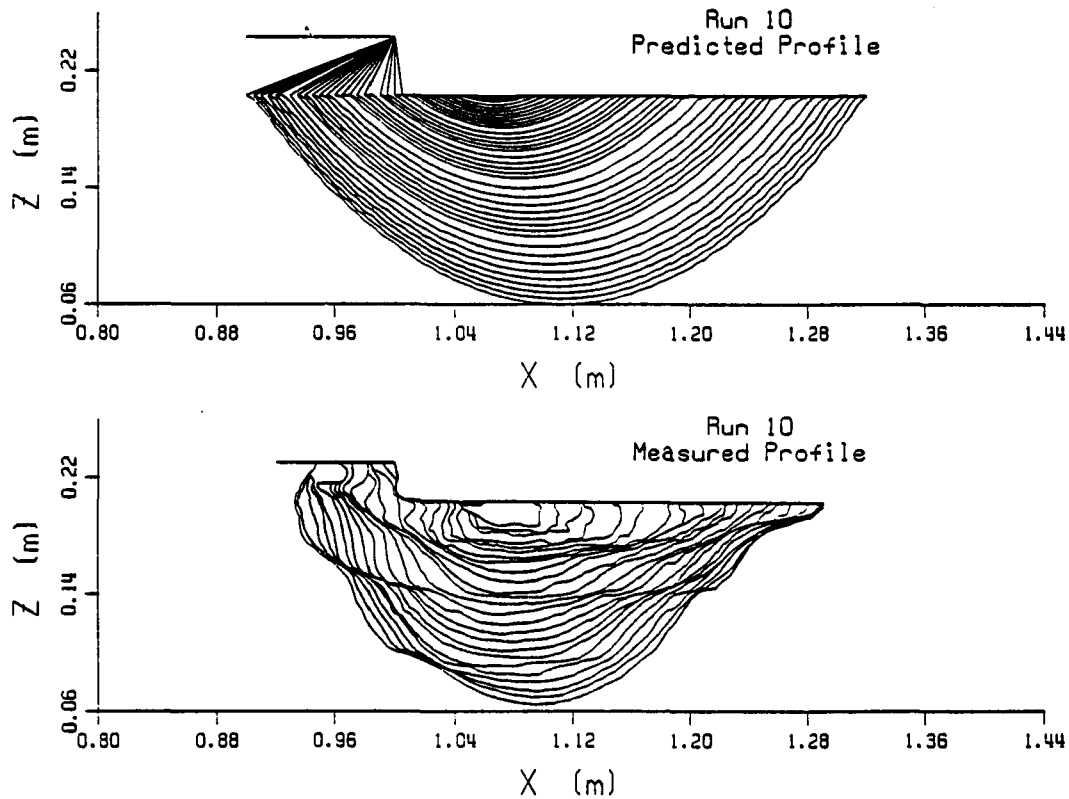


Figure 5.23: Comparison Measured and Predicted Profiles Non-Retreating Headcut time may be shifted somewhat. Because a sediment detachment equation for the sand runs has not been calibrated, these profiles are not predicted by the model.

A comparison of the measured and predicted scour profiles for Run 28, the only full retreating cohesive soil run in which profile measurements were taken, is given in Fig. 5.24. This run had a flow rate of $0.00313 \text{ m}^2/\text{s}$, a bed slope of 2.3% and a drop height of 4.0 cm.

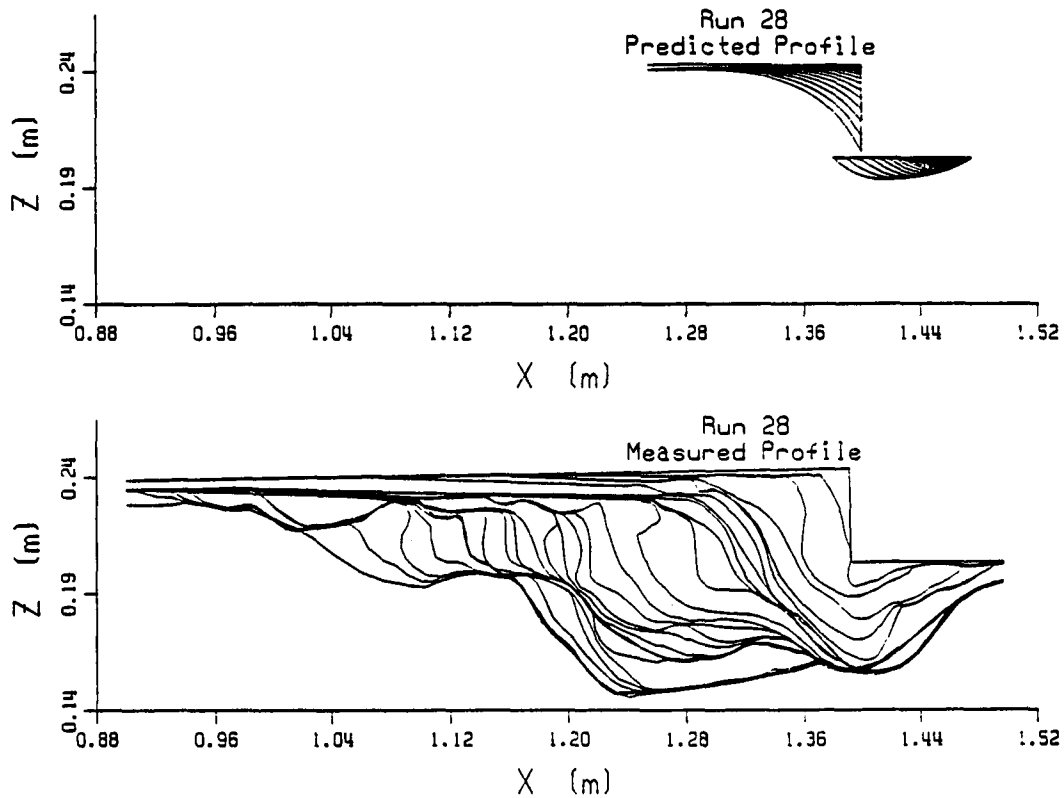


Figure 5.24: Comparison Measured and Predicted Profiles Retreating Headcut

The final measured profile is at 15 minutes, 49 seconds. No mechanism for headcut retreat has been developed within the model, therefore calculations are terminated when the headcut face has been completely obliterated, predicted at 2:26. This time corresponds to the upstream time scale T_U . Obviously the model in its present form cannot predict measured profiles for times greater than T_U . It would appear the model is underpredicting downstream erosion for times less than T_U , however the model predicts downstream erosion would be undercutting the headcut

face before the headcut is completely obliterated because the predicted time scale ratio T_U/T_D is 1.20. This can be seen in the predicted profiles of Fig 5.19. Because the ratio is close to unity neither upstream or downstream erosion clearly dominates, however it might be that downstream erosion insures that a small headcut drop height migrates upstream which would increase the predicted downstream scour depth. The measured profiles do show that upstream and downstream scour rates are about equal, as predicted.

Chapter 6

Conclusions and Recommendations

Although erosion in the vicinity of a headcut can significantly contribute to the total soil loss from a given storm very little previous research has attempted to determine the erosion potential and migration of a headcut. None of the existing studies consider headcut erosion or migration rate in terms of hydraulics properties near the headcut. The present study develops a conceptual model based on principles of open channel hydraulics and sediment detachment to predict the mode of upstream advancement and scour potential in the vicinity of a headcut. This model is then mathematically formulated and experimentally verified.

The conceptual model identifies two unique hydraulic regions, an accelerated flow region upstream from the headcut and an impingement region just downstream from a headcut. The effect of the hydraulics in these regions on shear stress is summarized below.

The abrupt end of the rill or gully channel at the headcut causes flow just upstream to accelerate increasing the velocity and applied shear stress by reducing the pressure. The Saint-Venant equations are analyzed to relate changes in shear stress at the bed to changes in velocity, flow depth and pressure. Three levels of sophistication can be used to calculate the upstream shear stress distribution. The

most simplistic ignores any changes in hydraulic variables by assuming a normal flow pattern through the entire upstream region. A more complex solution considers the effects of changes in velocity and flow depth has on shear stress. The most complex solution includes changes in pressure which are known to exist as well as depth and velocity. A depth integrated form of the Saint-Venant equations is proposed in Eq. 3.20 which includes changes in the pressure profile with the longitudinal coordinate. No analytical solution to this equation exists therefore experimental data from Rajaratnam and Muraldihar (1968) and Hager (1983) are used to determine the shear stress distribution upstream of the headcut. The equation is very sensitive to small changes in values of the derivatives of experimental data, therefore results are unstable. Shear stress should increase from a normal flow value as the headcut is approached, however the calculated value decreases from normal for some distance and eventually increases to a value greater than normal just at the brink.

A shear stress distribution for the reach just upstream of the headcut is calculated from water surface profiles just upstream from of fully aerated free overfall by combining Eqs. 2.12, 3.10 and 3.24. Though this method may slightly underestimate the shear stress at the headcut brink, it steadily increases from a normal flow value to maximum at the brink. This maximum as well as the total shear stress distribution is shown to be negatively correlated with bed slope and Reynolds number, as either of these independent variables increase, shear stress approaches the value for normal flow. In the limit for large Reynolds number of bed slope, the simplest solution for the shear stress distribution Eq. 3.10, based only on normal flow patterns is applicable.

Flow in the impingement region can be likened to that of an impinging jet produced by a free falling nappe. The hydraulics and scour potential of a jet impinging on non-cohesive bed material has been the subject of considerable past research. Two distinct hydraulic regions have been identified. Near the jet origin, a region called the potential core has a maximum velocity U_0 which is independent of the distance from the origin. Beyond this length, given as Eq. 2.17, the jet diffuses with the surrounding fluid and the maximum velocity, which occurs along the jet centerline, is proportional to one over the square root of the distance from the jet origin. The maximum shear stress given as Eq. 3.32 is shown to be proportional to the square of the maximum velocity by using a coefficient of friction and a characteristic shear velocity.

Most previous research on scour from jets has focused on the ultimate or maximum depth of scour, therefore only jet diffusion needs to be considered. Limited research on the change of scour depth with time (Rouse 1940 and others) has empirically concluded scour depth is proportional to the logarithm of time. Blaisdell et al. (1981) have concluded other empirical relations such as log-log or hyperbolic functions may be equally good. Review of this literature revealed great variability in the reported results. This is attributable to the empiricism and therefore lack of a sound hydraulically based theoretical development.

In regard to ultimate or maximum depth of scour of non-cohesive bed material, the method developed by Bormann (1988) using Eqs. 2.28 and 2.29 is shown to adequately predict results from 14 original tests on two sand sized bed materials. This method is shown to be an improvement on, but similar to, previous prediction

equations Eqs. 2.25 and 2.27 based on jet diffusion and the sediment transport related Shields parameter. A more general predictive equation Eq. 3.37 based on the same principles but applicable to scour from cohesive soil is presently proposed. This equation is tested against ten original experiment data sets. In only a few runs was the predicted ultimate depth approached as shown in Fig. 5.8, however the predicted depth was often greater than possible to measure with the given experimental equipment, and more importantly, an extrapolation of the change in scour depth with time indicates that the ultimate depth is asymptotically approached.

A dimensional analysis of the change in scour depth with time relates the maximum scour depth at any time normalized to the predicted ultimate scour depth to sediment detachment, Reynolds number, Froude number and time normalized to the jet velocity and thickness at tailwater impingement given as Eq. 3.4.

A theoretically based relation for the change in scour depth with time is presently proposed. While the bed is within the potential core of the impinging jet, maximum velocity and shear stress are independent of the distance between the bed and jet origin, defined as the point the plunging nappe impinges on the original bed. Therefore, the rate of scour given as Eq. 3.38 is constant with time for the time period the eroding bed is within the potential core. This time period, Eq.3.39 is inversely proportional to, and the constant rate directly proportional to, the sediment detachment capacity of the jet potential core.

When the eroding bed is beyond the potential core, at a depth given as Eq. 3.40, diffusion decreases the maximum velocity, maximum shear stress and sediment detachment rate of the impinging jet. A non-linear first order partial differential

equation Eq. 3.41 is proposed to describe the relation between maximum scour depth and time. This equation is developed by equating jet diffusion with a sediment detachment equation. An analytical solution to this differential equation exists only if the sediment detachment exponent is an integer. A solution, Eqs. 3.42 and 3.43 applicable when the exponent equals unity, gives time as a function of both arithmetic and log terms for depth, therefore depth cannot be explicitly related to time. A series expansion of the log terms results in Eq. 3.44 with considerable simplification as compare to Eqs, 3.42 and 3.43. This solution is shown to contain the same terms as developed from a dimensional analysis of basic hydraulic terms, Eq. 3.4. A graphical representation of the solutions to Eqs. 3.38 and 3.41 for four data sets are shown in Figs. 3.11 and 3.12.

An original data set, which appears to be the most exhaustive to date, has been collected to determine the validity of the dimensional analysis and the developed theoretical equation for the rate of scour. Three bed materials including a cohesive soil, representing three different sediment detachment rates, were eroded by an impinging jet created by a free falling nappe. Ten different combinations of Reynolds and impingement Froude numbers were conducted on the cohesive soil bed material. These experiments were repeated eight times on a sand with a mean diameter of 1.5mm and six times on a sand with a mean diameter 0.15mm. The measured scour profiles at various times for all runs given in Appendix B. Results show that for the range of parameters tested, scour depth for a given bed material could accurately be determined from a dimensionless time factor and impingement Froude number through the dimensional analysis (Eqs. 5.2- 5.4 and Figs. 5.9-5.12).

The data also supports the theoretically derived equation in trend as shown in Fig. 5.13. Cohesive soil scour depth clearly increases at two distinct rates corresponding to scour within and beyond the jet potential core. The depth corresponding to the break between rates, dependent only on flow hydraulics can be accurately determined from Eq. 3.40. However the time corresponding to the break Eq. 3.39, dependent on the sediment detachment rate, is over predicted using the best available sediment detachment equation. In addition to the change in maximum scour depth with time data for the change in total volume (Appendix C), sediment concentration (Eqs. 5.6-5.8, Figs 5.14 to 5.16 and Appendix A), and entire two dimensional scour profile has been collected (Appendix B).

As previously shown (Holland and Pickup, 1976), headcut migration can proceed in two distinct modes. This research proposes that the mode can be determined from a headcut stability parameter, defined as the ratio of time required for erosion upstream of the headcut to obliterate the headcut face over the time required for erosion downstream to undermine the headcut face. This stability parameter is related to five independent parameters, upstream and downstream sediment detachment, bed slope, Reynolds number and drop number. The drop number is defined as kinematic viscosity divided by the square root of the quantity gravity times drop height cubed. The same equation is developed from both dimensional analysis Eq. 3.2 and a physically based analysis of headcut hydraulics and geometry, Eq 3.46. This general equation is simplified to Eq. 3.51 by assuming upstream and downstream sediment detachments are similar and using the Blasius assumption for flow resistance. A graphical representation of headcut stability is

provided in Figs. 3.13 and 3.14. Eleven runs with a cohesive soil bed material were used to calibrate the developed equation. The results shown in Table 5.5 and Fig. 5.17 suggest Eq. 3.51 can be used to determine the mode of headcut migration, at least within the parameter ranges tested.

A computer model incorporating all of the above analysis has been developed to determine the bed profile changes with time. Usage of this model allows for a greater range of input parameters such as the sediment detachment exponent as compared to analytically derived solutions. This model can also be used to calibrate the headcut stability analysis. Comparison of the measured and predicted profiles, examples of which are provided in Figs. 5.21 and 5.22, is good though the model in its present form does not incorporate upstream advancement of the headcut.

The computer model as well as the determination of the change in scour depth with time requires that a sediment detachment equation be calibrated for each bed material. An excess shear equation shown as Eq. 2.10 has gained wide acceptance for sediment detachment of cohesive bed material (Nearing et al. 1989) despite limited validation. This equation was calibrated by measuring sediment discharge for 15 different applied shear stresses on one cohesive soil in small laboratory flume used for all other experimentation. The calibrated equation Eq. 5.1 verifies the applicability of an excess shear equation for cohesive soil detachment for this particular soil. Critical shear stress was determined to be 0.32 Pascals and the detachment exponent equal to unity, at least for the range of shear stresses measured. These shear stress values are representative of values expected to be found in rills formed in agricultural fields.

6.1 Conclusion Summary

The major conclusions of this research are as follows.

- 1) An excess shear equation for cohesive soil sediment detachment with an exponent equal to unity is applicable for the range of applied shear stresses expected in a small rill incised on typical agricultural soil.
- 2) Shear stress on a bed just upstream from a free overfall such as that produced by a headcut is maximum at the brink. This maximum is negatively correlated to bed slope and Reynolds number. The minimum brink shear stress occurring if either bed slope or Reynolds number are large corresponds to the normal flow shear stress value.
- 3) The change in maximum scour depth with time produced by an impinging jet such as that produced below a headcut proceeds at two distinct rates depending on the relative position the bed and the jet potential core. Scour rate is a maximum and proceeds linearly with time while the bed is within the jet potential core. For greater depths scour rate decreases with time in a relation which can be described by equating sediment detachment to jet diffusion.
- 4) An ultimate scour depth produced by an impinging jet can be determined by equating jet diffusion to the critical shear stress of the given bed material.
- 5) The mode of headcut migration can be determined from a headcut stability parameter defined as a time scale ratio of upstream and downstream sediment detachment. If the upstream erosion rate is greater than downstream erosion rate the headcut will tend to obliterate itself with time as the bed slope near the headcut approaches the average bed slope of the channel. If the downstream erosion rate is

greater than upstream a headcut with a near vertical face tends to migrate upstream because downstream erosion tends to undercut the headcut face.

6.2 Recommendations for Future Research

This dissertation has touched on three areas in which additional research is warranted. One is to determine the true shear stress distribution upstream from a free overfall. An equation derived from the Saint Venant equations which includes flow depth, velocity, and pressure gradient has been developed. The usage of the of this equation is severely hampered by a lack of quality data for the latter term. Two possible methods for remedying this situation are proposed. The most direct is to actually measure depth, velocity and pressure in a rigid walled flume in which conditions can be carefully controlled. This data set could be added to the one collected by Rajaratnam and Muralidhar (1968). A better method may be to use the finite difference or finite element schemes presently available to determine all parameters from the equation developed from the Saint Venant equations. of course this method still requires knowledge of the relevant parameters at the boundaries.

Another area which will and should continue to receive additional research attention is the development of sediment detachment and transport relations, especially for cohesive bed material. Despite decades of research in this area the fundamental principles are poorly understood. An excess shear detachment equation calibrated from data collected in this study by methods previously used appears to be applicable at least for one particular soil.

The next logical step in headcut stability analysis would be to incorporate the effects of grossly different upstream and downstream sediment detachment rates. One run was conducted to demonstrate this effect but no attempt has been made to predict the effect though a general framework for this has been developed. A project related to this would be to further the computer model for profile prediction incorporating a migrating headcut and different sediment strata.

References

- Al-Durrah, M.M. and J.M. Bradford. 1982a. Parameters for Describing Detachment Due to Single Waterdrop Impact. *Soil Sci. Soc. Am. J.* 46:836-840.
- Al-Durrah, M.M. and J.M. Bradford. 1982b. The Mechanism of Raindrop Splash on Soil Surfaces. *Soil Sci. Soc. Am. J.* 46:1086-1090.
- Albertson, M.L. et al. 1950. Diffusion of Submerged Jets. *Trans. ASCE* 115:639-697.
- Alonso, C.V., W.H. Neibling and G.R. Foster. 1981. Estimating Sediment Transport Capacity in Watershed Modeling. *Trans. ASAE* 24(5):1211-1220,1126.
- Akashi, N. and T. Saitou. 1986. Influence of Water Surface on Scour From a Vertical Submerged Jet. *J. of Hydroscience and Hydr. Engr.* 4(2):55-69.
- Arkhipov, G.A. 1984. Consideration of Sediment Transport When Calculating Local Scour. *Hydrotechnical Const* 18(4):149-153. Translated From: *Gidrotekhnicheskoe Stroitel'stvo* No. 4, pp. 14-16, April 1984.
- Ashida, K. and M. Michiue. 1971. An Investigation of River Bed Degradation Downstream of a Dam. *Inter. Asso. Hydr. Res. Proc. 14th Congress.* Vol. 3:247-255.
- Begin, Z.B. 1979. Aspects of Degradation of Alluvial Streams in Response to Base-Level Lowering. Ph.D. Dissertation, Colorado State University, Fort Collins CO. 239p.
- Begin, Z.B., D.F. Meyer and S.A. Schumm. 1980a. Sediment Production of Alluvial Channels in Response to Base Level Lowering. *Trans. ASAE* 23(5)1183-1188.
- Begin, Z.B., D.F. Meyer and S.A. Schumm. 1980b. Knickpoint Migration Due to Base Level Lowering. *J. Water., Port, Coastal, Ocean Div. ASCE* 106(WW3)369-389.
- Begin, Z.B. and S.A. Schumm. 1979. Instability of Alluvial Valley Floors : A Method for Its Assessment. *Trans. ASAE* 22(3)347-350.

- Beltaos, S. 1972. Normal Impingement of Plane Turbulent Jets on Sooth Walls. M.S. Thesis, University of Alberta, Edmonton, Alberta, Canada.
- Beltaos, S. 1974. Turbulent Impinging Jets. Ph.D. Dissertation, University of Alberta, Edmonton, Alberta, Canada.
- Beltaos, S. 1976a. Oblique Impingement of Plane Turbulent Jets. J. Hydr. Div. ASCE 102(HY9):1177-1192.
- Beltaos, S. 1976b. Oblique Impingement of Circular Turbulent Jets. J. Hydr. Res. 14(1):17-36
- Beltaos, S. and N. Rajaratnam. 1973. Plane Turbulent Impinging Jets. J. Hydr. Res. 11:29-59.
- Beltaos, S. and N. Rajaratnam. 1974. Impinging Circular Turbulent Jets. J. Hydr. Div. ASCE 100(HY10)1313-1328.
- Beltaos, S. and N. Rajaratnam. 1977. Impingement of Axisymmetric Developing Jets. J. Hydr. Res. 15(4)311-325.
- Blaisdell, F.W. 1954. Equation of the Free Falling Nappe. ASCE Proc. 80(August) Sep. No. 482:1-16.
- Blaisdell, F.W., C.L. Anderson and G.G. Hebaus. 1981. Ultimate Dimensions of Local Scour. J. Hydr. Div. ASCE 107(HY3)327-337.
- Blaisdell, F.W. and C.L. Anderson. 1988a. A Comprehensive Generalized Study of Scour at Cantilvered Pipe Outlets Pt.1. J. Hydr. Res. 26(4):357-376.
- Blaisdell, F.W. and C.L. Anderson. 1988b. A Comprehensive Generalized Study of Scour at Cantilvered Pipe Outlets Pt.2. J. Hydr. Res. 26(5):509-524.
- Blong, R.J. 1970. The Development of Discontinuous Gullies in a Pumice Catchment. Amer. Jour. Sci. 268:369-383.
- Blong, R.J. 1985. Gully Sidewall Development in New South Wales Australia. IN: Soil Erosion and Conservation pp. 574-584. El-Swaify, S.A., W.C. Moldenhauer and A. Lo Ed. Soil Conser. Soc. Am. Ankeny, Iowa
- Bogardi, J. 1974. Sediment Transport in Alluvial Streams. Akademiai Kiado, Budapest, Hungary.
- Bormann, N. 1988. Equilibrium Local Scour Depth Downstream of Grade Control Structures. Ph.D. Dissertation, Colorado State University, Fort Collins, Co.

- Bormann, N. 1989. Predicting Local Scour for Design of Hydraulic Structures in Alluvial Channels. In: Design of Hydraulic Structures 89 pp. 235-241. Albertson and Kia Ed. Balkema, Rotterdam, Netherlands.
- Bourque, C. and B.G. Newman. 1960. Reattachment of a Two Dimensional, Incompressible Jet to an Adjacent Flat Plate. *Aeronautical Quarterly*. 11(3):201-232.
- Bradford, J.M., D.A. Farrell and W.E. Larson. 1973. Mathematical Evaluation of Factors Affecting Gully Stability. *Soil Sci. Soc. Am. Proc.* 37:103-107.
- Bradford, J.M. and R.B. Grossman. 1982. In Situ Measurement of Near Surface Soil Strength by the Fall Cone Device. *Soil Sci. Soc. Am. J.* 46(4):685-688.
- Breusers, H.N.C. 1967. Time Scale of Two Dimensional Local Scour. *Inter. Asso. Hydr. Res. Proc. 12th Congress Vol. 3:275-282, Paper No. C32.*
- Breusers, H.N.C. 1975. Computation of Velocity Profiles in Scour Holes. *Inter. Asso. Hydr. Res. Proc. 16th Congress Vol. 2:300-306.*
- Brown, M.J., W.D. Kemper, T.J. Trout and A.S. Humpherys. 1988. Sediment, Erosion and Water Intake in Furrows. *Irrig. Sci.* 9:45-55.
- Brush, L.M., Jr. and M.G. Wolman. 1960. Knickpoint Behavior in Noncohesive Material: A Laboratory Study. *Geol. Soc. Am. Bul.* 71:59-73.
- Carstens, M.R. 1955. Free Overfall Has Rapidly Varying Characteristics. *Civil Engr.* 25(June):64-65.
- Carstens, M.R. 1966. Similarity Laws for Localized Scour. *J. Hydr. Div. ASCE* 92(HY3):13-37.
- Carstens, M.R. and R.W. Carter 1955. Discussion of "Hydraulics of the Free Overfall" Fathy and Amin. *ASCE Proc.* 81 (June) Sep. No. 719:18-28.
- Christodoulou, George C. 1985. Brink Depth in Nonaerated Overfalls. *J. Irr. Drain Engr.* 111(4):395-403.
- Chee, S.P. and T. Kung. 1971. Stable Profiles of Plunge Basins. *Water Res. Bul.* 7(2):303-308.
- Chee, S.P. and P.V. Padiyar. 1969. Erosion at the Base of Flip Buckets. *Engr. J. Canada* 52(11):22-24.
- Chee, S.P. and E.M. Yuen. 1985. Erosion of Unconsolidated Gravel Beds. *Can. J. Civ. Engr.* 12:559-566.

- Cola, Raffaele. 1965. Energy Dissipation of a High-Velocity Vertical Jet Entering a Basin. Inter. Asso. Hydr. Res. Proc. 11th Congress Vol. 1 Paper No. 1.52.
- Cruff, R.W. 1965. Cross-Channel Transfer of Linear Momentum in Smooth Rectangular Channels. USGS Water Study Paper 1592-B.
- Culling, W.E.H. 1960. Analytical Theory of Erosion. J. Geology 68:336-344.
- Daniels, R.B. and R.H. Jordan. 1966. Physiographic History and the Soils, Entrenched Stream of Systems and Gullies Harrison County Iowa. USDA Tech. Bul. 1348.
- Delleur, J.W., J.C.I. Dooge and K.W. Gent 1956. Influence of Slope Roughness on the Free Overfall. J. Hydr. Div. ASCE 82(Hy4):1038-30-1038-35.
- Diskin, M.H. 1961. End Depth at a Drop in Trapezoidal Channels. J. Hydr. Div. ASCE 87(Hy4) 11-32. Errata: 89(Hy1):165.
- Doddiah, D., M.L. Albertson and R. Thomas. 1953. Scour From Jets. Inter. Asso. Hydr. Res. Proc. 5th Congress Vol 1 161-169.
- Egboka, B.C.E. and E.I. Okpoko. 1984. Gully Erosion in the Agula-Nanka Region of Anambra State, Nigeria. In: Challenges in African Hydrology and Water Resources Inter. Asso. Hydro. Sci. (IAHS) Pub. No. 144:335-347.
- Ervine, D.A. and H.T. Falvey. 1987. Behavior of Turbulent Water Jets in the Atmosphere and in Plunge Pools. Proc. Instn. Civ. Engrs. Pt.2 83:294-314.
- Farhoudi, Javad and Kenneth V.H. Smith. 1985. Local Scour Profiles Downstream of Hydraulic Jump. J. Hydr. Res. 23(4)343-358.
- Fathy, A. and M.S. Amin 1954. Hydraulics of the Free Overfall. ASCE Proc. 80 (Dec) Sep. No. 564.
- Fink, L.E. 1974. Discussion of: Plane Turbulent Compound Wall Jets N. Rajatnam 1972. J. Hydr. Res. 12:133-139.
- Foster, G.R., L.F. Huggins and L.D. Meyer. 1984a. A Laboratory Study of Rill Hydraulics : I Velocity Relationships. Trans. ASAE 27(3):790-796.
- Foster, G.R., L.F. Huggins, and L.D. Meyer. 1984b. A Laboratory Study of Rill Hydraulics : II Shear Stress Relationships. Trans. ASAE 27(3)797-804.

Foster, G.R., and L.D. Meyer. 1975. Mathematical Simulation of Upland Erosion Using Fundamental Erosion Mechanics. In: Present and Prospective Technology for Predicting Sediment Yields and Sources. Proc. of the 1972 Sediment Yield Workshop, USDA Sedimentation Lab, Oxford, MS USDA-ARS, ARS-S40, pp. 190-207.

Foster, G.R., L.D. Meyer, and C.A. Onstad. 1977. An Erosion Equation Derived From Basic Erosion Principles. Trans. ASAE 20(4):678-682.

Gabriels, D., J.M. Pauwels and M. DeBoodt. 1977. A Quantitative Rill Erosion Study on a Loamy Sand in the Hilly Region on Flanders. Earth Surface Processes 2:257-259.

Gan, J.K.M, D.G. Fredlund and H. Rahardjo. 1988. Determination of the Shear Strength Parameter of an Unsaturated Soil Using the Direct Shear Test. Can. Geotech. J. 25:500-510.

Gessler, J. 1970. Self-Stabilizing Tendencies of Alluvial Channels. J. Waterways and Harbors Div. ASCE 96:235-249.

Gill, M.A. 1979. Hydraulics of Rectangular Vertical Drop Structures. J. Hydr. Res. 17(4):289-302.

Grissinger, E.H. 1982. Bank Erosion of Cohesive Materials. In: Gravel-Bed Rivers Hey, R.D., J.C. Bathurst and C.R. Thorne Ed. John Wiley and Sons Ltd.

Grissinger, E.H., W.C. Little and J.B. Murphey. 1981. Erodibility of Streambank Materials of Low Cohesion. Trans. ASAE 24(3):624-630.

Hager, Willi H. 1983. Hydraulics of Plane Free Overfall. J. Hydr. Engr. 109(12):1683-1697. Errata: 110(12):1687-1688.

Hager, W.H. and K. Hutter. 1984. Approximate Treatment of Plane Channel Flow. Acta Mechanica 51:31-48.

Hartley, D.M. 1987. Simplified Process Model for Water Sediment Yield from Single Storms. Part 1 - Model Formation. ASAE Trans. 30(3):710-717.

Hartung, F. and E. Häusler. 1973. Scours, Stilling Basins and Downstream Protection Under Free Overfall Jets at Dams. 11th Inter. Comm. Large Dams Trans. Vol II Q41 Paper R3 39-56.

Holland, W.N. and G. Pickup. 1976. Flume Study of Knickpoint Development in Stratified Sediment. Geol. Soc. Am. Bul. 87:76-82.

- Hooke, J.M. 1979. An Analysis of the Processes of River Bank Erosion. *J. of Hydrology* 42:39-62.
- Johnson, C.E., R.D. Grisso, T.A. Nichols, A.C. Bailey. 1987. Shear Measurement for Agricultural Soils - A review. *Trans. ASAE* 30(4):935-938.
- Johnson, G.M. 1967. The Effect of Entrained Air on the Scouring Capacity of Water Jets. *Inter. Asso. Hydr. Res. Proc. 12th Congress Vol. 3:218-226*, Paper No. C26.
- Johnson, G.M. 1977. Use of Weakly Cohesive Material for Scale Model Studies in Flood Spillway Design. *Inter. Asso. Hydr. Res. Proc. 17th Congress Vol. 4:509-512*, Paper No. C63.
- Johnson, P.L. 1974. Hydraulic Model Studies of Plunge Basins for Jet Flow. *USDI Bureau of Reclamation REC-ERC 74-9*.
- Julien, P.Y. and D.M. Hartley. 1986. Formation of Roll Waves in Laminar Sheet Flow. *J. Hydr. Res.* 24(1):5-17
- Julien, P.Y. and D.B. Simons. 1985. Sediment Transport Capacity of Overland Flow. *Trans. ASAE* 28(3):755-762.
- Kamoi, A. and H. Tanaka. 1972. Measurements of Wall Shear Stress, Wall Pressure and Fluctuations in the Stagnation Region Produced by Oblique Jet Impingement. In: *Fluid Dynamic Measurements Conference Papers Vol. 1*, D.J. Cockrell ED. Leicester University Press.
- Knisel, W.G. (Editor). 1980. CREAMS: A Field Scale Model for Chemicals, Runoff, and Erosion from Agricultural Management Systems. *USDA Conservation Report No. 26*, 640 pp.
- Kobus, H., P. Liester and B. Westrich. 1979. Flow Field and Scouring Effects of Steady and Pulsating Jets Impinging on a Moveable Bed. *J. Hydr. Res.* 17(3):175-192.
- Kuti, E.O. and C.L. Yen. 1976. Scouring of Cohesive Soils. *J. Hydr. Res.* 14(3):195-206
- Lambe, T.W. and R.V. Whitman. 1969. *Soil Mechanics*. John Wiley & Sons, New York, NY
- Lambermont, J. and G. Lebon. 1978. Erosion of Cohesive Soils. *J. Hydr. Res.* 16(1):27-44.

- Larsson, R., U. Bergdahl, and L. Eriksson. 1987. Evaluation of Shear Strength in Cohesive Soils with Special Reference to Swedish Practice and Experience. *Geotech. Test. J.* 10(3):105-112.
- Laursen, E.M. Observations on the Nature of Scour. *Proc. 5th Hydr. Conf., University of Iowa, Iowa City, Iowa Bul.* 34 pp. 179-197.
- Leopold, L.D., M.G. Wolman, and J.P. Miller. 1964. *Fluvial Processes in Geomorphology.* W.H. Freeman and Co., San Francisco, CA.
- Little, W.C., C.R. Thorne and J.B. Murphey. 1982. Mass Bank Failure Analysis of Selected Yazoo Basin Streams. *Trans. ASAE* 25(5):1321-1328.
- Markland, Eric 1965. Calculation of Flow at a Free Overfall by Relaxation Method. *Inst. Civ. Engr. Proc.* 31:71-78 (1965). Discussion 34:285-294 (1966).
- Martins, Rui. 1973. Contribution to the Knowledge on the Scour Action of Free Jets on Rocky River-Beds. 11th Inter. Comm. Large Dams Trans. Vol. II Q41 Paper R44 799-814.
- Martins, Rui B.F. 1975. Scouring of Rocky River-Beds by Free-Jet Spillways. *Inter. Water Pow. Dam Constr.* 27(4):152-153.
- Mason, P.J. 1984. Erosion of Plunge Pools Downstream of Dams Due to the Action of Free-Trajectory Jets. *Proc. Inst. Civ. Engrs. Pt. 1* 76:523-537.
- Mason, P.J. 1989. Effects of Air Entrainment on Plunge Pool Scour. *J. Hydr. Engr.* 115(3):385-399.
- Mason, P.J. and K. Arumugam. 1985. Free Jet Scour Below Dams and Flip Buckets. *J. Hydr. Engr.* 111(2):220-235.
- Mih, W.C. and J. Kabir. 1983. Impingement of Water Jets on Nonuniform Streambed. *J. Hydr. Engr.* 109(4):536-548.
- Mirtskhulava, Ts. E., I.V. Dolidze and A.V. Magomedova. 1967. Mechanism and Computation of Local and General Scour in Non-Cohesive, Cohesive and Rock Beds. *Inter. Asso. Hydr. Res. Proc. 12th Congress Vol. 3:169-176, Paper No. C20.*
- Moore, I.D. and G.J. Burch. 1986. Sediment Transport Capacity of Sheet and Rill Flow : Application of Unit Stream Power Theory. *Water Resources Res.* 22(8):1350-1360.
- Moore, W.L. 1943. Energy Loss at the Base of a Free Overfall. *ASCE Trans.* 108:1343-1360. Discussions 108:1361-1392.

- Nearing, M.A., L.T. West and L.C. Brown. 1988. A Consolidation Model for Estimating Changes in Rill Erodability. *Trans. ASAE* 31(3):696-700.
- Nearing, M.A., G.R. Foster, L.J. Lane and S.C. Finkner. 1989. A Processed-Based Soil Erosion Model for USDA Water Erosion Predictio Project Technology. *Trans. ASAE* 32(5):1587-1593.
- Nordin, C.F., Jr. 1964. Study of Channel Erosion and Sediment Transport. *J. Hydr. Div. ASCE* 90(HY4):173-192.
- Osman, A.M. and C.R. Thorne. 1988. Riverbank Stability Analysis. I: Theory. *J. Hydr. Engr.* 114(2):134-150.
- Parsons, D.A. 1960. Effects of Flood Flow on Channel Boundaries. *J. Hydr. Div. ASCE* 86(HY4):21-34.
- Partheniades, E. 1965. Erosion and Deposition of Cohesive Soils. *J. Hydr. Div. ASCE.* 91(HY1):105-138.
- Partheniades, E. 1972. Results of Recent Investigations on Erosion and Deposition of Cohesive Sediments. In: Shen, H.W. (Ed.), *Sedimentation: Symposium to Honor Professor H.A. Einstein*, pp. 20.1-20.29. H.W. Shen, Fort Collins, CO.
- Partheniades, E. and R.E. Paswell. 1970. Erodibility of Channels with Cohesive Boundary. *J. Hydr. Div. ASCE* 96:755-771.
- Patel, V.C. 1965. Calibration of the Preston Tube and Limitations on its Use in Pressure Gradients. *J. Fluid Mech.* 23 Pt 1:185-208.
- Patton, P.C. and S.A. Schumm. 1975. Gully Erosion, Northwestern Colorado : A Threshold Phenomenon. *Geology* 3:88-90.
- Piest, R.F., J.M. Bradford and G.M. Wyatt. 1975. Soil Erosion and Sediment Transport From Gullies. *J. Hydr. Div. ASCE* 101:65-80.
- Ponce, V.M. 1978. Generalized Stability Analysis of Channel Banks. *J. Irr. Drain. Div. ASCE* 104(IR4):343-350. Discussions: 1979. *J. Irr. Drain. Div. ASCE* 105(IR4):436-437. and 1980. *J. Irr. Drain. Div. ASCE* 106(IR3):255.
- Popova, K.S. and Y.E. Vedeneyev. 1988. Time Variation in the Depth of Local Scour Downstream of Dams. *Fluid Mech. - Soviet Res.* 17(3):123-134.
- Poreh, M. and E. Hefez. 1967. Initial Scour and Sediment Motion Due to an Impinging Submerged Jet. *Inter. Asso. Hydr. Res. Proc.* 12th Congress Vol. 3:9-16.

- Preston, J.H. 1953. The Determination of Turbulent Skin Friction by Means of Pitot Tubes. *J. Royal Aeronautical Soc.*, London 58(518):109-121.
- Rajaratnam, N. 1967. Plane Turbulent Wall Jets on Rough Boundaries. *Water Power* 29:(4):149-153, 29(5):196-201, 29(6):240-242 (April, May and June).
- Rajaratnam, N. 1972. Plane Turbulent Compound Wall Jets. *J. Hydr. Res.* 10:189-203.
- Rajaratnam, N. 1976. *Turbulent Jets : Development in Water Science #5*. Elsevier Scientific Publishing Co. Amsterdam, Netherlands.
- Rajaratnam, N. 1981. Erosion by Plane Turbulent Jets. *J. Hydr. Res.* 19(4):339-359.
- Rajaratnam, N. 1982. Erosion by Unsubmerged Plane Water Jets. In: *Applying Research to Hydraulic Practice*, ASCE Conf. Jackson, MS. pp. 280-288.
- Rajaratnam, N. and D. Muralidhar 1968. Characteristics of the Rectangular Free Overfall. *J. Hydr. Res.* 6(3):233-258.
- Rajaratnam, N. and D. Muralidhar 1970. The Trapezoidal Free Overfall. *J. Hydr. Res.* 8(4):419-447.
- Rajaratnam, N., D. Muralidhar and S. Beltaos 1976. Roughness Effects on Rectangular Free Overfall. *J. Hydr. Div. ASCE* 102(Hy5):599-614. Errata: *J. Hydr. Div. ASCE* 103(Hy3):337-338 1977.
- Rajaratnam, N. and K. Subramanya. 1968. Plane Turbulent Reattached Wall Jets. *J. Hydr. Div. ASCE* 94(HY1):95-112
- Rajaratnam, Nallamuthu and Spyridon Beltaos. 1977. Erosion by Impinging Circular Turbulent Jets. *J. Hydr. Div. ASCE* 103:1191-1205.
- Rand, W. 1955. Flow Geometry at Straight Drop Spillways. *ASCE Proc.* 81(Sept) Sep No. 791.
- Rauws, G. and G. Glovers. 1988. Hydraulic and Soil Mechanical Aspects of Rill Generation on Agricultural Soils. *J. of Soil Sci.* 39:111-124.
- Replogle, J.A. 1961. Discussion of "End Depth at a Drop in Trapezoidal Channels" Diskin. *J. Hydr. Div. ASCE* 88(Hy2):161-165.
- Robinson, K.M. 1988. Stress Distribution at an Overfall. *ASAE Paper No. 88-2135* Presented at ASAE Summer Meetings Rapid City, S.D., June 26-29, 1988.
- Robinson, K.M. 1989. Stress Distribution at an Overfall. *Trans. ASAE* 32(1):75-80.

Rooseboom, A. and F.J. Mulke. 1982. Erosion Initiation. Inter. Asso. Hydro. Sci. (IAHS) 137:59-66.

Rouse, Hunter. 1936. Discharge Characteristics of the Free Overfall. Civil Engr. 6(4):257-260.

Rouse, Hunter. 1937. Pressure Distribution and Acceleration at the Free Overfall. Civil Engr. 7(7):518.

Rouse, Hunter. 1940. Criteria for Similarity in the Transportation of Sediment. Proc. 1st Hydraulic Conf. State University of Iowa, Iowa City, Iowa. pp33-49.

Schauer, J.J. and R.H. Eustis. 1963. The Flow Development and Heat Transfer Characteristics of Plane Turbulent Impinging Jets. Tech. Rept. 3 Dept. of Mechanical Engr. Stanford University, Stanford, CA.

Shaikh, A., J.F. Ruff and S.B. Abt. 1986. Surface Erosion of Compacted Clays. Research Report Civil Engr. Dept. Colorado State Univ. Fort Collins, CO, Report No. CER85-86-AS-JFR-SRA29.

Sherard, J.L., L.P. Dunnigan, R.S. Decker and E.F. Steele. 1976. Pinhole Test for Identifying Dispersive Soils. J. Geotech. Engr. Div. ASCE 102(GT1):69-85.

Shields, A. 1936. Anwendung Der Aenlichkeitsmechanik Und Der Turbulenzforschung Auf Die Geschiebebewegung Mitteilungen Der Preussischen Versuchsanstalt Fur Wassererbau Und Schiffbau, Berlin, Germany. Translated to English by W.P. Ott and J.C. Van Ucheden California Institute of Technology, Pasadena, CA.

Shih, C.C. and D.F. Parsons. 1967. Some Hydraulic Characteristics of Trapezoidal Drop Structures. Inter. Asso. Hydr. Res. Proc. 12th Congress Vol. 3:249-259.

Simons, D.B. and F. Senturk. 1977. Sediment Transport Technology. Water Resources Publications, Fort Collins, Colorado 80522.

Soulliere, E.J. and T.J. Toy. 1986. Rilling of Hillslopes Reclaimed Before 1977 Surface Mining Law, Dave Johnston Mine, Wyoming. Earth Surface Processes and Landforms 11:293-305.

Southwell, R.V. and G. Vaisey 1946. Relaxation Methods Applied to Engineering Problems. Royal Soc. London Phil. Trans. Series A Vol A240:117-161.

Springer, F.M., C.R. Ullrich and D.J. Hagerty. 1985. Streambank Stability. J. Geotech. Engr. 111(5):624-640.

- Spurr, K.J.W. 1985. Energy Approach to Estimating Scour Downstream of a Large Dam. *Inter. Water Power and Dam Const.* 37(7):81-89.
- Stevens, M.A. and D.B. Simons. 1971. Stability Analysis for Coarse Granular Material. In: *River Mechanics Vol 1. (Chap 17)* H.W. Shen Ed. Fort Collins CO.
- Stieb, D.J. 1983. Surface Seal Development with Shallow Overland Flow. M.S. Thesis, Colorado State University, Ft. Collins, CO.
- Task Committee on Sedimentation. 1968. Erosion of Cohesive Sediments. *J. Hydr. Div. ASCE* 94:1017-1047.
- Thorne C.R. 1978. Processes of Bank Erosion in River Channels. Ph.D. Dissertation. School of Environmental Processes, University of East Anglia, England.
- Thorne, C.R. 1982. Processes and Mechanisms of River Bank Erosion. In : *Gravel Bed Rivers.* Hey, R.D., J.C. Bathurst, and C.R. Thorne, Ed. John Wiley and Sons Ltd.
- Thorne, C.R. and J. Lewin. 1979. Bank Processes, Bed Material Movement and Planform Development in a Meandering River. In : *Adjustment of the Fluvial System.* D.D. Rhodes and G.P. Williams Ed.
- Thorne, C.R. and A.M. Osman. 1988. Riverbank Stability Analysis. II: Applications. *J. Hydr. Engr.* 114(2):151-172.
- Thorne, C.R. and N.K. Tovey. 1981. Stability of Composite River Banks. *Earth Surface Processes and Landforms* 6:469-484.
- Thorne, C.R., N.K. Tovey and R. Bryant. 1980. Recording Unconfined Tension Tester. *J. Geotech. Engr. Div. ASCE* 106(GT11):1269-1273.
- Torri, D. and J. Poesen. 1988. Incipient Motion Conditions for Single Rock Fragments in Simulated Rill Flow Earth Surface Processes and Landforms. *13:225-237.*
- Vanoni, V.A. Editor. 1977. *Sedimentation Engineering.* 745 pages. ASCE Manuals and Reports on Engineering. Practice No. 54, Headquarters: 345 E. 47th St., New York, NY 10017.
- Van Der Meulen, T. and J.J. Vinje. 1975. Three Dimensional Local Scour in Non-Cohesive Sediments. *Inter. Assoc. Hydr. Res. Proc. 16th Congress.*
- Van Der Poel, P. and G.O. Schwab. 1985. Plunge Pool Erosion in Cohesive Channels Below a Free Overfall. *ASAE Paper No. 85-2038.*

Van Der Poel, P. and G.O. Schwab. 1988. Plunge Pool Erosion in Cohesive Channels Below a Free Overfall. Trans. ASAE 3(4):1148-1153.

de Vries, M. 1975. A Morphological Time-Scale for Rivers. Inter. Asso. Hydr. Res. Proc. 16th Congress Vol. 2:17-23.

Watkins, R.D. 1969. Local Scour in Beds of Sand and Gravel Downstream from a Solid Apron. Inst. of Engr. Australia, Civil Engr. Trans. Vol. CEII(1) April 1969; 97-106.

Yuen, E.M. 1984. Clearwater Scour by High Velocity Jets. M.S. Thesis, University of Windsor, Windsor, Ontario, Canada.

Appendix A

Measured Sediment Concentration Data

Table A1: Measured Sediment Concentration Data; Constant Slope Runs

Run	t (s)	C	Run	t (s)	C
CS1A	122	0.00648	CS4A	30	0.00013
CS1A	196	0.00401	CS4A	112	0.00010
CS1A	245	0.00341	CS4A	157	0.00007
CS1B	102	0.01656	CS4A	261	0.00002
CS1B	180	0.01226	CS4A	301	0.00006
CS1B	239	0.01256	CS4A	347	0.00005
CS1C	93	0.02550	CS4B	30	0.00099
CS1C	135	0.02146	CS4B	90	0.00076
CS1C	180	0.01782	CS4B	210	0.00050
CS2A	108	0.00172	CS4B	277	0.00046
CS2A	175	0.00104	CS4C	30	0.00234
CS2A	275	0.00094	CS4C	90	0.00331
CS2A	320	0.00102	CS4C	157	0.00439
CS2B	80	0.01171	CS4C	274	0.00253
CS2B	160	0.00880	CS5A	65	0.00065
CS2B	220	0.00938	CS5A	101	0.00152
CS2C	75	0.01627	CS5A	235	0.00170

Run	t (s)	C	Run	t (s)	C
CS2C	157	0.01389	CS5A	285	0.00113
CS2C	190	0.01141	CS5B	30	0.00736
CS3A	20	0.01111	CS5B	99	0.00516
CS3A	95	0.00540	CS5B	150	0.00393
CS3A	165	0.00337	CS5B	210	0.00628
CS3A	240	0.00284	CS5C	45	0.01401
CS3B	30	0.01224	CS5C	105	0.02089
CS3B	90	0.00814	CS5C	165	0.02306
CS3B	150	0.00798	CS5C	250	0.01989
CS3B	210	0.00783	CS5C	305	0.01710
CS3C	15	0.02688			
CS3C	90	0.01163			
CS3C	150	0.00805			
CS3C	215	0.00605			

Table A2: Measured Sediment Concentration; Non-Retreating Soil Runs

Run	t (s)	C	q _s (g/s)	Run	t (s)	C	q _s (g/s)
1	70	0.0136	3.1683	3&4	100	0.0063	1.4808
1	173	0.0133	3.0984	3&4	270	0.0040	0.9402
1	270	0.0137	3.1916	3&4	340	0.0037	0.8696
1	360	0.0119	2.7722	3&4	685	0.0024	0.5641
1	530	0.0138	3.2148	3&4	840	0.0020	0.4701
2	70	0.0045	1.1045	3&4	1060	0.0020	0.4701
2	120	0.0042	1.0308	3&4	1290	0.0020	0.4701
2	240	0.0039	0.9572	3&4	1680	0.0021	0.4936
2	425	0.0042	1.0308	3&4	2400	0.0017	0.3996
2	615	0.0039	0.9572	3&4	4760	0.0022	0.5171
2	795	0.0038	0.9327	3&4	4815	0.0013	0.3056
				3&4	4935	0.0016	0.3761
				3&4	5075	0.0019	0.4466
				3&4	5400	0.0014	0.3291
				3&4	5780	0.0029	0.6816
				3&4	6285	0.0009	0.2115
				3&4	6600	0.0008	0.1880

Run	t (s)	C	q _p (g/s)	Run	t (s)	C	q _p (g/s)
				3&4	6975	0.0007	0.1645
6	15	0.0165	7.7220	7	15	0.00933	1.4943
6	40	0.0112	5.2416	7	50	0.00681	1.0907
6	70	0.0092	4.3056	7	230	0.00377	0.6038
6	150	0.0065	3.0420	7	390	0.00395	0.6326
6	255	0.0043	2.0124	7	450	0.00283	0.4533
6	400	0.0026	1.2168	7	810	0.00155	0.2482
6	540	0.0022	1.0296	7	990	0.00118	0.1890
6	760	0.0021	0.9828	7	1200	0.00133	0.2130
6	1260	0.0017	0.7956	7	1420	0.00116	0.1858
6	1980	0.0011	0.5148	7	1750	0.00111	0.1778
6	2580	0.0011	0.5148	7	2030	0.00127	0.2034
6	3300	0.0014	0.6552	7	2220	0.00109	0.1746
6	3780	0.0008	0.3744	7	2575	0.00127	0.2034
6	4680	0.0007	0.3276	7	2920	0.00111	0.1778
6	5520	0.0005	0.2340	7	3270	0.00105	0.1682
6	5940	0.0008	0.3744	7	3940	0.00111	0.1778
				7	5057	0.00119	0.1906

Run	t (s)	C	q _p (g/s)	Run	t (s)	C	q _p (g/s)
				7	6185	0.00096	0.1538
8	11	0.01105	1.9766	9	10	0.03827	18.2288
8	90	0.00497	0.8890	9	30	0.01422	6.7733
8	180	0.00408	0.7298	9	50	0.01000	4.7632
8	255	0.00339	0.6064	9	80	0.00740	3.5248
8	390	0.00314	0.5617	9	115	0.00845	4.0249
8	615	0.00245	0.4383	9	175	0.00828	3.9439
8	880	0.00324	0.5796	9	295	0.00494	2.3530
8	1040	0.00433	0.7746	9	390	0.00518	2.4673
8	1440	0.00193	0.3452	9	710	0.00348	1.6576
8	1795	0.00151	0.2701	9	975	0.00352	1.6766
8	2065	0.00172	0.3077	9	1435	0.00220	1.0479
8	2520	0.00182	0.3256	9	1795	0.00298	1.4194
8	3240	0.00166	0.2969	9	2350	0.00180	0.8574
8	3830	0.00224	0.4007	9	2945	0.00157	0.7478
8	4530	0.00276	0.4937	9	3280	0.00151	0.7192
8	5110	0.00230	0.4114	9	4050	0.00106	0.5049
8	5595	0.00201	0.3595				

Run	t (s)	C	q _e (g/s)	Run	t (s)	C	q _e (g/s)
8	6120	0.00241	0.4311				
8	6780	0.00137	0.2451				
8	6970	0.00176	0.3148				
8	7705	0.00128	0.2290				
8	8377	0.00174	0.3113				
8	9817	0.00195	0.3488				
10	12	0.02108	7.7608	11	21	0.00704	2.5333
10	35	0.01461	5.3788	11	87	0.00368	1.3242
10	60	0.00979	3.6043	11	175	0.00336	1.2091
10	142	0.00514	1.8923	11	267	0.00332	1.1947
10	240	0.00338	1.2444	11	410	0.00353	1.2702
10	390	0.00238	0.8762	11	550	0.00364	1.3098
10	595	0.00187	0.6885	11	740	0.00406	1.4610
10	890	0.00231	0.8504	11	1048	0.00177	0.6369
10	1235	0.00126	0.4639	11	1312	0.00195	0.7017
10	1505	0.00121	0.4455	11	1762	0.00203	0.7305
10	1805	0.00093	0.3424	11	2162	0.00362	1.3026
10	2170	0.00116	0.4271	11	2347	0.00258	0.9284

Run	t (s)	C	q _s (g/s)	Run	t (s)	C	q _s (g/s)
10	2420	0.00116	0.4271	11	2820	0.00208	0.7485
10	2740	0.00114	0.4197	11	3315	0.00168	0.6045
10	3124	0.00106	0.3902	11	3988	0.00151	0.5434
10	3645	0.00097	0.3571	11	4725	0.00124	0.4462
10	3982	0.00093	0.3424	11	5593	0.00119	0.4282
10	4505	0.00100	0.3682	11	6393	0.00099	0.3562
10	5325	0.00086	0.3166	11	7238	0.00113	0.4066
10	6145	0.00173	0.6369	11	8160	0.00093	0.3347
10	6825	0.00099	0.3645	11	9000	0.00111	0.3994
10	7560	0.00116	0.4271				
10	8315	0.00109	0.4013				
10	8980	0.00098	0.3608				
12	18	0.00721	3.6667	13	40	0.00392	0.6401
12	50	0.01039	5.2839	13	110	0.00212	0.3462
12	95	0.00853	4.3380	13	285	0.00210	0.3429
12	195	0.00565	2.8734	13	415	0.00170	0.2776
12	480	0.00271	1.3782	13	600	0.00150	0.2449
12	953	0.00159	0.8086	13	854	0.00126	0.2057

Run	t (s)	C	q _s (g/s)	Run	t (s)	C	q _s (g/s)
12	1200	0.00169	0.8595	13	1383	0.00182	0.2972
12	1561	0.00126	0.6408	13	1685	0.00188	0.3070
12	2220	0.00122	0.6204	13	2075	0.00158	0.2580
12	2590	0.00092	0.4679	13	2640	0.00181	0.2955
12	3053	0.00083	0.4221	13	3255	0.00112	0.1829
12	3720	0.00037	0.1882	13	4022	0.00098	0.1600
12	4200	0.00039	0.1983	13	4730	0.00099	0.1616
12	4890	0.00155	0.7883	13	5354	0.00076	0.1241
12	5444	0.00087	0.4424	13	5975	0.00128	0.2090
12	5980	0.00035	0.1780	13	7150	0.00059	0.0963

Table A3: Measured Sediment Concentration; Non-Retreating Sand Runs

Run	t (s)	C	q _s (g/s)	Run	t (s)	C	q _s (g/s)
14	27	0.01673	2.9231	15	41	0.01435	3.5071
14	86	0.01338	2.3378	15	140	0.01110	2.7128
14	290	0.00337	0.5888	15	286	0.00383	0.9361
14	470	0.00161	0.2813	15	660	0.00049	0.1198
14	1040	0.00035	0.0612	15	995	0.00036	0.0880
14	1760	0.00030	0.0524	17	12	0.03073	15.3404
16	25	0.02549	9.6230	17	27	0.03173	15.8396
16	70	0.01785	6.7387	17	45	0.02583	12.8943
16	100	0.01266	4.7794	17	76	0.01545	7.7126
16	210	0.00461	1.7404	17	135	0.00921	4.5976
16	435	0.00288	1.0873	17	275	0.00422	2.1066
16	890	0.00089	0.3360	17	930	0.00095	0.4742
16	1780	0.00036	0.1359	17	1747	0.00037	0.1847
18	5	0.01559	7.9933	17	2958	0.00029	0.1448
18	17	0.02324	11.9156	17	5160	0.00033	0.1647
18	30	0.02427	12.4437	19	3	0.01815	6.5500
18	60	0.01386	7.1063	19	34	0.02164	7.8094

Run	t (s)	C	q _s (g/s)	Run	t (s)	C	q _s (g/s)
18	110	0.00819	4.1992	19	90	0.01222	4.4100
18	180	0.00676	3.4660	19	165	0.00687	2.4792
18	420	0.00185	0.9485	19	270	0.00363	1.3100
18	900	0.00086	0.4409	19	540	0.00152	0.5485
18	1785	0.00025	0.1282	19	975	0.00047	0.1696
20	8	0.01647	4.4021	19	1444	0.00039	0.1407
20	22	0.02130	5.6931	19	1785	0.00045	0.1624
20	50	0.01831	4.8939	21	10	0.00465	0.7834
20	120	0.00970	2.5926	21	45	0.01418	2.3890
20	260	0.00428	1.1440	21	80	0.01160	1.9544
20	465	0.00131	0.3501	21	295	0.00387	0.6520
20	1095	0.00026	0.0695	21	845	0.00043	0.0724
20	1440	0.00029	0.0775	21	1305	0.00067	0.1129
20	1790	0.00014	0.0374	21	1785	0.00014	0.0236
22	11	0.01408	2.4308	23	8	0.01688	4.0728
22	40	0.02199	3.7964	23	35	0.02083	5.0259
22	87	0.01057	1.8248	23	85	0.01118	2.6975
22	192	0.00607	1.0479	23	120	0.01299	3.1342

Run	t (s)	C	q _s (g/s)	Run	t (s)	C	q _s (g/s)
22	438	0.00418	0.7216	23	270	0.00701	1.6914
22	805	0.00345	0.5956	23	638	0.00423	1.0206
22	1360	0.00202	0.3487	23	736	0.00328	0.7914
22	1830	0.00259	0.4471	23	1205	0.00312	0.7528
22	2633	0.00251	0.4333	23	1835	0.00191	0.4608
22	3372	0.00217	0.3746	23	2340	0.00172	0.4150
22	4170	0.00160	0.2762	23	3190	0.00164	0.3957
22	5130	0.00147	0.2538	23	4345	0.00207	0.4994
22	5970	0.00091	0.1571	23	5525	0.00238	0.5742
22	7080	0.00116	0.2003	23	6660	0.00227	0.5477
22	8145	0.00102	0.1761	23	7965	0.00135	0.3257
22	8910	0.00071	0.1226	23	8985	0.00101	0.2437
24	6	0.04103	14.8922	25	11	0.04872	17.0754
24	19	0.02986	10.8380	25	35	0.05374	18.8348
24	45	0.03053	11.0812	25	76	0.03222	11.2925
24	80	0.01832	6.6494	25	160	0.02444	8.5657
24	140	0.01445	5.2448	25	225	0.01883	6.5995
24	261	0.00827	3.0017	25	442	0.00967	3.3891

Run	t (s)	C	q _p (g/s)	Run	t (s)	C	q _p (g/s)
24	440	0.00533	1.9346	25	713	0.00414	1.4510
24	800	0.00513	1.8620	25	995	0.00843	2.9545
24	1101	0.00117	0.4247	25	1223	0.00276	0.9673
24	1760	0.00104	0.3775	25	1540	0.00933	3.2700
24	2365	0.00269	0.9764	25	1718	0.00706	2.4744
24	2690	0.00153	0.5553	25	1944	0.00425	1.4895
24	3362	0.00258	0.9364	25	2349	0.00697	2.4428
24	4224	0.00090	0.3267	25	2662	0.00456	1.5982
24	4320	0.00186	0.6751	25	3030	0.00340	1.1916
24	5465	0.00281	1.0199	25	3175	0.00211	0.7395
24	6445	0.00170	0.6170	25	3670	0.00171	0.5993
24	7320	0.00202	0.7332	25	4335	0.00119	0.4171
24	8040	0.00128	0.4646	25	5496	0.00142	0.4977
24	8960	0.00180	0.6533	25	5717	0.00511	1.7910
26	10	0.04494	11.3105	27	10	0.02984	5.4309
26	34	0.04526	11.3910	27	40	0.02773	5.0469
26	94	0.02916	7.3390	27	184	0.02701	4.9158
26	190	0.01062	2.6728	27	245	0.03353	6.1025

Run	t (s)	C	q _e (g/s)	Run	t (s)	C	q _e (g/s)
26	393	0.01466	3.6896	27	300	0.02295	4.1769
26	700	0.00785	1.9757	27	484	0.01195	2.1749
26	1295	0.00984	2.4765	27	694	0.00821	1.4942
26	1462	0.00430	1.0822	27	969	0.00951	1.7308
26	1840	0.00519	1.3062	27	1279	0.00585	1.0647
26	2300	0.00426	1.0722	27	1600	0.00385	0.7007
26	2655	0.00497	1.2508	27	2131	0.00360	0.6552
26	3576	0.00318	0.8003	27	2602	0.00389	0.7080
26	4163	0.00275	0.6921	27	3285	0.00444	0.8081
26	4745	0.00276	0.6946	27	4063	0.00254	0.4623
26	5686	0.00255	0.6418	27	4660	0.00226	0.4113
26	6550	0.00227	0.5713	27	5359	0.00206	0.3749
26	7642	0.00197	0.4958	27	6265	0.00110	0.2002
26	8380	0.00162	0.4077	27	7303	0.00096	0.1747
26	8886	0.00100	0.2517	27	8093	0.00068	0.1238
26	8960	0.00079	0.1988	27	8975	0.00029	0.0528

Appendix B

Measured Scoured Profile Plots

The following plots are developed from the digitized slide data of the non-retreating headcut runs. Because each line of each plot contains from 50 to 250 x,y points the data is presented in graphical rather than tabular form. Runs 1 through 13 are for the cohesive soil runs, 14 through 21 the large sand runs ($d_{50} = 1.5\text{mm}$) and runs 22 through 27 the small sand runs ($d_{50} = 0.15\text{mm}$). The the time of each line is given in Appendix C.

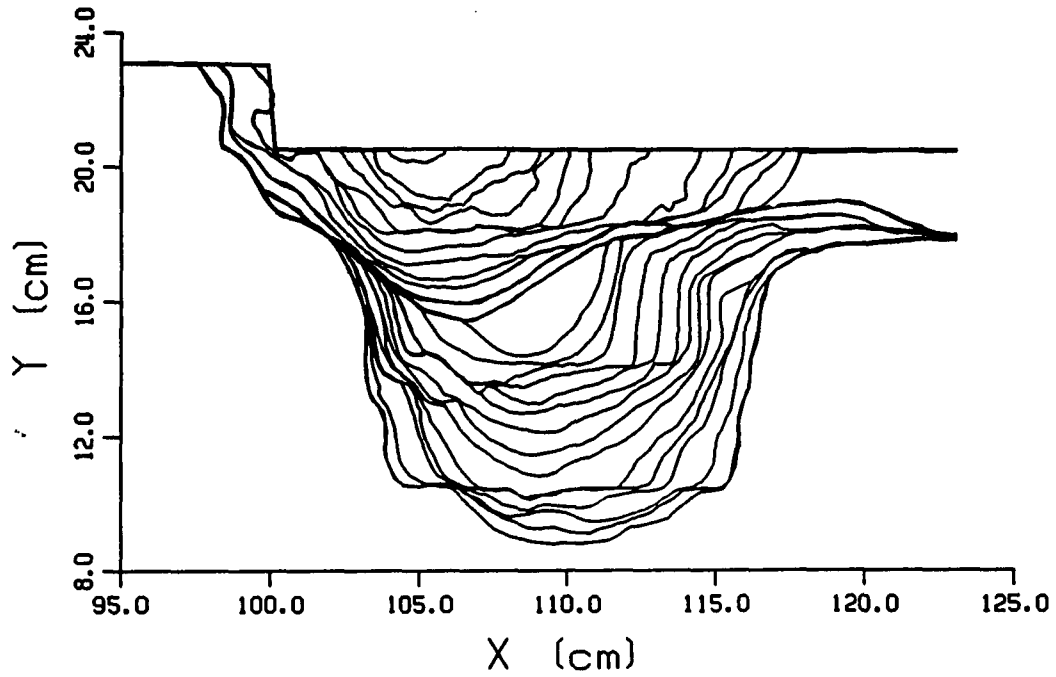


Figure A1: Run 1 Cohesive Soil $q=0.00230 \text{ m}^2/\text{s}$ $D_h=4.0 \text{ cm}$

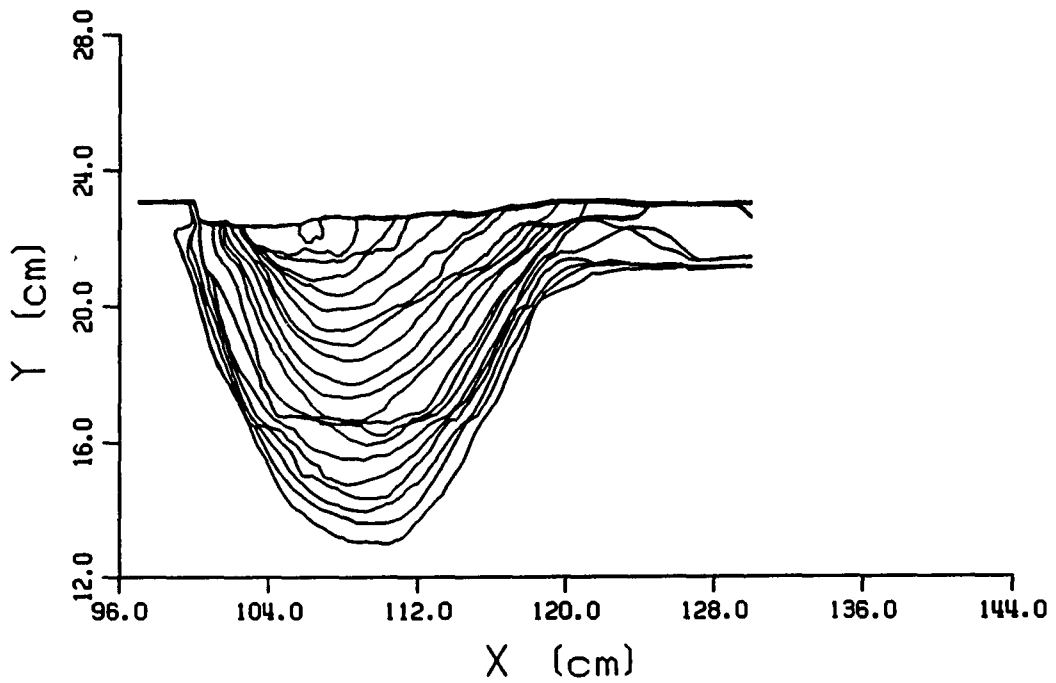


Figure A2: Run 3: Cohesive Soil $q=0.00236 \text{ m}^2/\text{s}$ $D_h=2.0 \text{ cm}$

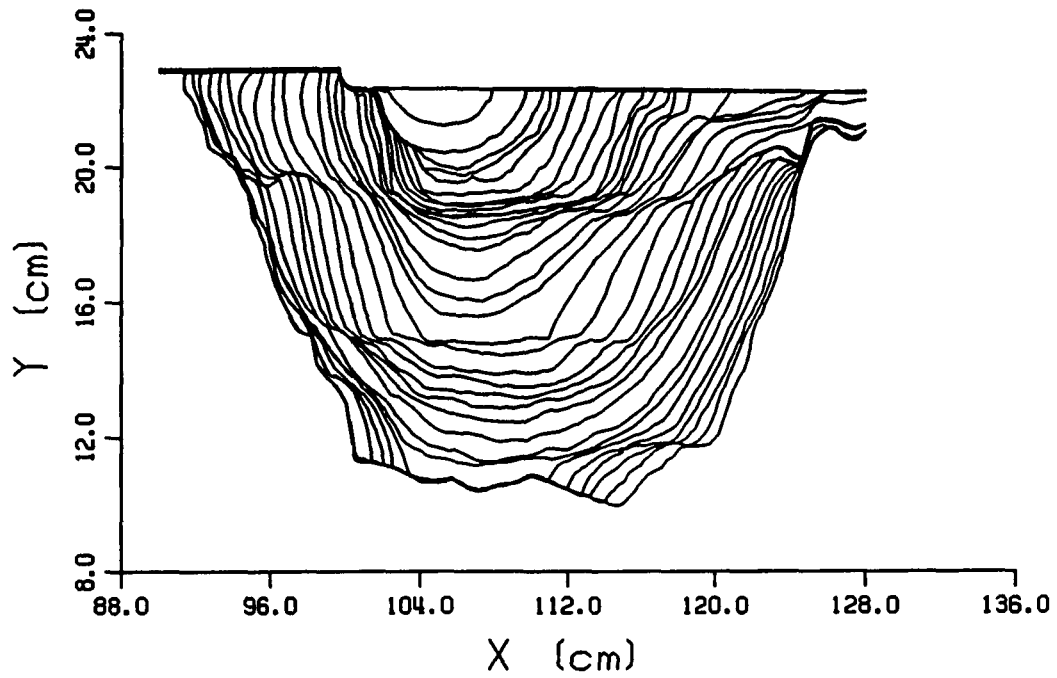


Figure A3: Run 6 Cohesive Soil $q=0.00450 \text{ m}^2/\text{s}$ $D_h=2.0 \text{ cm}$

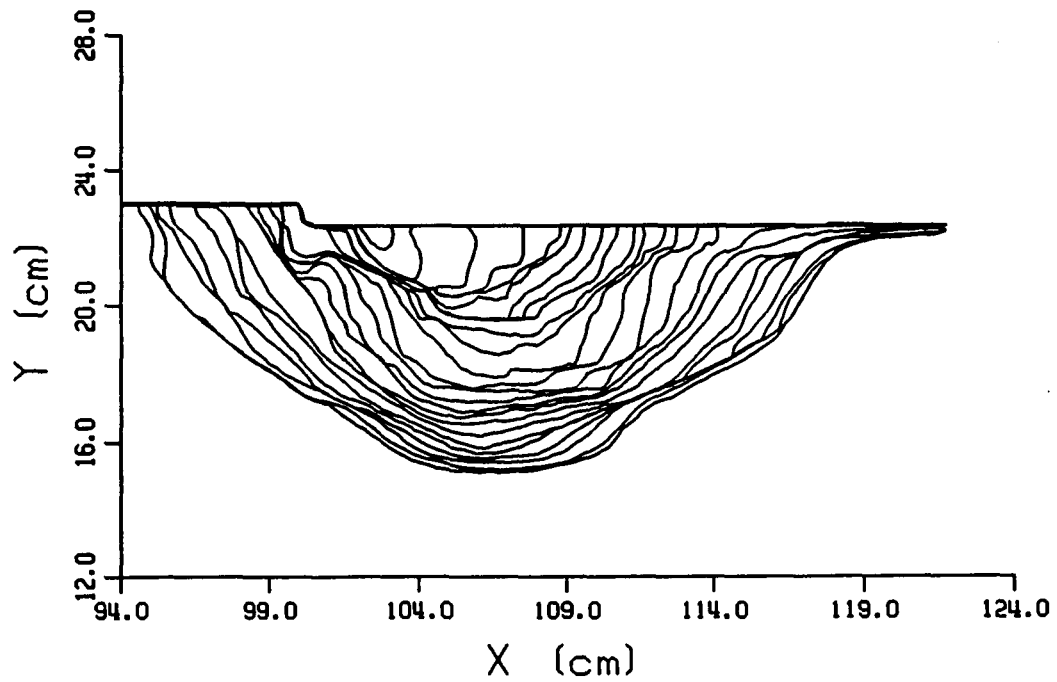


Figure A4: Run 7: Cohesive Soil $q=0.00154 \text{ m}^2/\text{s}$ $D_h=2.0 \text{ cm}$

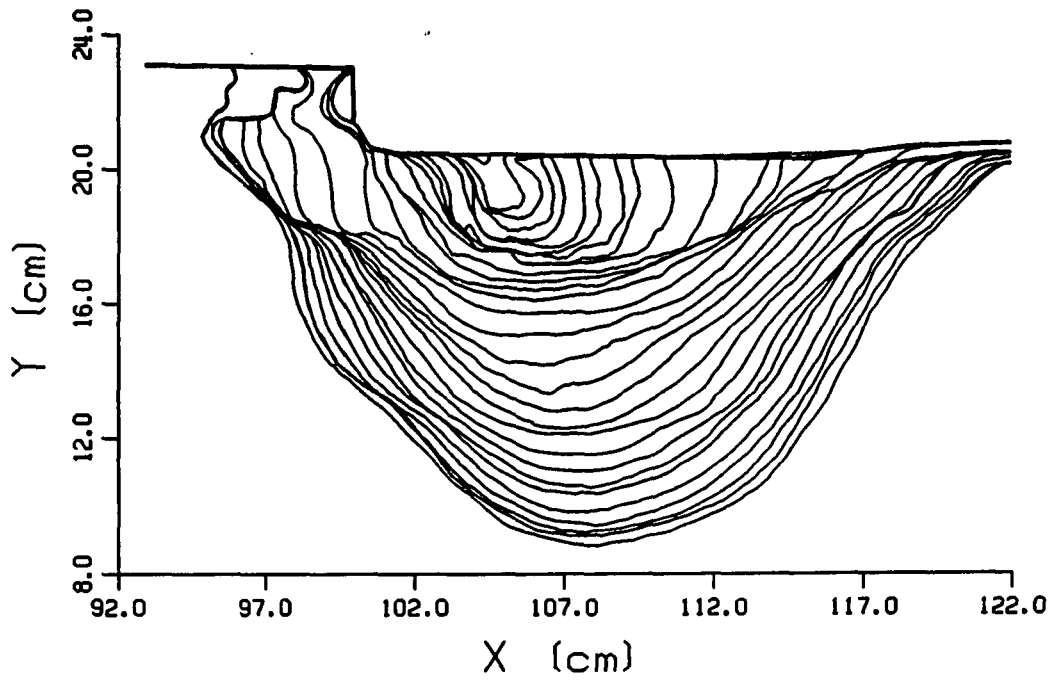


Figure A5: Run 8 Cohesive Soil $q=0.00172 \text{ m}^2/\text{s}$ $D_h=4.0 \text{ cm}$

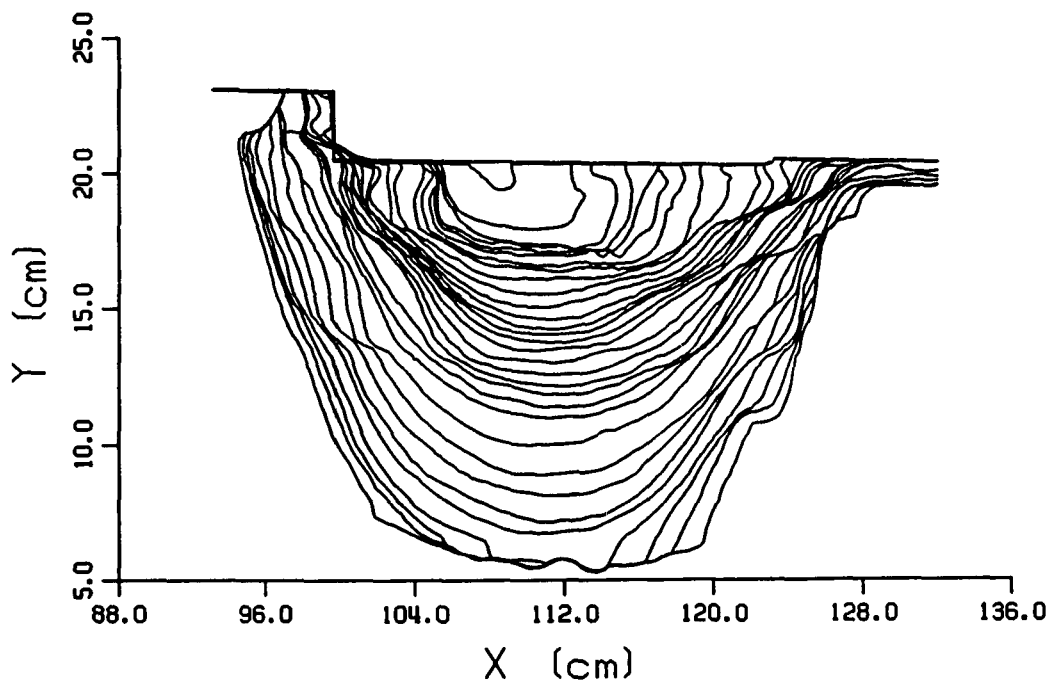


Figure A6: Run 9: Cohesive Soil $q=0.00458 \text{ m}^2/\text{s}$ $D_h=4.0 \text{ cm}$

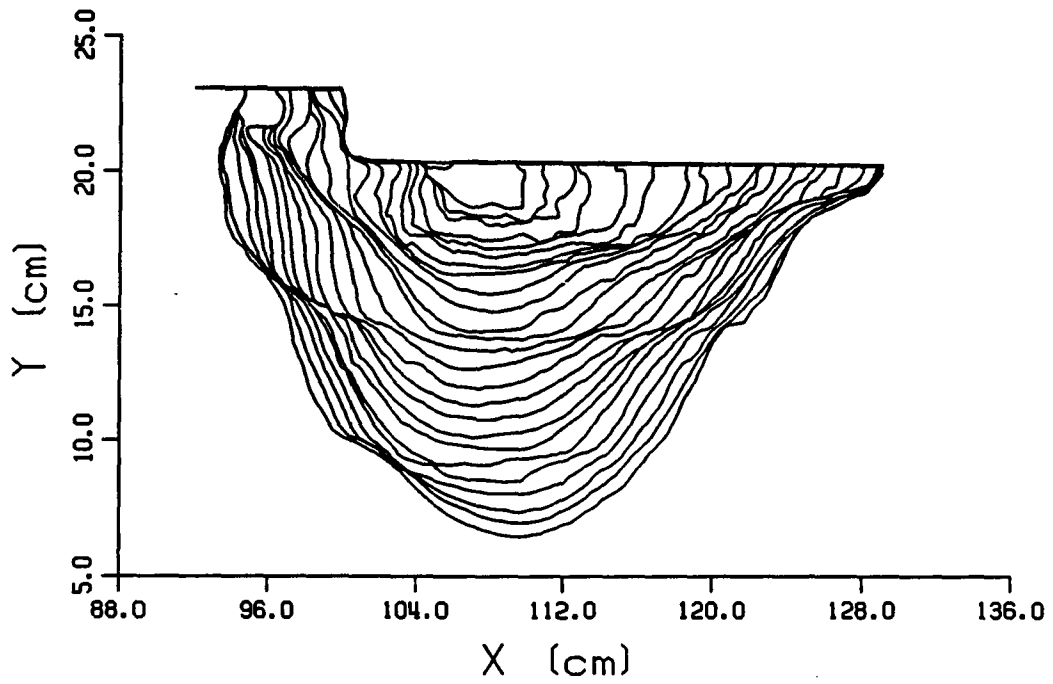


Figure A7: Run 10 Cohesive Soil $q=0.00354 \text{ m}^2/\text{s}$ $D_h=4.0 \text{ cm}$

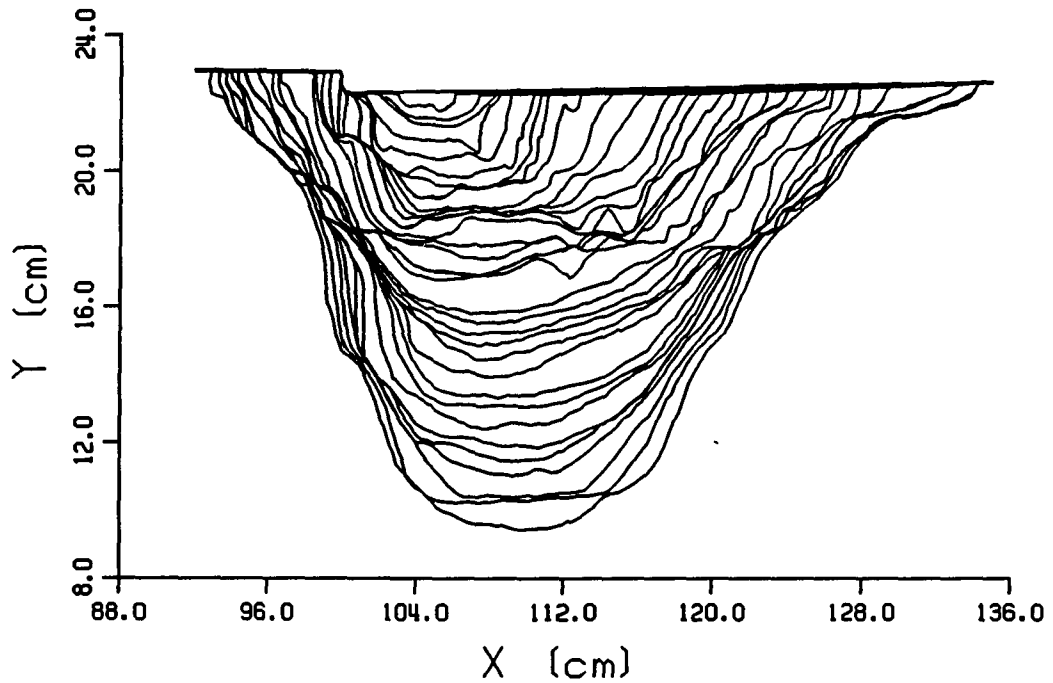


Figure A8: Run 11 Cohesive Soil $q=0.00346 \text{ m}^2/\text{s}$ $D_h=2.0 \text{ cm}$

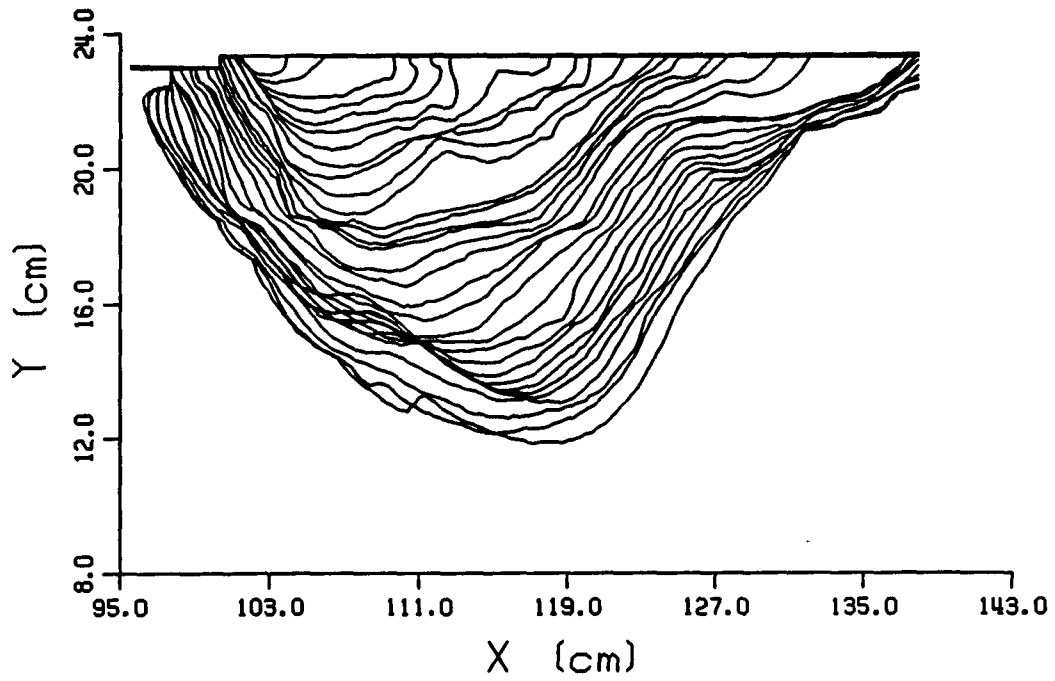


Figure A9: Run 12 Cohesive Soil $q=0.00489 \text{ m}^2/\text{s}$ $D_h=1.0 \text{ cm}$

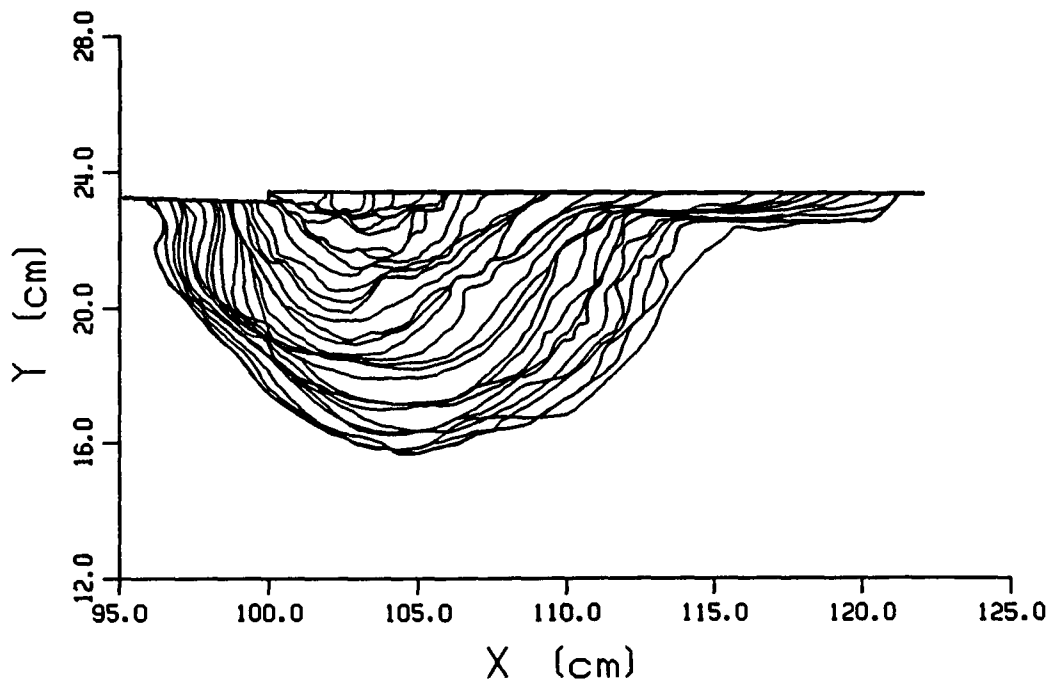


Figure A10: Run 13 Cohesive Soil $q=0.00157 \text{ m}^2/\text{s}$ $D_h=1.0 \text{ cm}$

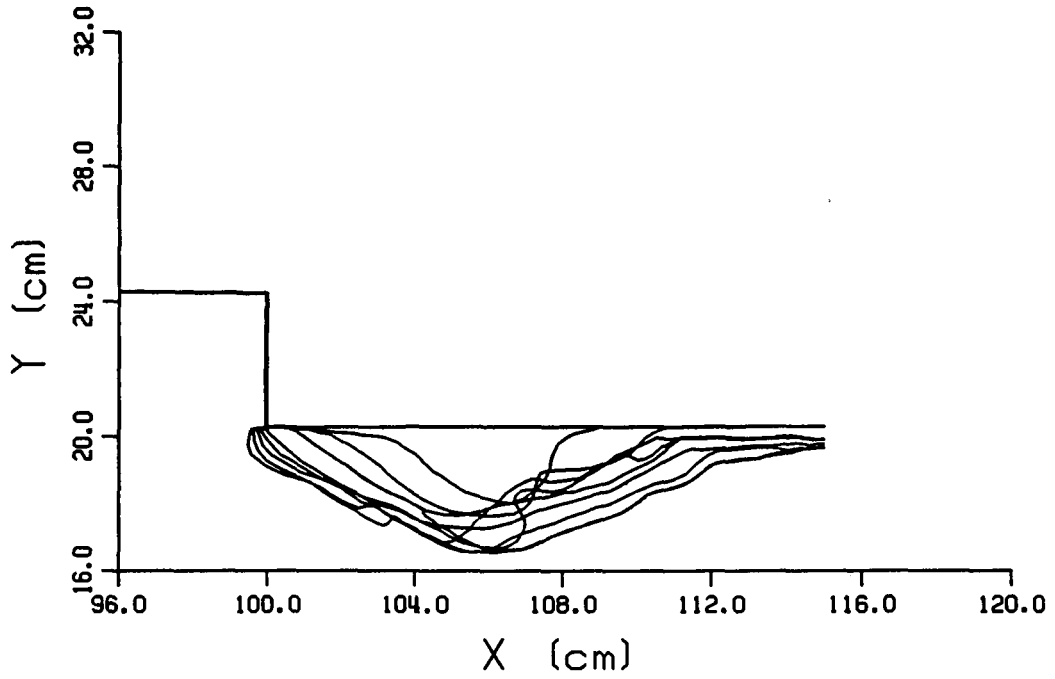


Figure A11: Run 14 Sand $D_{50} = 1.5\text{mm}$ $q = 0.00168 \text{ m}^2/\text{s}$ $D_h = 4.0 \text{ cm}$

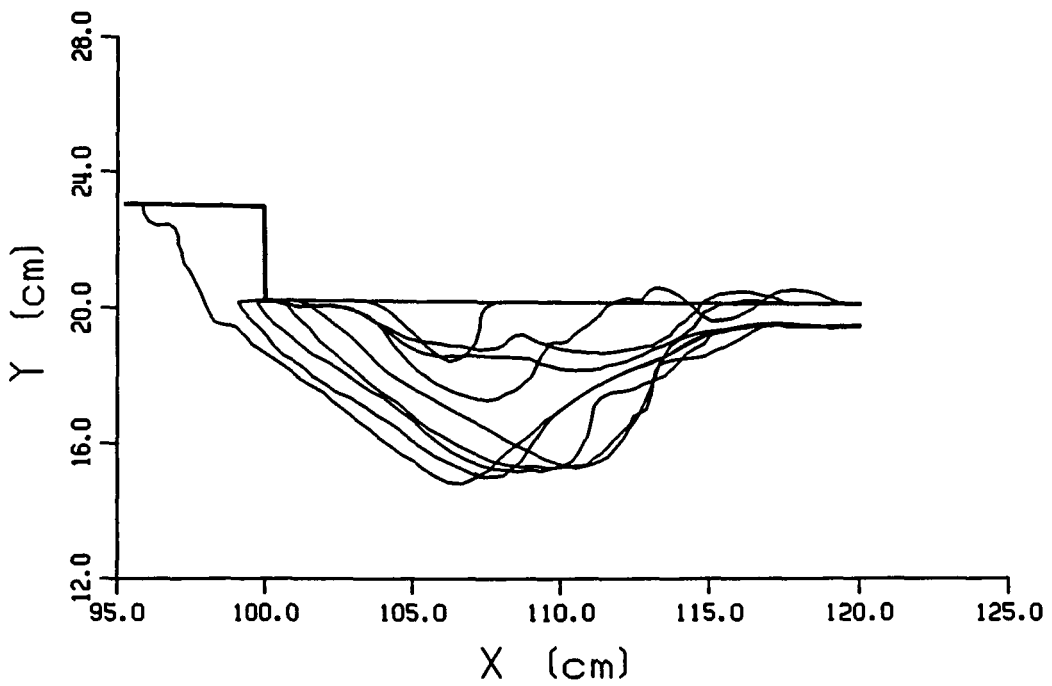


Figure A12: Run 15 Sand $d_{50} = 1.5\text{mm}$ $q = 0.00235 \text{ m}^2/\text{s}$ $D_h = 4.0 \text{ cm}$

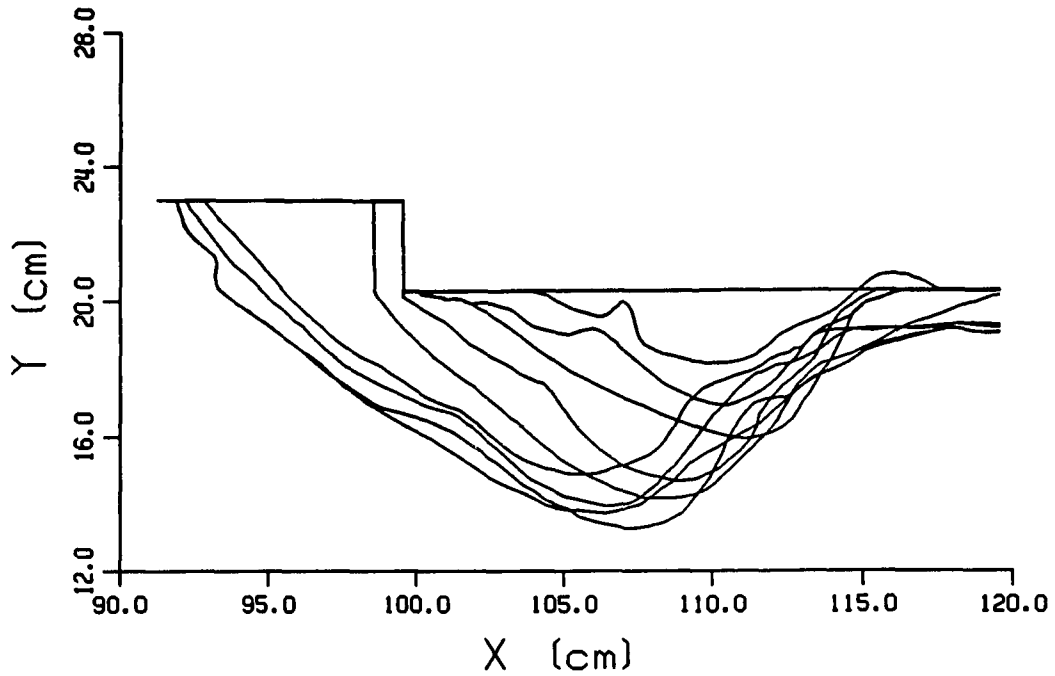


Figure A13: Run 16 Sand $D_{50} = 1.5\text{mm}$ $q = 0.00353 \text{ m}^2/\text{s}$ $D_h = 4.0 \text{ cm}$

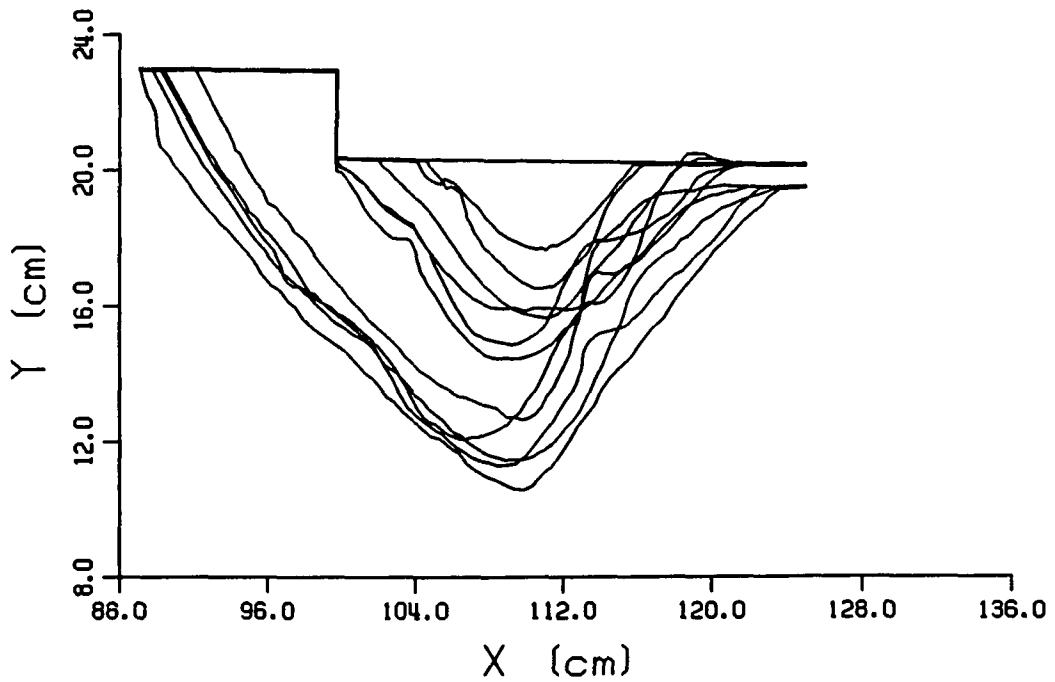


Figure A14: Run 17 Sand $d_{50} = 1.5\text{mm}$ $q = 0.00480 \text{ m}^2/\text{s}$ $D_h = 4.0 \text{ cm}$

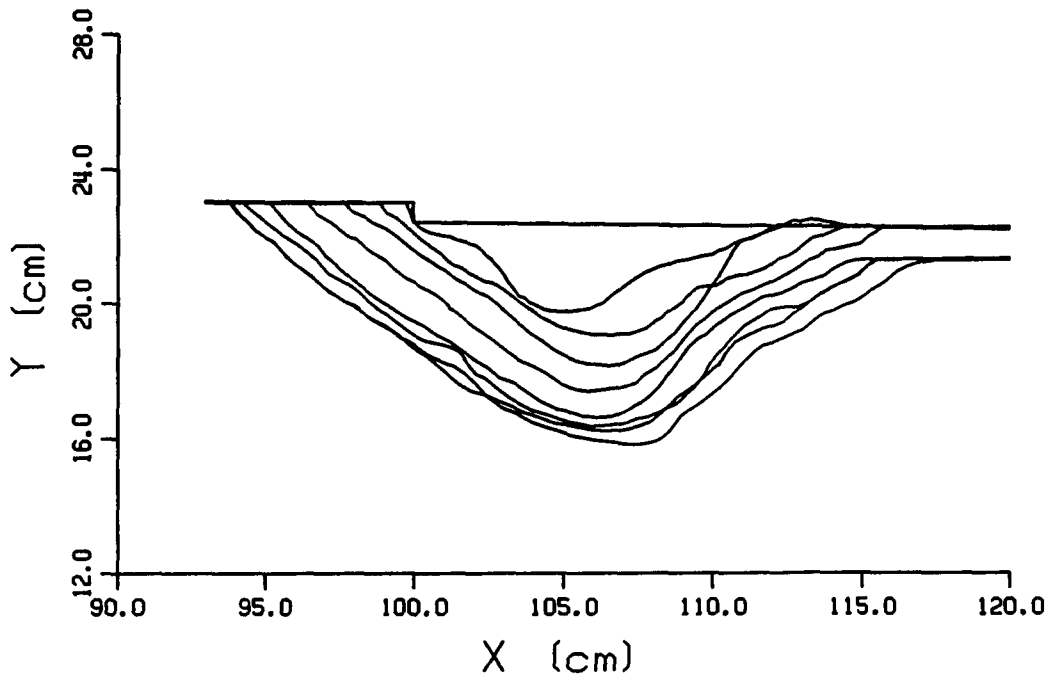


Figure A15: Run 19 Sand $D_{50} = 1.5\text{mm}$ $q = 0.00347 \text{ m}^2/\text{s}$ $D_h = 2.0 \text{ cm}$

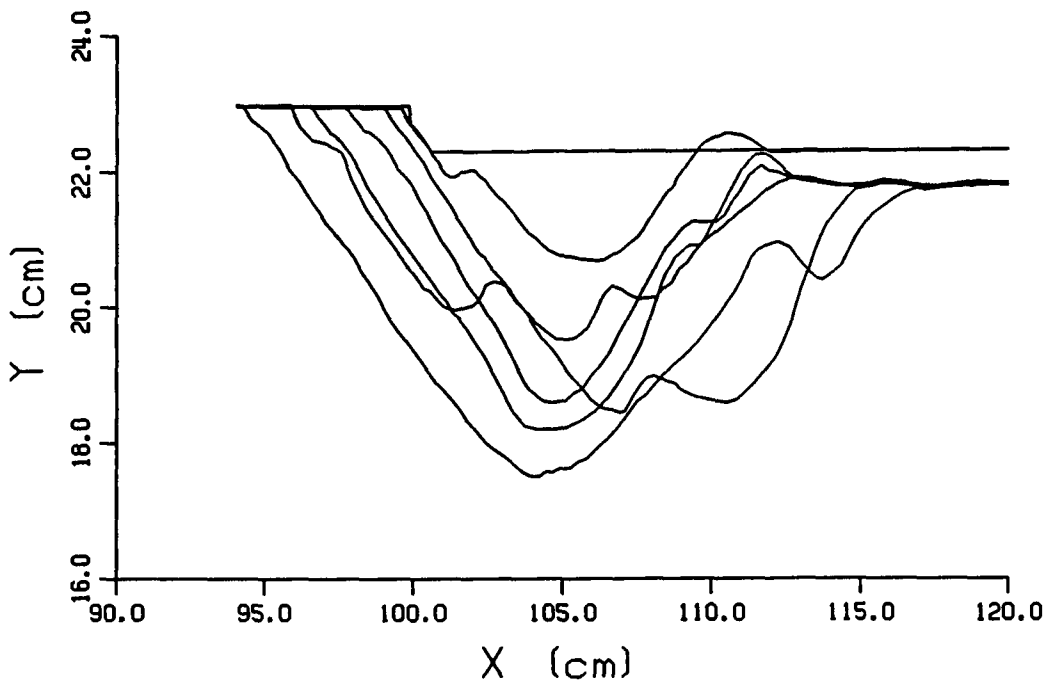


Figure A16: Run 20 Sand $d_{50} = 1.5\text{mm}$ $q = 0.00257 \text{ m}^2/\text{s}$ $D_h = 2.0 \text{ cm}$

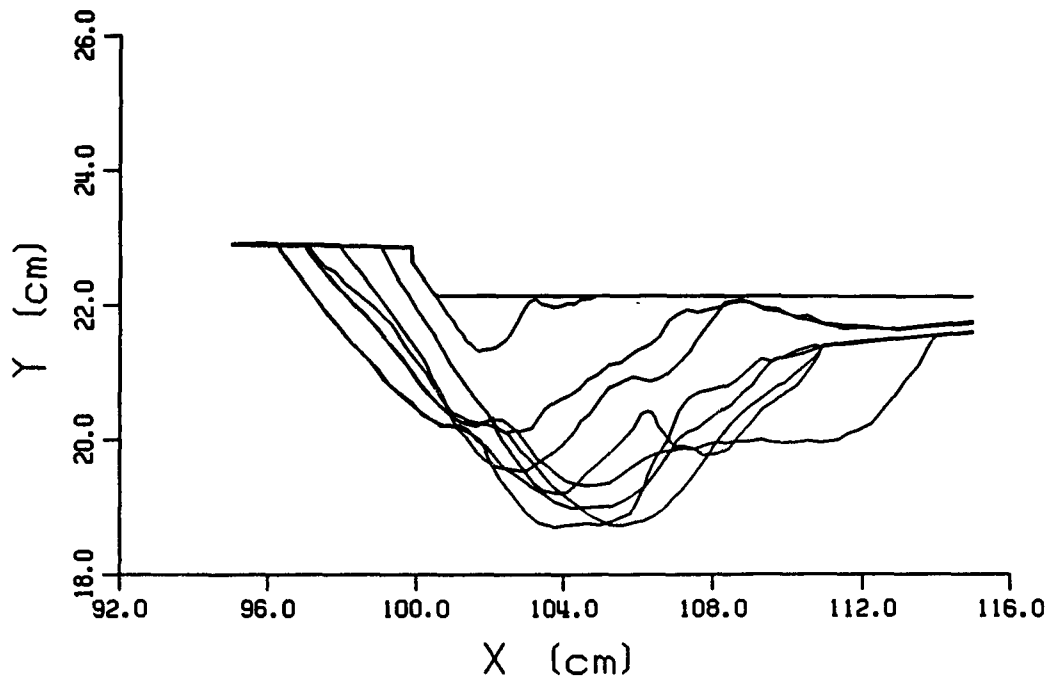


Figure A17: Run 21 Sand $D_{50} = 1.5\text{mm}$ $q = 0.00162\text{ m}^2/\text{s}$ $D_h = 2.0\text{ cm}$

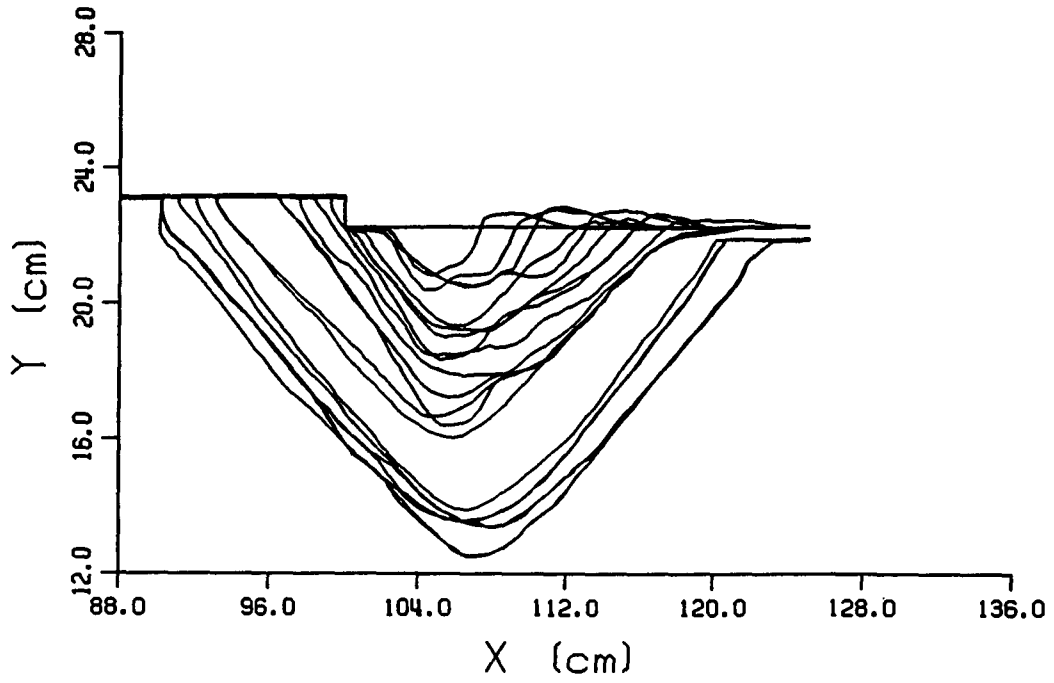


Figure A18: Run 22 Sand $D_{50} = 0.15\text{mm}$ $q = 0.00166\text{ m}^2/\text{s}$ $D_h = 2.0\text{ cm}$

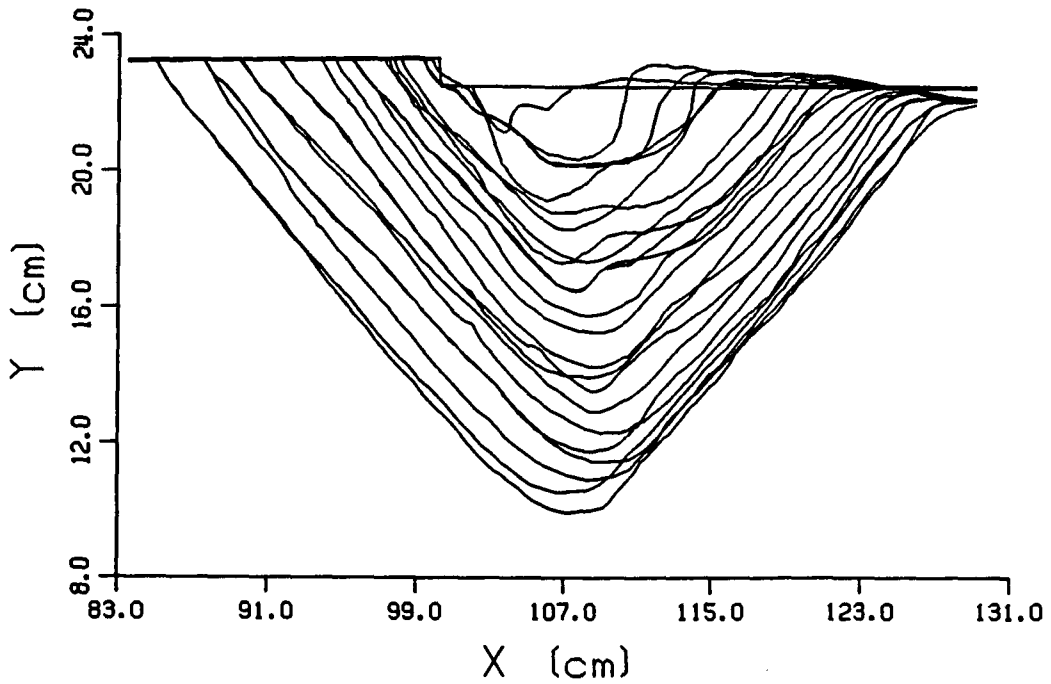


Figure A19: Run 23 Sand $d_{50} = 0.15\text{mm}$ $q = 0.00232\text{ m}^2/\text{s}$ $D_h = 2.0\text{ cm}$

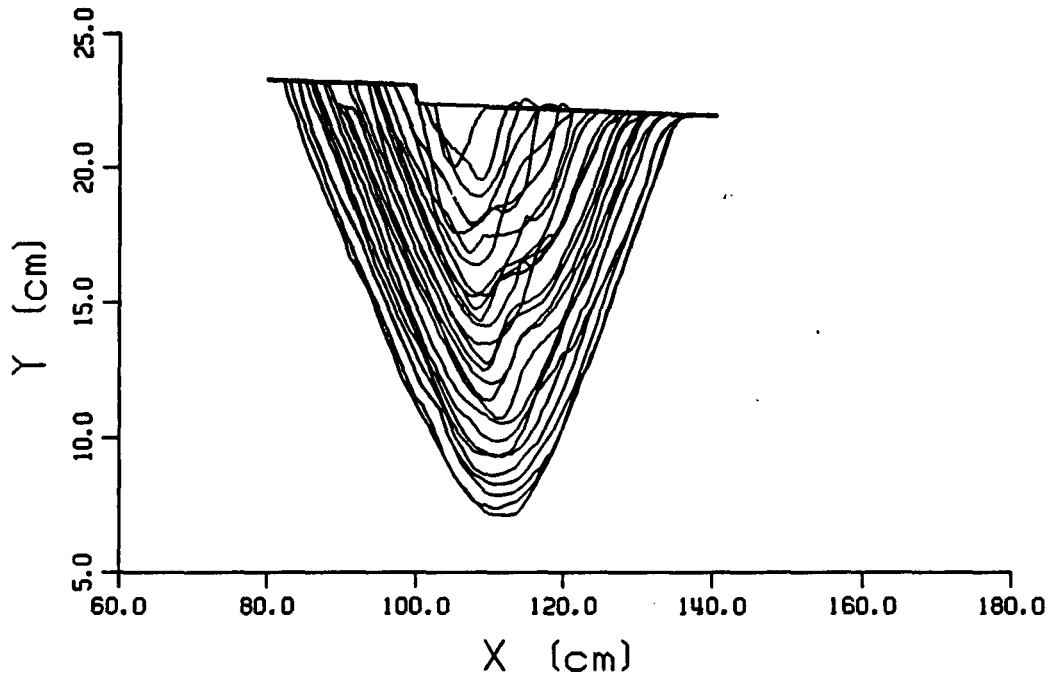


Figure A20: Run 24 Sand $D_{50} = 0.15\text{mm}$ $q = 0.00349 \text{ m}^2/\text{s}$ $D_h = 2.0 \text{ cm}$

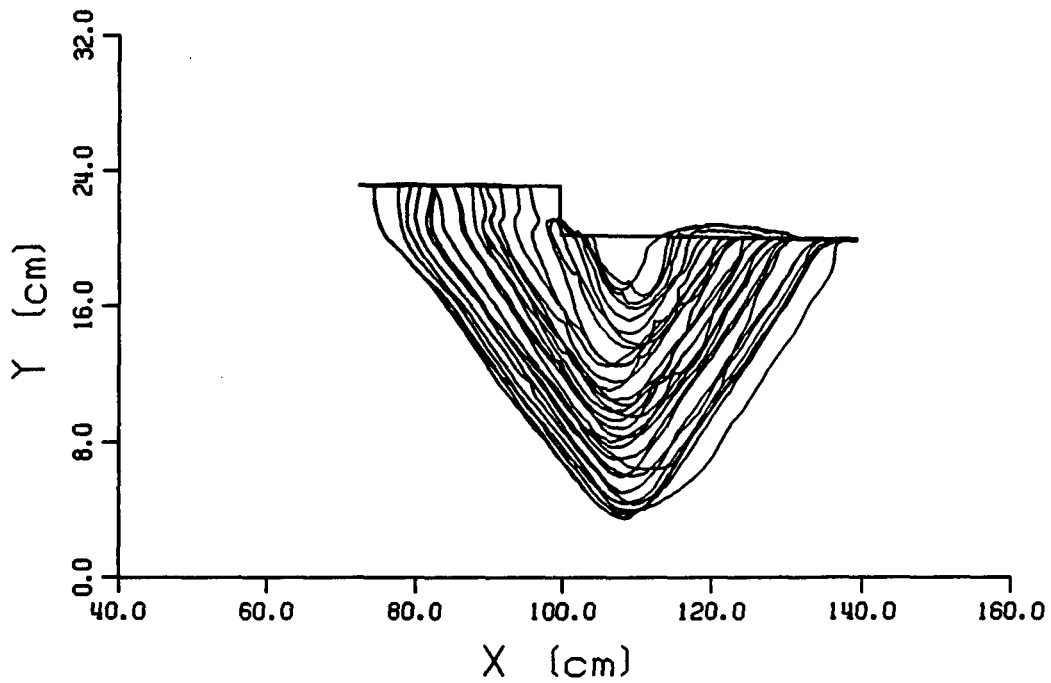


Figure A21: Run 25 Sand $D_{50} = 0.15\text{mm}$ $q = 0.00337 \text{ m}^2/\text{s}$ $D_h = 4.0 \text{ cm}$

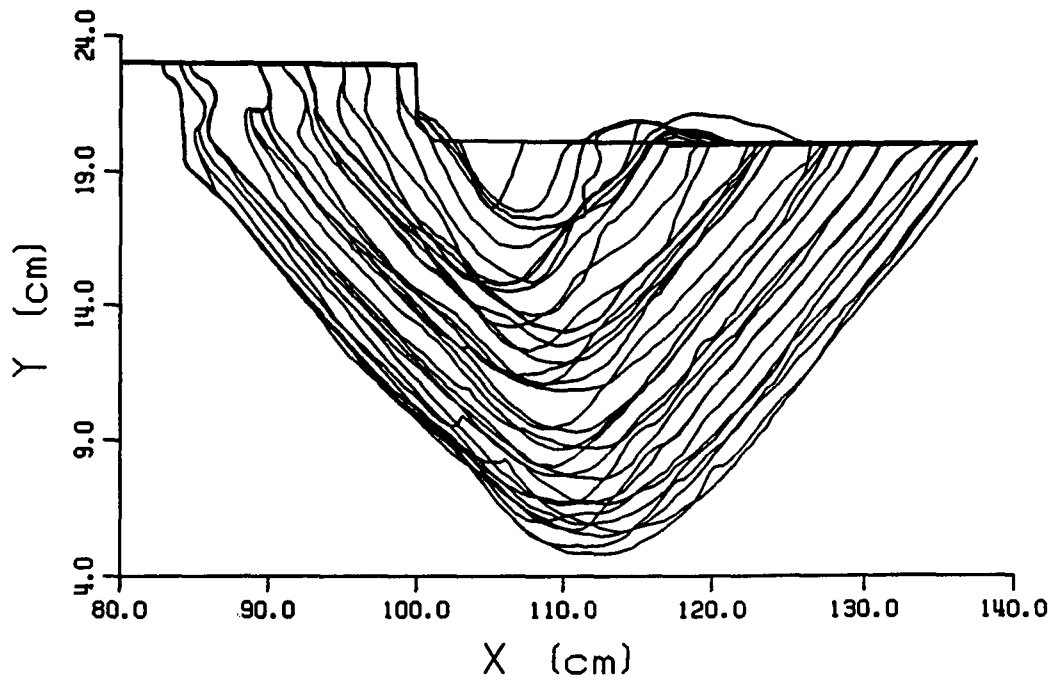


Figure A22: Run 26 Sand $d_{50} = 0.15\text{mm}$ $q = 0.00242\text{ m}^2/\text{s}$ $D_h = 4.0\text{ cm}$

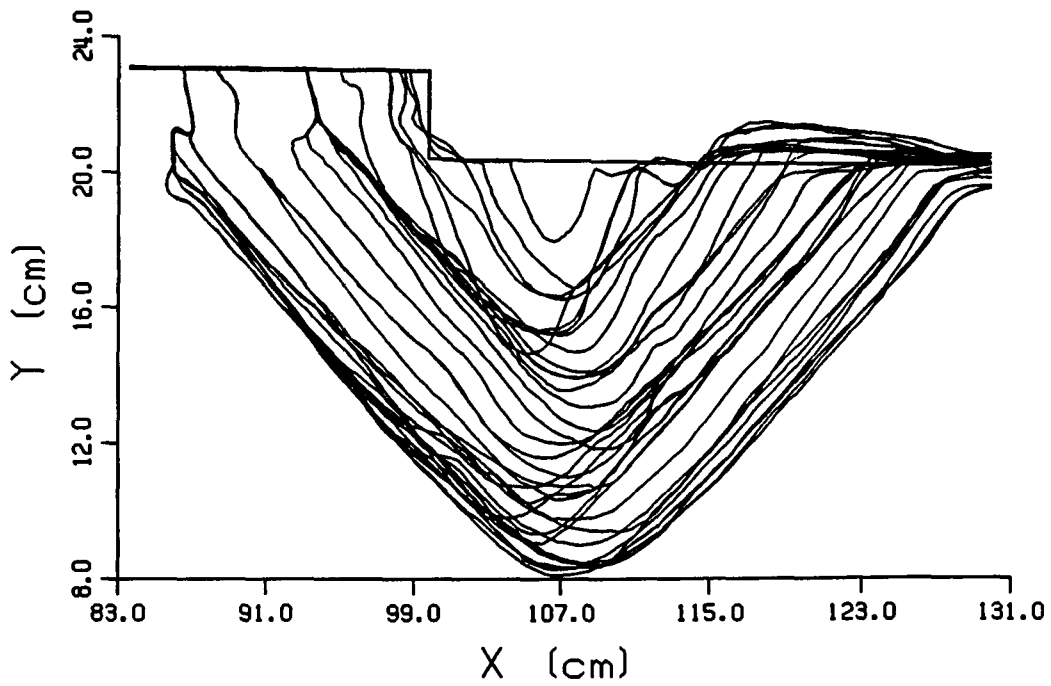


Figure A23: Run 27 Sand $d_{50} = 0.15\text{mm}$ $q = 0.00175\text{ m}^2/\text{s}$ $D_h = 4.0\text{ cm}$

Appendix C

Measured Eroded Volume and Maximum Depth of Scour Coordinates

**Table C1: Measured Scour Volume per Unit Width
and Maximum Depth Coordinate; Non-Retreating Soil Run**

Run	t (s)	Vol (cm ²)	X (cm)	Y (cm)	Run	t (s)	Vol (cm ²)	X (cm)	Y (cm)
1&2	0	0.0	105.5	20.3	3&4	0	0.0	103.9	22.3
1&2	10	0.6	105.2	20.1	3&4	50	0.0	103.9	22.3
1&2	20	4.3	106.0	19.0	3&4	60	0.8	106.0	21.9
1&2	30	7.2	105.5	18.6	3&4	90	4.9	107.7	21.5
1&2	60	10.9	105.4	18.3	3&4	120	7.4	106.8	21.3
1&2	90	16.6	104.3	18.0	3&4	180	10.7	106.4	20.8
1&2	120	20.1	103.9	18.0	3&4	270	14.8	107.7	20.3
1&2	180	25.6	104.5	17.5	3&4	480	21.4	107.2	19.9
1&2	300	36.9	104.4	17.1	3&4	840	27.8	107.1	19.3
1&2	420	42.6	105.9	16.6	3&4	1320	36.0	108.4	18.9
1&2	540	47.2	106.2	16.4	3&4	1740	43.1	108.1	18.4
1&2	660	51.7	106.2	15.9	3&4	2340	52.8	108.3	17.7
1&2	720	53.6	106.3	15.9	3&4	2940	60.9	108.1	17.3
1&2	745	60.0	106.3	15.5	3&4	3540	68.5	108.3	16.6
1&2	746	70.6	106.7	15.4	3&4	4740	80.1	110.5	16.6
1&2	776	77.8	108.3	14.4	3&4	5100	86.8	109.8	16.2
1&2	806	82.6	109.3	14.1	3&4	5460	89.7	109.2	15.9
1&2	836	87.2	107.6	13.5	3&4	5820	108.3	109.1	15.5
1&2	866	94.5	108.5	13.5	3&4	6180	118.5	108.2	14.7

Run	t (s)	Vol (cm ³)	X (cm)	Y (cm)	Run	t (s)	Vol (cm ³)	X (cm)	Y (cm)
1&2	926	100.4	108.7	13.0	3&4	6540	130.4	109.1	14.3
1&2	986	107.0	108.3	12.7	3&4	6900	138.6	109.2	13.9
1&2	1046	114.7	109.1	12.1	3&4	7440	147.4	109.5	13.6
1&2	1106	122.2	108.7	11.4	3&4	8340	157.6	110.1	13.0
1&2	1166	128.2	109.0	10.8					
1&2	1256	142.8	108.7	10.1					
1&2	1316	147.5	108.6	10.2					
1&2	1376	151.9	108.8	9.8					
1&2	1496	162.5	111.0	9.4					
1&2	1556	168.6	110.8	9.1					
1&2	1616	172.1	109.6	8.8					
6	0	0.0	105.2	22.3	7	0	0.0	103.3	22.3
6	10	0.0	105.2	22.3	7	80	0.0	103.3	22.3
6	20	4.6	105.3	21.2	7	90	0.6	102.8	21.6
6	30	11.6	105.4	20.4	7	100	2.5	103.7	20.8
6	40	15.3	106.0	19.9	7	110	5.9	104.5	20.5
6	50	17.7	106.5	19.7	7	120	8.6	105.0	20.3
6	60	20.1	105.8	19.5	7	150	10.3	105.0	20.3
6	90	25.6	106.0	19.2	7	180	12.4	104.9	19.9
6	120	30.7	106.3	18.8	7	210	15.3	107.0	19.6
6	150	34.4	105.4	18.9	7	240	16.9	107.1	19.6

Run	t (s)	Vol (cm ³)	X (cm)	Y (cm)	Run	t (s)	Vol (cm ³)	X (cm)	Y (cm)
6	180	38.8	105.1	18.7	7	300	18.9	106.6	19.5
6	210	44.4	105.6	18.5	7	420	24.3	107.4	19.1
6	240	46.9	105.8	18.5	7	540	27.3	106.7	18.6
6	270	50.3	106.4	18.2	7	720	33.1	106.6	17.9
6	300	55.5	106.5	17.9	7	900	40.6	105.7	17.6
6	360	61.0	107.0	17.5	7	1080	46.8	107.9	17.5
6	480	74.6	106.9	16.6	7	1320	54.1	106.9	17.2
6	600	87.4	107.4	16.0	7	1560	60.8	105.5	16.9
6	720	97.1	107.0	15.6	7	1800	67.7	105.4	16.7
6	960	116.8	108.0	14.8	7	2040	73.1	105.5	16.5
6	1260	134.5	108.5	14.4	7	2640	83.9	106.1	16.2
6	1560	158.0	108.0	13.9	7	3240	89.8	106.2	15.8
6	1860	174.4	109.2	13.5	7	3840	95.9	106.0	15.7
6	2160	188.5	109.3	13.2	7	4440	104.3	106.2	15.5
6	2460	201.5	108.4	12.9	7	5040	109.0	107.0	15.4
6	2760	213.8	109.3	12.4	7	5640	117.3	106.8	15.2
6	3300	228.8	108.4	11.9	7	6240	120.8	106.1	15.1
6	3900	250.4	107.6	11.3					
6	4200	261.8	106.9	11.1					
6	4500	273.8	107.1	10.4					
6	4800	283.2	107.1	10.4					

Run	t (s)	Vol (cm ³)	X (cm)	Y (cm)	Run	t (s)	Vol (cm ³)	X (cm)	Y (cm)
6	5100	290.6	112.7	10.3					
6	5400	297.1	113.1	10.2					
6	5700	306.0	113.8	10.1					
6	6000	311.0	114.6	10.0					
8	0	0.0	104.9	20.3	9	0	0.0	107.3	20.3
8	10	0.0	104.9	20.3	9	10	2.5	108.5	19.4
8	20	0.1	104.3	20.2	9	20	16.1	110.6	17.9
8	30	2.1	104.8	18.8	9	30	25.5	112.5	17.2
8	40	4.0	105.4	18.5	9	40	30.3	112.7	17.1
8	50	5.3	105.1	18.2	9	50	34.6	110.7	17.0
8	60	7.5	105.9	17.9	9	60	39.3	114.1	16.9
8	90	9.8	106.6	17.7	9	90	46.7	111.7	16.5
8	120	13.6	105.8	17.4	9	120	54.0	111.8	16.3
8	150	16.2	106.8	17.3	9	180	64.1	111.1	16.1
8	180	19.2	106.1	17.2	9	240	74.5	110.7	15.5
8	240	23.1	107.0	17.2	9	300	84.0	110.1	15.0
8	360	31.6	106.0	16.9	9	360	94.1	111.4	14.6
8	480	37.5	105.9	16.6	9	420	100.8	111.4	14.2
8	600	42.9	106.1	16.4	9	480	106.3	111.2	14.0
8	840	48.6	106.0	16.1	9	540	112.7	111.3	13.7
8	1440	60.6	105.7	15.7	9	600	119.9	110.5	13.5

Run	t (s)	Vol (cm ³)	X (cm)	Y (cm)	Run	t (s)	Vol (cm ³)	X (cm)	Y (cm)
8	2040	72.4	105.4	15.1	9	720	133.4	111.6	13.0
8	2640	84.8	106.2	14.2	9	840	143.8	111.6	12.6
8	3240	95.2	106.5	13.3	9	960	154.0	112.1	12.1
8	3840	105.2	106.8	12.8	9	1080	165.0	110.9	11.8
8	4440	114.7	107.0	12.3	9	1200	178.6	112.1	11.4
8	5040	122.9	107.6	12.1	9	1320	188.8	111.2	11.0
8	5640	134.7	107.0	11.5	9	1620	215.6	110.2	10.0
8	6240	144.0	107.5	11.0	9	1920	247.2	110.6	8.9
8	6840	152.1	107.9	10.5	9	2220	269.2	112.1	8.1
8	6960	161.6	107.4	10.3	9	2520	296.4	111.0	7.1
8	7560	174.2	107.3	9.8	9	2820	312.1	110.6	6.7
8	8160	184.1	108.0	9.4	9	3240	340.7	113.5	5.3
8	8760	192.4	107.5	9.2	9	3480	357.6	113.8	5.3
8	9360	197.5	108.3	9.1	9	3780	369.4	113.6	5.3
8	9960	205.8	107.8	8.8	9	4080	386.0	113.6	5.3
10	0	0.0	106.6	20.3	11	0	0.0	104.6	22.3
10	10	0.1	104.8	20.1	11	10	0.0	104.6	22.3
10	20	7.2	109.0	18.6	11	20	2.7	105.1	21.8
10	30	11.1	110.0	18.1	11	30	5.0	105.5	21.5
10	40	14.9	108.6	18.0	11	40	6.4	105.5	21.3
10	60	23.3	110.6	17.4	11	60	10.1	107.3	20.5

Run	t (s)	Vol (cm ³)	X (cm)	Y (cm)	Run	t (s)	Vol (cm ³)	X (cm)	Y (cm)
10	90	31.5	107.9	17.1	11	120	15.3	107.9	20.3
10	120	39.4	108.3	16.8	11	180	21.0	106.4	19.8
10	180	51.7	108.6	16.4	11	240	24.6	107.2	19.5
10	240	58.9	106.1	16.2	11	300	27.6	105.2	19.2
10	360	67.7	107.9	15.5	11	360	30.3	104.3	19.2
10	540	81.2	108.1	14.8	11	480	39.9	104.3	18.8
10	840	97.6	106.8	14.0	11	600	46.6	104.1	18.6
10	1200	110.4	109.3	13.8	11	720	52.2	103.5	18.6
10	1800	128.4	108.2	13.3	11	840	60.2	103.4	18.3
10	2400	144.2	106.6	12.6	11	960	62.8	112.7	18.3
10	3000	161.5	107.2	11.9	11	1200	72.0	104.7	18.0
10	3600	179.8	107.2	11.3	11	1440	82.0	112.7	17.8
10	4200	193.8	107.4	10.8	11	1800	87.9	107.6	17.4
10	4800	212.0	107.1	10.1	11	2100	98.3	107.1	17.0
10	5400	222.3	108.5	9.6	11	2400	101.8	107.5	16.9
10	6000	245.0	106.0	9.1	11	2700	109.4	104.9	16.8
10	6600	260.0	108.8	8.5	11	3000	129.9	107.0	15.8
10	7200	276.4	108.5	8.0	11	3300	138.0	107.3	15.5
10	7800	295.0	109.5	7.3	11	3600	149.5	106.7	15.2
10	8400	307.1	109.1	7.0	11	3900	161.0	107.3	14.9
10	9000	321.9	109.3	6.4	11	4200	169.0	107.2	14.4

Run	t (s)	Vol (cm ²)	X (cm)	Y (cm)	Run	t (s)	Vol (cm ²)	X (cm)	Y (cm)
					11	4500	180.6	108.1	13.9
					11	4800	196.2	108.4	13.3
					11	5400	206.3	110.0	13.0
					11	6000	215.2	107.6	12.4
					11	6600	234.6	110.7	11.8
					11	6900	239.0	109.3	11.4
					11	7200	247.8	109.3	11.0
					11	7800	262.5	107.2 ²⁰	10.4
					11	8400	273.3	106.2	10.2
					11	9000	289.3	109.4	9.4
12	0	0.0	103.8	23.3	13	0	0.0	102.3	23.3
12	40	0.0	103.8	23.3	13	20	0.0	102.3	23.3
12	50	0.2	102.8	22.7	13	30	0.3	102.3	22.8
12	60	2.2	103.4	22.5	13	40	1.3	102.8	22.7
12	90	6.9	105.0	22.1	13	50	2.2	102.9	22.6
12	120	10.4	105.3	21.7	13	60	2.4	102.8	22.6
12	150	15.3	105.3	21.3	13	90	3.2	102.9	22.6
12	180	19.5	105.3	21.1	13	120	3.3	103.1	22.3
12	240	27.9	106.4	20.5	13	150	4.8	103.3	22.2
12	300	37.3	106.8	20.0	13	180	6.9	104.3	21.6
12	360	43.3	106.0	19.7	13	240	7.4	103.8	21.5

Run	t (s)	Vol (cm ³)	X (cm)	Y (cm)	Run	t (s)	Vol (cm ³)	X (cm)	Y (cm)
12	480	52.5	106.6	19.2	13	360	9.6	102.9	21.2
12	600	62.6	107.2	18.6	13	540	12.6	102.5	21.0
12	660	80.7	108.8	18.2	13	960	17.0	102.3	20.5
12	720	86.1	109.0	18.0	13	1200	19.4	102.5	20.2
12	840	94.3	109.0	17.8	13	1320	20.5	102.7	19.9
12	960	100.0	108.4	17.6	13	1440	24.5	102.5	19.6
12	1080	114.8	109.5	17.0	13	1680	29.0	102.6	19.1
12	1200	126.5	110.3	16.5	13	1800	32.3	102.9	18.9
12	1500	152.2	110.2	15.9	13	2100	35.8	102.8	18.6
12	1800	160.5	111.3	15.5	13	2400	40.8	103.8	18.5
12	2100	174.4	110.8	15.0	13	2700	45.9	103.8	18.3
12	2400	188.5	114.3	14.9	13	3000	51.0	104.8	18.2
12	2700	199.4	112.9	14.6	13	3300	56.1	103.7	17.9
12	3000	209.2	114.4	14.2	13	3600	64.5	104.3	17.1
12	3300	217.8	114.2	13.9	13	3900	66.8	104.5	17.1
12	3600	224.2	114.5	13.6	13	4200	69.8	105.8	17.1
12	3900	229.7	115.1	13.4	13	4500	73.8	103.7	17.0
12	4200	234.2	116.7	13.3	13	4800	81.7	103.9	16.2
12	4500	243.6	118.7	13.0	13	5400	87.4	106.1	16.3
12	4800	249.2	115.5	13.1	13	5700	91.0	104.0	16.3
12	5100	269.2	115.8	12.6	13	6000	99.1	105.0	15.7

Run	t (s)	Vol (cm ³)	X (cm)	Y (cm)	Run	t (s)	Vol (cm ³)	X (cm)	Y (cm)
12	5400	280.1	115.1	12.1	13	6600	104.0	104.8	15.6
12	6000	291.2	117.2	11.8	13	6900	106.7	104.3	15.8
					13	7200	110.5	104.3	15.8

**Table C2: Measured Scour Volume per Unit Width
and Maximum Depth Coordinate; Non-Retreating Sand Runs**

Run	t (s)	Vol (cm ³)	X (cm)	Y (cm)	Run	t (s)	Vol (cm ³)	X (cm)	Y (cm)
14	0	0.0	104.8	20.3	15	0	0.0	105.6	20.3
14	10	7.8	106.6	18.0	15	5	3.8	106.2	18.4
14	60	14.0	106.0	17.6	15	20	12.8	111.3	18.7
14	110	20.1	106.2	16.6	15	30	17.5	110.5	18.2
14	120	19.2	105.2	17.6	15	40	14.7	107.5	17.3
14	180	21.3	104.8	16.8	15	180	42.3	110.5	15.3
14	300	25.3	105.7	17.3	15	360	50.5	109.6	15.3
14	600	31.6	105.6	16.5	15	600	50.0	108.6	15.2
14	1200	32.3	106.5	16.6	15	840	49.7	107.4	15.0
14	1800	34.9	105.5	16.5	15	1080	61.9	106.7	14.8
16	0	0.0	106.6	20.3	17	0	0.0	107.5	20.3
16	6	12.0	109.9	18.1	17	5	18.5	111.0	17.6
16	21	24.6	110.5	16.9	17	10	25.6	110.4	16.5
16	56	37.6	111.1	15.9	17	30	42.1	111.1	15.6
16	121	48.9	109.1	14.7	17	50	53.9	109.9	15.9
16	241	70.7	108.2	14.2	17	55	55.6	109.3	14.9
16	361	80.3	105.8	14.9	17	80	70.6	109.2	14.4
16	540	93.5	106.4	13.9	17	300	122.4	109.8	12.6
16	960	112.5	107.4	13.3	17	540	146.8	106.4	12.1

Run	t (s)	Vol (cm ³)	X (cm)	Y (cm)	Run	t (s)	Vol (cm ³)	X (cm)	Y (cm)
16	1800	112.3	106.4	13.7	17	1200	168.5	108.9	11.4
					17	2040	175.6	108.5	11.3
					17	5220	203.6	109.9	10.6
19	0	0.0	104.6	22.3	20	0	0.0	104.1	22.3
19	15	15.5	104.9	19.7	20	5	8.1	106.2	20.7
19	45	27.9	106.6	19.0	20	25	23.2	104.8	19.5
19	65	32.7	106.5	18.1	20	65	29.6	104.6	18.6
19	120	49.6	105.8	17.4	20	215	38.5	104.1	18.2
19	300	69.8	106.1	16.6	20	245	48.6	106.9	18.5
19	540	79.7	105.9	16.4	20	1800	60.9	104.0	17.5
19	900	86.3	106.4	16.2					
19	1740	93.0	107.3	15.8					
					21	0	0.0	103.4	22.3
					21	26	1.5	101.8	21.3
					21	36	11.7	102.4	20.1
					21	66	17.6	102.8	19.5
					21	236	28.4	104.6	19.3
					21	296	32.5	103.8	19.2
					21	896	29.6	105.4	18.7
					21	1256	31.3	103.8	18.7
					21	1800	31.1	104.2	19.0

Run	t (s)	Vol (cm ²)	X (cm)	Y (cm)	Run	t (s)	Vol (cm ²)	X (cm)	Y (cm)
22	0	0.0	103.4	22.3	23	0	0.0	103.9	22.3
22	11	3.7	104.8	20.8	23	5	1.9	103.6	21.1
22	21	7.4	104.9	20.4	23	15	7.6	107.7	20.3
22	31	8.1	106.9	20.5	23	25	15.4	107.4	20.1
22	61	11.9	106.4	20.5	23	45	18.4	107.0	20.2
22	110	19.4	106.2	19.3	23	85	26.3	106.0	19.1
22	210	27.7	105.5	19.0	23	135	40.7	107.1	18.3
22	300	29.0	107.5	19.2	23	245	49.6	107.6	18.8
22	420	34.1	105.2	18.3	23	485	65.5	106.9	17.3
22	660	42.8	105.1	18.5	23	605	70.3	107.6	17.4
22	1140	56.5	106.4	17.9	23	965	85.4	107.6	16.5
22	1260	61.6	106.2	17.2	23	1085	89.4	107.6	16.5
22	1380	66.4	105.7	16.4	23	1565	100.3	107.9	15.8
22	1500	81.2	104.6	16.7	23	1925	117.6	108.7	15.3
22	1800	88.6	105.9	16.0	23	2400	142.0	108.3	14.3
22	4800	144.0	106.6	13.9	23	3300	161.4	108.3	13.9
22	5400	154.8	106.7	13.5	23	3600	169.2	108.4	13.5
22	6000	164.1	106.4	13.6	23	4200	189.1	108.4	12.9
22	7200	177.3	108.0	13.4	23	4800	214.8	109.0	12.3
22	8100	185.9	107.1	12.5	23	5400	230.8	108.3	11.7
22	8400	186.2	106.7	12.5	23	6000	248.4	109.0	11.4

Run	t (s)	Vol (cm ³)	X (cm)	Y (cm)	Run	t (s)	Vol (cm ³)	X (cm)	Y (cm)
22	9000	185.3	107.7	13.4	23	7200	271.3	108.4	10.9
					23	7800	287.9	107.0	10.5
					23	9000	306.8	107.2	9.9
24	0	0.0	104.6	22.3	25	0	0.0	106.5	20.3
24	5	10.9	105.0	20.0	25	10	8.2	107.8	17.0
24	15	17.9	108.7	19.5	25	20	15.6	110.8	16.6
24	35	26.4	108.8	18.9	25	30	24.2	109.9	16.2
24	65	46.8	106.5	17.6	25	40	33.6	109.7	15.9
24	95	55.5	107.3	17.9	25	50	47.5	108.9	15.1
24	125	60.7	107.4	17.9	25	60	59.7	108.8	14.4
24	155	73.5	108.1	16.4	25	90	79.3	110.3	13.7
24	240	90.0	107.2	16.8	25	120	94.9	109.4	13.5
24	300	113.4	109.1	15.3	25	150	107.6	107.0	12.5
24	480	127.1	107.3	15.2	25	180	128.8	108.0	12.6
24	720	139.1	108.1	14.8	25	210	141.9	105.9	12.5
24	960	149.2	108.5	14.3	25	310	175.8	107.2	11.5
24	1200	159.6	109.4	14.1	25	360	186.7	106.4	11.1
24	1440	175.0	108.4	13.5	25	420	213.9	108.1	10.2
24	1800	196.6	109.7	12.7	25	480	228.8	106.4	10.5
24	2100	212.2	109.1	12.5	25	540	235.7	106.7	9.8
24	2400	236.8	110.4	12.0	25	600	258.3	109.3	9.5

Run	t (s)	Vol (cm ³)	X (cm)	Y (cm)	Run	t (s)	Vol (cm ³)	X (cm)	Y (cm)
24	3000	254.2	109.3	11.4	25	720	271.6	106.9	9.3
24	3600	279.8	111.1	10.7	25	960	292.6	107.9	8.8
24	4200	297.4	111.6	10.5	25	1080	315.5	108.1	8.3
24	4800	322.4	110.6	9.9	25	1200	327.3	106.5	8.0
24	5400	353.7	110.9	9.3	25	1500	351.8	106.7	7.7
24	6000	373.2	111.8	9.3	25	1800	378.9	107.0	7.0
24	6600	397.4	110.2	8.6	25	2160	412.8	108.0	6.0
24	7200	425.6	110.7	8.3	25	2280	434.0	111.1	6.4
24	7800	442.4	110.9	7.9	25	2400	451.5	109.2	6.0
24	8400	468.0	110.2	7.4	25	2640	467.4	108.0	5.0
24	9000	479.1	112.3	7.1	25	3000	519.4	109.6	4.3
					25	3600	532.8	108.2	4.4
					25	4200	574.1	107.9	3.8
					25	4800	594.2	108.4	3.5
					25	5400	599.0	107.8	3.6
					25	6000	640.1	108.6	4.0
26	0	0.0	105.6	20.3	27	0	0.0	104.9	20.3
26	5	7.8	105.1	17.6	27	5	8.7	106.6	17.9
26	15	9.7	107.2	17.5	27	15	9.6	107.7	16.6
26	25	15.1	108.3	17.3	27	25	23.3	107.1	16.2
26	35	21.1	108.0	16.9	27	55	27.7	107.0	16.3

Run	t (s)	Vol (cm ³)	X (cm)	Y (cm)	Run	t (s)	Vol (cm ³)	X (cm)	Y (cm)
26	65	36.0	107.1	16.2	27	85	42.5	105.1	14.6
26	95	44.6	108.0	14.9	27	95	48.6	106.3	15.2
26	125	64.0	106.3	14.8	27	115	51.8	105.5	15.3
26	155	72.6	106.1	14.8	27	145	60.0	106.9	15.2
26	185	82.1	106.6	14.5	27	175	73.3	107.7	14.7
26	225	103.6	107.9	13.6	27	205	84.6	108.0	14.1
26	295	118.1	106.7	13.2	27	235	90.0	108.0	13.9
26	362	133.1	109.8	13.0	27	265	94.4	107.8	13.9
26	422	139.1	110.2	13.0	27	295	104.9	107.0	13.6
26	452	146.5	107.8	12.3	27	355	113.0	108.0	13.0
26	542	154.0	109.6	12.5	27	480	132.1	108.7	12.4
26	660	169.8	110.2	11.8	27	720	151.4	108.8	11.8
26	900	186.5	108.6	11.0	27	840	160.5	106.8	12.0
26	1140	201.0	106.9	11.4	27	1080	187.0	106.4	11.6
26	1260	213.8	108.6	11.1	27	1320	202.2	107.5	11.0
26	1380	237.0	110.0	10.8	27	1680	218.5	106.7	10.3
26	1500	244.8	108.6	9.4	27	1920	225.0	104.9	10.7
26	1800	264.4	110.9	9.3	27	2160	235.4	103.8	9.8
26	2100	283.3	109.3	8.7	27	2280	243.3	108.9	10.6
26	2400	305.9	109.3	8.0	27	2400	249.1	105.3	10.2
26	2700	332.9	112.3	8.7	27	2700	262.8	106.1	9.3

Run	t (s)	Vol (cm ³)	X (cm)	Y (cm)	Run	t (s)	Vol (cm ³)	X (cm)	Y (cm)
26	3000	354.9	109.9	7.7	27	3000	272.9	106.0	9.0
26	3300	369.2	112.7	7.6	27	3300	281.5	106.5	9.8
26	3600	376.3	109.6	6.6	27	3600	295.6	110.1	9.4
26	4200	409.7	111.6	6.7	27	4200	308.2	108.0	9.0
26	4800	426.7	110.6	5.7	27	4800	318.4	107.9	8.4
26	5400	446.8	113.1	6.7	27	5100	324.9	106.5	8.1
26	6000	458.9	108.5	6.0	27	5400	326.1	108.4	8.4
26	6600	480.0	111.9	5.9	27	7200	335.9	109.4	8.4
26	7200	491.5	112.6	5.5	27	7800	342.0	107.1	8.3
26	7800	504.3	111.4	5.1	27	8400	341.2	107.1	8.3
26	8400	507.0	113.8	5.6	27	9000	342.4	107.5	8.3
26	9000	528.0	112.8	4.8					

Appendix D

Source Code for Headcut Migration Model

As much as possible variable names are the same as presented in this text. The model is structured as a main driver program which reads inputs such as slope, flow rate, drop height and soil bulk density, calculates simple values, prints outputs and call various subroutines to determine subprocesses, mainly upstream and downstream bed profiles. These can be run independently or in combination.

Program Headcut

```

c
c To calculate bed profiles in the vicinity of a headcut
c
c It uses an excess shear model assuming an airtated nappe to calculate
c upstream profiles (see the subroutines "Rajarcomp" and "Upstream" for details) and
c uses modifications of Noel Bormann's dissertation to calculate downstream
c profiles (see the subroutines "nappe" and "downstream" for details)
c There are two possible levels of sophistication which can be used to
c calculate upstream profiles, the simpler uses only water surface
c profiles calculated from "hagercomp" subroutine (levcom = 0).
c The more sophisticated uses both water surface profiles and
c a pressure defect profile calculated from "rajarcomp" subroutine.
c See these and the "upstream" subroutine for more details.
c The "rajarcomp" subroutine is called from the "hagercomp" subroutine.
c
c
c Variable Dictionary Units are in the (m,k,s) system
c
c Name      I/O      Description
c
c *          an arrayed variable
c
c betap     SI      angle of the nappe from horizontal at impingement (radians)
c brinkst   I       initial x position of headcut brink (m)
c bulkden   I       bulk density of the soil (kg/m3)
c clu,c2u   BI      regression coefficients in upstream detachment model
c c1d,c2d   BI      regression coefficients in downstream detachment model
c cd        BI      coefficient of nappe
c cf        BI      ratio of shear stress to rho*ub2
c delh *    SI      change in bed elevation with respect to x (m/m)
c delpk *   SI      change in pressure coefficient with respect to x (1/m)
c dh        I       effective drop height of headcut (m)
c dhinit    I       initial drop height of headcut (m)
c dwncomp   0       character output from flag idwnon
c dwnprt    0       character output from flag idwnprt
c flwflag   SI      flag set .true. if flow is laminar
c flwhead   0       character header printing message on normal flow
c frnorm    0       Froude number in normal flow region
c g         BI      gravitational constant (m/s2)
c gamma     BI      specific weight of water (kg/m2/s2)
c h *       SI      flow depth at nodes (m)
c he        I       flow depth at brink (m)
c hnorm     SI/O    normal depth of flow (m)
c idwnon    I       flag to activate downstream subroutine if needed
c idwnprt   I       flag to suppress downstream printing if desired
c inhead    I       character header inputted with data
c iproprt   I       flag to suppress shear stress distribution printing if desired
c ittime    I       number of time steps
c iupon     I       flag to activate upstream subroutine if needed
c iupprt    I       flag to suppress upstream printing if desired
c kill      I       flag to stop program if upstream values are unstable
c levcom    0       flag determining different methods for upstream calculations
c levcomp   0       output from flag levcom
c napprt    I       flag set true if printing from nappe subroutine desired
c rmax      I       most downstream node effected by downstream scour
c rmin      I       most upstream node effected by downstream scour
c nodebrk   I       node value of brink coordinate and number of upstream nodes
c nodecdn   I       number of nodes
c oldtime   I       time from the previous iteration
c pk *      SI      pressure coefficient at nodes
c proprt    0       character output from iproprt flag
c q         I       flow rate per unit width (m2/s)
c qs *      I       soil detachment rate at nodes (kg/s/m2)
c qsnorm    I       soil detachment rate in normal flow region (kg/s/m2)
c reach     I       length of channel (m)
c rey       SI/O    Reynolds number
c rho       BI      density of water (kg/m3)
c s *       I       bed slope at upstream nodes
c scoumax   I       predicted maximum downstream scour from Bormann (m)
c se        I       slope at the brink node (m/m)

```

```

c sinit      I      initial bed slope (m/m)
c tauc       BI     critical shear stress for erosion initiation (Pa)
c taunorm    BI     applied bed shear stress in normal flow region (Pa)
c time       BI     present run time (s)
c tmax       I      run end time (s)
c timestep   BI     time between each iteration (s)
c unorm      SI/O   flow velocity in normal flow region (m/s)
c uo         SI     impingement velocity (m/s)
c upcomp     0      character output from flag iupon
c upprt      0      character output from flag iupprt
c x *        BI     longitudinal length scale (m)
c xmax      SI     most downstream point effected by scour (m)
c xnap       SI     longitudinal coordinate of nappe impingement (m)
c xnu       BI     kinematic viscosity of water (m2/s)
c xscmax     0      x coordinate of maximum downstream scour non-retreating headcut
c xspace     BI     distance between nodes (m)
c yo        SI     thickness of nappe at impingement (m)
c zd *       BI     bed elevation at downstream nodes (m)
c zdinit     BI     initial downstream bed elevation (m)
c znorm      0      bed elevation in the normal flow region (m)
c zscmax     0      z coordinate of maximum downstream scour non-retreating headcut
c zu *       BI     bed elevation at upstream nodes (m)
c zuinit     I      initial upstream bed elevation (m)
c
c -----
c Declare variables and set or read initial values
c -----
c
  implicit real (a-h,o-z)
  implicit integer (i-n)
  character inhead*80,flwhead*60,upcomp*3,dwncomp*3,upprt*3
  character dwnprt*3,proprt*3,levcomp*30
  logical flwflag,kill,napprt
c
  dimension x(1000),zd(1000),zu(1000),s(1000)
  dimension h(1000),delh(1000),pk(1000),delpk(1000)
  common /down/ cd,cf,scoumax
  common /input/ q,sinit,dhinit,zuinit,brinkst,reach,bulkden,tmax
  common /nap/ uo,yo,betap,xnap
  common /norm/ hnorm,unorm,fnorm,znorm,taunorm,qsnorm
  common /param/ time,tstep,xspace,nodebrk,nodedch
  common /physcon/ g,gamma,xnu,rho
  common /taucon/ clu,c2u,c1d,c2d,tauc
  data kill / .false. /
  data napprt / .true. /
  data upcomp / ' on' /
  data dwncomp / ' on' /
  data upprt / ' on' /
  data dwnprt / ' on' /
  data levcomp / 'water surface profiles only.' /
  data proprt / ' on' /
c
  gamma= rho * g
c
c Read input data
c
  read (5,1) inhead
  1 format (a80)
  read (5,*) q,sinit,dhinit,zuinit,brinkst,reach,bulkden,tmax
  read (5,*) iupon,idwnon,iupprt,idwnprt,iproprt,levcom
c
c -----
c Determine values in the normal flow region which are constant in time
c -----
c
  call normcalc(rey,flwflag,hnorm,unorm)
c
c The subroutine returns all passed variables
c
  fnorm= sqrt (q**2 / g / hnorm**3)
  znorm= zuinit

```

```

c
c Determine shear stress and soil detachment in normal flow region
c
  taunorm= gamma * hnorm * sin (atan (sinit))
c
  if (taunorm .gt. tauc) then
    qsnorm= c1u * (taunorm - tauc)** c2u
  else
    qsnorm= 0.0
  endif
c
-----
c Print initial conditions and normal flow values with appropriate headers
c -----
c
  write (6,100) inhead
c
c First the program controls change flag outputs if necessary
c
  if (iupon .eq. 1) upcomp= 'off'
  if (idwnon .eq. 1) dwncomp= 'off'
  if (iupprt .eq. 1) upprt= 'off'
  if (idwnprt .eq. 1) dwnprt= 'off'
  if (iproprt .eq. 1) proprt= 'off'
  if (levcom .eq. 1) levcomp= 'water and pressure profiles.'
  write (6,150)
  write (6,160) upcomp,dwncomp,upprt,dwnprt,proprt
  write (6,165) levcomp
c
c Input and normal flow values
c
  write (6,110)
  write (6,120) brinkst,dhinit,zuinit,reach,bulkden,tmax
  write (6,130)
  write (6,140) sinit,q,hnorm,unorm,rey,frnorm
c
c Use the flag to print normal flow calculation heading
c
  if (flwflag) then
    flwhead='Normal flow values computed from laminar flow equation.'
  else
    flwhead='Normal flow values computed from Blasius equation.'
  endif
  write (6,135) flwhead
c
c Sediment detachment parameters
c
  write (6,170)
  write (6,180) tauc,taunorm,c1u,c2u,c1d,c2d
c
c Set up an output file for profiles
c
  zdinit= zuinit - dhinit
  write (7,700) inhead,brinkst,zuinit,zdinit
c
-----
c Set the initial values of upstream and downstream nodes
c -----
c
  zdinit= zuinit - dhinit
  nodebrk= int (brinkst/ xspace) + 1
  nodedn= int(reach / xspace) + 1
  x(1)= 0.0
  zu(1)= zuinit
  zd(1)= zdinit
  s(1)= sinit
  do 10 i=2,nodebrk
    s(i)= sinit
    zu(i)= zuinit
10 continue
  do 20 j=2,nodedn

```

```

        x(j)= x(j-1) + xspace
        zd(j)= zdinit
20    continue
c
c -----
c Use subroutines to determine other initial values
c -----
c
c     call hagercomp (frnorm,hnorm,brinkst,nodebrk,x,h,delh,levcom,
c     $ ipropt)
c
c     Hagercomp subroutine returns the arrays h & delh; requires other variables
c     If levcom= 1 rajarcomp returns pk & delpk; requires other variables
c
c     he= h(nodebrk)
c     se= s(nodebrk)
c     call nappe (q,sinit,brinkst,dhinit,he,se,napprt)
c
c     Subroutine prints and returns values in "nap" common statement
c
c     if (idwnprt .eq. 1) napprt= .false.
c
c     Determine maximum predicted scour coordinates from initial conditions
c
c     cf= taunorm / (rho * unorm**2)
c     scoumax= sin(betap) * (cf * cd**2 * rho / tauc) * uo**2 * yo
c     xscmax= xnap + 0.4 * (scoumax / tan (betap))
c     zscmax= zuinit - dhinit - scoumax
c     fdout= 1000000.0 * xnu / sqrt( g * dhinit**3)
c
c     write (6,185)
c     write (6,190)
c     write (6,200) fdout,cf,cd,xscmax,zscmax
c     write (6,210)
c
c -----
c Start erosion process iterate using given time step
c -----
c
c     if (iupon .ne. 0 .and. idwnon .ne. 0) go to 99
c
c     If only downstream profiles are required the time steps can be relaxed
c
c     if (iupon .ne. 0 .and. idwnon .eq. 0) then
c       do 30 k=1,5000
c         if (time .lt. 60) then
c           tstep= 10.0
c         elseif (time .lt. 300) then
c           tstep= 30.0
c         elseif (time .lt. 600) then
c           tstep= 60.0
c         elseif (time .lt. 1200) then
c           tstep= 120.0
c         elseif (time .lt. 3600) then
c           tstep= 300.0
c         else
c           tstep= 600.0
c         endif
c         oldtime= time
c         time= time + tstep
c
c     Adjust time and tstep if next time is greater than tmax
c
c     if (time .ge. tmax) then
c       time= tmax
c       tstep= time - oldtime
c     endif
c     write (6,900) time
c     call downstream (x,zd,xmax,idwnprt)
c
c     Adjust the effective drop height for next iteration to account

```

```

c      for water surface drop due to scour width and slope
c
c dh= dhinit + sinit * (xmax - xnap) - hnorm
c dh= dhinit + sinit * (xmax - xnap)
c call nappe (q,sinit,brinkst,dh,he,se,napprt)
c
c      Write the profiles to a file
c
c      nmax= int (xmax / xspace) + 2
c      nmin= nodebrk + 1
c
c      Determine most upstream node which has been scoured
c
c      do 40 n=1,nodebrk
c      if (zd(n) .ne. zd(n+1) .and. n .lt. nmin) nmin= n
40      continue
c      write (7,710) time,x(nodebrk),zu(nodebrk)
c      do 45 n=nmin,nmax
c      write (7,710) time,x(n),zd(n)
45      continue
c
c      if (time .eq. tmax) then
c
c      Redetermine maximum predicted scour coordinates
c
c      scoumax= sin(betap) * (cf * cd**2 * rho / tauc) * uo**2 * yo
c      xscmax= xnap + 0.4 * (scoumax / tan (betap))
c      zscmax= zuinit - dhinit - scoumax
c
c      write (6,186)
c      write (6,190)
c      write (6,200) cf,cd,xscmax,zscmax
c      write (6,210)
c      go to 99
c      endif
30      continue
c      endif
c
c      Both upstream and downstream profiles are desired:
c      Use the default time step
c
c      ittime= int (tmax / tstep) + 1
c      do 50 i=1,ittime
c      oldtime= time
c      time= time + tstep
c      if (time .ge. tmax) then
c      time= tmax
c      tstep= time - oldtime
c      endif
c      write (6,900) time
c
c      Determine upstream profiles if desired
c
c      if (iupon .eq. 0) then
c      call upstream (x,zu,s,h,levcom,iupprt,kill)
c
c      Subroutine requires all passed variables and will modify zu and s
c      If kill flag was turned on, terminate program after this iteration
c      This flag is on if a slope instability is detected
c
c      endif
c
c      Determine downstream profiles if desired
c
c      if (idwnon .eq. 0) then
c      call downstream (x,zd,xmax,idwnprt)
c      if (zd(nodebrk) .lt. zdinit .and. td .eq. 0.0) td = time
c
c      Determine the effective drop height for next iteration
c
c dh= dhinit - (zuinit - zu(nodebrk)) + sinit * (xmax - xnap) - hnorm

```



```

dh= dhinit - (zuinit - zu(nodebrk))
if (dh .le. 0.0) then
  dh= 0.0
  write (6,220)
endif
se= s(nodebrk)
call nappe (q,sinit,brinkst,dh,he,se,napprt)
endif
c
c Write profiles to a file at ten second intervals
c
if (amod (time,10.0) .eq. 0.0) then
  nmax= int (xmax / xspace) + 2
  nmin= nodebrk + 1
  do 60 n=1,nodebrk
    if (zu(n+1) .ne. zu(n)) write (7,710) time,x(n),zu(n)
    if (zd(n) .ne. zd(n+1) .and. n .lt. nmin) nmin= n
60  continue
    write (7,710) time,x(nodebrk),zdinit
    do 70 n=nmin,nmax
      write (7,710) time,x(n),zd(n)
70  continue
    endif
    if (kill) go to 99
    if (dh .eq. 0.0) then
      tu = time
      go to 99
    endif
50  continue
99  continue
fd= xnu / sqrt( g * dhinit**3)
a= 1.0 / (fd**(1.0/3.0) * sinit**(1.0/3.0) * rey**(5.0/12.0))
b= 0.011 / (fd**(1.0/3.0) * sinit**(4.0/3.0) * rey**(2.0/3.0))
c= 0.182 / (fd * (0.011 * rey + sinit * rey**(1.25)))
sum= a+b+c
if (td .ne. 0.0) tratio= tu/td
const= tratio/sum
write (6,230) fd,a,b,c,sum,tu,td,tratio,const
write (7,720)
c
c -----
c Format statements
c -----
c
100 format (10x,a80/)
110 format (//10x,24x,'Initial Values'//
$ 10x,' Headcut Headcut Soil Length'/
$ 10x,'Longitudinal Drop Upstream Channel Bulk of'/
$ 10x,' Coordinate Height Elevation Length Density Storm'/
$ 10x,' (m) (m) (m) (m) (kg/m^3) (s)'/)
120 format (10x,f9.3,f10.3,f11.3,f9.3,f10.0,f8.0)
130 format (//
$ 10x,' Slope Flow Depth Velocity Reynolds Froude'/
$ 10x,' Rate Number Number'/
$ 10x,' (m/m) (m^2/s) (m) (m/s)'/)
135 format (/10x,5x,a60)
140 format (10x,4x,f5.3,4x,f7.5,3x,f7.5,2x,f6.3,5x,f6.0,2x,f6.3)
150 format (//10x,' Program Controls'//
$10x,' Upstream Downstream Upstream Downstream Initial Flow'/
$10x,' Subroutine Subroutine Printing Printing Profile Printing'/)
160 format (10x,3x,a3,8x,a3,7x,a3,7x,a3,11x,a3)
165 format (/10x,' Upstream shear stress calculated by ',a30)
170 format (//10x,' Detachment Parameters'//
$ 10x,' Critical Normal'/
$ 10x,' Shear Shear -----Detachment Coefficients-----'/
$ 10x,' Stress Stress Upstream Downstream'/
$10x,' (PA) (PA) Constant Power Constant Power'//)
180 format (10x,4x,f5.3,5x,f5.3,4x,f6.4,5x,f4.2,4x,f6.4,6x,f4.2)
185 format (//10x,8x,' Initial Downstream Degradation Values')
186 format (//10x,8x,' Recalculated Downstream Degradation Values')
190 format (/

```

```

$ 10x,' Drop      Shear      Impinging      Maximum Predicted'/
$ 10x,' Froude    Stress      Jet            Scour Coordinates'/
$ 10x,' Number   Coefficient Coefficient    X              Y'/
$ 10x,' Fd 10^6  Cf          Cd             (m)           (m)'/)
200 format (10x,f8.3,4x,f8.6,9x,f4.2,7x,f5.3,5x,f8.4)
210 format ('1')
220 format (/10x,'THE HEADCUT HAS ROTATED! QUESTION DOWNSTREAM ',
$ 'DEGRADATION VALUES')
230 format (/10x,' fd      a      b      c      sum',
$' tu      td      tu/td      const'/10x,10f10.5)
900 format (///10x,'Time (sec)=' ,f5.0)
c
700 format (1x,a80/1x,3f10.5/1x,6x,'time',6x,'x',10x,'z')
710 format (1x,f10.0,2f10.5)
720 format (1x,7x,'-1.1')
stop
end

```

```

c
c -----
c Initialize values in the common blocks
c -----
c

```

```

c
c      blockdata
c      implicit real (a-h,o-z)
c      implicit integer (i-n)
c      common/ down/ cd,cf,scoumax
c      common /param/ time,tstep,xspace,nodebrk,nodedn
c      common/ physcon/ g,gamma,xnu,rho
c      common/ taucon/ c1u,c2u,c1d,c2d,tauc

```

```

c
c      data cd /2.3/
c      data cd /2.67/
c      data cf /0.005/
c
c      data time / 0.0 /
c      data tstep /2.0/
c      data xspace /0.005/

```

```

c
c      data g /9.807/
c      data xnu /1.4e-6/
c      data rho / 1000.0/

```

```

c
c      data c1 / 0.0256058/
c      data c2 /0.6412797/
c      data tauc /0.58/

```

```

c
c      data c1u /0.0201650673/
c      data c2u /1.0/
c      data c1d /0.048076923/
c      data c2d /1.5/
c      data c1d /0.0201650673/
c      data c2d /1.0/
c      data tauc /0.333176/

```

```

c      end
c      Subroutine Normcalc (rey,flwflag,hnorm,unorm)

```

```

c
c To calculate depth of flow and velocity in normal flow region

```

```

c
c Variable Dictionary Units in the (m,k,s) system

```

```

c
c Name      I/O      Description
c
c g          I          gravitational constant (m/s**2)
c hnorm      0          normal flow depth (m)
c flwflag    0          flag set .true. if flow is laminar
c q          I          unit flow rate (m**3/s*m)
c rey        0          Reynolds number
c snorm      I          bed slope (m/m)
c unorm      0          normal flow velocity (m/s)
c xlamb      0          constant in laminar flow equation
c xnu        I          kinematic viscosity of water (m**2/s)

```

```

c
  implicit real (a-h,o-z)
  implicit integer (i-n)
  logical flwflag
  common/physcon/ g,gamma,xnu,rho
  common/input/ q,snorm,dh,zinit,brinkst,reach,bulkden,tmax
  data xlank/ 24.0/
c
  rey= q/ xnu
  if (rey .lt. 1700.0) then
c
c Flow is laminar use appropriate equations for depth and velocity
c
  flwflag= .true.
  hnorm= (xlank* xnu/ 8.0/ g)** (1.0/3.0)/ snorm** (1.0/3.0)*
$   q** (1.0/3.0)
  unorm= (8.0* g/ xlank/ xnu)** (1.0/3.0)* snorm** (1.0/3.0)*
$   q** (2.0/3.0)
  else
c
c Flow is turbulent use Blasius equation for depth and velocity
c
  flwflag= .false.
  hnorm= (0.22/ 8.0/ g)** (1.0/3.0)* xnu** (1.0/12.0) /
$   snorm** (1.0/3.0) * q** (7.0/12.0)
  unorm= (8.0* g/ 0.22)** (1.0/3.0)/ xnu** (1.0/12.0) *
$   snorm** (1.0/3.0) * q** (5.0/12.0)
  endif
  return
  end
  Subroutine Rajarcomp (irajpt,nodebrk,xu)
c
c To calculate the flow depth and pressure at nodes upstream of
c a fully airated nappe
c
c A fully airated nappe at the brink is assumed. This generates a varying
c non-hydrostatic pressure distribution for some distance upstream from the
c brink defined as reach L1. The pressure is hydrostatic upstream of the
c reach L1 where the flow is normal and is at a minimum just at the brink.
c The decrease in pressure as the brink is approached causes a flow
c acceleration which in turn causes a decrease in flow depth. Data from
c experiments conducted by Rajaratnam and Muralidhur (1968) are used to
c determine the pressure and flow depth distributions in the reach L1. These
c calculated distributions will be used by the "Upstream" subroutine to
c determine the shear stress distributions and bed degradation in this reach.
c
c Variable Dictionary Units in the (m,k,s) system
c
c * an arrayed variable
c
c Name I/O Description
c a1,a2 regression coefficients in normalized depth equation
c accelng length of the reach L1 (m)
c b1,b2 regression coefficients in pressure coefficient equation
c brinkst I initial x coordinate of headcut brink (m)
c delh * SO change in flow depth with respect to x (m/m)
c dhhat * O change in flow depth with respect to normalized x (m)
c delpk * SO change in pressure coefficient with respect to x (1/m)
c dpkhat * O change in pressure coefficient with respect to normalized x
c gamma CI specific weight of water (kg/m^2/s^2)
c fr Froude number at a transfered node
c h * SO flow depth at upstream nodes (m)
c hatleng distance between normalized nodes (m)
c hhat * O flow depth at normalized nodes
c hnorm I depth of flow in normal flow region (m)
c irajpt I print control: if = 1 supress printing
c nodebrk I node value of brink coordinate
c nodehat number of normalized nodes in reach L1
c pk * SO pressure coefficient at upstream nodes
c pkhat* O pressure coefficient at normalized nodes
c tauck calculated shear stress at a transfered node (Pa)

```

```

c taunorm CI normal flow shear stress (Pa)
c xhat * normalized longitudinal length scale
c xu * I upstream longitudinal length scale (m)
c
c The normalizing parameters are:
c hhat= h / hnorm
c xhat= (accelng - x) / accelng
c
c -----
c Declare variables
c -----
c
c implicit real (a-h,o-z)
c implicit integer (i-n)
c real nu
c dimension xhat(110),hhat(110),pkhat(110),dhhat(110),dpkhat(110)
c dimension xu(1000)
c common/input/q,sinit,dh,zinit,brinkst,reach,bulkden,tmax
c common/physcon/ g,gamma,nu,rho
c common/norm/ hnorm,unorm,fnorm,znorm,taunorm,qsnorm
c common/rajar/ h(1000),pk(1000),delh(1000),delpk(1000)
c
c data a1/ -2.9/
c data a2/ -1.15/
c data b1/ -5.0/
c data b2/ -0.06/
c data nodehat /100/
c
c -----
c Determine values needed for the nodes
c -----
c
c Determine the length of the reach L1
c
c accelng= 2.5 * hnorm
c
c Set normalized x values of the nodes
c
c hatleng= accelng / float(nodehat)
c xhat(1)= 0.0
c do 10 i=2,nodehat+1
c xhat(i)= xhat(i-1) + (1.0 / float(nodehat))
10 continue
c nodehat= nodehat+1
c
c -----
c Determine specific values at the normalized nodes assuming an airated nappe
c -----
c
c do 20 j=1,nodehat
c
c Determine the depth and pressure coefficient at nodes. Use regression
c coefficients determined from Rajaratnam and Muralidhar's (1968) data
c
c hhat(j)= 1.0- exp (a1* (xhat(j)- a2))
c pkhat(j)= 1.0- exp (b1* (xhat(j)- b2))
c
c Determine the changes in these values with xhat at nodes
c
c dhhat(j)= -a1* exp (a1* (xhat(j)- a2))
c dpkhat(j)= -b1* exp (b1* (xhat(j)- b2))
20 continue
c
c Remove some error induced by regression by setting values at the most upstream
c node to normal flow values and adjusting all other nodes accordingly
c
c do 25 i=1,nodehat
c hhat(i)= hhat(i) + (1.0 - hhat(nodehat))
c pkhat(i)= pkhat(i) + (1.0 - pkhat(nodehat))
c dhhat(i)= dhhat(i) + (0.0 - dhhat(nodehat))
c dpkhat(i)= dpkhat(i) + (0.0 - dpkhat(nodehat))

```

```

25 continue
c
c Convert the normalized values to real values
c
kk= 0
do 30 k=1,nodehat
inc= nodebrk - kk
if (abs(brinkst - (float(k-1) * hatleng) - xu(inc))
$ .le. (hatleng / 2.0)) then
h(inc)= hnorm * hhat(k)
pk(inc)= pkhat(k)
delh(inc)= -(hnorm / accelng) * dhhat(k)
delpk(inc)= -(1.0 / accelng) * dpkhat(k)
c
c Insure the calculated shear stress is not less than normal shear stress
c
fr= sqrt(q**2 / g / h(inc)**3)
tauck= gamma * h(inc) * (sin(atan(sinit)) - h(inc) / 2.0 *
$ delpk(inc) - delh(inc) * (pk(inc) - fr**2))
if (tauck .lt. taunorm) then
h(inc)= hnorm
pk(inc)= 1.0
delh(inc)= 0.0
delpk(inc)= 0.0
endif
kk= kk + 1
endif
30 continue
c
c Set the values to normal values in the normal flow region
c
do 40 m= 1,nodebrk - kk
h(m)= hnorm
pk(m)= 1.0
delh(m)= 0.0
delpk(m)= 0.0
40 continue
c
c Print the normalized values if desired
c
if (irajpr .eq. 1) go to 50
write (6,100)
write (6,200)
do 50 n=1,nodehat,5
write (6,300) xhat(n),hhat(n),pkhat(n),dhhat(n),dpkhat(n)
50 continue
c
c -----
c Format Statements
c -----
c
100 format (///20x,'Normalized values from Rajaratnam s data'//)
200 format (16x,'xhat hhat k dhhat/dxhat dk/dxhat'//)
300 format (14x,f6.2,4f11.5)
return
end
Subroutine Nappe (q,sinit,brinkst,dh,he,se,napprt)
c
c To calculate impingment parameters of a free falling nappe as needed
c for subroutine "downstream".
c
c Variable Dictionary Units are in the (m,k,s) system
c
c Name I/O Description
c
c betad 0 angle of the nappe from horizontal at impingement (degrees)
c betar 80 angle of the nappe from horizontal at impingement (radians)
c brinkst I longitudinal coordinate of brink (m)
c dh I effective drop height of the headcut (m)
c g I gravitational constant (m/s**2)
c he I flow depth at brink (m)

```

```

c napprt  I      flag set true if printout desired
c q       I      unit flow rate (m**3/m**s)
c se      I      bed slope at the brink (m/m)
c sinit   I      initial bed slope (m/m)
c tnap    I      fall time between brink and impingement (s)
c ue      I      average velocity at the brink (m/s)
c uex     I      velocity in x direction at brink (m/s)
c uey     I      velocity in y direction at brink (m/s)
c uo      BO/O   impingement velocity (m/s)
c uox     BO/O   velocity in x direction at impingement (m/s)
c uoy     BO/O   velocity in y direction at impingement (m/s)
c xnap    BO/O   longitudinal coordinate of impingement (m)
c yo      BO/O   thickness of nappe at impingement (m)
c
c -----
c Declare variables
c -----
c
c implicit real (a-h,o-z)
c implicit integer (i-n)
c logical napprt
c common/ physcon/ g,gamma,xnu,rho
c common/ nap/ uo,yo,betar,xnap
c
c -----
c Determine the values
c -----
c
c if (dh .lt. 0.0) dh= 0.0
c
c Determine values at the brink
c
c ue= q / he
c uex= ue * cos (atan(se - sinit))
c uey= ue * sin (atan(se - sinit))
c
c Determine values at the point of impingement
c
c uox= uex
c uoy= uey + sqrt (2.0 * g * dh)
c uo= sqrt (uox**2 + uoy**2)
c yo= q / uo
c betar= atan (uoy / uox)
c tnap= sqrt (2.0 * dh / g)
c xnap= brinkst + uex * tnap
c
c -----
c Print the value for the initial conditions
c -----
c
c if (napprt) then
c   betad= (180.0 / 3.1416) * betar
c   write (6,100)
c   write (6,150) dh,uo,yo,betad,xnap
c endif
c
c 100 format (//10x,'          Values of the Nappe at Impingement'//
c $ 10x,' Effective Jet Jet Impingement Impingement'//
c $ 10x,' Drop Height Velocity Thickness Angle X Coordinate'//
c $ 10x,' (m) (m/s) (m) (degrees) (m)'//)
c 150 format (10x,f9.6,1x,f11.6,1x,f9.6,1x,f9.2,3x,f11.6)
c return
c end
c Subroutine Upstream (xu,zu,s,h,levcom,iupprt,kill)
c
c To calculate Bed Profiles Upstream of a Headcut
c
c A fully airated nappe at the brink is initially assumed. This generates
c varying non-normal flow depth and non-hydrostatic pressure distributions
c for a distance upstream from the brink defined as reach L. These
c distributions cause an increase in applied bed shear stress from normal

```

c in this reach. Two levels of sophistication for calculating the shear
c stress distribution are possible. The simpler one uses only the water
c surface profiles, the more complex uses water surface and pressure
c distributions. The user decides which method to use by choosing the value
c of the parameter "levcom" (0= simple). In either case, shear stress
c decreases from a maximum at the brink to the value computed assuming a
c normal flow pattern. A normal flow pattern is assumed upstream of this
c reach.
c Soil detachment is calculated at each point along the bed from an
c excess shear model and the calculated shear stresses. Bed profile
c degradation is calculated from the soil detachment model. This process
c is iterated with time. After some time a fully aerated nappe at the brink
c can no longer be assumed due to the degradation in this area.

c
c Variable Dictionary Units in the (m,k,s) system

c Name I/O Description

c * an arrayed variable

c brinkst	BI	initial x position of headcut brink (m)
c bulkden	BI	bulk density of the soil (kg/m ³)
c c1u,c2u	BI	regression coefficients in transport model
c cin		sine of slope angle at nodes
c delzu *	O	change in bed elevation for each time step at nodes (m)
c delznor	O	change in bed elevation for each time step in normal flow
c delh *	BI	change in flow depth with respect to x (m/m)
c dh	BI	headcut drop height (m)
c delpk *	BI	change in pressure coefficient with respect to x (1/m)
c fr		Froude number at nodes
c g	BI	gravitational constant (m/s ²)
c gamma	BI	specific weight of water (Kg/m ² /s ²)
c h *	I	flow depth at nodes (m)
c hnorm	BI	normal depth of flow (m)
c iupprt	I	flag to suppress printing if set equal to 1
c kill	I/SO	flag to stop program if node values become unstable
c levcom	I	flag determining desired method of shear stress calculation
c nodebrk	BI	number of nodes
c xru	BI	kinematic viscosity of water (m ² /s)
c pk *	BI	pressure coefficient at nodes
c q	BI	flow rate per unit width (m ² /s)
c qs *	O	soil detachment rate at nodes (kg/s/m ²)
c qsnorm	BI/O	soil detachment rate in normal flow region (kg/s/m ²)
c reach	BI	total length of channel (m)
c rho	BI	density of water (kg/m ³)
c s *	I/O	bed slope at nodes (m/m)
c sinit	BI	initial bed slope (m/m)
c tau *	O	applied bed shear stress at nodes (Pa)
c tauc	BI	critical shear stress for erosion initiation (Pa)
c taunorm	BI/O	applied bed shear stress in normal flow region (Pa)
c theta		weighting parameter of bed slope calculation
c time	BI/O	present run time (s)
c tmax	BI	run end time (s)
c xspace	BI	distance between nodes (m)
c xu *	I/O	longitudinal length scale (m)
c zinit	BI	initial bed elevation (m)
c znorm	BI/O	bed elevation in the normal flow region (m)
c zu *	I/O	bed elevation at nodes (m)

c -----
c Declare variables and set or read initial values

c
c implicit real (a-h,o-z)
c implicit integer (i-n)
c logical kill
c common /input/ q,sinit,dh,zinit,brinkst,reach,bulkden,tmax
c common /norm/ hnorm,unorm,frnorm,znorm,taunorm,qsnorm
c common /param/ time,tstep,xspace,nodebrk,nodedn
c common /physcon/ g,gamma,xru,rho
c common /taucon/ c1u,c2u,c1d,c2d,tauc

```

dimension xu(1000),zu(1000),s(1000),sdeg(1000),tau(1000)
dimension delzu(1000),qs(1000)
dimension h(1000),delh(1000),pk(1000),delpk(1000)
data theta / 0.5 /

c
c -----
c Calculate values at the time determined by main program
c -----
c
c Determine bed degradation and new bed elevation in the normal flow region
c
delznor= qsnorm * tstep / bulkden
znorm= znorm - delznor
c
c Determine the same at each node
c
do 10 i= 1,nodebrk
  cin= sin(atan(s(i)))
c
c Use the given level of sophistication to determine shear stress
c
  if (levcom .eq. 0) then
    tau(i)= taunorm * (cin / sin(atan(sinit))) *
$      (hnorm / h(i))**2
  else
    fr= sqrt (q**2 / g / h(i)**3)
    tau(i)= gamma * h(i) * (cin - h(i) / 2.0 * delpk(i) -
$      delh(i) * (pk(i) - fr**2))
  endif
c
c Determine soil detachment, bed degradation and new bed elevation at nodes
c
  if (tau(i) .gt. tauc) then
    qs(i)= c1u * (tau(i) - tauc)** c2u
  else
    qs(i) = 0.0
  endif
  delzu(i)= qs(i) * tstep / bulkden
  zu(i)= zu(i) - delzu(i)
10 continue
c
c Set slope at first and last node
c
s(1)= sinit + (zu(1) - zu(2)) / xspace
s(nodebrk)= sinit + (zu(nodebrk-1) - zu(nodebrk)) / xspace
c
c Set slope at all other nodes; use weighting function
c
do 20 j= 2,nodebrk-1
  s(j)= sinit + theta * (zu(j-1) - zu(j+1)) / xspace
20 continue
do 30 k=1,nodebrk
  sdeg(k)= (180.0 / 3.1416) * atan (s(k))
30 continue
c
c Test for stability
c
do 40 m=2,nodebrk
  if (s(m) .lt. s(m-1)) then
    write (6,500) time
    kill= .true.
    iupprt= 0
  endif
40 continue
c
c -----
c Print expanded results for this iteration if desired
c -----
c
  if (iupprt .eq. 0) then
    write (6,100)

```



```

write (6,150) znorm,taunorm,delznr,sinit
do 50 n=1,nodebrk-1
  if (zu(n+1) .eq. zu(n)) go to 50
  write (6,200) xu(n),zu(n),tau(n),delzu(n),s(n),sdeg(n)
50 continue
  write (6,200) xu(nodebrk),zu(nodebrk),tau(nodebrk),
    $ delzu(nodebrk),s(nodebrk),sdeg(nodebrk)
endif
c
c -----
c Format statements
c -----
c
100 format (//10x,'                Upstream Degradation Values'//
  $ 10x,'Profile Coordinates Shear Change in Bed Bed Bed'//
  $ 10x,' X Z Stress Elevation Slope Slope'//
  $ 10x,' (m) (m) (PA) (m) (%) (degrees)'//)
150 format (10x,1x,'normal',f10.5,f10.5,e11.3,f10.5,f7.3)
200 format (10x,1x,f6.3,f10.5,f10.5,e11.3,f10.5,f7.3)
500 format (///
  $ 10x,'!!!!!!!!!!!!!!!!!!!!!!!!!!!! WARNING !!!!!!!!!!!!!!!!!!!!!!!!!!!!!/'
  $ 10x,'UPSTREAM VALUES HAVE BECOME UNSTABLE AT TIME (SEC)=' ,F6.0/
  $ 10x,'!!!!!!!!!!!!!!!!!!!!!!!!!!!!!!!!!!!!!!!!!!!!!!!!!!!!!!!!!!!!!!!!')
  return
end
Subroutine Downstream (xd,zd,xmax,icnprt)
c
c To Calculate Bed Profiles Downstream From Headcut
c
c Variable Dictionary Units in the (m,k,s) system
c
c Name I/O Description
c
c * an arrayed variable
c
c a1,a2 regression coefficients V* vs Ds*
c beta angle of the nappe from horizontal at impingement (radians)
c betap I predicted value of beta
c brinkst I initial x position of headcut brink (m)
c bulkden I bulk density of the soil (kg/m^3)
c c1d,c2d I regression coefficients in detachment model
c cd I diffusion constant of jet impingement
c cf I constant in relation between shear stress and velocity
c delscoud change in scour depth (m)
c delxt shift in x direction of maximum scour pt. since last time
c dhinit I initial drop height (m)
c idnprt I suppresses some printing if equal to 1
c impinx downstream node just upstream from maximum scour point
c itiltrn node number in scour profile corresponding to impingement pt.
c newscd flag set true if delxt does not equal zero
c nodebrk I node value of brink coordinate
c nodedn I number of downstream nodes
c notil number of nodes in scour hole profile
c p1,p2 coefficients of parabola fitted for scour hole profile
c qsb soil detachment rate at point of maximum scour (kg/s/m^2)
c rho density of water (kg/m^3)
c scoud 0 present depth of scour (m)
c scoumax I predicted maximum scour depth (m)
c scouvol volume of scour hole per unit width (m^2)
c scoum half-width of scour hole (m)
c so length of jet potential core (m)
c taub 0 shear stress in vicinity of maximum scour depth (Pa)
c tauc I critical shear stress for erosion initiation (Pa)
c tilflag flag set true if the value of notil is increased
c tilleng distance between nodes in scour hole profile (m)
c time 0 present run time (s)
c tmax I run end time (s)
c tstep I time between each iteration (s)
c ub velocity of jet in vicinity of maximum scour (m/s)
c uo I velocity of jet entering tailwater (m/s)
c width I width of channel (m)

```

```

c xd *      I      longitudinal coordinate of downstream nodes (m)
c xls       distance along jet centerline from tailwater to impingement (m)
c xlsflag   flag set true if bed still within the potential core
c xmax     SO     most downstream coordinate affected by scour (m)
c xnap      0      longitudinal coordinate of jet entering tailwater (m)
c xscoud    0      longitudinal coordinate of maximum scour (m)
c xscoup    predicted longitudinal coordinate of maximum scour (m)
c xspace    I      distance between downstream nodes (m)
c xtil *    longitudinal scale to determine scour hole shape (m)
c yo        I      thickness of jet entering tailwater (m)
c zd *      1/SO   elevation at downstream nodes (m)
c zdtrans   value of ztil transferred to zd (m)
c zeroscd   flag set true if impingement pt. beyond previous scour profile
c zscoud    0      elevation of maximum scour depth (m)
c zinit     I      initial upstream bed elevation (m)
c ztil *    vertical scale to determine scour hole shape (m)
c
c -----
c Declare variables and set or read initial values
c -----
c
c implicit real (a-h,o-z)
c implicit integer (i-n)
c logical xlsflag,zeroscd,newscd,tilflag
c dimension xtil(1010),ztil(1010),zd(1000),xd(1000)
c common /down/ cd,cf,scoumax
c common /input/ q,sinit,dhinit,zinit,brinkst,reach,bulkden,tmax
c common /nap/ uo,yo,betap,xnap
c common /param/ time,tstep,xspace,nodebrk,nodedn
c common /physcon/ g,gamma,xnu,rho
c common /taucn/ c1u,c2u,c1d,c2d,tauc
c
c data a1 /0.453368882412/
c data a2 /1.650725892649/
c
c -----
c Calculate values at the time passed by main program
c -----
c
c xlsflag= .false.
c newscd= .true.
c tilflag= .false.
c zeroscd= .false.
c
c Set values for first time iteration
c
c if (time .eq. tstep) then
c   xscoud= xnap
c   xmax= xscoud
c   scoud= 0.0
c   scouw= 0.0
c   notil= 10
c   tilleng= 0.0
c   do 10 i= 1,notil+1
c     xtil(i)= 0.0
c     ztil(i)= 0.0
10  continue
c   endif
c
c Increase the impingement angle to account for a non-aerated nappe
c
c beta= atan (tan (betap) / 0.4)
c
c Determine the bed depth beneath the jet centerline
c
c itiltrn= 0
c delxt= abs (xscoud - (xnap + scoud / tan(beta)))
c if (delxt .eq. 0.0) then
c
c Headcut and maximum depth of scour have not moved and
c scoud= scoud

```

```

c
  newscd= .false.
  elseif (delxt .gt. scouw) then
c
  Previous scour profile does not effect new scour depth
c
  scoud= 0.0
  zeroscd= .true.
  else
c
  Maximum depth of scour has moved from previous maximum but still
c  in previous profile
c
  do 20 i= 1,notil+1
    if (abs(xtil(i) - delxt) .le. tilleng / 2.0) then
      scoud= -ztil(i)
      itilrn= i
    endif
  20 continue
  endif
c
  Determine length of potential core and velocity at boundary
c
  so= cd**2 * yo
  xls= scoud / sin (beta)
  if (xls .le. so) then
    ub= uo
    xlsflag= .true.
  else
    ub= cd * uo * sqrt (yo / xls)
  endif
c
c Determine the bed degradation at maximum scour point
c
  taub= cf * rho * ub**2
  if (taub .gt. tauc) then
    qsb= c1d * (taub - tauc)**c2d
  else
    qsb= 0.0
  endif
  delscoud= qsb * tstep / bulkden
c
c Determine coordinates of maximum scour point
c
  scoud= scoud + delscoud
  xscoup= xnap + scoud / tan (betap)
  xscoud= xnap + scoud / tan (beta)
c
  xscoud= 0.6* (xnap - xscoup) + xscoup
  zscoud= zinit - dhinit - scoud
c
c -----
c Fit a parabola to the scour hole profile Form: ztil= p1* xtil^2 + p2
c -----
c
c Determine dimensions of scour hole
c
  scouvol= scoumax**2 * exp(a1 + a2 * alog(scoud / scoumax))
  p2= -scoud
  p1= -(16.0 / 9.0) * p2**3 / scouvol**2
  scouw= sqrt(-p2 / p1)
  if ((xscoud + scouw) .gt. xmax) xmax= xscoud + scouw
c
c Determine node spacing and increase number of nodes if necessary
c
  tilleng= scouw / float(notil)
  if (tilleng .gt. (xspace / 2.0)) then
    notil= 10 * notil
    tilleng= scouw / float(notil)
    tilflag= .true.
  endif
c

```

```

c   Fit the parabola from the center to one end
c
  xtil(1)= 0.0
  ztil(1)= p2
  do 30 i= 2,notil+1
    xtil(i)= xtil(i-1) + tilleng
    ztil(i)= p1 * xtil(i)**2 + p2
30  continue
c
c -----
c Set downstream nodes
c -----
c
  impinx= int(xscoud / xspace) + 1
  kk=1
  kkk=0
  do 40 k=1,notil+1
c
c   Transfer values to nodes downstream from absolute from maximum scour
c
    if (abs(xscoud + xtil(k) - xd(impinx + kk)) .le.
$     (tilleng / 2.0)) then
      zdtrans= zinit - dhinit + ztil(k)
c
c     If the transfer value is less than the old value transfer it
c
      if (zdtrans .lt. zd(impinx + kk)) zd(impinx + kk)= zdtrans
      kk= kk + 1
    endif
c
c   Transfer values to nodes upstream from absolute from maximum scour
c
    if (abs(xscoud - xtil(k) - xd(impinx - kkk)) .le.
$     (tilleng / 2.0)) then
      zdtrans= zinit - dhinit + ztil(k)
c
c     If the transfer value is less than the old value transfer it
c
      if (zdtrans .lt. zd(impinx - kkk)) zd(impinx - kkk)= zdtrans
      kkk= kkk + 1
    endif
40  continue
c
c -----
c Print results for iteration
c -----
c
  if (idnprt .eq. 0) then
    write (6,100)
    if (xlsflag) write (6,150)
    if (zeroscd) write (6,160)
    if (newscd) write (6,170) xtil(itiltrn)
    if (tilflag) write (6,200)
    write (6,250)
    write (6,300) xscoud,zscoud,xscoup,scoud,scouw,taub
    write (6,350)
    if ((impinx - kkk) .lt. nodebrk) then
      imin= impinx - kkk
    else
      imin= nodebrk
    endif
    do 50 i=imin,impinx + kk
      write (6,400) xd(i),zd(i)
50  continue
  endif
c
c -----
c Format statements
c -----
c
100 format (//10x,'          Downstream Degradation Values!')

```

```

150 format (10x,'The potential core of the jet still impinges on ',
$ 'the bed.'//)
160 format (10x,'The jet impinges on an unscoured portion of the ',
$ 'bed.'//)
170 format (10x,'The jet impingement point was moved (m) ',f9.6//)
200 format (10x,'The number of profile nodes was increased by a ',
$ 'factor of ten.'//)
250 format (
$ 10x,' Maximum Scour Coordinates      Scour Hole Shape  Maximum'/
$ 10x,'      X          Z   Predicted X   Depth    Width    Shear'//
$ 10x,'      (m)      (m)      (m)      (m)      (m)    Stress',
$ ' (PA)'//)
300 format (10x,3f9.5,3x,2f9.5,1x,f9.5)
350 format (/10x,'Scour Profiles'/
$ 10x,' X          Zd'/10x,' (m)      (m)'//)
400 format (10x,f6.3,3x,f9.6)
return
end

```